5 June 2009 | $10

Science

AAAS

GE Healthcare

Coordinate your application focus. Achieve greater operational efficiency.

GE Healthcare is focused on helping you develop efficient biopharmaceutical process flows and eliminating wasteful practices, taking your value stream to new frontiers. Through our wide range of technology platforms and services, upstream and downstream from process development to final manufacturing scale, GE Healthcare can connect you to the power of operational excellence.

Learn more about operational excellence at: www.gelifesciences.com/opex

imagination at work

GE Healthcare Bio-Sciences AB, a General Electric Company
Björkgatan 30, 751 84 Uppsala, Sweden

GE04-09. First printetd 09/2008.

CONTENTS

Volume 324 Issue 5932

CONTENTS continued **>>**

page 1254

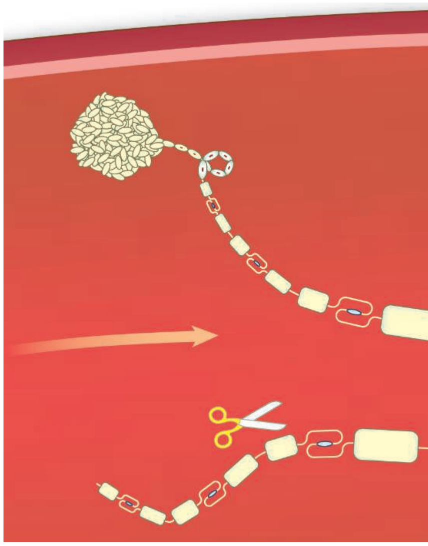

pages 1278 & 1330

COVER

Herbert Newman's 1960s love song about the birds, bees, flowers, and trees inspired this cover, which celebrates the sixth essay, "On the Origin of Sexual Reproduction," in *Science*'s monthly series honoring Darwin's 200th birthday. See page 1254.

Photos: Getty Images (birds, flower, tree); iStockphoto.com (bee)

DEPARTMENTS

CONTENTS continued >>

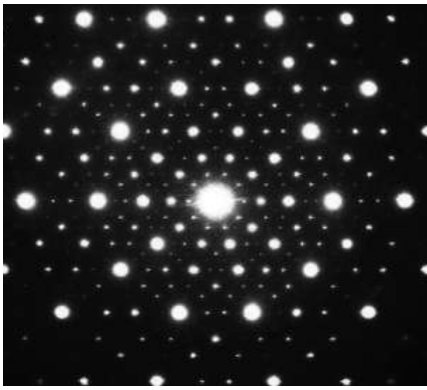

page 1306

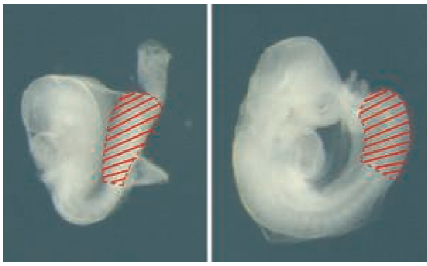

page 1320

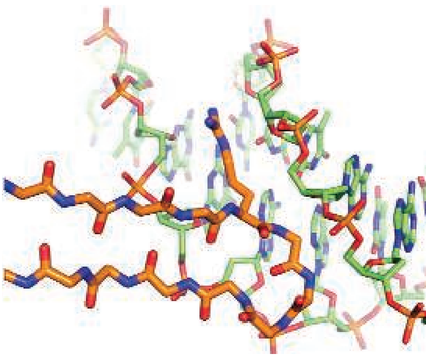

page 1323

Published by AAAS

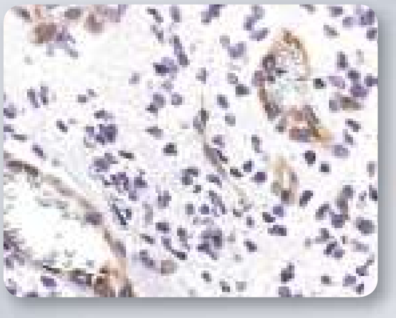

Immunohistochemical analysis of paraffin-embedded human astrocytoma using **VEGF Receptor 2 (55B11) Rabbit mAb #2479**.

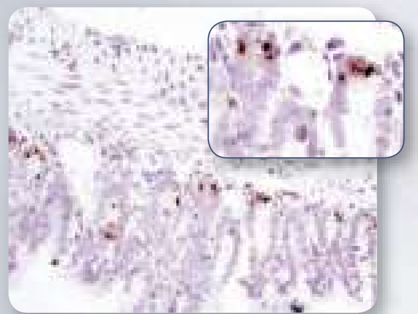

Immunohistochemical analysis of paraffin-embedded mouse small intestine using **MMP7 (D4H5) Rabbit mAb #3801**.

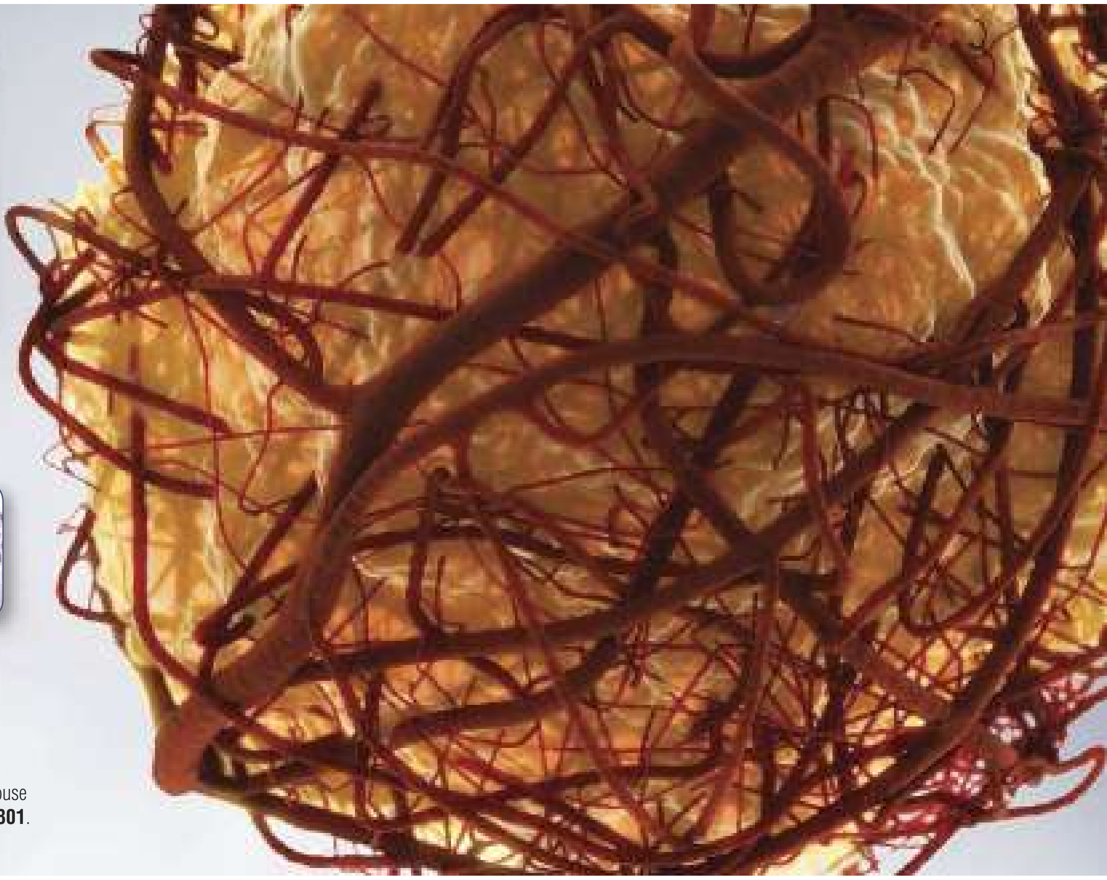

The Highest Quality Antibodies for the Study of

Angiogenesis

...from Cell Signaling Technology®

Unparalleled product quality, validation and technical support.

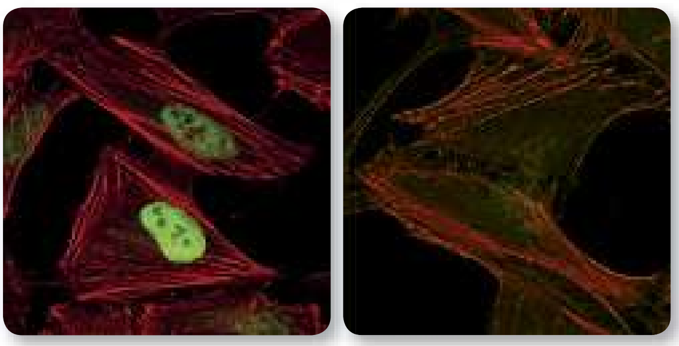

Confocal immunofluorescent analysis of HeLa cells, treated with either 10 µM MG132 (left) or 10 µM MG132 and 1 mM DMOG (right), using **Hydroxy-HIF-1α (Pro564) (D43B5) Rabbit mAb #3434** (green). Actin filaments have been labeled using DY-554 phalloidin (red).

- Cell Signaling Technology's innovative products offer unsurpassed sensitivity, specificity and performance.
- Extensive in-house validation means that optimization is not left up to you, the user.
- Technical support provided by the same scientists who produce and validate the products translates into a thorough, fast and accurate response.

for quality products you can trust...

www.cellsignal.com

Cell Signaling TECHNOLOGY®

Orders (toll-free) 1-877-616-2355 | **Technical support** (toll-free) 1-877-678-8324 support@cellsignal.com | **Inquiries** info@cellsignal.com | **Environmental Commitment** eco.cellsignal.com

*SCIENCE*ONLINE

SCIENCE**XPRESS**
www.sciencexpress.org

Amplified Trace Gas Removal in the Troposphere
A. Hofzumahaus et al.

A yet undescribed pathway for hydroxyl radical production is needed to account for reaction rates of highly polluted air.
10.1126/science.1164566

Extending Universal Nodal Excitations Optimizes Superconductivity in $Bi_2Sr_2CaCu_2O_{8+\delta}$
A. Pushp et al.

Scanning tunneling spectroscopy reveals strong electronic correlations in the insulating state of a cuprate superconductor.
10.1126/science.1174338

Auxin-Dependent Patterning and Gamete Specification in the *Arabidopsis* Female Gametophyte
G. C. Pagnussat et al.

An auxin gradient is involved in cell fate specification of the female sex cells in flowering plants.
10.1126/science.1167324

IRAP Identifies an Endosomal Compartment Required for MHC Class I Cross-Presentation
L. Saveanu et al.

Immunological dendritic cells contain an endocytic compartment involved in the cross-presentation of internalized antigens.
10.1126/science.1172845

RIP3, an Energy Metabolism Regulator That Switches TNF-Induced Cell Death from Apoptosis to Necrosis
D.-W. Zhang et al.

The protein kinase RIP3 mediates necrotic cell death, likely through regulation of metabolic enzymes.
10.1126/science.1172308

SCIENCE**NOW**
www.sciencenow.org
Highlights From Our Daily News Coverage

Thin the Air, Save the Biosphere?
A team suggests a way to prevent plant Armageddon.

Embryonic-Like Cells Advance Toward Disease Treatment
Researchers find ways to increase safety and to generate genetically tailored cells.

A Billion-Year Hard Drive
A new process could preserve digital data, essentially forever.

SCIENCE**SIGNALING**
www.sciencesignaling.org
The Signal Transduction Knowledge Environment

RESEARCH ARTICLE: Involvement of the Protein Kinase CK2 in the Regulation of Mammalian Circadian Rhythms
Y. Tsuchiya et al.

Protein kinase CK2 promotes PERIOD2 degradation and modulates the mammalian circadian clock.

PERSPECTIVE: Allosteric Effects Govern Nuclear Receptor Action—DNA Appears as a Player
H. Gronemeyer and W. Bourguet

DNA sequences regulate glucocorticoid receptor activity.

NETWATCH: PANTHER
Explore a database of proteins classified by function; in Bioinformatic Resources.

NETWATCH: Inside Cancer
Learn about the cell biology of cancer through interactive multimedia resources; in Educator Sites.

SCIENCE**CAREERS**
www.sciencecareers.org/career_magazine
Free Career Resources for Scientists

A Bioethicist's Work Bridges Science, Law, and Religion
C. Wald

An erroneous conference invitation prompted Jennifer Miller to pursue a bioethics career.

Taken for Granted: Building a Culture of Safety
B. L. Benderly

An investigation of a fatal UCLA fire shows how many academic labs can be made safer.

Weighty Research in Microgravity
E. Pain

A physician and an engineering student are preparing experiments in microgravity for a European Space Agency competition.

SCIENCE**PODCAST**
www.sciencemag.org/multimedia/podcast
Free Weekly Show

Download the 5 June *Science* Podcast to hear about returns on science investments, human social evolution, the origin of sexual reproduction, and more.

ORIGINS**BLOG**
blogs.sciencemag.org/origins
A History of Beginnings

SCIENCE**INSIDER**
blogs.sciencemag.org/scienceinsider
Science Policy News and Analysis

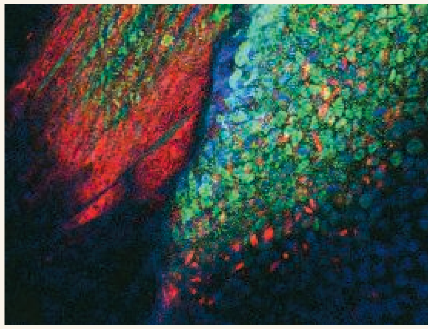

SCIENCE**NOW**
Genetically corrected cells.

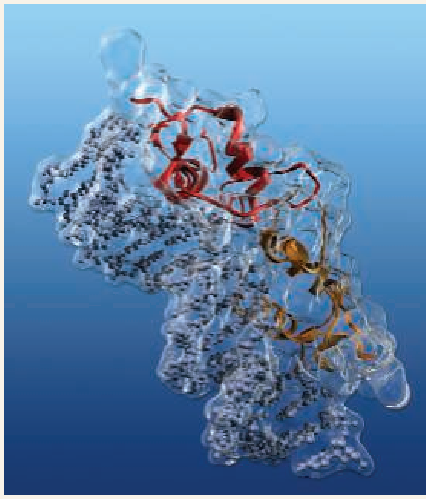

SCIENCE**SIGNALING**
Glucocorticoid receptor–DNA complex.

CREDITS: (*SCIENCE NOW*) JUAN CARLOS IZPISÚA BELMONTE; (*SCIENCE SIGNALING*) CHRIS BICKEL

SCIENCE (ISSN 0036-8075) is published weekly on Friday, except the last week in December, by the American Association for the Advancement of Science, 1200 New York Avenue, NW, Washington, DC 20005. Periodicals Mail postage (publication No. 484460) paid at Washington, DC, and additional mailing offices. Domestic individual membership and subscription (51 issues): $146 ($74 allocated to subscription). Domestic institutional subscription (51 issues): $835; Foreign postage extra: Mexico, Caribbean (surface mail) $55; other countries (air assist delivery) $85. First class, airmail, student, and emeritus rates on request. Canadian rates with GST available upon request, GST #1254 88122. Publications Mail Agreement Number 1069624. **Printed in the U.S.A.**

Change of address: Allow 4 weeks, giving old and new addresses and 8-digit account number. **Postmaster:** Send change of address to AAAS, P.O. Box 96178, Washington, DC 20090–6178. **Single-copy sales:** $10.00 current issue, $15.00 back issue prepaid includes surface postage; bulk rates on request.

EDITED BY STELLA HURTLEY

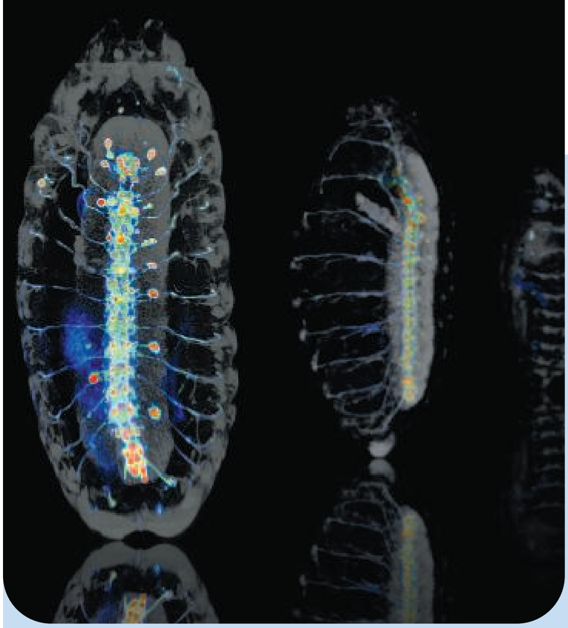

<< Signaling Signature in Situ

Upon activation, signaling proteins trigger response pathways, but knowing when and where they are activated within animals has been difficult. **Kamiyama and Chiba** (p. 1338) describe an in vivo bioprobe imaging technology that reveals the restricted pattern for endogenous activities of a ubiquitously expressed signaling protein Cdc42 within individual cells and in whole animals. Genetic experiments confirmed that it is the activation within individual cells and tissues, not simply the protein's presence, which defines its function during development.

Two Ways to Redox Regulation

Eukaryotic cells control the redox environment within their cytoplasm to be generally reducing. However, the endoplasmic reticulum provides an oxidizing environment for secretory and membrane proteins. In addition, a subcompartment of mitochondria—the powerhouses of the cell—also generates an oxidizing environment for constituent and itinerant proteins. **Riemer *et al.*** (p. 1284) review the current understanding of both eukaryotic redox machineries and highlight their implications for the biogenesis and regulation of protein function, focusing on the impact of these systems on health and disease.

Coordinating Response to Stress

Sirtuin 1 (Sirt1) (a protein deacetylase implicated in aging), senses the metabolic state of the cell and modulates the activity of substrate proteins that in turn regulate cellular transcriptional responses. In response to hypoxia, cells activate the transcription factor hypoxia-inducible factor 2 alpha (HIF-2α), which promotes adaptive responses. **Dioum *et al.*** (p. 1289; see the Perspective by **Guarente**) discovered a link between these two important cellular stress response systems—HIF-2α is a substrate of Sirt1. Direct interaction between Sirt1 and HIF-2α results in deacetylation of HIF-2α and enhances its transcriptional activity. In mice lacking Sirt1, the ability of HIF-2α to promote synthesis of the growth factor erythropoietin is diminished. Thus, the regulation of HIF-2α helps to coordinate responses of cells to various stresses.

Extending Platinum Catalysts

Platinum performs extremely well as a catalyst for the oxygen-reduction reaction that runs under highly acidic conditions in proton-exchange membrane fuel cells, but is expensive. One strategy for reducing costs is to increase the surface area of the platinum. **Lim *et al.*** (p. 1302, published online 14 May) describe a simple chemical route, in which Pt ions in solution are reduced onto Pd seed crystals, which creates faceted Pt nanocrystals with a high area owing to their dendritic architecture. On a Pt mass basis, these catalysts are several times more active than conventional Pt catalysts.

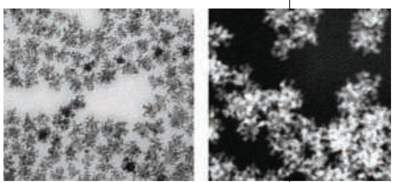

War and Peace?

Modern behavior, including the development of advanced tools, musical instruments, and art, seems to have arisen in humans in stages. The earliest hints are seen in Africa about 70 to 90,000 years ago, but later in Europe about 45,000 years ago. An ongoing discussion centers on the origins and significance of human prosociality. During early human development, could the benefits of altruistic behavior have outweighed its costs (see the Perspective by **Mace**)? **Bowles** (p. 1293) constructed a model of conflict between groups of humans and extracted estimates of the critical parameters from archaeological and ethnographic data sets. Provocatively, it appears that warfare might have enhanced the emergence and persistence of altruistic behavior. **Powell *et al.*** (p. 1298) present a population model that shows that the development of modern behaviors may rely on the attainment of critical population densities and migratory patterns required for stable cultural transmission. The model is consistent with genetic inferences of population dynamics in Africa and Europe and suggests that these cultural changes may not solely reflect increased cognitive evolution.

Mergers and Acquisitions

The crystallization of small molecules or polymers is often described in terms of a nucleation stage, where initial clusters form, followed by a distinct growth stage. Growth can come from the addition of unbound molecules, or through "Ostwald ripening" where larger crystals grow at the expense of smaller ones due to thermodynamic effects. **Zheng *et al.*** (p. 1309) studied the growth of platinum nanocrystals inside a transmission electron microscope using a special liquid cell, allowing observation of crystal growth in situ. Both monomer addition to growing particles and the coalescence of two particles were observed. The specific growth mechanism appeared to be governed by the size of each of the particles. The combination of growth processes makes it possible for an initially broad distribution of particles to narrow into an almost uniform one.

Growing Graphene

The highest quality graphene samples, single-atom-thick layers of carbon, are suspended flakes exfoliated from graphite, but these samples are very small in size (square micrometers). For many electronics applications, larger areas are needed. **Li *et al.*** (p. 1312, published online 7 May) show that graphene grows in a self-limiting way on copper films as large-area sheets (one square centimeter) from methane through a chemical vapor deposition process. The films, which are mainly one layer in thickness, can be transferred to other substrates and have electron mobilities as high as 4300 square centimeters per volt second.

Continued on page 1240

CREDITS (TOP TO BOTTOM): DAICHI KAMIYAMA AND AKIRA CHIBA; LIM *ET AL.*

Published by AAAS

Continued from page 1239

Defeating the Cuckoo

Brood parasite-host interactions show ongoing antagonistic coevolution. What mediates rapid behavioral changes that do not reflect genetic change? **Davies and Welbergen** (p. 1318) show that reed warblers learn from their neighbors to behave aggressively toward models of the parasitic common cuckoo. Furthermore, reed warblers seem to be predisposed to learn to respond to cuckoos as enemies: Hosts that witnessed neighbors mobbing a harmless parrot model did not increase their aggression toward a cuckoo model. Thus, birds have templates for threats, and relevant antithreat behaviors can be turned on or off depending on social experience.

Hox Clocks

Homeobox or *Hox* genes are historically significant for demonstrating evolutionary conservation and homology in developmentally important genes. In addition, in many species, the *Hox* genes are fundamental to the organization of the embryo. Modifications in the regulation of their colinear, temporal activation may represent a way of altering their expression patterns and to elaborate body plans during evolution. **Soshnikova and Duboule** (p. 1320) now report highly dynamic modifications of chromatin marks along with progressive *Hox* gene activation during axial extension in the mouse. This work supports the proposal that the "*Hox* clock" may be controlled, at least in part, by epigenetic mechanisms.

Starving T Cells

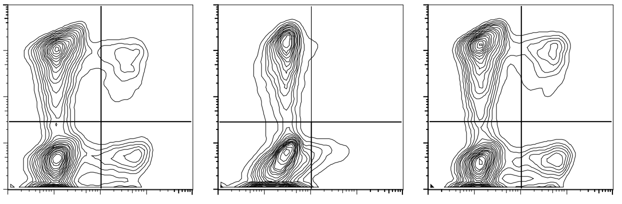

The T_H17 lineage of $CD4^+$ helper T cells, characterized by the ability to secrete IL-17, is an important mediator of inflammation and autoimmunity. Dampening the responses of these cells or inhibiting their differentiation is of great therapeutic interest. **Sundrud *et al.*** (p. 1334; see the Perspective by **Blander and Amsen**) now show that the small molecule halofuginone inhibits the differentiation of T_H17 cells but not other $CD4^+$ T cell helper lineages both in vitro and in a mouse model of multiple sclerosis. This selective inhibition was mediated by activation of the amino acid starvation response. Amino acid depletion mimicked the effects of halofuginone, whereas excess amino acids rescued T_H17 differentiation. The results highlight the importance of amino acid metabolism in regulating inflammation.

Rhes-olving Huntington's Disease?

Huntington's disease (HD) is caused by a single dominant mutation of huntingtin (Htt), a protein that occurs in all tissues of the body and that is uniformly distributed throughout the brain. How mutant Htt (mHtt) selectively damages striatal neurons with negligible alterations elsewhere has been a mystery. **Subramaniam *et al.*** (p. 1327) show that Rhes, a small G protein very highly localized to the striatum, binds mHtt and augments its neurotoxicity. Rhes promotes sumoylation of mHtt, leading to its disaggregation and augmented cytotoxicity. The findings establish how mHtt selectively kills cells in the striatum and suggest that Rhes-Htt binding might provide a therapeutic target.

Dissecting VWF's Thrombogenic Potential

Von Willebrand factor (VWF) is secreted from cells in an ultralarge form (ULVWF) in response to thrombogenic stimuli. Shear forces expose a binding site for platelets, enabling formation of a hemostatic plug. The thrombogenic potential of VWF correlates with its length and is regulated by proteolytic cleavage of the A2 domain. **Zhang *et al.*** (p. 1330; see the Perspective by **Gebhardt and Rief**) now combine single molecule data and polymer dynamics theory to show that shear forces in the circulation are sufficient to unfold the A2 domain and allow cleavage of multimers with more than about 200 monomers. The A2 domain may thus represent the "shear bolt" of VWF, unfolding when multimers experience high forces to allow cleavage and down-regulation of thrombogenic potential.

CREDIT: SUNDRUD *ET AL.*

Published by AAAS

Sharon Long is Steere-Pfizer Professor of Biological Sciences and dean emerita of Humanities and Sciences at Stanford University. E-mail: srl@stanford.edu

Robert Alpern is dean and Ensign Professor at Yale University School of Medicine. E-mail: robert.alpern@yale.edu

Science for Future Physicians

BIOMEDICAL RESEARCH IS RAPIDLY TRANSFORMING OUR UNDERSTANDING OF HEALTH AND DISEASE, with major implications for medical practice. But the science education of physicians has not kept pace with these advances. Today, the Association of American Medical Colleges (AAMC) and the Howard Hughes Medical Institute release a report that addresses this issue.* The analysis, by a committee of U.S. undergraduate and medical school faculty that we co-chaired, comes 6 years after the U.S. National Academies report *BIO 2010*, which noted that undergraduate premedical course requirements and the content of the Medical College Admissions Test (MCAT) constrain innovation in undergraduate science education.

The new report, *Scientific Foundations for Future Physicians*, emphasizes that physicians must have a firm grounding in the biomedical sciences and understand their relation to the physical sciences and mathematics. For physicians to be prepared for inquisitive, critical thinking and lifelong learning, they should also be able to incorporate the methods of science into their practice, including skeptical and critical analysis. These goals should be reflected across the entire span of a physician's education, from undergraduate study through medical school.

Medical school faculty have a short time in which to convey an in-depth understanding of specific medical knowledge and recent research. Students should arrive at medical school prepared in the sciences, including some areas not currently required, such as statistics and biochemistry. If all beginning medical students understand general biochemistry, for example, then faculty can build on this knowledge, creating more opportunities to explore the synergistic relationships among biomedical science, research, and clinical medicine. Medical schools should also increase their emphasis on the importance of the physical sciences and mathematics in biomedical research and clinical practice.

How should preparation for medical study be assessed? Medical schools generally determine scientific readiness for admission by course requirements and scores on the MCAT, which mainly reflects the traditional content of those courses. In contrast, medical schools have long evaluated readiness for medical practice in terms of competency—specific learned abilities that can be put into practice—rather than by mandating standard courses and curricula for all medical schools. The report recommends that scientific readiness for medical school entry be assessed similarly: The current list of required premedical school courses should be replaced with required science competencies. Instead of a nationwide requirement that premedical undergraduates take specific chemistry classes, for example, a required competency might be described as being "able to apply knowledge of the chemistry of carbon compounds to biochemical reactions." The report suggests competencies for premedical and medical school science education, recognizing that there may be multiple routes to gaining a competency. An integrated approach to both undergraduate and medical education may help both to innovate.

A change in competency-based educational goals would allow undergraduate institutions the option to design new curricula. Chemistry competencies, for example, might be gained either in traditional chemistry courses or in rigorous interdisciplinary courses. Such innovations, aimed at increasing relevant scientific content and understanding, should also yield more efficient teaching. While recommending new competencies such as biochemistry and statistics, the report's committee opposes a net increase in premedical science requirements. As the report states, "the undergraduate years should not be designed primarily to prepare students for professional school, but for creative engagement in a broad, intellectually expansive education." In conjunction with the shift to competencies, the MCAT could be modified to test for competencies proposed by the committee. The new report coincides with an AAMC review of MCAT content, a multiphase process that will consider the report, among other inputs.

In a system with so many participants, dialogue is essential to progress. Outreach to and feedback from the scientific disciplines and medical community will enhance the success of these efforts. We urge colleagues to engage in this national discussion. **– Sharon Long and Robert Alpern**

*See www.aamc.org/scientificfoundations.

10.1126/science.1176994

CREDITS: (TOP LEFT) LINDA CICERO, STANFORD COMMUNICATIONS, STANFORD UNIVERSITY; (BOTTOM LEFT) TERRY DAGRADI; (RIGHT) ISTOCKPHOTO.COM

GEOLOGY

How Heat Stirs the Mantle

In the aftermath of earthquakes, seismic tomography offers a window into mantle dynamics through large-scale inversion of recorded seismic velocities along different paths. Observed variations in velocity generally reflect mantle density, but the patterns could also indicate shifts in temperature, composition, grain size, or water content. To address this conundrum, Dalton *et al.* conducted a global inversion of seismic attenuation, which responds differently to variations in these parameters than does the shear-wave velocity. The data (constrained further by recent laboratory studies of the mineral olivine, abundant in the upper mantle) imply that temperature variations of about 150° to 200°C can explain most of the patterns beneath ocean basins in the upper mantle but that a different composition must be invoked beneath continents at depths less than 250 km. In a complementary approach, Schuberth *et al.* focused on the lower mantle, comparing seismic data with a numerical mantle circulation model. They also found that much of the observed seismic data, including an apparent large upwelling beneath Africa, can be well accounted for by temperature variations alone (of up to 1000°C) produced by high heat flow from the core. — BH

Earth Planet. Sci. Lett. 10.1016/j.epsl.2009.04.009 (2009); *Geochem. Geophys. Geosyst.* **10**, 10.1029/2009GC002401 (2009).

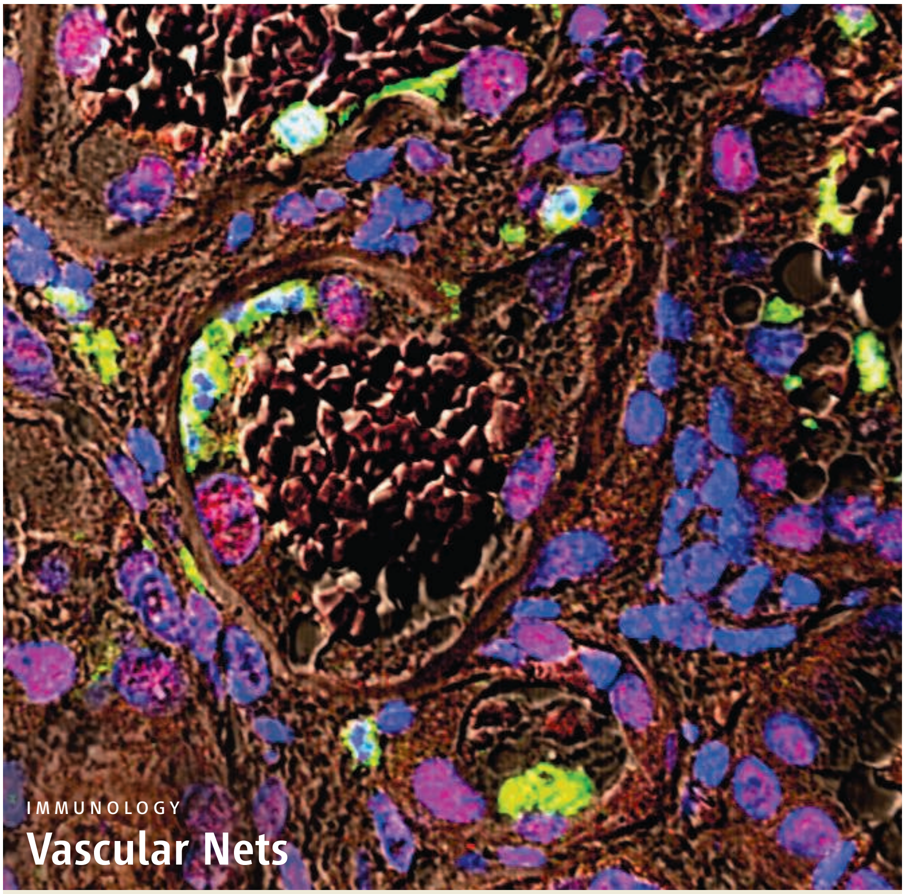

IMMUNOLOGY

Vascular Nets

During an infection, invading microbes can be caught in sticky webs of chromatin (DNA + histones) that are released by neutrophils. These neutrophil extracellular traps are decorated with granules that are laden with lytic enzymes and antimicrobial peptides; these weapons facilitate the rapid killing of pathogens.

In small-vessel vasculitis (SVV), the body generates antibodies against two antigenic proteins that are expressed by neutrophils, and this leads to the inflammation of small blood vessels. How this chronic condition is sustained has not been clear, but Kessenbrock *et al.* have found that these nets are also produced in the absence of infection and that they may perpetuate autoimmune disorders. It appears that when neutrophils are attacked by these autoantibodies, they release their fibrous chromatin nets (shown above), which contain the two antigens. Kidney biopsies from patients with SVV confirmed the presence of neutrophils and nets near deteriorating capillaries. This immune response probably maintains the exposure of the autoantigens to other immune cells (dendritic and B cells), whose consequent activation could play a pathogenic role in the disease. — LC

Nat. Med. **15**, 10.1038/nm.1959 (2009).

MATERIALS SCIENCE

A Basic Deposit

Manganese dioxide (MnO_2) meets many of the requirements as an electrode in lithium (Li) batteries, but the bulk material exhibits low capacity and poor cycling because Li ion intercalation distorts the crystal lattice. Nanostructuring of the bulk material can alleviate some of the problems, but typical templating routes for creating mesoporous MnO_2 have not been cost-effective. Liu *et al*. report on the deposition of mesoporous MnO_2 films through a two-step cathodic deposition process driven by water electrolysis. Hydroxide ions generated at the cathode in a 0.1 M Mn^{2+} solution formed $Mn(OH)_2$, which precipitated, and after exposure to air, formed $MnO_2 \cdot 0.5\ H_2O$. This material has a nanowall-array morphology (shown at left) with high surface area (96 $m^2\ g^{-1}$) and an energy storage capacity with Li ions of 256 mA·hour g^{-1}. The higher capacity and better cycle life of this material, relative to the material formed directly in an anodic version of the process (80 mA·hour g^{-1}), were attributed to the mesoporous structure of the nanowalls. — PDS

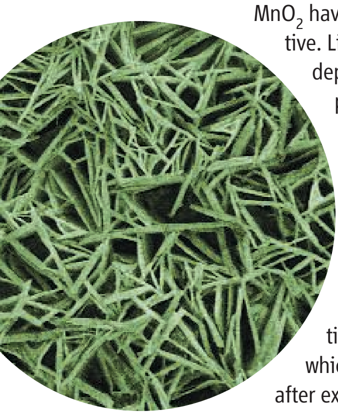

Adv. Funct. Mater. **19**, 1015 (2009).

BEHAVIOR

Intervening to Reduce Risk

There have been many discussions of how genes and environment might interact in the context of human behavior. Brody *et al.* have studied the effects of a randomized behavioral intervention on adolescents who have a genetic polymorphism associated with the initiation of risky behavior.

CREDITS (TOP TO BOTTOM): KESSENBROCK *ET AL.*, *NAT. MED.* **15**, 10.1038/NM.1959 (2009); LIU *ET AL.*, *ADV. FUNCT. MATER.* **19**, 1015 (2009)

Roughly 600 11-year-olds were randomly assigned to the Strong African American Families (SAAF) program or to a control group. The SAAF group (and their caregivers, usually mothers) participated in separate and joint training sessions on parenting practices, stress management, dealing with racism, setting goals, and norms for the use of alcohol and other substances. Sessions occurred over the course of 1 year, and the initiation of risky behaviors was assessed at the beginning of the program and for the next 2.5 years. Two years later, saliva samples were collected to look for a polymorphism in the promoter region of the serotonin transporter. Possession of a short form of the allele has been associated previously with impulsivity, substance abuse, and early sexual activity. In the control group, adolescents with the short allele were twice as likely to have engaged in risky behaviors as those assigned to the SAAF group or those with the long allele in either group. Only one genetic polymorphism was examined, and the results need to be confirmed in a variety of populations; however, this provides further evidence of the value of this intervention and the mutability of the effects of genetic predisposition. — BJ

Child Devel. **80**, 645 (2009).

BIOCHEMISTRY

Stuck in the On Position

Protein kinases are of course central components of many signaling pathways in cells. Cascades of kinases, in which the first kinase in a series modifies the second and enhances its enzyme activity, are not uncommon, and BRAF sits in a pathway that begins with a membrane-bound receptor tyrosine kinase and ends with the movement of the extracellular signal-regulated kinase into the nucleus. The special interest in BRAF arises from the frequent association of a mutation (V600E) of a valine to a glutamate with malignant melanoma. Xie *et al.* describe kinetic and structural studies of the interaction of wild-type and mutated forms of BRAF with kinase inhibitors built on a ruthenium (fuschia above) half-sandwich scaffold. They provide a structure-based explanation for the higher potency of one such inhibitor (CS292) for the V600E mutant versus the wild-type enzyme and use this information to design a more specific and more potent derivative. They also explain how the substitution of a glutamate electrostatically mimics the normal, activating phosphorylation of nearby serine and threonine residues, but with the critical distinction that activation in the BRAF mutant is irreversible. — GJC

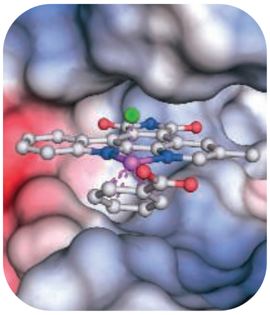

CREDIT: JIE QIN

Biochemistry **48**, 10.1021/bi802067u (2009).

CHEMISTRY

Microscopic Window Washing

High-resolution imaging of organic polymers in a transmission electron microscope (TEM) is hampered by the accumulating residue of electron beam–induced sample decomposition. Horiuchi *et al.* solve this problem through gentle cleaning of their microscope with oxygen radicals generated in a low-temperature plasma near one of the accessory ports. An extra pumping system added at the objective aperture pulled the oxygen radicals into the sample chamber. The authors used their TEM to examine brushes of a phosphorylcholine that had been grafted onto silicon nanoparticles via a surface initiator. Once oxidation (and hence volatilization) of the residue cleared the field, they could see the brushes extending from a nanoparticle, and even visualize the intermingling of brushes in two neighboring particles. Mapping of the intensity profiles distinguished the initiator, with a high carbon density near the particles and the broader brushes where the carbon density was lower. — MSL

ACS Nano **3**, 1297 (2009).

CELL BIOLOGY

Wrestling with Heat Shock

Golebiowski *et al.* have conducted a comprehensive large-scale analysis of protein SUMOylation. Small ubiquitin-like modifier (SUMO) proteins, when covalently attached to target proteins, can alter properties such as the cellular localization, activity, or stability of the targets. By combining an affinity-tagging isolation method with sensitive mass spectrometry detection, the authors obtained a glimpse of 766 proteins that experienced increased or decreased SUMOylation in cells exposed to the stress of heat shock (a temperature increase from 37° to 43°C). Three-quarters of these proteins had not been identified previously as targets of SUMOylation. These proteins provide clues to the extent of the biological processes that are altered by heat shock—from DNA repair and protein folding to cell death and cell cycle control. Furthermore, this regulatory mechanism operates quickly, within 5 min, although reversal of SUMOylation was generally slower, taking up to 2 hours—and for those proteins that underwent deconjugation in response to stress, an even longer recovery time was needed for re-SUMOylation. — LBR

Sci. Signal. **2**, ra24 (2009).

Published by AAAS

www.sciencemag.org

Science

1200 New York Avenue, NW
Washington, DC 20005
Editorial: 202-326-6550, FAX 202-289-7562
News: 202-326-6581, FAX 202-371-9227
Bateman House, 82-88 Hills Road
Cambridge, UK CB2 1LQ
+44 (0) 1223 326500, FAX +44 (0) 1223 326501

Subscription Services For change of address, missing issues, new orders and renewals, and payment questions: 866-434-AAAS (2227) or 202-326-6417, FAX 202-842-1065. Mailing addresses: AAAS, P.O. Box 96178, Washington, DC 20090-6178 or AAAS Member Services, 1200 New York Avenue, NW, Washington, DC 20005

Institutional Site Licenses please call 202-326-6755 for any questions or information

Reprints: Author Inquiries 800-635-7181
Commercial Inquiries 803-359-4578

Permissions 202-326-7074, FAX 202-682-0816

Member Benefits AAAS/Barnes&Noble.com bookstore www.aaas.org/bn; AAAS Online Store www.apisource.com/aaas/ code MKB6; AAAS Travels: Betchart Expeditions 800-252-4910; Apple Store www.apple/eppstore/aaas; Bank of America MasterCard 1-800-833-6262 priority code FAA3YU; Cold Spring Harbor Laboratory Press Publications www.cshlpress.com/affiliates/aaas.htm; GEICO Auto Insurance www.geico.com/landingpage/go51.htm?logo=17624; Hertz 800-654-2200 CDP#343457; Office Depot https://bsd.officedepot.com/portalLogin.do; Seabury & Smith Life Insurance 800-424-9883; Subaru VIP Program 202-326-6417; VIP Moving Services www.vipmayflower.com/domestic/index.html; Other Benefits: AAAS Member Services 202-326-6417 or www.aaasmember.org.

science_editors@aaas.org	(for general editorial queries)
science_letters@aaas.org	(for queries about letters)
science_reviews@aaas.org	(for returning manuscript reviews)
science_bookrevs@aaas.org	(for book review queries)

Published by the American Association for the Advancement of Science (AAAS), *Science* serves its readers as a forum for the presentation and discussion of important issues related to the advancement of science, including the presentation of minority or conflicting points of view, rather than by publishing only material on which a consensus has been reached. Accordingly, all articles published in *Science*—including editorials, news and comment, and book reviews—are signed and reflect the individual views of the authors and not official points of view adopted by AAAS or the institutions with which the authors are affiliated.

AAAS was founded in 1848 and incorporated in 1874. Its mission is to advance science, engineering, and innovation throughout the world for the benefit of all people. The goals of the association are to: enhance communication among scientists, engineers, and the public; promote and defend the integrity of science and its use; strengthen support for the science and technology enterprise; provide a voice for science on societal issues; promote the responsible use of science in public policy; strengthen and diversify the science and technology workforce; foster education in science and technology for everyone; increase public engagement with science and technology; and advance international cooperation in science.

Information for Authors
See pages 807 and 808 of the 6 February 2009 issue or access www.sciencemag.org/about/authors

editor-in-chief **Bruce Alberts**
executive editor **Monica M. Bradford**
news editor **Colin Norman**
managing editor, research journals **Katrina L. Kelner**
deputy editors **R. Brooks Hanson, Barbara R. Jasny, Andrew M. Sugden**

Editorial senior editor/perspectives Lisa D. Chong; **senior editors** Gilbert J. Chin, Pamela J. Hines, Paula A. Kiberstis (Boston), Marc S. Lavine (Toronto), Beverly A. Purnell, L. Bryan Ray, Guy Riddihough, H. Jesse Smith, Phillip D. Szuromi (Tennessee), Valda Vinson; **associate editors** Kristen L. Mueller, Nicholas S. Wigginton, Jake S. Yeston, Laura M. Zahn; **online editor** Stewart Wills; **associate online editors** Robert Frederick, Tara S. Marathe; **web content developer** Martyn Green; **book review editor** Sherman J. Suter; **associate letters editor** Jennifer Sills; **editorial manager** Cara Tate; **senior copy editors** Jeffrey E. Cook, Cynthia Howe, Harry Jach, Barbara P. Ordway, Trista Wagoner; **copy editors** Chris Filiatreau, Lauren Kmec; **editorial coordinators** Carolyn Kyle, Beverly Shields; **publications assistants** Ramatoulaye Diop, Carlos L. Durham, Joi S. Granger, Jeffrey Hearn, Lisa Johnson, Scott Miller, Jerry Richardson, Jennifer A. Seibert, Brian White, Anita Wynn; **editorial assistants** Emily Guise, Michael Hicks, Patricia M. Moore; **executive assistant** Sylvia S. Kihara; **administrative support** Maryrose Madrid

News deputy news editors Robert Coontz, Eliot Marshall, Jeffrey Mervis, Leslie Roberts; **contributing editors** Elizabeth Culotta, Polly Shulman; **news writers** Yudhijit Bhattacharjee, Adrian Cho, Jennifer Couzin, David Grimm, Constance Holden, Jocelyn Kaiser, Richard A. Kerr, Eli Kintisch, Andrew Lawler (New England), Greg Miller, Elizabeth Pennisi, Robert F. Service (Pacific NW), Erik Stokstad; **intern** Jackie D. Grom; **contributing correspondents** Dan Charles, Jon Cohen (San Diego, CA), Daniel Ferber, Ann Gibbons, Robert Koenig, Mitch Leslie, Charles C. Mann, Virginia Morell, Evelyn Strauss, Gary Taubes; **copy editors** Linda B. Felaco, Melvin Gatling, Melissa Raimondi; **administrative support** Scherraine Mack, Fannie Groom; **bureaus** New England: 207-549-7755, San Diego, CA: 760-942-3252, FAX 760-942-4979, Pacific Northwest: 503-963-1940

Production director James Landry; **senior manager** Wendy K. Shank; **assistant manager** Rebecca Doshi; **senior specialists** Steve Forrester, Chris Redwood; **specialist** Anthony Rosen; **Preflight director** David M. Tompkins; **manager** Marcus Spiegler; **specialist** Jason Hillman

Art director Yael Kats; **associate art director** Laura Creveling; **illustrators** Chris Bickel, Katharine Sutliff; **senior art associates** Holly Bishop, Preston Huey, Nayomi Kevitiyagala; **art associates** Jessica Newfield, Matthew Twombly; **photo editor** Leslie Blizard

***Science* International**

Europe (science@science-int.co.uk) **editorial: international managing editor** Andrew M. Sugden; **senior editor/perspectives** Julia Fahrenkamp-Uppenbrink; **senior editors** Caroline Ash, Stella M. Hurtley, Ian S. Osborne, Peter Stern; **associate editor** Maria Cruz; **locum editor** Helen Pickersgill; **editorial support** Deborah Dennison, Rachel Roberts, Alice Whaley; **administrative support** John Cannell, Janet Clements, Louise Moore; **news: europe news editor** John Travis; **deputy news editor** Daniel Clery; **contributing correspondents** Michael Balter (Paris), John Bohannon (Vienna), Martin Enserink (Amsterdam and Paris), Gretchen Vogel (Berlin); **intern** Claire Thomas

Asia Japan Office: Asca Corporation, Eiko Ishioka, Fusako Tamura, 1-8-13, Hirano-cho, Chuo-ku, Osaka-shi, Osaka, 541-0046 Japan; +81 (0) 6 6202 6272, FAX +81 (0) 6 6202 6271; asca@os.gulf.or.jp; **asia news editor** Richard Stone (Beijing: rstone@aaas.org); **contributing correspondents** Dennis Normile (Japan: +81 (0) 3 3391 0630, FAX +81 (0) 3 5936 3531; dnormile@gol.com); Hao Xin (China: +86 (0) 10 6307 4439 or 6307 3676, FAX +86 (0) 10 6307 4358; cindyhao@gmail.com); Pallava Bagla (South Asia: +91 (0) 11 2271 2896; pbagla@vsnl.com)

executive publisher **Alan I. Leshner**
publisher **Beth Rosner**

Fulfillment Systems and Operations (membership@aaas.org); **director** Waylon Butler; **senior systems analyst** Nomuna Nyamaa; **customer service supervisor** Pat Butler; **specialists** Latoya Casteel, LaVonda Crawford, Vicki Linton, April Marshall; **data entry supervisor** Cynthia Johnson; **specialists** Shirlene Hall, Tarrika Hill, William Jones

Business Operations and Administration director Deborah Rivera-Wienhold; **assistant director, business operations** Randy Yi; **manager, business analysis** Michael LoBue; **manager, business operations** Jessica Tierney; **financial analysts** Priti Pamnani, Celeste Troxler; **rights and permissions: administrator** Emilie David; **associate** Elizabeth Sandler; **marketing director** Ian King; **marketing manager** Allison Pritchard; **marketing associates** Aimee Aponte, Alison Chandler, Mary Ellen Crowley, Julianne Wielga, Wendy Wise; **marketing executive** Jennifer Reeves; **director, site licensing** Tom Ryan; **director, corporate relations** Eileen Bernadette Moran; **publisher relations, eresources specialist** Kiki Forsythe; **senior publisher relations specialist** Catherine Holland; **publisher relations, east coast** Phillip Smith; **publisher relations, west coast** Philip Tsolakidis; **fulfillment supervisor** Iquo Edim; **fulfillment coordinator** Laura Clemens; **marketing associate** Mary Lagnaoui; **electronic media: manager** Lizabeth Harman; **project manager** Trista Snyder; **assistant manager** Lisa Stanford; **senior production specialists** Christopher Coleman, Walter Jones; **production specialists** Nichele Johnston, Kimberly Oster

Advertising director, worldwide ad sales Bill Moran

Product (science_advertising@aaas.org); **midwest/west coast/w. canada** Rick Bongiovanni: 330-405-7080, FAX 330-405-7081; **east coast/e. canada** Laurie Faraday: 508-747-9395, FAX 617-507-8189; **uk/europe/asia** Roger Goncalves: TEL/FAX +41 43 243 1358; **japan** Mashy Yoshikawa: +81 (0) 3 3235 5961, FAX +81 (0) 3 3235 5852; **senior traffic associate** Deiandra Simms

Commercial Editor Sean Sanders: 202-326-6430

Project Director, Outreach Brianna Blaser

Classified (advertise@sciencecareers.org); **u.s.: sales manager** Daryl Anderson: 202-326-6543; **inside sales representative** Tina Burks: 202-326-6577; **key account manager/midwest** Joribah Able; **east coast** Alexis Fleming: 202-326-6578; **west/south central** Nicholas Hintibidze: 202-326-6533; **sales coordinators** Rohan Edmonson, Shirley Young; **international: sales manager** Tracy Holmes: +44 (0) 1223 326525, FAX +44 (0) 1223 326532; **sales** Susanne Kharraz, Dan Pennington, Alex Palmer; **sales assistant** Lisa Patterson; **japan** Mashy Yoshikawa: +81 (0) 3 3235 5961, FAX +81 (0) 3 3235 5852; **advertising support manager** Karen Foote: 202-326-6740; **advertising production operations manager** Deborah Tompkins; **senior production specialist/graphic designer** Amy Hardcastle; **senior production specialist** Robert Buck; **senior traffic associate** Christine Hall

AAAS Board of Directors retiring president, chair James J. McCarthy; **president** Peter C. Agre; **president-elect** Alice Huang; **treasurer** David E. Shaw; **chief executive officer** Alan I. Leshner; **board** Alice Gast, Linda P. B. Katehi, Nancy Knowlton, Cherry A. Murray, Julia M. Phillips, Thomas D. Pollard, David S. Sabatini, Thomas A. Woolsey

AAAS
ADVANCING SCIENCE, SERVING SOCIETY

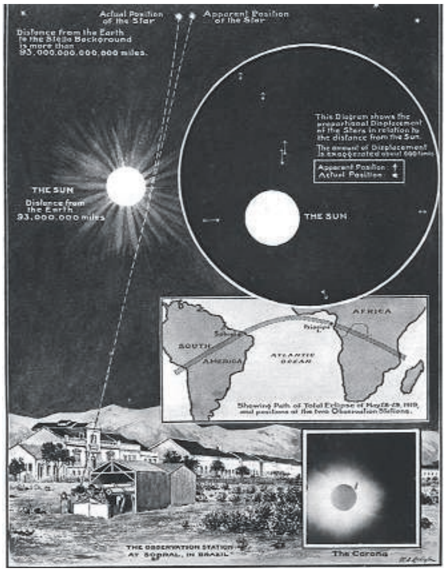

The Eclipse That Proved Relativity

Last week, a trio of U.K. scientists trooped to the little-known island of Principe off the West Coast of Africa to celebrate one of the most renowned experiments of the 20th century.

Astronomers Pedro Ferreira of the University of Oxford, Richard Massey of the University of Edinburgh, and Oxford anthropologist Gisa Weszkalnys visited the site where a team led by British astrophysicist Arthur Stanley Eddington photographed stars during a total solar eclipse on 29 May 1919 (noted above in the 22 November 1919 edition of *The Illustrated London News*). The stars in the constellation Hyades appeared to be slightly in the wrong place. The shift showed that the sun's mass had warped the path the starlight followed through space, a key prediction of Albert Einstein's then-new general theory of relativity. The 21st century scientists gave talks and unveiled a plaque at the plantation where Eddington's observations were made.

Tuned to Bond

If music be the food of love, could there be an overlap between genes for musicality and social bonding? Researchers in Finland claim to have found an association between musical aptitude and certain versions of a hormone related to attachment behavior.

A team led by geneticist Irma Järvelä of the University of Helsinki gave 343 people from 19 Finnish families—all containing musicians—aptitude tests for pitch discrimination, time discrimination, and auditory structuring ability (detecting changes in the order or number of small tone sequences). They then collected blood samples from 298 participants.

The team found musical aptitude to have a strong genetic component, with heritability from the combined tests estimated at 0.44. The scientists looked for associations between musicality and several behavior-related genes and found one: two variants of a receptor gene for arginine vasopressin (*AVPR1A*). That's the stuff implicated in turning promiscuous voles into monogamous ones; it's also been associated with social attachment in humans (*Science*, 7 November 2008, p. 892).

The finding suggests that the "neurobiology of musicality is related to pathways affecting … attachment behavior," the authors reported last week in *PLoS ONE*. Neuroscientist Nina Kraus of Northwestern University in Evanston, Illinois, says the paper addresses a "hot topic." Experts debate whether music is just an evolutionary frill. If a genetic link is established between music and social bonding, she says that "could have far-reaching implications … [meaning] that music plays a role in human evolution."

But No Cats for Rover

The next Mars rover will be named Curiosity, thanks to a 12-year-old girl from Lenexa, Kansas. Clara Ma's essay suggesting that name was one of 9000 proposals NASA received from students around the country.

"Curiosity is an everlasting flame that burns in everyone's mind," Ma wrote. "It makes me get out of bed in the morning and wonder what surprises life will throw at me that day. Curiosity is such a powerful force. Without it, we wouldn't be who we are today. Curiosity is the passion that drives us through our everyday lives. We have become explorers and scientists with our need to ask questions and to wonder. … We will never know everything there is to know, but with our burning curiosity, we have learned so much."

Ma is being rewarded with a trip to NASA's Jet Propulsion Laboratory in Pasadena, California, where she will get to sign her name on the rover. Currently being assembled, it is scheduled for launch in 2011.

PUTTING A FACE ON ANCIENT APES

When workers dug up a fossil while building a dump for a country house in the hills west of Barcelona, Spain, a half-dozen years ago, they had no idea that they had uncovered a treasure trove of fossils. Among them was a new species of ape that lived 11.9 million years ago, according to a report in the current issue of the *Proceedings of the National Academy of Sciences*. The discovery literally puts a face on a type of Miocene ape that may have given rise to African apes—gorillas, chimpanzees, bonobos, and humans—says paleontologist Salvador Moyà-Solà of the Institut Català de Paleontologia in Barcelona.

The new ape, called *Anoiapithecus brevirostris*, may offer clues about whether apes in Eurasia or Africa gave rise to great ape lineages, says Moyà-Solà. The jaw has traits that could tie it to later African apes: a deep upper palate and thick tooth enamel. The relatively flat midface and high-crowned canines are also reminiscent of hominids, the offshoot that led to modern humans. But the authors also acknowledge that the traits could have arisen independently both in Europe and in Africa. This ape would have been an evolutionary dead end if, as most scientists believe, great apes emerged in Africa.

CREDITS (TOP TO BOTTOM): SOURCE: THE ROYAL ASTRONOMICAL SOCIETY; NASA; COURTESY PNAS

Published by AAAS

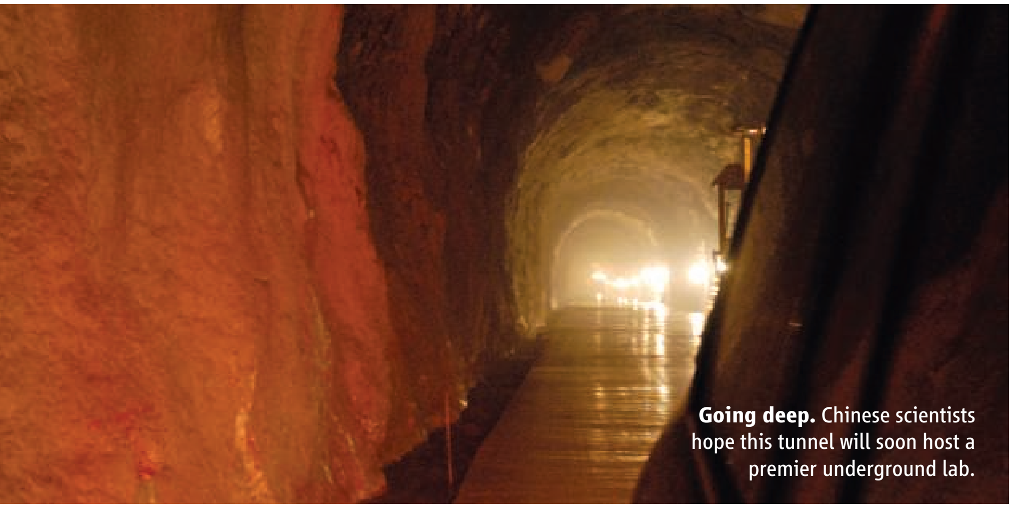

Going deep. Chinese scientists hope this tunnel will soon host a premier underground lab.

PARTICLE PHYSICS

Chinese Scientists Hope to Make Deepest, Darkest Dreams Come True

Particle physicist Yue Qian had his eureka moment in front of the TV set. For over a decade, Chinese scientists have longed for an underground laboratory that would enable them to join efforts across the globe to detect dark matter, observe neutrinos, and watch for exotic particle physics phenomena. Searches for suitable sites repeatedly came up empty-handed. But last August, after Yue caught a news report on the completion of two tunnels piercing Jinping Mountain in Sichuan Province, he felt that the long quest for such a lab might finally be over.

After months of negotiations, on 8 May Tsinghua University in Beijing, where Yue is an associate professor, signed an agreement with the tunnels' owner, Ertan Hydropower Development Co., to hollow out an experimental chamber. The Jinping lab would be the deepest underground science facility in the world, edging out—by 100 meters or so—the Deep Underground Science and Engineering Laboratory that the U.S. National Science Foundation may build in an abandoned mine in Lead, South Dakota. By placing sensors deep in the earth, physicists hope to reduce spurious signals from cosmic rays. China's subterranean aspirations have been circulating in Asia for months; the international community will get its first glimpse of the project at a dark-matter workshop in Shanghai on 15 June and at an astroparticle and underground physics conference in Rome next month.

An underground lab has been a dream for several generations of Chinese scientists, says Wang Yifang, a particle physicist at the Institute of High Energy Physics of the Chinese Academy of Sciences in Beijing. Past candidate sites, including an underground aviation museum near Beijing and coal and gold mines around the country, all were judged too shallow or impractical.

Short cut. Tunnels between the Jinping dams on the Yalong River offer a serendipitous lab site.

Jinping, on the other hand, "looks ideal," Wang says. The lab would have approximately 2500 meters of marble and sandstone above it: more shielding than any similar site in the world. Researchers will be able to make a 1-hour drive from a regional airport to the lab's front door. And the tunnels are sized for construction equipment, promising smooth delivery of instruments and supplies.

Wang cautions that the lab is not a done deal. "It's really at a very early stage," he says. To start with, Yue's group must verify that the rock overburden really does screen out unwanted cosmic rays and that there is no unexpected radiation emanating from nearby rock or groundwater. To provide space for instruments, by the end of the year the team plans to have hollowed out a 5-meter-high, 5-meter-wide, 30-meter-long chamber. They will then measure cosmic ray flux and background radiation for about 6 months. And they will begin at least one experiment. Yue is forming a collaboration to install a germanium detector to search for a postulated component of dark matter known as WIMPs, or weakly interacting massive particles. Chinese physicists are also talking about observations of atmospheric and solar neutrinos as well as experiments to watch for neutrinoless double-beta decay, an extremely rare phenomenon that might help refine estimates of neutrino mass.

Yue doesn't yet know what the first phase will cost, as design efforts are just starting. "But [Tsinghua] university has promised strong support," he says, and they are seeking funds from the science ministry. If the project develops as hoped, says Yue, "we would want to get more universities and institutions from China and around the world to join us and push this project ahead."

The good fortune befell physicists thanks to a mammoth hydroelectric project about 350 kilometers southwest of Chengdu, the capital of Sichuan Province, where the Yalong River makes a 150-kilometer-long U-turn around Jinping Mountain. Ertan Hydropower is building two dams: Jinping 1 at the start of the U-turn and Jinping 2 at the end. To move workers and materials between the construction sites, Ertan blasted a pair of 17-kilometer-

CREDITS (TOP TO BOTTOM): YUE QIAN; INTERNATIONAL WATER POWER & DAM CONSTRUCTION

Published by AAAS

Hydrogen pullback prompts backlash
1257

Galaxy evolution in isolation
1262

long access tunnels through the mountain. One will host the lab.

The hydropower project is controversial because some geologists think the weight of the impounded water could destabilize faults in the earthquake-prone region (*Science*, 8 May, p. 714). The prospect of an underground lab, though, is warmly welcomed by physicists throughout Asia. "It certainly is good news," says Henry Wong, a physicist at Academia Sinica in Taiwan, who will collaborate with Yue on the dark-matter experiment. Wong says he expects the lab to strengthen scientific ties between Taiwan and mainland China. Kim Sun Kee, a particle physicist at Seoul National University, is also enthusiastic. "Compared to other regions, in Asia, we don't have many underground labs," he says. Kim spearheads a collaboration hunting for dark matter in a lab in South Korea's Jeombong Mountain (*Science*, 6 July 2007, p. 32). But the Korean lab is only 700 meters beneath the surface, and more sensitive detectors now being contemplated by the community would need better shielding. Jinping, says Kim, "will be a great place for next-generation experiments."

–DENNIS NORMILE

RESEARCH FACILITIES

European Neutron Source Finally Finds a Home

After a frustrating decade watching their preeminence in neutron-beam science ebb away to newer facilities in the United States and Japan, European researchers got some good news last week: Their €1.4 billion dream machine, the European Spallation Source (ESS), which has been on the drawing board for more than 15 years, overcame a major hurdle when the countries interested in funding the project picked a site on which to build it in Lund, Sweden. "This is the real thing, something we can focus on and move forward," says Robert Cywinski of the University of Huddersfield in the United Kingdom, spokesperson for the ESS preparatory phase project.

Research fields. An artist's impression of ESS at Lund, with the doughnut-shaped MAX IV synchrotron.

Government ministers are not getting out their checkbooks yet, as there is still much to sort out, including a final site-specific design and an environmental impact assessment, as well as obtaining planning permission and figuring out exactly which countries want to join. But as with other major European research facilities, choosing a site—Lund won out over rivals Debrecen in Hungary and Bilbao in Spain—is always a tense and deeply political part of the process. ESS will be "the first European experimental facility in Sweden and the first outside the big five E.U. nations." says Colin Carlile of Lund University, who headed the effort to bring ESS there.

ESS will surpass current U.S. and Japanese neutron sources in power, unless they upgrade in the meantime. Neutron beams are used by a wide variety of researchers to probe how atoms are arranged within materials and how they interact. Beams of the particles can be produced using a nuclear reactor or by smashing a proton beam into a metallic target, a process known as spallation.

In the 1990s, Europe had the top two neutron sources: a reactor in France and a spallation source in the United Kingdom. U.S. researchers at the time were facing a neutron drought after a planned reactor was canceled in 1995. But the Spallation Neutron Source in Oak Ridge, Tennessee, got the green light in 1998 and opened for business in 2007 with a 1.5-megawatt beam. J-PARC, a multiaccelerator facility in Tokai-mura, Japan, is in the process of commissioning its 1-MW neutron beamline.

Although Europe drew up plans for a 10-MW spallation source in 1995, no European government seemed to want to pick up the ball and run with it. By 2003, ESS seemed all but dead, despite a cost reduction by downgrading to 5 MW. Cywinski blames this impasse on the fact that Europe "doesn't have one doorstep on which to put a proposal." Instead, researchers have to find a government to champion their idea and build a group of collaborators, a process known in E.U. circles as "variable geometry." Says Cywinski: "Variable geometry doesn't work, or we would have had ESS years ago."

ESS finally got a shot in the arm from the European Strategy Forum on Research Infrastructures, an E.U. body that in 2006 drew up a list of facilities that would benefit European research, describing ESS as a mature project. That stamp of approval led to E.U. money for preparatory work and several countries stepping up to offer possible sites. The Swedish government, for example, offered to pay 50% of ESS's construction cost and 20% of operating expenses. The site at Lund will also be home to a new Swedish-built synchrotron, an intense source of x-rays for research, and ESS will aim to be carbon-neutral through a joint project with a wind-energy company.

Sweden worked hard to get neighboring countries in Scandinavia and the Baltic on board before the vote. The final decision was made on 28 May after a group of research ministers from 12 countries interested in participating met to discuss the bids and then the non-bidding countries voted. Seven declared they would join the Lund effort—Germany, France, Poland, Denmark, Norway, Estonia, and Latvia—and two others, Italy and Switzerland, backed the Lund site. Portugal voted for Bilbao.

Sweden must cement the collaboration over the next few months with a memorandum of understanding signed by the partners and attempt to bring Italy and Switzerland as well as defeated rivals Spain and Hungary into the collaboration. Construction is penciled in to start in 2012.

–DANIEL CLERY

CREDIT: ESS SCANDINAVIA

Published by AAAS

GEOSCIENCE

The Quaternary Period Wins Out in the End

Geoscientists have cut the Gordian knot of geologic timekeeping. Ever since 19th century geologists divided the history of Earth into four periods—the Primary, Secondary, Tertiary, and Quaternary, oldest to most recent—their intellectual descendants have been dismantling that time scale. But the geologists, anthropologists, glaciologists, and paleoecologists studying the last couple of million years became quite attached to the Quaternary. They gave its name to their journals and even themselves—to the disgruntlement of strict constructionists, who have been insisting for decades that the modern rules for dividing up geologic time permitted neither the Quaternary nor quaternarists (*Science*, 25 January 2008, p. 402).

On 21 May, the final committee vote on the question was announced: The quaternarists will endure. Pending an almost certain ratification by the ultimate authority—the International Commission on Stratigraphy (ICS)—the Quaternary will officially take over the past 2.6 million years of the geologic time scale, when humans took up tools and the world began slipping in and out of the ice ages.

"The Quaternary Commission is greatly relieved and pleased," says Philip Gibbard of the University of Cambridge in the United Kingdom, who is president of the commission, a subgroup of ICS. Nomenclature "is not set in stone, even in geology," says Gibbard. "It's just a question of changing the label."

Not quite. "It makes no sense, it creates havoc, we're going to ignore it pretty much," says marine geologist Marie-Pierre Aubry of Rutgers University in Piscataway, New Jersey, who with others vociferously opposed the change. The ICS committee's 16-to-2 vote, she notes, not only usurps the last 2.6 million years of the Neogene period for the Quaternary but also extends the subsidiary Pleistocene epoch from 1.8 million years ago to 2.6 million years at the expense of its predecessor, the Pliocene epoch. Everyone had agreed on how to identify the original time boundaries according to consistent rules, she says; the vote throws those rules out the window. "You have to respect scientific principles," Aubry says. "If you don't, things don't make sense any more."

"Technically, [Aubry] is absolutely right, but I don't think it's going to make a great deal of difference in our community," says paleoceanographer Lloyd Keigwin of Woods Hole Oceanographic Institution in Massachusetts, who was not involved in the debate. Researchers analyzing the marine record are usually concerned with changes through time, he says, not so much where an event stands in relation to broadly spaced time markers. "From a practical standpoint, we may have to move on," he concludes.

–RICHARD A. KERR

*Science*NOW.org

From *Science*'s Online Daily News Site

Preventing a Plant Apocalypse. Sometime between 100 million and 1 billion years from now, Earth will have lost so much carbon dioxide from its atmosphere that plants and trees will literally begin suffocating, eventually taking all life with them. In a new study, researchers propose one way to delay this Armageddon: reduce the pressure of the atmosphere, effectively creating conditions where we all feel like we're living at high altitudes. http://tinyurl.com/kqj3sc

A Billion-Year Hard Drive. That embarrassing home movie of you naked in the tub could still be around millions of years from now, along with your less-than-eloquent posts on Facebook and Twitter. Researchers have developed a new technology based on carbon nanotubes that promises to permanently preserve individual bits of data, such as those found on computer hard drives and DVDs. If so, the technology could lead to data archives holding the entirety of human thought and communications potentially forever. http://tinyurl.com/lxrffu

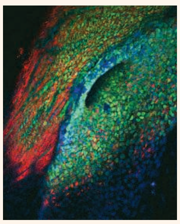

iPS Cells to the Rescue. Two papers published this week appear to bring the day closer when embryonic-like stem cells can be used to treat human diseases. One study describes what scientists say is the safest method yet to produce these cells. The other reports success in using the cells to begin correcting a rare genetic disorder known as Fanconi anemia. http://tinyurl.com/mogfdz

Quantum Widget. The strange rules of quantum mechanics govern the behavior of tiny objects and explain the structure of atoms, the subtleties of chemical bonding, and the inner working of electronic microchips. Ironically, although the theory is called quantum mechanics, physicists have never produced a machine whose motion demonstrates quantum weirdness. Now a team from the National Institute of Standards and Technology in Boulder, Colorado, has taken a step in that direction by forging a bizarre quantum connection called entanglement between two mechanical widgets. The devices don't look much like typical machines, however: Their moving parts are ions oscillating in electric fields.

So Long Aspirin, Hello Silver. Millions of people around the world are prone to dangerous blood clots. Now researchers have had early success with a new way to prevent them—and the strokes, heart attacks, and pulmonary embolisms they cause. Nano-sized particles of silver can stop sticky blood cells called platelets from clinging together in laboratory strains of mice, the team reports. http://tinyurl.com/lcof8s

CREDITS (TOP TO BOTTOM): PETER HOEY; JUAN CARLOS IZPISÚA BELMONTE

Published by AAAS

U.S. HIGHER EDUCATION

Report Finds No Gender Bias in Faculty Hiring, Resources

A new report by the U.S. National Academies says that women are getting a fair shake from major research universities in being hired, promoted, and given access to resources—once they can grab onto the academic ladder and start climbing the rungs.

That conclusion may surprise those familiar with a stream of recent reports on the topic, including a 2006 academies' study that demanded an end to what it called the "bias and outmoded practices" hindering the progress of women in academic science. The good news, says the report, is that "men and women faculty … have enjoyed comparable opportunities, and gender does not appear to have been a factor in a number of important career transitions and outcomes." The bad news, however, is that too many scientifically trained women are rejecting academia in favor of other career paths.

"I'd hate for anybody to read this report and think that we can be complacent," says physicist Claude Canizares, vice president for research at the Massachusetts Institute of Technology in Cambridge and co-chair of the new report, *Gender Differences at Critical Transitions in the Careers of Science, Engineering, and Mathematics Faculty*. "While women can take some encouragement from the fact that there is no evidence of large-scale bias at these key transition points, the reasons for their continued underrepresentation need to be examined more closely."

The study, requested by Congress in 2002 and supported by a $1.3 million grant from the National Science Foundation, focuses on three important transitions: getting a tenure-track position, winning tenure, and being promoted to full professor. It's based on surveys of 500 departments at 89 institutions and of 1800 faculty members in those departments. Although legislators had initially wanted a sweeping review of "gender differences" among all faculty members at all institutions, the academy panel decided to save time and money by concentrating on full-time faculty members from six disciplines—biology, chemistry, civil and electrical engineering, mathematics, and physics—who work at the top tier of research universities.

Within that population, the panel found that women are actually more likely than men to be interviewed for and offered tenure-track jobs (see graphic, p. 1251) and just as likely to be successful when they come up for tenure. But taking the first step is where the problems seem to lie. According to the report, many fewer women bid for tenure-track positions than would be expected based on their proportion of the Ph.D. pool. Although university outreach efforts had no apparent effect on attracting more women applicants, one factor did make a difference: Women are more likely to apply if a woman is chairing the selection committee or serving on it.

Once women take the job, they also often face a tougher climb up the ladder than their male colleagues. The survey found that faculty women "were less likely to engage in conversation with their colleagues on a wide range of professional topics," including research, salary, and benefits. The panel also found that women remain assistant professors significantly longer and that the attrition rate is higher before coming up for tenure.

Donna Nelson, a chemistry professor at the University of Oklahoma who has done pioneering work on the status of women in academic science, says that the panel's findings match what she hears on campuses. "Women tell me all the time that they feel isolated. It's harder to feel good about your work, and be productive, if you're not being included in conversations and collaborations." Nelson also emphasized the need for more women applicants to entry-

NEWSMAKER INTERVIEW

Eugenie Scott Toils in Defense of Evolution

As executive director of the California-based National Center for Science Education, anthropologist Eugenie Scott has spent the past 2 decades on the frontlines of the contentious battle over teaching evolution in U.S. public schools. She doesn't confine herself to the classroom and courthouse: Every year, she and geologist Alan Gishlick lead a rafting trip through the Grand Canyon, teaching a general audience about the science and natural history of the canyon and comparing the evidence with the creationist explanation of its origins.

Last week, Scott won the inaugural Stephen Jay Gould Prize from the Society for the Study of Evolution, only weeks after *Scientific American* ranked her among the country's top 10 science and technology leaders for her self-described role as "Darwin's golden retriever." Scott spoke to *Science* last week about where things now stand.

–YUDHIJIT BHATTACHARJEE

Hard facts. Eugenie Scott leads rafting trips through the Grand Canyon.

Q: How has this battle changed in the past 20 years?

E.S.: The enemy has become more diverse. When I started, it was just creation science. Now we have creation science, intelligent design [ID], and straight-up antievolution in the form of "evidence against evolution." It used to solely be a K–12 issue. Now we are seeing that it crops up frequently in community colleges and even 4-year colleges.

Q: What's the current situation in the various states?

E.S.: Besides periodic assaults on science standards as we recently saw in Texas, we are concerned about antievolution legislation in different states under the guise of academic freedom bills. Just in the last few weeks, antievolution bills awaiting decisions in a number of states—Oklahoma, South Carolina, Alabama—died in committee. Louisiana passed antievolution legislation last year; we're now waiting to see how it plays out. We are also seeing closet creationism being introduced through wording not obvious to those unfamiliar with the history of the controversy.

Q: Why has the ID movement survived the 2005 Dover trial?

E.S.: ID proponents have repackaged ID

CREDIT: EDWARD COTTER

STAYING AFLOAT IN ACADEMIA

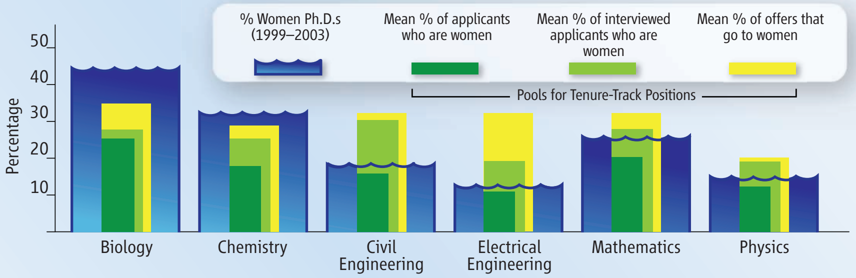

	TENURED		TENURE TRACK	
	Actual % of All-Male Interview Pools	Probability of All-Male Pools	Actual % of All-Male Interview Pools	Probability of All-Male Pools
Biology	25	18	22	24
Chemistry	50	24	22	37
Civil Engineering	46	35	33	42
Electrical Engineering	42	62	35	56
Mathematics	39	44	13	33
Physics	32	35	38	50

Job hunting. Women are underrepresented in the applicant pool (*top*), but once in the running, their chances generally improve. The exception is for tenured jobs (*above*) in biology, chemistry, and civil engineering.

SOURCE: U.S. NATIONAL ACADEMIES

level, tenure-track positions. "If universities narrow the pool at the onset," she notes, "then women will have a harder time even getting on the radar screen."

Canizares said that the panel took the unusual step of conducting its own research because "there were no data to answer the questions we were interested in addressing." He hopes that federal agencies and universities will recognize the need to gather longitudinal data on the career paths of women. "And I'd suggest that we start with our own graduate students."

–JEFFREY MERVIS

and are promoting it as "evidence against evolution." The Discovery Institute, an ID think tank, has published *Explore Evolution* that quotes a "number of problems" with evolution that they would like taught in biology class. Of course, these are standard creationist arguments.

Q: Why hasn't the general public rejected ID?

E.S.: Only 40% of adult Americans understand the nature of a scientific experiment. Remember that ID is primarily a marketing strategy to the general public, and unless that is directly opposed, people are going to be miseducated about science. We don't have to worry about medical schools teaching that AIDS is a curse from God, but we have to worry about teachers teaching well.

Q: Why is it important to teach evolution? Can't doctors and most life scientists do their jobs without accepting evolution?

E.S.: You can be a mechanic without understanding the niceties of the internal combustion engine. [But] wouldn't you rather go to a mechanic who has the big picture?

Q: What should scientists do to help the cause?

E.S.: Universities need to do a better job of teaching evolution because that's where high school teachers get their training. Evolution needs to be brought into every course of biology instead of getting tacked on as a unit to the intro class.

What university scientists should not do is to force students to choose between religion and science. If a professor were to say that evolution proves there is no God, that's not just bad philosophy of science, it ensures that a significant number of students will stick their fingers in their ears.

When explaining biological questions, such as the evolution of the eye, there is no need to say that God had nothing to do with it. It's an irrelevant comment. I don't think a classroom is an appropriate place to try to create more atheists any more than it is an appropriate place to create more fundamentalist Christians.

*Science*Insider

From the *Science* Policy Blog

A call to include damage to oceans in climate policy, a trio of new government ministers in India, and a contrarian analysis of swine flu data were among the stories covered by *Science*Insider in the past week.

Scientific academies have joined forces to warn world leaders about the **dangers of ocean acidification.** The InterAcademy Panel on International Issues, with members representing 69 countries, issued a statement this week recommending that the United Nations Framework Convention on Climate Change take up the issue before the U.N. Climate Change Conference in Copenhagen in December. The oceans are absorbing a quarter of industrial emissions of carbon dioxide, increasing their acidity and harming marine life.

India's **prime minister, Manmohan Singh**, has named leaders with deep technical expertise to his cabinet. The new science minister is Prithviraj Chavan, a politician from western India who was educated as a mechanical engineer at the University of California, Berkeley. Singh appointed Kapil Sibal, a lawyer and respected former science minister, as minister of human resources development, which includes the education portfolio. Mechanical engineer Jairam Ramesh becomes minister of environment and forests.

*Science*Insider's ongoing coverage of the **swine flu outbreak** includes an analysis that contradicts the view of the U.S. Centers for Disease Control and Prevention that cases in the country might have crested. Donald Olson, a New York City–based epidemiologist who runs the influenza monitoring project at the International Society for Disease Surveillance, says his data show "massive increases" in Boston and New York City, which look "mild" in the CDC regional data. Olson says New York City's drop and then rise in cases may soon be repeated around the country.

Stay on top of the latest science policy news at **blogs.sciencemag.org/scienceinsider**.

Water Flea Boasts Whopper Gene Count

Packed into a body no bigger than the letters on this page is a whale of a genome. The body belongs to *Daphnia pulex*, a crustacean common in lakes and ponds around the world. Since 2004, the Department of Energy Joint Genome Institute in Walnut Creek, California, and a consortium that now numbers 350 investigators from 17 countries have been sequencing and analyzing the 200-million-base genome from a *Daphnia* that lived in a pond along the Pacific coast of Oregon. It is one of just two noninsect arthropods to be deciphered to date.

At first glance, the genome seemed to have about 25,000 genes—a lot, but no record-breaker. Eventually, however, gene-finding programs found 31,000, John Colbourne of Indiana University, Bloomington, reported at the meeting. And a variety of experiments have revealed as many as 8000 more genes that gene-finding annotation programs missed, he said. That tops the gene count of the newly sequenced genome of another tiny creature: the pea aphid, which sports 34,600 genes (see p. 1253).

"It's a big surprise that critters that you think wouldn't have a high gene count do," says Eric Green of the National Human Genome Research Institute in Bethesda, Maryland. These findings are further evidence that biological complexity does not directly correlate with gene number. But we are also "probably naïve in defining what is biological complexity," Green adds.

Part of the appeal for sequencing the genome of *Daphnia* is its ability to adapt—it usually clones itself but reproduces sexually under certain conditions. Eggs can hatch right away or lay dormant for more than a century. *Daphnia* thrive on algae and in turn are fodder for many fish and other predators, making them a key link in aquatic food webs. But, depending on the predator, they can sprout helmets, tail spines, or ridges called neck teeth. The genome is already helping researchers get to the genetic basis of this plasticity.

All-purpose genome. An extraordinary number of genes may help *Daphnia* cope with diverse environments and predators.

Colbourne and his colleagues first made a microarray of all the organism's genome sequence rather than just pieces of the genes themselves. "The array is blind relative to the annotation," Colbourne explains, and thus can pick up expressed DNA that gene-finding programs might miss. They have started using the array to study how gene expression changes under different conditions. In experiments that looked at *Daphnia* exposed to different predators, for example, they found "a set of genes that were hidden," Colbourne reported. "And we expect there are still more" to be unearthed as they evaluate different environmental conditions. The new genes they're finding seem to code for proteins but not for any that look familiar.

Colbourne wonders whether this gene-packed genome arose in part because of the complexity of the aquatic environment—this species can live where it's salty, acidic, hot, and so shallow that exposure to the sun is hazardous. "It's almost as if they have more than one genome" to be able to cope with this diversity, he said. Another reason for the high gene count could be a consequence of having both sexual and asexual reproduction.

Whatever the cause, the high gene count comes from having many duplicated genes. This stands in contrast to the human genome, which generates a variety of different proteins by splicing genes into different configurations. Why the *Daphnia* genome evolved this way is a mystery, says John Werren of the University of Rochester, New York. "Some feature of the genome of *Daphnia* has pushed it to make more copies as opposed to [evolving] splicing."

Some RNA May Play Key Role in Repressing Genes, Slowing Cancer

Protein-coding genes have long been the stars of the Human Genome Project, but now RNA is moving into the limelight. Over the past 3 years, researchers have come to realize that protein-coding genes account for barely a quarter of the DNA that gets transcribed. The rest leads to RNA strands of various lengths—but toward what end has been a mystery, because that RNA doesn't seem to lead to any proteins. Some experts have even argued that this RNA is little more than "transcriptional noise." Yet, just as junk DNA proved to be more than junk, at least some of this "noise" translates into meaningful molecules that may play key roles in turning genes on and off.

"For the past 5 to 10 years, researchers have been cataloging the presence of the noncoding RNAs," says Thomas Gingeras, a molecular biologist at Cold Spring Harbor Laboratory in New York. "Now people want to understand what they do." Chris Ponting of the University of Oxford in the United Kingdom and his colleagues took some of the first steps in that direction in 2007 by showing that 3000 long noncoding RNAs were conserved in evolution, with sequences that were quite similar among mice, rats, and humans—an indication that they serve some vital function.

At the meeting, another team described progress in quantifying and assessing the function of a particular group of long RNA molecules. John Rinn of Harvard Medical School in Boston and his colleagues presented further evidence that at least some of these molecules seem to be important to a cell's survival, and they reported that by studying the molecules these RNAs associate with, they are beginning to glean how some of them may actually work. One, for example, seems critical to helping the tumor suppressor gene *p53* keep cancer in

CREDIT: PAUL HEBERT/THE UNIVERSITY OF GUELPH

Published by AAAS

The Bug and the Bacterium: Interdependent Genomes

Any successful relationship demands sacrifices. The partnership between the pea aphid and a tiny bacterium called *Buchnera aphidicola* is no exception. The newly sequenced DNA of this tiny insect, a common pest of legume crops, reflects a long history of give-and-take between the genomes of the bug and the bacterium. "The bargaining chips are genes, and the inventory reflects concessions during the course of negotiations," says John Colbourne, an evolutionary biologist at Indiana University, Bloomington.

Sappy diets. The aphid genome revealed that making essential amino acids was a joint venture with this plant pest's microbial partners.

Like other aphids, *Acyrthosiphon pisum* live off plant sap, a sugary mix low in protein. To make up for this nutritional shortfall, the insects depend on their microbial guests to supply essential amino acids. In return, the pea aphid has given up some of the genes that normally help fend off infections by Gram-negative bacteria such as *Buchnera*, Stephen Richards of Baylor College of Medicine in Houston, Texas, reported at the meeting. This loss "might account for the evolutionary success of aphids to obtain beneficial symbionts," reported aphid consortium collaborator Shuji Shigenobu of Princeton University.

Buchnera bacteria have tiny genomes, and genes number about 640. But they include key ones for providing the aphid with about nine amino acids that are missing from the sap that aphids feed on. A big surprise however, was that making almost every essential amino acid was a joint venture, with some steps occurring in each species. For example, *Buchnera* lacks the enzyme needed for the last step in making leucine, but it's in the aphid genome, so the finishing touches take place in the aphid. This division of responsibilities "dramatically underscores the dependent nature of symbiont-host relationships at the molecular level," says Colbourne.

The consortium had expected that some bacterial genes—such as ones missing in amino-acid-synthesis pathways—might have worked their way into the aphid genome. But relatively few have, Richards reported. The consortium found about 11. At least two are important to *Buchnera* for making the microbe's cell wall, and these are active in the nuclei of aphid cells specialized to house the microbes. Surprisingly, those genes didn't come from *Buchnera*, Richards reported: They appear to have come from a different type of microbe altogether, an alpha protobacteria.

The aphid was rife with duplicated genes, with an estimated 34,604 protein-coding genes in all, double the number in *Drosophila*. It also has several new genes, not known in other species, that code for saliva proteins that likely help keep plant juices flowing once the aphid has broken into the plant. "If you ask how we are going to control aphids on plants, this is the interaction that you have to stop," Richards says. "And now you have a molecular entry into that."

–E.P.

check. "There are a lot more of these [RNAs], and they are probably more important than we thought," says Richard Myers of the HudsonAlpha Institute for Biotechnology in Huntsville, Alabama.

Rinn and his colleagues study what he calls "large intervening noncoding RNAs" (lincRNAs), 2300 to 17,200 bases long, that are coded for in DNA between genes. Until recently, researchers knew of only about a dozen lincRNAs, notably XIST, an RNA that turns off the extra X chromosome in females, and HOTAIR, an RNA that directs the specialization of skin cells.

Rinn's team has searched systematically for lincRNAs by looking outside gene boundaries for chemical signatures that they know mark the coding regions of active genes. They initially looked in four types of mouse cells, assuming that such marks signaled additional transcription. The survey initially turned up about 1500 candidates, Rinn graduate student Mitchell Guttman and colleagues reported online 1 February in *Nature*.

At the meeting, Guttman reported that the team has expanded the search to 10 human tissues and has come up with 4000 definite lincRNAs. He estimates there are about 1000 more. Not everyone agrees that lincRNAs represent a true subclass of noncoding RNAs, as they worry that some of the DNA sequence encoding long noncoding RNAs may extend into genes, blurring the definition of "intervening." "Making a new class may be premature," Gingeras says.

Guttman, Rinn, and their colleagues have also looked for patterns of coexpression between protein-coding genes and lincRNAs in 21 tissues. They found quite a few gene-lincRNA overlaps, from which they concluded that, broadly speaking, lincRNAs are involved in the regulation of the cell cycle, immunity, and stem cell differentiation, Guttman reported. For example, 39 associated with the tumor suppressor gene *p53*. One "is directly regulated by *p53*," Rinn reported at the meeting. He thinks that particular lincRNA acts as a global repressor of the *p53* pathway, because 1000 genes increased their expression when he disabled either *p53* or that particular lincRNA.

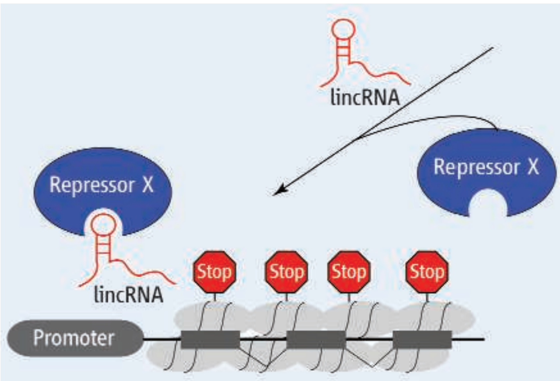

Gene stopper? LincRNAs may bind and lead repressor proteins to promoters so as to silence genes.

The story sounded vaguely familiar, for that is how HOTAIR and XIST seem to work. So Rinn and Guttman did an experiment to assess how many lincRNAs bind to polycomb protein complexes. These complexes remodel chromatin, reconfiguring this DNA-protein matrix to shut out transcription factors and silence certain genes. They found that almost 25% of the lincRNAs latch onto these complexes in one cell type or another. Furthermore, the RNAs were required for gene silencing. In total, 38% of the lincRNAs are tied in with one of four chromatin-remodeling complexes, Rinn reported. "We think RNA is a scaffold to [help] bring in the right proteins," says Rinn.

"Those results are very exciting," says David Haussler, a bioinformaticist at the University of California, Santa Cruz. "This is far from being a mature scientific story, but there are tantalizing hints [of a repressive function]." Adds cancer geneticist Victor Velculescu of Johns Hopkins Kimmel Cancer Center in Baltimore, Maryland: "It reinforces the fact that these lincRNAs are likely to be important physiologically."

–ELIZABETH PENNISI

CREDITS (TOP TO BOTTOM): NANCY MORAN/UNIVERSITY OF ARIZONA; JOHN RINN

On the Origin of Sexual Reproduction

For Darwin, sex was a big question mark. "We do not even in the least know the final cause of sexuality; why new beings should be produced by the union of the two sexual elements," he wrote in 1862. "The whole subject is as yet hidden in darkness."

Today, biologists understand the molecular nuts and bolts of sex fairly well. Each new human being (or bird or bee) needs a set of chromosomes from each parent. But that's the *how*. The *why* of sex is still fairly mysterious. Bacteria don't have to search for a mate; they just grow and divide in two. An aspen tree can simply send out shoots that grow into new trees. No muss, no fuss with finding a partner, fertilizing an egg, and joining two genomes. Why should so many species take such a labyrinthine path to reproduction, when straightforward routes are available?

Biologists first began to give the question "Why sex?" serious attention about 40 years ago, and today they're using genomics and other 21st century tools to search for the answer. They are finding hidden signs of sex in the DNA of supposedly asexual organisms and are tracking the evolutionary impact of sex among living populations of animals and plants. Some use sophisticated mathematical models to assess the conditions under which sex can arise.

These efforts are providing new hints about how sex first emerged some 2 billion years ago and about the forces that have made it so widespread. The studies bolster a handful of hypotheses: Sex may speed up evolution, for example, or it may provide a better defense against parasites. In the past, scientists have focused on just one of these hypotheses at a time, but today many argue that several forces may be at work at once.

Mating of molecules

Sex gives nature much of its spice. Fireflies flash through the night to find a mate; a flower's perfume lures insects to carry pollen to distant partners; male bullfrogs croak to impress females. But despite this dizzying diversity, all sexually reproducing organisms take the same key steps to make new offspring: They shuffle their own DNA and then combine some of it with the DNA of another member of their species to produce a new genome. The key to this novelty is a process called meiosis.

As with those of other vertebrates, almost all human cells are diploid: Each one contains two copies of very similar, or homologous, chromosomes. As precursor sex cells divide, they give rise to haploid sex cells of sperm and eggs, each with only one chromosome from each pair. Only when one sex cell fuses with another does it become part of a new diploid genome.

Meiosis creates new variations in two ways. There's a 50-50 chance that a parent will pass down either chromosome of a given pair to his or her offspring. And during the development of sex cells, homologous chromosomes undergo recombination: They line up with each other and swap segments of their DNA. So even if two siblings get the same chromosome from their mother, their chromosomes aren't identical.

In 1971, the late British evolutionary biologist John Maynard Smith helped kick off the modern study of the evolution of sex by pointing out how costly sons are to a mother. An asexual female lizard, for example, produces just daughters, all of whom can reproduce. A sexually reproducing female lizard, on the other hand, produces, on average, a son for every daughter, half the reproductive potential. Yet despite this "twofold cost of sex," as Maynard Smith called it, he observed that sex is widespread, as most animals and plants produce males and females.

And he didn't even realize how widespread sex is. It's starting to seem as if just about all eukaryotes—the lineage that includes animals, plants, fungi, and protozoans—have some sort of sex. (Fungi and protozoans don't have males and females like we do; instead, they produce two or more "mating types.") In April, for example, signs of sexual recombination were discovered in the seemingly asexual *Leishmania*, a protozoan that causes the tropical disease leishmaniasis (*Science*, 10 April, pp. 187, 265).

Other asexual eukaryotes show signs of having evolved from sexual ancestors. *Trichomonas vaginalis*, a protozoan that causes vaginal infections, doesn't appear to reproduce sexually, for example. But in 2007, John Logsdon of the University of Iowa in Iowa City and his colleagues discovered that its genome contains almost all the genes necessary for meiosis, suggesting that it was once a sexual creature. Given how widespread sex and sex-related genes are, Logsdon says, "it's hard to escape the conclusion" that sex first evolved in the common ancestor of all eukaryotes some 2 billion years ago.

The road to sex

In trying to understand how this transition occurred, most scientists thought that meiosis and sex evolved together, as a package. But Adam Wilkins of the University of Cambridge in the United Kingdom and Robin Holliday of the Australian Academy of Sciences have recently argued that some key steps in meiosis—namely, the reduction of diploid cells into haploids—took place long before full-blown sex existed. "It turns the conventional thinking on its head," says Wilkins.

Wilkins and Holliday's scenario starts with the ballooning of the genomes of the early, asexual eukaryotes. Although the most ancient single-celled, amoebalike creatures were probably haploid, like modern bacteria, today the eukaryote genome can be thousands of times the size of a bacterial one, and many studies suggest that it was inflated billions of years ago by invading viruslike segments of DNA called mobile elements.

At first, these early eukaryotes reproduced simply by duplicating their giant haploid genomes and dividing. But at some point, Wilkins and Holliday propose,

THE YEAR OF DARWIN

This essay is the sixth in a monthly series. For more on evolutionary topics online, see the Origins blog at **blogs.sciencemag.org/origins**. For more on sexual reproduction, listen to a podcast by author Carl Zimmer at **www.sciencemag.org/multimedia/podcast**.

CREDITS: DEA PICTURE LIBRARY/GETTY IMAGES; WIKIPEDIA/GEORGE RICHMOND, FROM ORIGINS, RICHARD LEAKEY AND ROBERT LEWIN

Published by AAAS

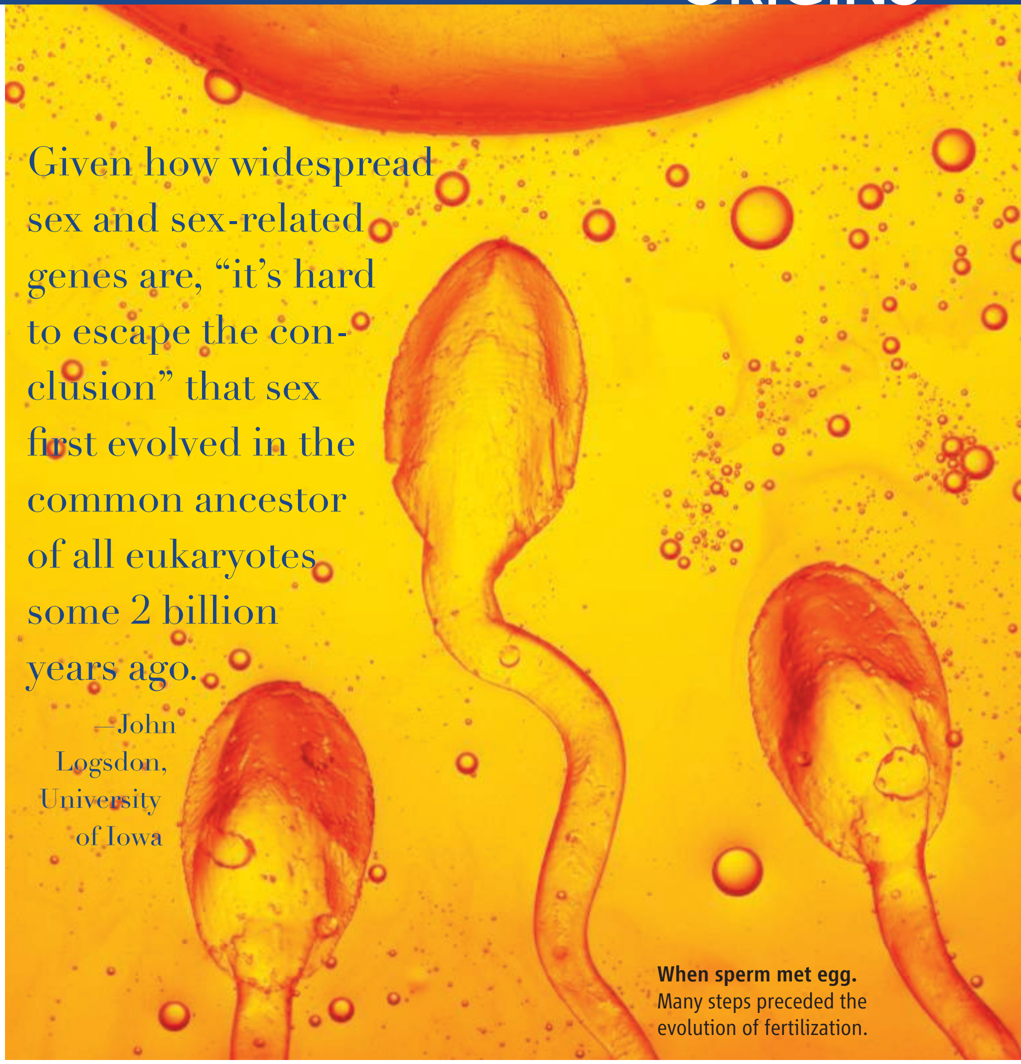

Given how widespread sex and sex-related genes are, "it's hard to escape the conclusion" that sex first evolved in the common ancestor of all eukaryotes some 2 billion years ago.

—John Logsdon, University of Iowa

When sperm met egg. Many steps preceded the evolution of fertilization.

CREDIT: DENNIS WILSON/CORBIS

diploid cells arose. Two haploid cells might have fused, for example, or a cell may have failed to divide after duplicating its DNA. Today, some fungi pass through these kinds of diploid stages.

The combination of a big genome and a new diploid stage raised the risk that eukaryotes would make fatal mistakes while copying their DNA. A chromosome can potentially join any other chromosome wherever they share similar sequences. It's safe for this to happen between homologous chromosomes, because they will swap versions of the same genes during recombination. But when one chromosome recombines with a nonhomologous chromosome, "that leads to terrible problems," says Wilkins. Each chromosome donates some of its genes but doesn't get the same genes back. A cell that inherits one of these deficient chromosomes may die.

Wilkins and Holliday argue that this risk drove the evolution of a new defense. In one or more lineages of early eukaryotes, homologous chromosomes began to line up tightly with one another before cells divided. Now recombination could take place safely. If a chromosome swapped some of its genes with another chromosome, it would get versions of the same genes back. Meiosis thus evolved as a way to reduce the damage from mismatched recombinations.

It would take millions of years more before eukaryotes shifted from a mostly haploid existence to spending most of their life cycle as diploids (as we do) and only sometimes producing the haploid cells necessary today for sexual reproduction. That shift to a sexual life cycle, however, still had to overcome the twofold cost of sex.

Lilach Hadany of Tel Aviv University in Israel and Sarah Otto of the University of British Columbia, Vancouver, in Canada, have been building mathematical models to explore the evolutionary pressures that might have allowed a population of asexual eukaryotes to become sexual. They find that sex can come to predominate if it's only optional.

Hadany and Otto created a mathematical model of eukaryotes in which most of the organisms were asexual, but some carried genes that let them reproduce sexually when under stress. This reflects real life: Today, yeast and many species of plants reproduce sexually only during times of stress and reproduce asexually the rest of the time. The researchers found that over the generations, from one crisis to the next, the sex genes spread. By triggering organisms to reproduce sexually, these genes could become combined with new sets of genes that were better able to withstand the crisis, leading to the greater proliferation of the "sexual" individuals. Once the crisis was over, the sex genes turned off, allowing the advantageous combinations of genes to remain intact.

However, this strategy "doesn't happen because sex is good for the population," Hadany points out. Instead, the model suggests that genes for sex spread thanks to their own selfish drive to generate ever more copies of themselves.

If sex started out as an optional way to reproduce, then a new question emerges: How did sex later become mandatory in many species, including our own? Hadany suspects that the answer has to do with sexiness—that is, with the preference sexually reproducing organisms often have to mate with some individuals over others. Female guppies, for example, like to mate with male guppies with bright spots; in some frog species, the females choose to mate with the males that croak loudest.

Hadany and Tuvik Beker, then at Hebrew University of Jerusalem, built a mathematical model in which the frequency of sex as well as the mating preferences could evolve. Under these conditions, they found, the population evolved to reproduce sexually more and more often until asexual reproduction ceased all together. The sexy individuals were driving this evolution. Because they could attract so many more mates from the opposite sex, they could have more offspring through sexual reproduction than by just cloning themselves. (The female's advantage comes in part from sexy sons that achieve reproductive success through mate preference.) As a result, mutations that increased the amount of sex increased these organisms' success. These genes passed down to more offspring and eventually spread through the entire population.

Here to stay

Although sexiness may help explain how sexual reproduction took over, it can't fully explain why sex has managed to reign for billions of years. Because they don't have to pay the twofold cost of sex, under the right conditions, any new cloners ought to spread rapidly in a population, challenging sexual reproduction. However, given the rarity of asexuals, something must be getting in the way. Over the years, scientists have proposed about

20 different hypotheses to explain the failure of asexuality to regain much of a foothold. Logsdon calls the three with the most support from both experiments and mathematical analysis "the good, the bad, and the ugly."

The "good" refers to the ability sexual species have to adapt faster than asexual ones. If an asexual organism picks up a beneficial mutation, it can only pass the mutation down to its direct offspring. If another organism picks up a different beneficial mutation in a different gene, then there's no way for it to be combined into the same genome as the first mutation to make a more optimal genome. Sexual reproduction, on the other hand, splits up genes and recombines them into new arrangements, joining beneficial mutations.

In this way, sexual reproduction may improve the fitness of a population faster than asexual reproduction. In 2005, Matthew Goddard and colleagues at the University of Auckland in New Zealand genetically engineered some yeast that could only reproduce sexually and others that could only reproduce asexually. (Typically, yeast can do both.) When Goddard raised both mutants on a near-starvation diet, the sexual yeast were able to adapt faster. As they evolved, their growth rate increased 94%, while the asexual strain increased only 80%. The difference in growth would allow the sexual yeasts to rapidly take over a population.

The "bad" refers to slightly harmful mutations and what sex does to purge them. Over time, a population of asexual organisms may pick up mutations that slow their growth rate. Each mutation may be only slightly deleterious, and so natural selection fails to eliminate it from the population. As generations pass, more and more harmful mutations accumulate, dragging down the expansion of the population. Eventually, these slightly deleterious variants may replace all the undamaged versions of these genes in a population, permanently compromising fitness. Sexual organisms, on the other hand, can trade in a defective version of a gene for a working one through recombination, keeping healthy genomes intact.

Real examples that celibacy can be bad for the genome exist. In 2006, for example, Susanne Paland and Michael Lynch of Indiana University, Bloomington, looked at mutations in *Daphnia pulex*, a species of water flea. Populations of asexual water fleas carried more harmful mutations than sexual ones.

Along with the "good" and the "bad," there is the "ugly": namely, parasites, against which sex may be a powerful defense. In the 1970s, several researchers built mathematical models of how parasites influenced the evolution of their hosts and vice versa. Their research suggested that both partners go through cycles of boom and bust. Natural selection favors parasites that can infect the most common strain of host. But as they kill off those hosts, another host strain rises to dominate the population. Then a new parasite strain better adapted to the new host strain begins to thrive, leaving the old parasite strain in the dust.

This model of host-parasite coevolution came to be known as the Red Queen hypothesis, after the Red Queen in Lewis Carroll's book *Through the Looking Glass*, who takes Alice on a run that never seems to go anywhere. "Now *here*, you see, it takes all the running *you* can do to keep in the same place," the Red Queen explains.

The Red Queen conundrum, some researchers have argued, may give an evolutionary edge to sex. Asexual strains can never beat out sexual strains, because whenever they get too successful, parasites build up and devastate the strain. Sexual organisms, meanwhile, can avoid these dramatic booms and busts because they can shuffle their genes into new combinations that are harder for parasites to adapt to.

Red Queen models for sexual reproduction are very elegant and compelling. But testing them in nature is fiendishly hard, because biologists need asexual and sexual organisms that share the same environment and parasites. One of the few test cases scientists have found is *Potamopyrgus antipodarum*, a snail that lives in New Zealand lakes. Some snails have to mate to reproduce; others don't.

Curt Lively of Indiana University, Bloomington, and his colleagues have spent nearly 30 years painstakingly studying the snails and one of their parasites, a fluke that can sterilize them. In a paper in press at *The American Naturalist*, Lively and collaborators Jukka Jokela of the Swiss Federal Institute of Aquatic Science and Technology and Mark Dybdahl of Washington State University, Pullman, present some of the most compelling evidence gathered so far for the Red Queen at work.

Over the course of the past 15 years, Lively and his colleagues have documented a parasite-driven boom-and-bust cycle in asexual snails, a cycle just as the Red Queen would predict. In a New Zealand lake in 1994, the most common strains of asexual snails were initially resistant to the most common flukes. Over time, the snails became more and more vulnerable, as a well-adapted fluke strain infected them. By 2004, the snails had all but disappeared. Meanwhile, a rare strain of asexual snails in 1994 became the most common, apparently because it was resistant to the fluke strain sickening the previous dominant strain of snails. "We didn't expect to see such a dramatic shift in our lifetimes," says Lively.

As the flukes drove the asexual snails through boom and bust, the population of sexual snails has remained relatively steady, Lively says. That stability is consistent with the idea that the Red Queen effect can give sexual organisms an edge.

Yet Lively doesn't think that the Red Queen on its own can fully account for the staying power of sex. Once an asexual strain of hosts becomes rare, its parasites become rare, too. So the Red Queen can't wipe out asexual reproduction altogether.

It's possible that the Red Queen may be able to work more effectively to promote sex by cooperating with another force. For example, the Red Queen may drive asexual populations down to small numbers, which may make it easier for harmful mutations—the "bad"—to build up.

"There are a lot of people who don't like this fusing of hypotheses," admits Lively. "It gets messy, and it gets hard to test." Yet Lively and some other researchers think that messiness is no reason to reject the possibility that sex has many masters. It won't be surprising if a mystery so hidden in darkness turns out to have more than one answer. **–CARL ZIMMER**

Carl Zimmer's latest book is *Microcosm: E. coli and the New Science of Life*.

Oh, how sexy. That animals as diverse as (*left to right*) guppies, peacocks, and dung beetles are picky about their mates may help ensure that sexual reproduction prevails.

CREDITS: JUPITERIMAGES

Published by AAAS

Deceleration? Ford engineers celebrate breaking 200 mph with the company's hydrogen car, a technology now out of favor with the Obama Administration.

TRANSPORTATION RESEARCH

Hydrogen Cars: Fad or the Future?

The Obama Administration wants to end the hydrogen fuel cell vehicles program, which proponents see as the ultimate clean-car technology

In May 2007, engineers from General Motors pumped 8 kilograms of compressed hydrogen gas into each of two GM Sequels, among the company's most advanced hydrogen fuel cell cars. The fuel, produced by splitting water into hydrogen and oxygen, was generated using renewable electricity from nearby Niagara Falls, on the U.S.-Canadian border.

The two cars were driven 482 km, from Rochester to Tarrytown, New York. Instead of emitting roughly 90 kilograms of carbon dioxide (CO_2) during the journey, their tailpipes puffed only water vapor. "It was the world's first 300-mile drive that was petroleum-free and emissions-free on a single tank of fuel," explained GM's R&D chief, Larry Burns, at an alternative fuel vehicles meeting in March 2008.

The drive may have been historic, but it didn't impress the Obama Administration. Last month, Energy Secretary Steven Chu announced that the Department of Energy (DOE) was putting the brakes on research into automotive hydrogen fuel cells. Chu cites the cost and durability of vehicle fuel cells, the inability to store large volumes of hydrogen fuel, the absence of a carbon-free way of generating the hydrogen, and the need to build a nationwide refueling infrastructure. The issue came down to a simple question, says Chu: "Is it likely in the next 10 or 15 or even 20 years that we will convert to a hydrogen-car economy? The answer, we felt, was no."

But many scientists and energy experts believe Chu asked the wrong question and, therefore, made the wrong call. No alternative-vehicle technology will make a major impact on carbon emissions, petroleum use, or anything else within the next 20 years, they say, because it takes longer than that for a new technology to displace what is already on the road. In the long run, they say only two technologies—hydrogen fuel cells and electric vehicles—are capable of getting the job done. And only one variation, plug-in hybrids, will be on the market anytime soon. "There are uncertainties with both these technologies," says Joan Ogden, who heads the sustainable transportation energy program at the University of California, Davis. "So the idea of taking one off the table seems shortsighted."

Some influential politicians are also unhappy with Chu's proposed policy shift and have vowed to block the cuts. "I, for one, am not interested in shutting down these research projects," says Senator Byron Dorgan (D–ND), who chairs the spending panel that will act on the president's 2010 budget request, which saves $100 million by eliminating the vehicle portions of the program while maintaining $68 million for stationary fuel-cell power plants viewed as closer to the market. Speaking at a hearing last month during which Chu laid out the Administration's plans, Dorgan declared, "We are going to do everything we can to continue the [vehicle program]."

Making the case

Invented in 1839, fuel cells use catalysts to combine hydrogen and oxygen to produce water and electricity. Their ability to generate electricity without CO_2—at least within the fuel cell itself—has spawned recurring visions of a carbon-free hydrogen economy. The Bush Administration embraced the idea in 2003 when it rolled out what became a $1.5 billion research program to make hydrogen fuel cell vehicles practical and affordable. Since then, car companies have spent billions of dollars of their own money and produced two generations of cars, 318 of which remain on the road. Toyota, GM, and Honda have said that they will continue to invest in the technology regardless of what DOE decides to do.

Hydrogen proponents don't dispute that hydrogen fuel cell technology lags a few years behind plug-in hybrids. However, they argue that it's improving rapidly in virtually all areas. "We cannot abandon one of the most promising technologies around just because it is not ready for commercialization in the next 2 years," says Ronald Grasman, an automotive engineer who manages fuel-cell market development for Daimler in Kirchheim, Germany.

Grasman and others point out that the ultimate goal is not how quickly alternative-fuel vehicles are adopted but how fast greenhouse gas emissions and the use of petroleum can be reduced. Even if plug-in hybrids hit the market first, their impact on carbon emissions will be modest initially because they rely on electricity generated primarily by burning fossil fuels. A recent analysis by C. E. "Sandy" Thomas, whose Virginia company H2Gen Innovations makes reformers that convert natural gas into hydrogen, found that hydrogen cars would actually reduce CO_2 emissions more than plug-ins would by 2030, and the gap widens as the decades pass.

A big reason is their source of power. Most electricity in the United States is generated by burning coal, Thomas notes, and coal emits nearly twice as much carbon as does natural gas, the fuel most commonly used to generate hydrogen. In addition, fuel-cell electric engines are twice as efficient as the combustion engines that are still required in hybrids. A clean, carbon-free source of energy is needed for either fuel cell or electric vehicles to meet their potential, Thomas acknowledges.

The Obama Administration has already called for cutting U.S. carbon emissions 80% below 1990 levels by 2050. In the transporta-

CREDIT: WENN/NEWSCOM

Published by AAAS

THE CASE **AGAINST** HYDROGEN FUEL CELL CARS...

Energy Secretary Steven Chu says there are no quick fixes to these pressing technological challenges:

- Inexpensive and long-lasting fuel cells
- Adequate fuel storage capacity at a reasonable price
- A carbon-free way to generate the hydrogen
- A nationwide refueling system

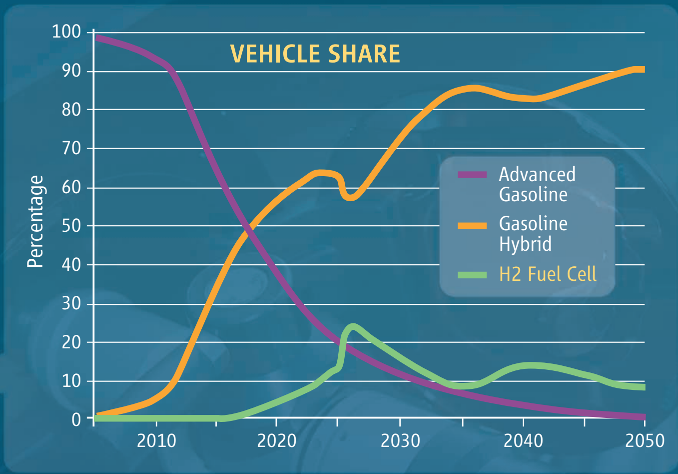

▲ **Niche player.** Hydrogen cars lose out to gasoline hybrids under this DOE scenario, in which storage costs remain high.

tion sector, which accounts for more than one-quarter of all carbon emissions, "you can't accomplish that without hydrogen vehicles," says Robert Shaw Jr., a venture capitalist and founder of Aretê Corp. in Center Harbor, New Hampshire. Shaw was vice chair of a National Research Council (NRC) panel that looked at the viability of hydrogen cars and their potential impact by 2050.

The NRC report, published last year, concluded that improvements in conventional vehicles, switching to gas-electric hybrids, and using biofuels would be the best first step in reducing CO_2 emissions. But "hydrogen offers greater longer-term potential," reads the report. "The greatest benefits will come from a portfolio of R&D technologies that would allow the United States to achieve deep reductions in oil use" by 2050. A follow-on NRC panel is now reviewing the role of plug-ins.

An uphill road

DOE officials, from Chu on down, would probably agree with that overall assessment of the promise of hydrogen vehicles. But that doesn't mean they think they're a safe bet. "There is really a lot of progress, but issues remain," says Sunita Satyapal, who directs DOE's hydrogen program.

One major concern is price, in particular, the high cost of precious-metal catalysts. Today's fuel cell engines could be built for $73 a kilowatt if mass-produced, according to a recent DOE estimate, a 74% drop since 2002 but still more than twice the 2015 target price.

The range of today's cars is also a problem. High-pressure tanks used by today's fuel cell cars hold enough fuel for the average fuel cell car to travel 320 km, according to the latest tally from researchers at the National Renewable Energy Laboratory in Golden, Colorado. By 2015, DOE hopes to achieve 480 km, a distance that would satisfy consumers.

Durability is another issue. Some of the fuel cell cars have operated for 2000 hours without need of servicing, the equivalent of driving 96,000 km, and DOE would like to boost that number to 5000 hours. Finally, despite hydrogen's widespread use in industry, no infrastructure exists for producing vast amounts of hydrogen and delivering it to drivers when and where they need it.

Given these hurdles, Chu and his DOE colleagues argue that it makes more sense to focus on areas with the potential to make the quickest impact, notwithstanding that the average car stays on the road for 15 years. "With plug-in vehicles, you can start that process now," says Patrick Davis, who heads DOE's Vehicle Technologies Program in Washington, D.C. "With other technology, you have to start that clock later." Mass-produced hydrogen cars may be 2 decades away. And if the onboard hydrogen-storage problem isn't solved, customers simply won't buy the cars.

Fuel-cell cars aren't the only alternatives facing a rough road, however. Battery electric vehicles (BEVs) have cost and technology problems of their own. Mass-produced BEVs with a range of more than several dozen kilometers are years away. And better batteries will be expensive.

A 2007 study by automotive engineers John Heywood and Matthew Kromer at the Massachusetts Institute of Technology in Cambridge projected the cost of various advanced technologies and found that all make a bigger dent in the wallet than advanced internal combustion engines. A plug-in hybrid with an all-electric range of only 16 km would cost an extra $3000, for example, whereas an electric vehicle with a range of 320 km would add $10,200 to the sticker price. The long-distance winner, a hydrogen car that could travel 400 km between fill-ups, would cost an extra $3600.

"None of these technologies are free," Shaw says. Adds Heywood: "It's really battery cost versus fuel-cell cost. Cost reduction is a major challenge for both these paths." Klaus Bonhoff, managing director for Germany's National Organization for Hydrogen and Fuel Cell Technology, agrees: "People are overselling battery technology today. They will not be able to do the [complete] job that people expect."

(IMAGES) PEG SKORPINSKI; NATIONAL HYDROGEN ASSOCIATION; (GRAPH) ADAPTED FROM D. L. GREENE *ET AL.*, OAK RIDGE NATIONAL LAB (2009)

THE CASE **FOR** HYDROGEN FUEL CELL CARS...

Proponents say hydrogen cars are a good bet because:

- They will eventually deliver the biggest reduction in greenhouse gas emissions
- Electric vehicles face similarly tough challenges
- The nation needs a balanced fleet of alternative vehicles
- The cost of making the fuel cells is approaching DOE targets

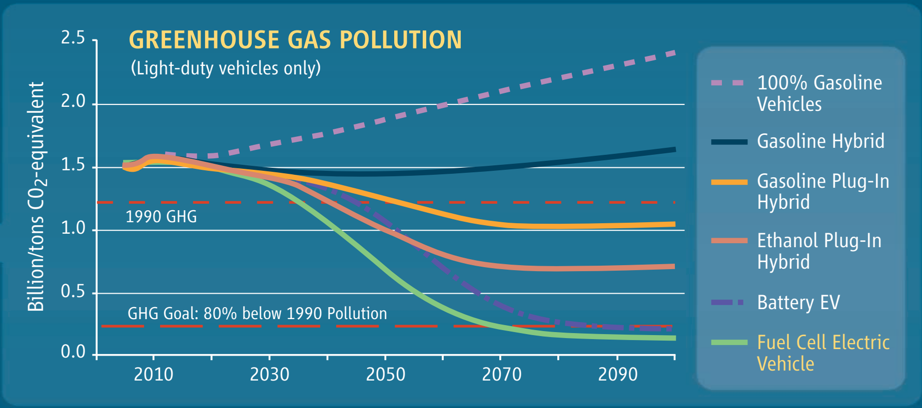

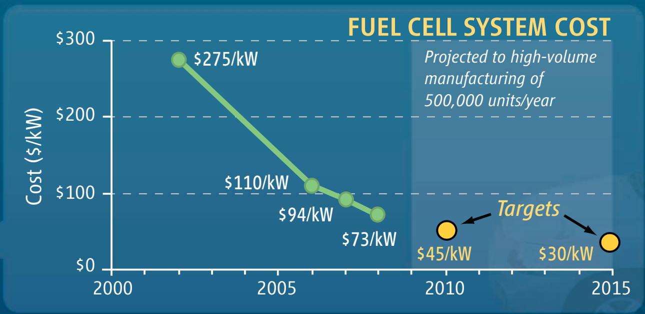

Clean sweep. Fuel cell vehicles reduce greenhouse gas emissions faster than any other technology in the U.S. fleet.

Both technologies need to develop a better way to deliver energy to consumers. Hydrogen would appear to face the bigger challenge: Only 71 hydrogen refueling stations exist in the United States and Canada, and the distribution system is likewise scant. The NRC panel estimated that the U.S. federal government would need to spend about $10 billion between 2008 and 2023 to develop a self-sustaining hydrogen-fuel infrastructure and another $44 billion on tax credits and other subsidies, while industry invests $145 billion.

In comparison, the nation already has an electric utility grid, and a 2006 study by researchers at the Pacific Northwest National Laboratory found that the existing grid could charge up to 70% of all cars and light trucks in the United States if they were plug-ins that were charged overnight when idle generation capacity is available. But battery-powered cars also need sockets into which to plug. A 2008 study by researchers at the Idaho National Laboratory estimated it would cost $878 to $2146 to add the home circuits needed to charge a plug-in. And recharging takes several hours, compared with just a few minutes for a hydrogen fill-up.

Then there's fuel storage, which DOE's Satyapal says remains a "significant challenge" for hydrogen cars. In recent years, DOE has backed research on some 200 different storage materials, ranging from packing hydrogen into metal solids called metal hydrides to a slurry of alane powder in a light mineral oil. To date, none meets DOE's targets for storing and releasing enough hydrogen fuel on demand.

But automotive engineers don't seem overly concerned. Daimler's new B-class fuel-cell engines have a range of 400 km using a tank that pressurizes hydrogen to 700 bar, and GM's Sequels have already gone farther than that. In addition, reducing the size and weight of the fuel cells and other electronic systems has left more room for larger storage tanks. "Storage technology is not the issue," Daimler's Grasman concludes.

The trends are similarly positive with respect to improving the durability of fuel-cell engines, lowering the cost of producing hydrogen, and finding a low-carbon means of doing so. Lab-based fuel cells have far surpassed DOE's 5000-hour benchmark, and natural gas can be turned into hydrogen for $3 per kilogram of hydrogen (the equivalent to how far a car will go on a gallon of gasoline). As renewable-energy technologies improve, they can be used to generate hydrogen as well as electricity.

The road ahead

Given this progress, many hydrogen experts were caught off-guard by Chu's announcement last month. "Everybody I know in the hydrogen field is just puzzled by this decision," Shaw says. Philip Ross, a retired chemical engineer from Lawrence Berkeley National Laboratory and member of a DOE technical panel that is supposed to advise DOE's upper management on the hydrogen program, says Chu did not contact the committee before announcing his new direction.

Chu and his aides also did not reply to requests from *Science* for comment. However, when he announced DOE's fiscal year 2010 budget, Chu said the department is not giving up on fuel cells altogether. In addition to continuing to support stationary fuel cells, DOE will back basic research to improve the catalysts and other components of the systems.

Even if Congress restores the program's funding, some hydrogen backers worry that Chu's statements have already damaged the industry. "It has really hurt the public perception of this field," Grasman adds. Such skepticism, when combined with the industry's overall financial woes, could undermine corporate support for the technology, Grasman contends.

That outcome would leave Chu in the position of supporting a policy that could significantly delay the potential climate and energy-security benefits he believes alternative vehicles can deliver. Says Shaw: "If you want to get to the volumes [of cars] necessary to make an impact, you have to begin immediately."

–ROBERT F. SERVICE

CREDITS (TOP TO BOTTOM): C. E. THOMAS/NATIONAL HYDROGEN ASSOCIATION ANNUAL CONFERENCE (2009); SUNITA SATYAPAL/DOE (2009)

Published by AAAS

"Magnificent achievement." Japan has broken through a key bluefin tuna breeding barrier.

MARINE BIOLOGY

Persevering Researchers Make a Splash With Farm-Bred Tuna

A 30-year effort has paid off in raising bluefin tuna in captivity, but the benefit for wild stocks of the embattled predator may be years more away

OHSHIMA, JAPAN—With a snap of its jaws, a meter-long bluefin tuna grabs a fish tossed into its circular enclosure and darts away in murky Kushimoto Bay. "They're excellent swimmers," says Yoshifumi Sawada, a fisheries biologist at Kinki University's Ohshima Experiment Station, as he shovels fish into the water. The note of pride in his voice is understandable: The bluefins in the pen are the product of a 30-year effort to rear second-generation captive tuna—something no other group in the world has accomplished. It's "a magnificent achievement," says Daniel Pauly, a fisheries biologist at the University of British Columbia, Vancouver.

The feat could hold vital significance for one of the ocean's keystone predators. In recent decades, the bluefin tuna's succulent belly meat has become the favorite of sushi and sashimi aficionados, driving the price sky high. Tunas auctioned at Tokyo's Tsukiji fish market routinely fetch tens of thousands of dollars; in 2001, a prize 202-kilogram specimen sold for an astounding ¥20.2 million, or roughly $1000 per kilogram.

To satiate rising demand, dozens of tuna farms have sprung up off Japan's coasts. Each year, Japanese fishers capture 300,000 to 400,000 young bluefins from the open ocean and fatten them in pens before shipping them off to wholesalers. But removing juveniles from the wild has only increased pressure on the heavily fished species, leaving some populations on the brink of collapse (see sidebar).

The bluefin's eccentricities have contributed to its downfall. "The bluefin tuna has habits that are completely wrong for species survival," says Gary Sakagawa, a fisheries biologist at the U.S. National Oceanic and Atmospheric Administration's Southwest Fisheries Science Center in San Diego, California. For instance, young tuna congregate in coastal areas in spring and summer as they feed on schooling fish, making them easy prey for fishers, Sakagawa says.

The researchers at Kindai, as the university is known locally, hope their breakthrough will give wild tuna a reprieve. "We want to supply all of the farmed bluefin tuna harvested in Japan," says Sawada. They have a long way to go. This year, Sawada says they hope to sell up to 20,000 juveniles to fish farms, a small fraction of what's needed. "This technology will take a while to have a positive impact on the conservation of tuna," says Pauly.

Tuna kahuna. Fisheries biologist Yoshifumi Sawada.

Kindai's tuna program started in 1970, when "it seemed Japanese were eating up all the world's tuna," says university trustee Hidemi Kumai, a fisheries biologist who led the Kindai research for years. Concerned that the country would be blamed for depleting wild tuna stocks, Japan's Fisheries Agency funded three groups, including one at Kindai, to try raising bluefin tuna from eggs.

As a private university with campuses scattered across a rugged peninsula that juts into the Pacific Ocean southeast of Osaka, Kindai emphasizes "practical studies" attuned to the needs of local agricultural and fishing communities, Kumai says. Kindai had already succeeded in raising yellowtail, sea bream, sole, and other fish from eggs. The university sells fry to farmers and harvests mature fish for the market, then sinks the proceeds into research.

The know-how gleaned from farming other fish, however, didn't readily transfer to bluefins. "Tuna have many unique characteristics that make culturing them difficult," says Sawada. For starters, bluefin tuna, one of the larger oceanic predators, are simply much bigger than other farmed fish. A half-century ago, before overfishing started to take its toll, 4-meter-long tuna tipping the scales at half a ton were common. These days, mature bluefins can exceed 2 meters in length and weigh 250 kilograms.

When it comes to captive breeding, more than size matters. Tuna, unlike most pelagic fish, are warm-blooded. And like some sharks, they must move continuously to force water over their gills; otherwise, they suffocate. "They swim all day, all through their lives," Sawada says. Bluefins are built for both speed and endurance: They can accelerate as quickly as a sports car, and they crisscross the Atlantic several times a year. For these reasons, tunas require pens much bigger than those used for other captive fish.

It took the Kindai group 4 years to learn how to keep penned tuna alive longer than a few months. Then it took another 5 years, until 1979, to get them to spawn. That was a world first, Kumai says, but his team couldn't keep the spawned fish alive. Then, for more than a decade, they couldn't get captive tuna to spawn at all.

Facing similar difficulties, the two competing research groups gave up, and Kumai worried that Kindai's program would get the ax. At one point, he confessed to Kindai's

CREDITS (TOP TO BOTTOM): FISHERIES LABORATORY OF KINKI UNIVERSITY; DENNIS NORMILE/*SCIENCE*

Published by AAAS

president that his team had "no results despite spending a lot of money." "The president said to me, 'You have to take the long view when considering living creatures,' " Kumai recalls. With such encouragement, he says, the group resolved to "succeed in this project at any cost." (The price of success is hard to quantify, he says, as the Fisheries Laboratory, with an annual budget of about $25 million, doesn't itemize expenses by project.) Finally, in 1994 their captive tunas spawned again.

Through sheer persistence, the team has gained a trove of information about tuna biology. Postmortems on dead juveniles revealed that many fish were snapping their necks by swimming into the walls of the square enclosures. Such injuries tapered off after fish passed their 80th day. In juvenile tuna, the tail fin, used for propulsion, develops more quickly than the pectoral and abdominal fins, which adults use to steer and brake, Kumai says. "The only thing [juvenile] tuna can do is dash straight ahead," he says. To reduce the number of deadly collisions, the researchers switched to circular enclosures.

After numerous other tweaks to rearing techniques, the Kindai team eventually bred mature fish. Six fish spawned in 1995, and 16 from the class of 1996 survived to adulthood. Those fish spawned in 2002, and Kindai is now rearing the third generation. "We've completed the life cycle," Kumai says. That, says Sakagawa, "gives us some idea what may be going on in nature." The Kindai group has identified behavioral triggers for spawning and clarified that the time of first spawn is more closely related to size than age. The group acknowledges that they still have a lot to learn. Kumai figures they get mature fish from only about 1% of eggs, compared with 60% for sea bream.

The Kindai group now hopes to develop an attractive product. They are selectively breeding tuna for fast growth, disease resistance, and higher-quality meat, Sawada says. The group does not plan to genetically engineer tuna out of concerns about unforeseen consequences if fish were to escape into the wild. But they are introducing the use of molecular markers, small DNA fragments that identify desirable traits, says Yasuo Agawa, a molecular biologist who cut his teeth on Drosophila and recently joined the Kindai team. Pauly, however, worries that the feed requirements of scaled-up tuna farming could harm wild stocks of feed fish, many of which are a staple for people in developing countries.

That might be avoided if the Kindai group's most ambitious plan succeeds: to transform their captives into vegetarians. Sawada says they intend to gradually substitute plant protein for fish feed, in part to improve the program's sustainability. Pauly, for one, is skeptical. "This is where these plans veer off into science fiction," he says. He notes that despite decades of trying, the Norwegian salmon industry has not weaned farmed salmon off a fish diet.

It is unclear what impact the landmark breeding success might have on wild tuna stocks. Sakagawa worries that replacing fish caught for farms with juveniles raised from eggs might simply expand the market, as happened when Australian fisheries started pen-rearing captured Southern Pacific bluefins. He says he appreciates Kindai's contributions to understanding tuna reproductive biology. However, Sakagawa says, "I don't think it's a solution for conservation of wild stocks."

Toward that end, Japan's Fisheries Research Agency is working to raise tuna from eggs for release. To have an impact on natural populations, a restocking effort would have to be massive—and "many issues need to be solved before [we can] start to release tuna," says agency official Kazumasa Ikuta. But as the Kindai team has demonstrated in their decades-long effort to breed tuna, patience is a virtue.

–DENNIS NORMILE

Scientists Get No Respect From Fishery Managers

Last June, when a scientific panel met to review the health of the bluefin stock in the East Atlantic and Mediterranean, they were miffed to find they had so little to go on. Only three of 48 member countries and regions of the International Commission for the Conservation of Atlantic Tunas (ICCAT) had reported 2007 catch data. Despite that handicap, the ICCAT advisory panel gleaned that the situation was grave: The 2007 bluefin catch, they estimated, was roughly 61,000 tons—more than double ICCAT's limit.

In its report,* the Standing Committee on Research and Statistics warned that overfishing "will most probably lead to further reduction in spawning stock biomass with high risk of fisheries and stock collapse." To forestall that disaster, the scientists recommended that ICCAT set a quota of 15,000 tons starting in 2009. ICCAT's response: quotas of 22,000 tons in 2010, 19,950 tons in 2011, and 18,500 tons in 2012. "Even in 3 years, the quotas will be higher than what scientists recommended the quotas be immediately," fumes Rebecca Lent, an economist in charge of international affairs for the U.S. National Oceanic and Atmospheric Administration's National Marine Fisheries Service.

ICCAT's problems run deeper than quota setting. In a September 2008 report, an independent review panel chaired by Glenn Hurry, CEO of the Australian Fisheries Management Authority in Canberra, concluded that ICCAT's management of bluefin tuna fisheries for sustainable fishing "is widely regarded as an international disgrace."

In response to an e-mail asking for comment on the catch quotas, ICCAT Assistant Executive Secretary Victor Restrepo wrote, "We abstain from interpreting how or why the Commission makes decisions." He added that a meeting on ICCAT's future planned for next August will address questions raised by the review panel.

Stock mismanagement hasn't yet dealt a crippling blow to bluefin stocks in the Western Atlantic and the Pacific. Although stock assessments are clouded by gaps in the data, scientists recommended there be no increase in Pacific bluefin catches above the current 23,000 tons a year. This covers taking mature tuna but not capturing juveniles for pen-fattening. **–D.N.**

*www.iccat.int/Documents/Meetings/Docs/2008_SCRS_ENG.pdf

Reported Catch

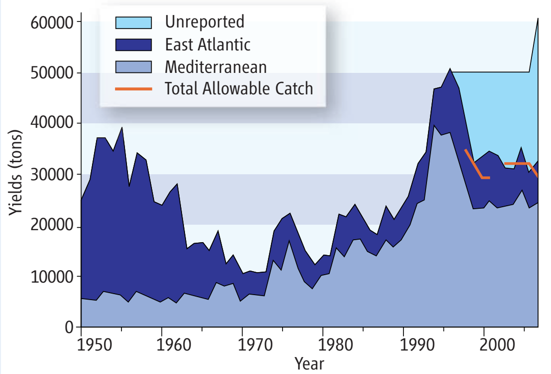

Under the radar. By official numbers, East Atlantic and Mediterranean bluefin tuna catches have declined, but unreported catches have soared.

CREDIT: ICCAT

ASTRONOMY

The Tales Told by Lonely Galaxies

To what extent is a galaxy shaped by its surroundings? To find out, astronomers are seeking the rare ones that appear to be isolated

Unblemished beauty. Isolated galaxies like NGC 7217 may have evolved undisturbed for billions of years.

GRANADA, SPAIN—Laden with 400 billion stars, countless planets, and vast clouds of gas, our Milky Way galaxy pinwheels through the void. Its spiral arms stretch 50,000 light-years and revolve once every 220 million years, as we plunge at 400,000 kilometers per hour toward the neighboring Andromeda galaxy. That's well known, but it's less clear how the Milky Way—or any other galaxy—came to appear as it does.

In the century since the first distant ones were recognized, astronomers have learned much about how galaxies form and evolve. But they still don't know to what extent a galaxy's properties are determined by its inner workings or through interactions with its surroundings—such as the Milky Way's potential collision with Andromeda in 3 billion years. In short, astronomers want to know how much of a galaxy's character is set by nature and how much by nurture.

To solve that puzzle, some astronomers are searching for rare galaxies well isolated from their neighbors. By comparing these loners to their more-gregarious brethren, researchers hope to tease apart the inherent inner workings of galaxies and the effects of interactions. Last month, 120 researchers gathered here to discuss such efforts.*

"If there really are significant numbers of isolated galaxies, and if we can collect large enough samples of them, then they're certain to provide some sort of fundamental insight into galaxy evolution," says Jack Sulentic, an astronomer here at the Institute for Astrophysics of Andalusia (IAA). Astronomers have searched for isolated galaxies before, but recent massive galaxy surveys may unearth many more of the gems.

The notion of an isolated galaxy may be something of an oxymoron, however. Galaxies form through a "hierarchical process" in which smaller ones merge to make bigger ones, researchers think. So each galaxy is in fact the product of galaxy interactions. "I think there are no isolated galaxies," says Bärbel Koribalski, an astronomer at the Australia Telescope National Facility in Epping. Still, the few galaxies that appear to be lingering alone are worth studying, says Christian Theis, a theoretical astrophysicist at the University of Vienna in Austria. "Even if they're not formed in isolation, they may have evolved in isolation for some time," he says. "So they can give some insight into the inherent processes of evolution."

Gathering the outcasts

The first major catalog of isolated galaxies was created in 1973 by Valentina Karachentseva of Taras Shevchenko National University of Kyiv in Ukraine, working with her husband, Igor Karachentsev of the Special Astrophysical Observatory in Nizhnij Arkhyz, Russia. "We divided our work," she says. "Igor worked with the pairs, and I work on the isolated galaxies."

Karachentseva analyzed photos taken in the 1950s with a 1.2-meter telescope in the famed Palomar Observatory Sky Survey. She declared a galaxy isolated if no neighboring galaxy lay closer than 20 times the neighbor's radius or was more than four times as big in diameter as the galaxy in question. Those rules selected galaxies that had not suffered an interaction in roughly 3 billion years. The Karachentseva catalog of 1051 galaxies is "still the best game in town," say Sulentic, who works on the Analysis of the Interstellar Medium of Isolated Galaxies (AMIGA) project at IAA.

Now, however, astronomers are trawling the enormous data sets produced in the past decade in ever-bigger sky surveys. In optical wavelengths, the Six-Degree Field Galaxy Redshift Survey has used a 1.2-meter telescope on Siding Spring Mountain, Australia, to pinpoint a total of 125,071 galaxies; the Two-Degree Field Galaxy Redshift Survey has used a neighboring 4-meter telescope to spot 221,414 more; and the Sloan Digital Sky Survey has used a 2.5-meter telescope on Apache Point, New Mexico, to bag 930,000 of them.

The new data allow astronomers to fix a galaxy's position in three-dimensional space, not just on the two-dimensional celestial sphere. As the universe expands, the galaxies speed apart. The more distant a galaxy, the faster it recedes. The motion stretches a galaxy's light to longer, redder wavelengths, so by measuring that "redshift," astronomers can deduce the galaxy's speed and distance.

Using Sloan data, Hong Bae Ann of Pusan National University in South Korea has sifted through 100,000 galaxies lying between 275 million and 700 million light-years away to find about 500 isolated ones. Meanwhile, Karachentsev has used data from all three big surveys to pick out 513 isolated galaxies lying within 135 million light-years. Karachentseva has spied 3227 of them using data from the near-infrared Two Micron All-Sky Survey conducted with twin 1.3-meter telescopes on Mount Hopkins, Arizona, and Cerro Tololo, Chile.

*Galaxies in Isolation: Exploring Nature vs. Nurture, 12–15 May.

CREDIT: MISCHA SCHIRMER (ING) AND GILLES BERGOND (IAA, GRANADA)

Published by AAAS

But as catalogs proliferate, so do the criteria used to define isolation and the tensions between them. Ann focuses on the galaxies' masses and separations, and he can set his criteria so that his list recaptures 80% of the 1973 Karachentseva catalog. However, Ann seeks extremely isolated galaxies, and when he tightens his criteria the lists do not overlap at all, he says.

Whether a galaxy appears isolated may also depend on the method used to observe it, says Oded Spector of Tel Aviv University in Israel. He used the 1-meter telescope at the Wise Observatory near Mitzpe Ramon, Israel, to spot 27 extremely isolated galaxies. He then compared the optical data with data from ALFALFA, a radio survey using the 305-meter dish at the Arecibo Observatory in Puerto Rico that can detect hydrogen gas and reveal galaxies too faint to be seen with optical and infrared instruments. The ALFALFA data showed that nine of Spector's galaxies had companions after all. "One of these had seven neighbors," he says.

Compare and contrast

Still, the few isolated galaxies there are may shed light on galaxy content, behavior, and structure, researchers say. Theorists generally agree that the cosmos took shape after the big bang as dark matter—the mysterious stuff whose gravity binds the galaxies—coalesced into clumps. Smaller clumps merged to make bigger clumps and form a vast "cosmic web" of filaments and sheets separated by voids. Meanwhile, the dark matter clumps or "halos" drew in hydrogen gas from which stars and galaxies formed like raindrops condensing in clouds.

Researchers hope to fill in some of the details within this big picture. One question is whether star formation depends on a galaxy's environment. Galaxies in crowds are often "red and dead": Their stars are reddish in color, and the galaxies have stopped making new ones. That could be a natural effect of aging, as the radiation from the galaxies themselves blows out the gas needed to make new stars. Or interactions with other galaxies may have stripped out the gas.

Striking a blow for interactions and nurture, Angela Iovino of the Astronomical Observatory of Brera in Milan, Italy, and colleagues tallied galaxies as far away as 11 billion light-years (a redshift of 100%) using the Very Large Telescope on Cerro Paranal, Chile. They find signs that isolated galaxies fade from blue to red more slowly than those in groups do. "Isolated galaxies stay younger longer," Iovino says.

But Jeremy Tinker, a theorist at Lawrence Berkeley National Laboratory in California, argues for nature. Simulations of the large-scale structure of the cosmos reproduce the observed distribution of galaxy clusters and voids only if a galaxy's color and fertility depend on the mass of its dark matter halo alone, he says. "The probability of being red has to be independent of the environment," he says.

Other studies are probing the tricks of a galaxy's heart. A galaxy can possess a radiation-spewing "active galactic nucleus" (AGN) that presumably arises when gas falls into the supermassive black hole in the galaxy's center and heats up to a temperature of millions of degrees. Researchers think that can happen when one galaxy jostles another. But can it happen in an isolated galaxy?

To find out, IAA's José Sabater looked for AGNs as part of the AMIGA project, which reanalyzes the galaxies in Karachentseva's 1973 catalog using new data. With data from the Sloan survey and elsewhere, he found that 21% of 353 isolated galaxies had AGNs. That's well below the 33% rate that M. Angeles Martinez of the University of Zaragoza in Spain found in her study of galaxies in groups. The results don't necessarily prove that a galaxy can toss gas on its own heart to make an AGN, Sabater says: An isolated galaxy with an AGN may have been perturbed while consuming a now-vanished companion.

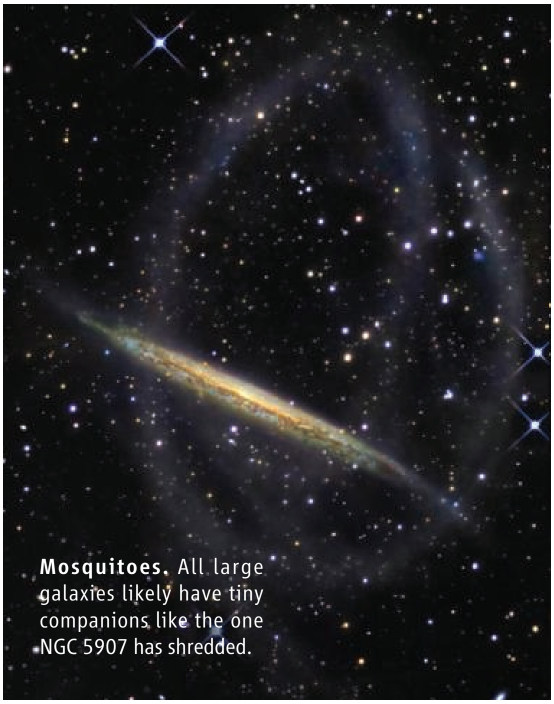

Mosquitoes. All large galaxies likely have tiny companions like the one NGC 5907 has shredded.

CREDIT: R. JAY GABANY/COSMOTOGRAPHY.COM

Still, the results put a limit on what a galaxy can do alone. AGNs come in two types: those that emit radio waves and those that are "radio quiet." Sabater finds only radio-quiet AGNs in isolated galaxies. "We can conclude that the environment is fundamental for triggering a radio AGN," he says.

Astronomers would also like to know what sorts of structures a galaxy can generate by itself. Theorists generally agree that bloblike elliptical galaxies can form only through galaxy mergers, whereas a well-isolated galaxy has a strong tendency to form a spiral. Data seem to back that up: The various studies suggest that fewer than 20% of isolated galaxies are elliptical.

Isolated galaxies have already given theorists modeling structure something to puzzle over, however. AMIGA researchers find that at least two-thirds of the isolated spirals lack the prominent bulges often seen in spiral galaxies such as the Milky Way. "Bulgeless spirals are a challenge to the simulations, because they don't produce them in great numbers," says Evangelia Athanassoula of the Astronomy Observatory of Marseilles Provence in France. So theorists may have to rethink certain details of galaxy structure formation.

A loner and its companions

The question of what counts as isolation among galaxies can be subtle, as becomes clear when researchers turn to the Milky Way. The Milky Way has remained relatively unmolested for billions of years, and theorists need invoke no external influence to explain its properties, says François Hammer, an astronomer at the Observatory of Paris. By that measure, "I would say that the Milky Way is isolated," Hammer says.

But the Milky Way is surrounded by tiny dwarf galaxies—"mosquitoes," conference attendees call them—some of which it is shredding. "The companions of the Milky Way definitely feel its effect," says Eric Wilcots of the University of Wisconsin, Madison. Given that it's ripping its neighbors apart, the Milky Way might also exemplify an interacting galaxy.

Such ambiguity aside, the search for isolated galaxies seems likely to continue as ever more data become available. The Sloan survey measured the positions of 930,000 galaxies; the proposed 8-meter Large Synoptic Survey Telescope would pinpoint billions. The data might reveal inherent and environmental effects too small to be seen now. "I think we have a good chance to solve this problem" of the relative importance of nature and nurture in galaxy evolution, Hammer says. However, the answer may depend on how precisely you define the question.

–ADRIAN CHO

Summer reading

1267

Glimpsing platinum nanoparticles growth

1276

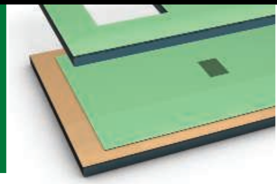

LETTERS

edited by Jennifer Sills

Stem Cell Debate Extends to Scientists

IN AN ARTICLE PUBLISHED AS "NEWS" ("A FIRST STEP IN RELAXING RESTRICTIONS ON STEM CELL research," C. Holden, News of the Week, 13 March, p. 1412), a one-sided depiction of the debate among scientists on embryonic stem cell research is presented. The article reports President Obama's signing of an executive order that lifts the restrictions on stem cell research laid down by President Bush in 2001. Instead of beginning the article "Scientists are breathing a huge sigh of relief," Holden should have begun by stating that "*Some* scientists are breathing a huge sigh of relief." She should have recognized that not all scientists support embryonic stem cell research and not all are relieved at President Obama's recent action.

SUSAN BOACKLE

University of Colorado Denver, Aurora, CO 80045, USA. E-mail: susan.boackle@ucdenver.edu

A Step Ahead on the HIV Collaboratory

IN THE REVIEW "THE CHALLENGE OF FINDING a cure for HIV infection" (6 March, p. 1304), D. D. Richman *et al*. suggest that a "collaboratory"—a consortium involving government [here referring to the National Institutes of Health (NIH)], academia, and the pharmaceutical industry—work together to address the specific and unique challenges required to eradicate HIV from latently infected cells while simultaneously continuing viral suppression with conventional combination therapies.

The term "collaboratory" was first used by the National Science Foundation to describe a computer and information science network in 1989 (*1*). Eight years ago, the term was used to describe one of the NIH's Centers for AIDS Research that had partners located in four states (*2*). In 2001, with support from the Bettencourt Schueller Foundation of France, we set up Objectif Recherche Vaccin Sida (ORVACS), a not-for-profit organization that networked major academic institutions in France (Université Pierre et Marie Curie–Paris), the United Kingdom, Spain, Belgium, Italy, and the United States. Our objective was to speed up the evaluation of new treatment strategies based on therapeutic immunization to control HIV as an alternative to conventional antiretroviral regimens (*3*). Among other achievements, the network recently completed a clinical trial that described the deleterious effect on viral control and need for resumption of antiviral therapy in HIV-infected patients following immunization with an HIV-recombinant live vector anti-HIV candidate vaccine (*4*). Over the past year, ORVACS decided to focus on a rapid way to evaluate HIV eradication strategies in an approach similar to the proposed HIV Latency Collaboratory described in the Richman Review. Our model combines treatment intensification with immune interventions aimed at activating latently infected cells and/or targeting actively replicating cells with the goal of purging the reservoirs of HIV. Our first two trials are evaluating three immunomodulatory strategies plus intensification in patients with optimal viral suppression. Our protocols have been quickly developed at a reasonable cost and are being submitted to regulatory authorities in the various jurisdictions.

We were convinced that only an international effort could achieve this objective because many of the smaller biotechnology companies and academics with products of interest or expertise are scattered around the globe. The funding necessary to coordinate such activities does not exist under current government and industry mechanisms. Setting up this network in such a challenging environment would have been impossible without the original private seed funding plus the collaboration of multiple government and private institutions. Thanks to these unconventional sources and partnerships coupled with the exceptional enthusiasm from our scientific, industrial, and institutional partners, we overcame the obvious obstacles. We have now extended our previous global ORVACS network by including representatives from other major academic institutions, two major pharmaceutical firms, four biotechnology firms, and the NIH.

ROBERT L. MURPHY,[1]* BRIGITTE AUTRAN,[2] CHRISTINE KATLAMA,[3] GILLES BRUCKER,[4] PATRICE DEBRE,[2] VINCENT CALVEZ,[5] BONAVENTURA CLOTET,[6] NATHAN CLUMECK,[7] DOMINIQUE COSTAGLIOLA,[8] STEVEN G. DEEKS,[9] LUCY DORRELL,[10] JOSE GATELL,[11] ASHLEY HAASE,[12] MICHEL KLEIN,[13] ADRIANO LAZZARIN,[14] ANDREW J. MCMICHAEL,[10] LAURA PAPAGNO,[2] TIMOTHY W. SCHACKER,[15] SIMON WAIN-HOBSON,[16] BRUCE D. WALKER,[17] MICHAEL YOULE[18]

[1]Division of Infectious Diseases, Northwestern University, Chicago, IL 60611, USA. [2]Laboratoire d'Immunologie Cellulaire et Tissulaire, University Pierre et Marie Curie–Paris, Paris 75013, France. [3]Service Maladies Infectieuses et Tropicales, University Pierre et Marie Curie–Paris, Paris 75013, France. [4]Objectif Recherche Vaccin Sida, Paris 75013, France. [5]Department of Virology, University Pierre et Marie Curie–Paris, Paris 75013, France. [6]Irsicaixa Foundation, Hospital Universitari Germans Trias I

Letters to the Editor

Letters (~300 words) discuss material published in *Science* in the previous 3 months or issues of general interest. They can be submitted through the Web (www.submit2science.org) or by regular mail (1200 New York Ave., NW, Washington, DC 20005, USA). Letters are not acknowledged upon receipt, nor are authors generally consulted before publication. Whether published in full or in part, letters are subject to editing for clarity and space.

CREDIT: ZBIGNIEW BZDAK/MCT/LANDOV

Forces of wound healing

1278

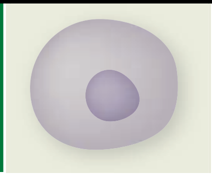

T cell sensitivity

1282

Pujol, Badalona, Catalonia 08916, Spain. [7]Division of Infectious Diseases, Saint-Pierre Hospital, Brussels, Belgium. [8]Department of Epidemiology, University Pierre et Marie Curie–Paris, Paris 75013, France. [9]Department of Medicine, University of California, San Francisco, CA 94143, USA. [10]Weatherall Institute of Molecular Medicine, Oxford University, Oxford, UK. [11]Sevicio de Infecciones, University of Barcelona, Villaroel 170, Barcelona, Spain. [12]Department of Microbiology, University of Minnesota, Minneapolis, MN 55455, USA. [13]CSO AmVac, Metalstrasse 4, Zug 6300, Switzerland. [14]Clinic of Infectious Diseases, San Raffaele Scientific Institute, Milan, Italy. [15]Department of Medicine, University of Minnesota, Minneapolis, MN 55455, USA. [16]Institut Pasteur, Paris 75015, France. [17]Ragon Institute, Harvard University, Charlestown, MA 02129, USA. [18]HIV Resource and Training Initiative, London, UK.

*To whom correspondence should be addressed. E-mail: r-murphy@northwestern.edu

References

1. J. Lederberg, K. Uncapher, "Towards a national collaboratory: Report of an invitational workshop at the Rockefeller University" (Directorate for Computer and Informational Science, National Science Foundation, Washington, DC, 1989).
2. S. Teasley, S. Wolinsky, *Science* **292**, 2254 (2001).
3. B. Autran, P. Debre, B. Walker, C. Katlama, *Nat. Rev. Immunol.* **3**, 503 (2003).
4. B. Autran *et al.*, *AIDS* **22**, 1313 (2008).

Keeping Mars Clean

C. P. MCKAY ("BIOLOGICALLY REVERSIBLE EXPLOration," Policy Forum, 6 February, p. 718) recommends that "COSPAR [the international Committee on Space Research] … set a policy that all Mars exploration be biologically reversible." I agree; it allows rigorous scientific study of past and current life there without presupposing that it will be easily recognizable or accessible. However, several assertions may not go far enough to enable remediation, which could make cleanup politically or fiscally impossible. Key are clear statements as to the purpose and urgency of exploration that may contaminate; biological discovery and mining may not be compatible.

McKay asserts that "hitchhiking organisms" exposed to the martian environment are killed quickly by ultraviolet (UV) solar radiation but that bacteria inside spacecraft may survive and remain dormant because of the dry conditions. This theory does not account for the environments beneath the surface. Biological contamination from a crashed vehicle could be buried by the impact or deposited by Mars' winds in UV-shielded crevasses far from the crash site. A nighttime introduction would not expose bacteria to UV, allowing them time to work into cracks or other protected niches. Second, the surface may be dry, but the Phoenix Mars Lander found water ice at 5 cm below the surface. Should bacteria reach subsurface liquid water, they could propagate rapidly. Third, the Policy Forum states that contaminants "will remain local and static and can be removed without requiring an effort vastly larger than the missions that carried the contamination." Such conclusions don't account for wind dispersal of contaminants not exposed to UV or possible burial by meteor strikes or landslides.

LIFE IN SCIENCE

It Takes a Village

A couple of years ago, we set out along with a team of ecologists to sample 100 lakes along the east coast of South America. We discovered that the task was easier said than done. Our four-wheel-drive pickup was stolen in Brazil and had to be restored by airplane. In the far south of Argentina, our boat sank with all of our equipment—and us—on it. But perhaps the most memorable adventure was the quest for our missing samples and the villagers in a small town in Argentina who came to our aid.

We had been in the field, traveling from lake to lake, for almost 2 months straight. Our precious samples were stored in coolers in the back of our pickup truck. At night, we would park the pickup in guarded car-parks. One early morning, we took the truck to lake El Paraiso. After a long day of fieldwork, we went to store the "catch of the day" in the cooler, only to discover that the cooler was no longer there.

We drove back the 30 km to the previous day's worksite in the hope that we had left the cooler there. Upon realizing that we did not have the key to the gate of the lake, we decided to climb the fence and walk the last 2 km through a mosquito-infested swamp. But it was for naught; the cooler was not there.

Back in the village, at the suggestion of a local, we sent a plea for help through the local radio station. Even before we arrived back at our hotel, three people had called with information. Apparently, someone had stolen the cooler during the night. Disappointed with its contents, the thief had thrown the cooler with samples in a garden adjacent to the hotel. The owner of the garden found them and, thinking they were veterinary samples, informed the police. The police, in turn, contacted all vets in the area. The neighbor, the police, and a veterinarian all contacted the radio show as soon as they heard our story. What a relief: We recovered almost all of our samples and became local celebrities in the process!

SARIAN KOSTEN[1]* AND GISSELL LACEROT[2]

[1]Aquatic Ecology and Water Quality Management Group, Wageningen University, Droevendaalsesteeg 3a, Wageningen 6708PG, Netherlands. [2]Facultad de Ciencias, Universidad de la República, Iguá 4225, CP 11400 Montevideo, Uruguay.

*To whom correspondence should be addressed. E-mail: sarian.kosten@wur.nl

Note

1. Supported by The Netherlands Organization for Scientific Research and National Geographic Society.

EDITOR'S NOTE

This is an occasional feature highlighting some of the day-to-day humorous realities that face our readers. Can you top this? Submit your best stories at www.submit2science.org.

CREDIT: PETER HOEY/WWW.PETERHOEY.COM

"Biologically reversible exploration" (putting off cleaning up) may be impossible given experiences on Earth. Remediation is often extremely expensive, requiring political resolve. In Hawaii, for example, there is no effective control that is affordable and politically feasible for scores of alien species. If an invasive weed cannot be controlled in Hawaii [as in the case of *Miconia calvescens*, an invasive tree (*1*)], what are the probabilities that a microbe on Mars can be contained and eradicated? How would costs be apportioned among space-faring nations?

Lastly, McKay posits that discovering martian life "may open discussions of warming Mars to help that alien life to flourish." Although it is true that warming generally speeds metabolism, it may be prudent to complete noninvasive studies of martian life processes and its evolutionary path and critique our motives for intervention first. While human-initiated warming of the planet may help humans, it would not necessarily "help" endemic life that has adapted to the present martian environment. If a goal of exploration is mineral extraction, early contamination, and plenty of it, would best justify a later conclusion that Mars is too contaminated to clean; exploitation with decreased regard for contamination would be facilitated. As industries gain a foothold on Mars, their influence on governance there will strengthen. If COSPAR requires clean Mars vehicles, the astrobiological value of a more pristine Mars would be enhanced. Now is the time for caution, while it is still an option.

WILLIAM R. KRAMER

Department of Political Science, University of Hawaii, Manoa, Honolulu, HI 96822, USA. E-mail: wkramer@hawaii. edu

Reference

1. L. L. Loope, "Harmful non-indigenous species report: Report for *Miconia calvescens*" (Haleakala National Park Field Station, USGS/BRD, 1997).

CORRECTIONS AND CLARIFICATIONS

Reports: "Regulators of PP2C phosphatase activity function as abscisic acid sensors" by Y. Ma *et al*. (22 May, p. 1064; published online 30 April). The date of receipt was 27 October 2008, not the later date in the original *Science* Express publication. The date has been corrected both online and in print.

Reports: "Human induced pluripotent stem cells free of vector and transgene sequences" by J. Yu *et al*. (8 May, p. 797). Karyotypes were performed on each of the vector-free iPS cell clones analyzed and were reported to be normal. Through subsequent high-resolution chromosomal analysis by comparative genomic hybridization, a small interstitial deletion of chromosome 15 was identified in one of the clones (iPS-DF6-9-12T). Re-review of the original karyotypes revealed that this small deletion was present and missed, and that the initial karyotype depicted in Fig. 3B was not normal, but should have been reported as: 46,XY,del(15)(q14q15). The karyotypes for the other vector-free iPS cell clones analyzed were also re-reviewed, and all are apparently normal. The revised karyotype for clone iPS-DF6-9-12T does not change the substance of the paper given that the karyotypes of the remaining vector-free clones appear normal.

Books *et al.*: "Many worlds in tiny grains" by R. Holman (6 March, p. 1291). The photographs of sand samples were not printed as intended. From top to bottom, the sands are actually from Rodeo Beach, Marin County, California; Agate Beach, Oregon; Daytona Beach, Florida; Santorini, Greece; Ayers Rock, Australia; Saraha Desert, Mauritania; Santorini, Greece (again); and Old Course Golf Course, Scotland. The photograph of shell-rich sand from Bermuda (shown here) mentioned in the original caption was inadvertently replaced.

Published by AAAS

SUMMER READING

Pages to Turn on a Lazy Day

In the past, we have looked to senior scientists for suggestions of thoughtful and enjoyable books for summer reading. This spring, we turned to graduate students, postdocs, and recent AAAS interns and media fellows for recommendations. We encouraged them to consider nonfiction and fiction, requesting only that the books be linked in some way (however tenuous) to science. As in 2007 (see *Science* **316**, 1845), we indicated a preference for titles from the last few years. We hope that these brief descriptions lead you to some relaxed reading, whether at home or while on vacation.

–Sherman J. Suter

Amos Nur and Dawn Burgess, *Apocalypse: Earthquakes, Archaeology, and the Wrath of God*. This fascinating multidisciplinary insight into the effects of earthquakes on ancient civilizations suggests how cooperation between geoscientists and archaeologists can benefit both fields. The authors' intriguing arguments challenge the long-held archaeological precept that violent tremors were not important catalysts in the collapse of past societies. Nur and Burgess suggest that archaeological records of major quakes can extend modern seismic catalogs and provide more accurate estimates of seismic hazards. Their lucid accounts of the impact of earthquakes at sites such as Troy, Jericho, Knossos, Mycenae, and Teotihuacán will appeal to scientists and nonscientists alike.

–Aubreya Adams (Pennsylvania State University)

Simon Singh, *The Code Book: The Evolution of Secrecy from Ancient Egypt to Quantum Cryptography*. This history of codes and ciphers focuses on the ongoing "arms race" between cryptography and codebreaking technologies. It charts developments in these fields through a variety of time periods and applications, including examples from ancient Greece, the Middle Ages, World War II, and modern computer encryption. The engaging narrative spotlights influential and interesting personalities in cryptography through the years. Singh's carefully chosen examples illustrate concepts so vividly that I promptly and clearly understood each concept. Hugely enjoyable and intellectually stimulating.

–Gloria Brar (University of California, San Francisco)

Leonard Mlodinow, *Feynman's Rainbow: A Search for Beauty in Physics and in Life*. Mlodinow documents his first year as a postdoc in the physics department at Caltech in the early 1980s. Struggling with the "impostor syndrome," he approaches Richard Feynman for career advice. As time progresses, they develop a close friendship, and their conversations reach far beyond physics—Feynman becomes a mentor to Mlodinow in all aspects of life. The book offers a unique and intimate view of the personality of one of the 20th century's most prolific thinkers and the journey of a young scientist searching for his niche in the world.

–Ian B. Burgess (Harvard University)

Richard Lewontin, *It Ain't Necessarily So: The Dream of the Human Genome and Other Illusions*. This collection of beautifully written and highly engaging essays by evolutionary biologist Richard Lewontin provides an informative account of developments in genetics research over the past few decades. The author's fresh and thoughtful views call attention to the profound differences between the genetic profile of an organism and the complex interactions that make living beings whole. The essays raise far-reaching questions that are rarely discussed in the field and remain timely reading in this age of the genome.

–Laura Colgin (Norwegian University of Science and Technology)

William W. Warner, *Beautiful Swimmers: Watermen, Crabs, and the Chesapeake Bay*. A classic in natural history writing, this 1977 Pulitzer Prize winner takes its title from a famous symbol of the Chesapeake Bay: the blue crab, *Callinectes sapidus*. Warner offers an excellent introduction to the ecology and behavior of this feisty animal, weaving together views of scientists and detailed observations by the watermen who hunt it. His fascinating and entertaining read also records a way of shore life that, threatened even over 30 years ago now, may soon disappear.

Richard A. Fortey, *Trilobite! Eyewitness to Evolution*. This journey through time and behind the scenes of museums around the world showcases the bewildering diversity of the once-ubiquitous trilobites and their geological importance. Conveying his passion and something approaching trembling awe, Fortey gives readers a sense of the excitement of studying extinct creatures and the feelings that come from touching small pieces of life's history.

–Elizabeth A. Diamond (Rutgers University)

Daniel Kehlmann (translated by Carol Brown Janeway), *Measuring the World*. Tapping the lives of two very different but contemporary scientists, mathematician Carl Friedrich Gauss and explorer Alexander von Humboldt, Kehlmann creates an enjoyable adventure story that manages to entertain in an intelligent way. He draws Gauss as a grumpy genius, Humboldt as an eccentric obsessed traveler. Although he may not portray the historical characters accurately, they become amazingly alive. While attempting to measure the world in their own ways, both have the same passion for science.

–Barbara Fischer (University of Bonn)

Margaret Atwood, *Oryx and Crake*. Nothing says summer like a good dystopian-turned-postapocalyptic future. Atwood's deeply disturbing novel paints a fascinating, sometimes nauseating, picture of biotechnology gone awry (for example, food of the future "Chickie Nobs" are meaty protrusions sprouted from a headless, footless chicken base) but also delves into human psychology. Word-guy Jimmy and science-guy Crake—a classic juxtaposition—are best friends, colleagues, and elites housed in a gated compound in this near-future world; Oryx, a tragic love interest, comes from the far grimmer landscape outside. This tangled human web erupts in a global cataclysm that leaves only Jimmy to care for a Crake-engineered posse of posthumans. The chilling conclusion will keep you pondering this cautionary tale well into the fall.

–Erika Gebel (former AAAS media fellow)

Jennifer L. Rohn, *Experimental Heart*. Describing the daily life of lovestruck postdoc Andy, this scientific novel can't be put down. It realistically and humorously portrays the inner workings of a biology research lab, relations between the scientific community and the public, and the highs and lows of research life.

CREDIT: PETER HOEY/WWW.PETERHOEY.COM

That would be enough to captivate scientists (been there, done that, felt that way) and give nonscientists an inkling of what life in a lab is like. To spice things up, Rohn spins a riveting thriller—replete with scientific discovery, fraud, falsified reagents, romantic darkroom encounters, threats, and even abduction—as Andy searches for personal and scientific fulfillment.

–**Alice Genevet** (Cancer Research UK)

Rick Weiss and Jonathan D. Moreno, Eds., *Science Next: Innovation for the Common Good.* This fairly short, readable collection of essays from the progressive Center for American Progress addresses a wide variety of science policy topics, including climate change, digital communications, stem-cell research, innovation, and education. The often thought-provoking, if occasionally relatively simple, pieces are intended to illuminate the intersection of science and policy and to explore science as a "social enterprise" in the public interest.

Alan Lightman, *Einstein's Dreams.* Novelist and former physicist Lightman offers a wonderfully literary meditation on the theory of relativity. He begins with a young patent clerk in Berne who, while working out his new theory, can't help but drift off to sleep. Subsequent chapters (fables) present a series of individual "dreams" of fantastical worlds with physical rules very different from our own. An exploration of the nature of time, human society, and even spirituality, this former bestseller is often whimsical and highly rereadable.

–**Matt Hourihan** (AAAS intern)

Brian Greene, *The Fabric of the Cosmos: Space, Time, and the Texture of Reality.* How did the universe begin? Why does time seem to flow one way but not the other? How many dimensions does the universe really have? Theoretical physicist Greene tackles some of the deepest and most challenging questions in science, taking readers on a guided tour of physicists' search for answers. His enjoyable examples and analogies feature characters from *The Simpsons*, *The X-Files*, and more. He vividly explains breakthroughs in relativity, quantum mechanics, and string theory using language simple enough for a layperson but with enough depth to engross any professional physicist.

–**Daniel Hummer** (Pennsylvania State University)

John Derbyshire, *Prime Obsession: Bernhard Riemann and the Greatest Unsolved Problem in Mathematics*. Although the topic of the distribution of prime numbers may seem inaccessible and boring to most nonmathematicians, Derbyshire's accounts of Riemann's hypothesis and life provide an exciting and rewarding read. Chapters on mathematics alternate with ones giving historical and biographical background. Some familiarity with basic math makes the former easier to digest, but anyone can enjoy the book.

–**Jussi Lehtonen** (University of Helsinki)

A. J. Jacobs, *The Know-It-All: One Man's Humble Quest to Become the Smartest Person in the World*. To achieve his goal, Jacobs attempts to audition for *Jeopardy,* competes on *Who Wants to Be a Millionaire?,* and hobnobs with his newfound Mensa peers, all while reading the Encyclopedia Britannica from cover to 32nd cover. His hilariously quirky adventures juxtaposed with his insightful ideas regarding the difference between knowledge and intelligence will keep you entertained from A-ak to Zywiec.

–**Cassandra Leigh** (AAAS intern)

Neal Stephenson, *Quicksilver*. In this work of historical fiction, set in the early Enlightenment, scientific giants such as Newton, Huygens, Hooke, and Leibniz share center stage with the theories of gravity and calculus. Painstakingly detailing a world in which scientific thought is emerging, Stephenson captures the excitement of discovery against a background of religious, political, and social upheaval. The adventures of a thoroughly entertaining vagabond "Half-Cocked Jack" and his companion Eliza allow an expansive description of Western Europe at the time, while the book still keeps an eye on broader political intrigue.

–**Steven Lockton** (University of California, Berkeley)

Isaac Asimov, The *Foundation* series. These books chart the rise and fall of a galactic empire and ultimately the search for Earth. The series is best read in chronological order according to the books' time frames (not the order of publication): *Prelude to Foundation*, *Forward the Foundation*, *Foundation*, *Foundation and Empire*, *Second Foundation*, *Foundation's Edge*, and *Foundation and Earth*. *Foundation* was originally written as a collection of short stories and, at times, may be difficult to follow. The novels broach fundamental aspects of what it means to be human.

Orson Scott Card, The *Ender's Game* series. These novels (and prequel short stories) on the life of a boy military genius who saves humanity from an alien race only to be banished for genocide should also be read in chronological order: *First Meetings*, *Ender's Game*, *A War of Gifts*, *Ender's Shadow*, *Shadow of the Hegemon*, *Shadow Puppets*, *Shadow of the Giant*, *Ender in Exile*, *Speaker for the Dead*, *Xenocide*, and *Children of the Mind*. Over the course of the series, the focus shifts from military tactics and troop relationships to the true nature of religion and the political basis of morality. The Shadow titles form an entertaining spin-off within the series. The early books are fast reads, great for the beach. The later ones may take a little more focus than you can muster after your second or third piña colada.

–**Kathryn Luke** (AAAS)

Jonathan Haidt, *The Happiness Hypothesis: Finding Modern Truth in Ancient Wisdom*. Looking for "great ideas" that might bring meaning to life, Haidt explores philosophies from many cultures and time periods to determine which wisdoms are pervasive. He weaves together examples of

CREDIT: PETER HOEY/WWW.PETERHOEY.COM

human nature and psychological theory to describe how the human mind works and the competition for control between our conscious mind (head brain) and our instincts (gut brain).

–**Victoria Miller** (Pennsylvania State University)

Richard Wiseman, *Quirkology: How We Discover the Big Truths in Small Things/The Curious Science of Everyday Lives*. Like the following suggestion, this book celebrates possibly the most important quality for a scientist, curiosity. Summarizing years of quirky research, psychologist Wiseman turns simple, everyday questions into scientific matters through which we can learn about human behavior. His subjects range from how birthdays influence personal luck to how to spot a liar by looking at his eyes. Entertaining and witty, his account is rich in anecdotes and trivia. Do you know the funniest joke in the world?

Richard P. Feynman and Ralph Leighton, edited by Edward Hutchings, *Surely You're Joking, Mr. Feynman! Adventures of a Curious Character*. These autobiographical stories follow physicist Feynman from childhood, through his formative years at MIT and Princeton and his participation in the Manhattan project, to his years of stardom at Caltech. Moved by an enthusiastic spirit of enquiry and a playfully skeptical attitude, he fixes radios, tracks books by smelling them, investigates his sleep, and experiments with drugs. This clever collection is a monument to curiosity as an invaluable ingredient of a passionate and adventurous life.

–**Andrea Orsi** (Cancer Research UK)

Penny Le Couteur and Jay Burreson, *Napoleon's Buttons: How 17 Molecules Changed History*. Two organic chemists discuss how certain molecules—from coffee sweeteners that don't add calories to drugs that fight malaria to possibly the greatest killer of all time—have influenced everyday lives and helped shape history. They balance chemistry, history, and culture in an accessible and enjoyable account that gets one looking at the world around us in a whole new light.

–**Olga Pantos** (University of Queensland)

Walter Isaacson, *Einstein: His Life and Universe*. Who knew one could snuggle with a 700-page biography? Isaacson toes a nearly ideal line between the personal and private Einstein, illustrating how each shaped the other. As a graduate student, I was both inspired and daunted by challenges that a young Einstein had to overcome from the scientific and political establishment before he developed into the face of the very same establishment. Although biographers can never provide the full picture of a life, the author's expansive scope and exhaustive referencing suggest he has come pretty close.

Robert Charles Wilson, *Spin*. A modern sci-fi novel in classical style, this epic is rich in imagination and filled with "whoa" moments firmly rooted in hard science. But it is really about people and what happens to them when something unimaginable occurs. Wilson describes the effects through the lenses of both children and adults while addressing religion, politics, romance, and science. It is the kind of book that leaves one thinking "I wish I lived in this type of world," only to realize that we very well may. Read it without any background knowledge of the plot. Don't even let the back cover tempt you.

–**Aaron Price** (Tufts University)

Daniel Gilbert, *Stumbling on Happiness*. Looking at the science behind how people understand and attempt to achieve happiness, Gilbert blends explanations of numerous psychology experiments with witty narrative to highlight the predominantly unnoticed tricks that our minds play on us when interpreting past and present information. Acknowledging and compensating for these tricks increase the possibilities of future happiness. Well written and extremely entertaining, the book should please both those who just want a good laugh and those seeking a deeper understanding of the processes by which we make decisions for the future.

–**Sarah Remmert** (Oxford University)

Doris Lessing, *Mara and Dan*. This topical and captivating novel by the 2007 Nobel laureate in literature describes the journey of two children in a future era after climate change. Mara and Dan inhabit a world that combines preindustrial resources with the remnants of Western science and technology. With the American continent only a legend and Europe lost under glaciers, their adventure takes place in drought-struck Ifrik (Africa), among telltale signs of the dire losses humanity has suffered. For them, our civilization is a semi-mythical memory, enduring through strange objects, such as skyscrapers abandoned underwater or surrounded by great deserts. This tale of human survival, kinship, and love echoes the greatest human epics, while sounding the alarm about the urgent need to halt global climate change.

–**Deborah Talmi** (University College London)

Rivka Galchen, *Atmospheric Disturbances: A Novel*. The Royal Academy of Meteorology hides secret messages in the *New York Post*. These coded instructions to Harvey are part of their clandestine war with the mysterious 49 Quantum Fathers, who seek to control the weather to reap fortunes in crop futures. Harvey may be delusional. So, too, may be his psychiatrist, the protagonist Leo, who is convinced his wife Rema has been kidnapped, replaced by a doppelganger. Sensing the influence of the Academy, Leo scrutinizes the atmospheric studies of Tzvi Gal Chen for clues, which lead him to Patagonia. Along the way we learn about Doppler radar, mental health, and the ever-shifting shapes of aging romantic love.

–**Brad Wible** (former AAAS media fellow)

10.1126/science.1176528

ECOLOGY

A Story of Symbiosis

Leigh Krietsch Boerner

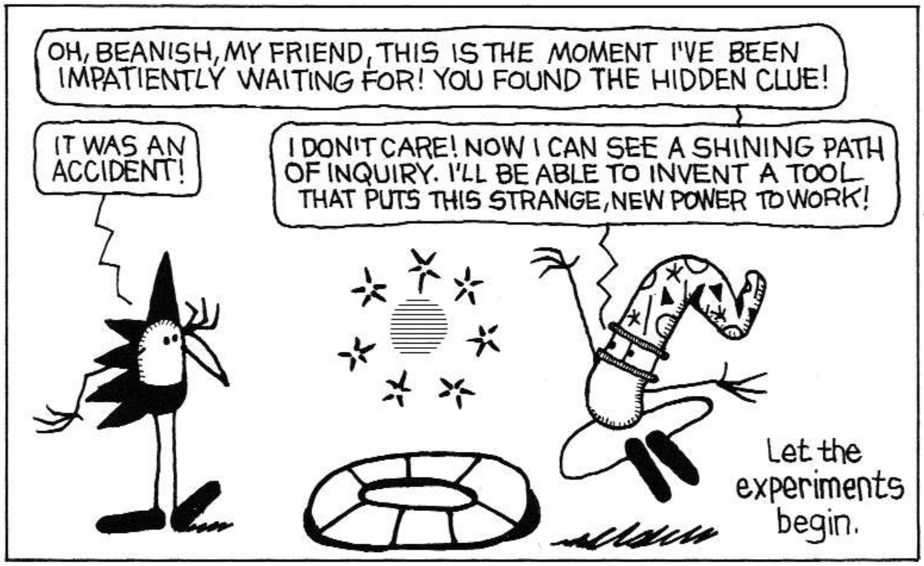

CREDIT: LARRY MARDER, FROM *BEANWORLD: WAHOOLAZUMA!*/COURTESY DARK HORSE COMICS

Larry Marder's *Tales of the Beanworld* series is best described as an ecological fairy tale. What the cover proclaims a "most peculiar comic book experience," the deceptively simple black-and-white cartoons concern how a race of creatures interacts with their environment. "Beanworld is about the affinity of life," Marder states in the beginning of the story. "All the characters, whether they are friends or adversaries, understand that ultimately they depend on each other for survival."

Marder first drew his minimalist, "bean" characters while an editorial cartoonist for his university newspaper in the early 1970s. He started *Tales of the Beanworld* in the mid-1980s under Eclipse but then abruptly ended it, mid-storyline, in 1993. The story so far is being re-released though Dark Horse Comics in two hardcover graphic novels: the already available *Wahoolazooma!* and *A Gift Comes!*, due out in early August. Much to the delight of his long-term fans, Marder is picking up the narrative and continuing from where he left off.

The tale is one that's a bit … different. Even in the comic book world, where nerds have secret super-powers and aardvarks go on hero quests, Beanworld is unusual: "a weird fantasy dimension operating under its own rules and laws." The world is populated by Beans, and the story chronicles their struggle to find a place in their universe, which Marder calls "The Big Big Picture." That picture is unlike anything you've seen before.

The gist is this: Mr. Spook, the hero and protector, leads the Chow Sol'jer army on raids to steal a substance called chow, the Beans' food, from the Hoi-Polloi ring herd. The Hoi-Polloi are a race of one-armed gamblers that live below the four realities, the elemental forms (slats, hoops, twinks, and chips) the Beans use to make tools. The exchange between the Beans and the Hoi-Polloi is a violent one: spears are thrown, and chow is stolen. But Mr. Spook always leaves behind a sprout-butt, an object donated by Gran'Ma'Pa, the Beans' silent but sentient spiritual guardian. The Hoi-Polloi send mental love rays to the sprout-butt, and it dissolves into more chow, which they use as currency. The Beans will eventually come back for this chow and leave another sprout-butt behind. It's closed, it's cyclical, and it's ideal, at least in the Beans' opinions. As Mr. Spook says in *A Gift Comes!* "The life Gran'Ma'Pa provides is perfect, as long as we all carry out our duties."

Beanworld
Book 1: Wahoolazuma!
by Larry Marder
Dark Horse, Milwaukie, OR, 2009. 272 pp., illus. $19.95. ISBN 9781595822406.

Beanworld
Book 2: A Gift Comes!
by Larry Marder
Dark Horse, Milwaukie, OR, August 2009. 272 pp., illus. $19.95. ISBN 9781595822994.

This is the overarching theme in the Beanworld story: symbiosis. The Beans and the Hoi-Polloi, although enemies, need the other to live. The Beans need one another as well. Each has a specific job to do that contributes to the good of the tribe. Those who don't go on chow raids have other important vocations.

Among the most intriguing characters are the scientist-thinker, Professor Garbanzo, and the artist-in-residence, Beanish. The interactions between the two are fascinating to watch, mostly because they employ the same methods (experiment and observation) to come to completely different ends. Both use the four realities as raw materials. Professor Garbanzo fashions tools for the Beans and invents things to promote the upward movement of Bean society. Beanish creates his "Fabulous Look-See Show," an artistic endeavor that challenges the Beans' ideas of perception and reality. But even though their respective outcomes are so different, the story often has Garbanzo and Beanish cooperating. Through simple exchanges between two bulbous cute things, Marder raises some erudite questions. Does science need art? Does art need science?

This reflects one of Marder's great talents: taking complex ideas and distilling them down to their basic components. Throughout the series, the reader encounters many lessons about ecology, invention, and cooperation. But they are presented so subtly that you won't realize you are being taught. Instead of shoving ideas at his readers, Marder simply tells a story. You can take from it what you will.

All this food for thought comes in an enjoyable and easily digestible package. The characters and ideas just make sense; the storyline clicks and whirs with the utter precision of a well-known folktale. Likewise, the drawings in Beanworld are eerily apt. It is almost as if they were not drawn but instead grew from the pages. Simple yet viscerally attractive, the art is charming. But it also has an odd sophistication, a hint of something more lying beneath.

It is this dichotomy that makes Beanworld appealing to children and adults alike. The cartoony drawings and unpretentious storyline make it kid-friendly, and the delightfully weird and rhythmic language begs to be read aloud. Adults get to enjoy the deeper meanings and themes and appreciate it for the unlikely work of art that it is. Both can wonder together, what will happen next? Whereas longtime Beanworld fans have been kept in suspense for 16 years, new readers will only have to wait a few months to find out. The next episode in Marder's far-out fantasy, *Remember Here When You Are There!* should appear in mid-November.

10.1126/science.1176005

The reviewer, a former AAAS media fellow, is at the Department of Chemistry, Indiana University, Bloomington, IN 47405, USA. www.ljkboerner.wordpress.com

MATHEMATICS

Numbers to Remember By

Katharine Ott

Yoko Ogawa's novel *The Housekeeper and the Professor* tells the story of an unexpected kinship between a Japanese mathematician, his hired housekeeper, and her son. The Professor, who studied mathematics at Cambridge, held a prominent university position until a car accident in 1975, when he was 47 years old. The crash left him with a short-term memory resembling a videotape that erases and records over itself every 80 minutes. Isolated from the present day by this memory impairment but able to recall everything he knew prior to the accident 17 years ago, the Professor finds his only peace in the world of numbers. The Housekeeper of the title, a single mother, narrates the story. Every day, and numerous times within each day, the Housekeeper and her son appear as strangers to the Professor. In order to help ease their frequent introduction, he wears a note clipped to his suit containing a crude drawing of her face and the simple words: "The new housekeeper ... and her son, ten years old, $\sqrt{\ }$."

The Housekeeper and the Professor

by Yoko Ogawa

Translated from the Japanese (*1*) by Stephen Snyder. Picador, New York, 2009. 190 pp. Paper, $14, $C18. ISBN 9780312427801.

The Professor nicknames the Housekeeper's son Root because the flat shape of his head resembles the square root sign, $\sqrt{\ }$. The Professor's love for mathematics is equaled only by his love for Root and children in general. In his words, "primes were the base on which all other natural numbers relied; and children were the foundation of everything worthwhile in the adult world." Accordingly, Root's character serves as a fundamental link between the Professor and the Housekeeper because he resolves their differences. To draw an analogy in mathematics, as the Professor is fond of doing, Root acts as the 1 in Euler's formula: he resolves the relationship between e and π into one harmonious equation, $e^{\pi i} + 1 = 0$.

The principal events in this quiet novel (a trip to a baseball game and a party celebrating Root's 11th birthday) are not its important moments. Instead, the narrative blossoms in the passages describing the Housekeeper's journey into mathematics. The Housekeeper is not inclined toward math—in fact the subject made her feel ill in school—but she is inspired by the Professor's passion for it. She brings numbers alive for herself and the reader by giving them human traits and emotions. For instance, when learning about "twin primes" (pairs of prime numbers that differ by 2, such as 3 and 5 or 11 and 13), the Housekeeper imagines that "the twins had matching outfits and stood holding hands as they waited in the number line." In another example, the "abundant number" 18 (its divisors sum to a number great than 18) "secretly carried a heavy burden," whereas the "deficient number" 14 (its divisors sum to a number less than 14) "fell mute in the face of its terrible lack."

One climactic moment occurs when the Housekeeper finds a formula for adding all consecutive integers from 1 to 10. It is not an original proof, but any student of mathematics who has struggled with a problem will recognize the Housekeeper's accomplishment in solving it on her own. Her moment of discovery is momentous, "the clarity and purity of the solution was even more extraordinary in light of the confusion it had emerged from, as if I'd unearthed a shard of crystal from the floor of a dark cave." The Professor deserves some credit for the Housekeeper's discovery. He excels where many math teachers fall short, encouraging her to ask questions and instructing her on the process of problem-solving. "It's important to use your intuition. You swoop down on the numbers, like a kingfisher catching the glint of sunlight on the fish's fin."

The novel ends swiftly and predictably. Readers will quickly forget its conclusion and recall instead the miraculous connections between numbers revealed by the Professor and the Housekeeper. One such numerical bond that lingers in the imagination links the Housekeeper's birthday, February 20 (or 220), to the number 284 engraved on the back of the Professor's watch. This pair of "amicable numbers" (the sum of the factors of 220 excluding itself equals 284, and the sum of the factors of 284 excluding itself equals 220) is extremely rare. Pythagoras knew of amicable numbers and associated mystical properties to these friendly pairs. One is led to hope that although the Professor's memory prevents him from remembering the Housekeeper and Root, perhaps numbers do reveal to him the true nature of their friendship.

The reviewer, a former AAAS media fellow, is at the Department of Mathematics, University of Kentucky, Lexington, KY 40506–0027, USA. E-mail: katharine.ott@uky.edu

References

1. Y. Ogawa, *Hakase no Aishita Sushiki* (Shinchosha, Tokyo, 2003).

10.1126/science.1175075

BROWSINGS

Wave. Suzy Lee. Chronicle Books, San Francisco, 2008. 40 pp. $15.99. ISBN 9780811859240.

In this wordless story, a carefree little girl and a flock of gulls play with the encroaching tide. She grows progressively bolder and ends up drenched—but delighted with the shells left on the sand. Lee's simple, lively, and evocative charcoal and acrylic illustrations will charm adults and children of any age. The book kindles desires for one's own bright day at the beach.

CREDIT: SUZY LEE, FROM *WAVE*/COURTESY CHRONICLE BOOKS

Published by AAAS

SCIENCE INNOVATION

Assessing the Impact of Science Funding

Quantifying the outcomes of investment in science is not an easy task.

Julia Lane

Science supporters were rightly excited by the passage of the American Reinvestment and Recovery Act (ARRA, i.e., the stimulus package). Headlines in *Science* (*1*) and *Nature* (*2*) rejoiced at the new value placed on science as a basis for economic growth and associated job creation. Indeed, federal investment was at least partly based on a belief that the result would be more competitive firms and more, and better, jobs—and soon! (*3*). That belief was bolstered by advocacy groups: For example, a report by the Information Technology and Innovation Foundation (ITIF) estimated that an additional \$20 billion investment in research in the stimulus package would create ~402,000 American jobs for 1 year.

Within 2 years, the public will want to be informed about the impact of the stimulus on the economic recovery. Were the estimates accurate? How can they be validated? And, in the longer term, what were the impacts of the reinvestment strategy on scientific knowledge, economic growth, and job creation? But we should also want to be informed about questions that go beyond the immediate accounting issues raised by ARRA. For example, what deeper understanding did we gain about the mechanisms whereby knowledge is created and how it contributes to both economic and social outcomes? Given the global nature of both economic and scientific activity, how did the science investments of other countries affect the United States? What new measures and indicators were developed to measure those contributions, and how can they be used to inform future investments and the response to future economic downturns? Answers to these questions will need to be based on theory and empirical evidence, as well as conveyed in a manner that is understandable. Some insights can be drawn from research into the science of science and innovation policy (SciSIP) (*4*).

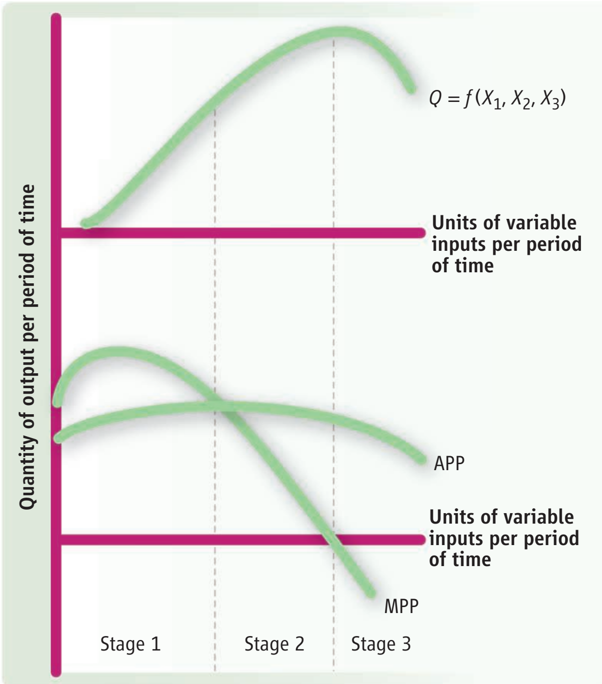

A standard approach to linking inputs and outputs that has been used to study innovation. Output (Q) is shown as as a linearizable function of inputs (X_1, X_2, and X_3). The efficiency of different stages of production is described by the relationship between average physical product (APP) and marginal physical product (MPP).

CREDIT: ADAPTED BY P. HUEY/*SCIENCE*

Much of the public discussion about the "science stimulus," consistent with the apparent precision of the ITIF estimates, suggested that the outcomes of scientific investments were both certain and tied to economic growth. It is true that science policy in the United States and abroad is largely predicated on such beliefs. The United Kingdom's *Innovation Agenda* identifies basic research as critical to productivity and employment growth (*5*), as does the Organization for Economic Cooperation and Development's (OECD's) innovation strategy (*6*). Saudi Arabia has invested \$6 billion to set up a new science and technology university (*7*), and the Japan Science and Technology Agency has made investment in basic research a cornerstone of its economic strategy (*8*). Certainly, there are a number of anecdotes that make the case that science investments create jobs. For example, four researchers at the University of California at San Diego have been credited for the vibrant growth of San Diego, creating more than 40,000 jobs in life sciences and over 12,800 in electronics (*9*). The emergence of Google has been traced to National Science Foundation support of one of its founders, Sergey Brin, who was an NSF Graduate Research Fellow, and a \$4.5 million Digital Library Initiative grant from NSF to Stanford that helped support early Google prototypes.

However, much of the research in science policy is cautious about the impact of science investments—consistent with Congressional Budget Office expectations that increased spending for basic research and education would have very wide ranges of expected impacts and might affect output only after a number of years. Cross-national evidence also suggests that investment in science, while often successful, is not a guarantee of short-term economic growth and job creation. The U.S. experience of the past decade, in which more than three-quarters of post-1995 increase in productivity growth could be traced to science investments (*10*), was not duplicated in all other countries. For example, massive investments in university and government research institutes had little short-term impact on Japan's economic growth and "demonstrates that science, technology, and innovation policy cannot compensate for adverse framework conditions (e.g., dysfunctional financial systems)" [(*11*), page 8]. Similarly, Sweden, despite having invested heavily in research and development (R&D), has employment that is still below the precrisis level in 1990 despite a population growth of more than 5% (*12*). In sum, we do not understand the mechanisms through which investments in R&D, and their immediate products (knowledge and technologies) interact with other aspects of societies and economies.

Understanding the reasons for these cross-national differences is important not only for answering questions about the impact of the "science stimulus" and guiding policy deci-

Science of Science and Innovation Policy, National Science Foundation, Arlington, VA 22230, USA. E-mail: jlane@nsf.gov

Published by AAAS

sions but also for responding to a fascinating scientific challenge. Similar policy-related challenges have resulted in scientific advances in the past. Jim Heckman's analysis of the econometric issues associated with labor policy not only earned him the Nobel Prize in 2000 but also guided government policy in training (*13*); Vernon Smith's research in alternative market mechanisms not only earned him the Nobel Prize in 2002 but also guided the design of broadband communication spectrum auctions and allocating landing slots at airports.

The challenge in the field of SciSIP is greater than in many policy areas for a number of reasons. The relation between science and innovation is nonlinear in nature, with complex outcomes that can vary substantially by discipline and be subject to considerable time lags. The units of analysis can similarly be quite complex, ranging from the individual to project teams to organizations to political systems: As a result, relevant research takes place in separate disciplines such as economics, sociology, political science, and psychology. This complexity has created a substantial empirical challenge: Because the creation and transmission of knowledge and technologies result from complex human and social interactions, new ways need to be developed to capture data on those interactions, and new data need to be developed to characterize the eventual outcomes. Finally, a related and equally interesting scientific challenge is how best to convey the results of scientific analysis to policy-makers and the public. Even the terms "innovation," "science," "technology," and "research and development," used interchangeably in the popular press, mean very different things to the scientists who study the science and innovation enterprise.

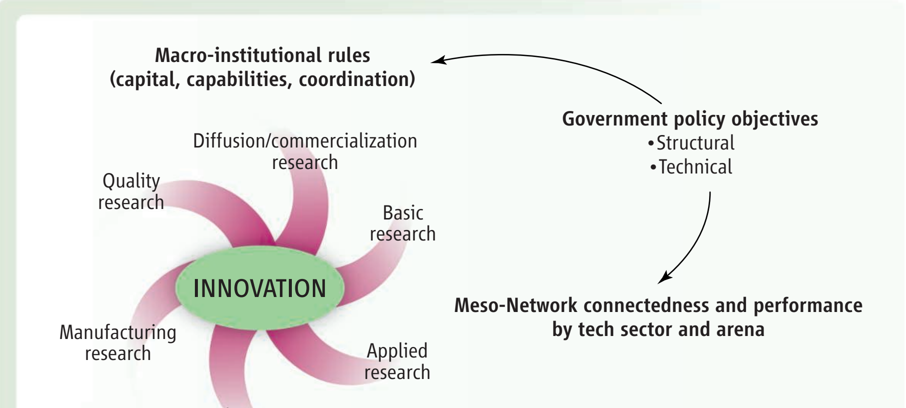

A few of the complex interrelationships in an innovation ecosystem. From (*29*).

The Scientific Challenge

The ITIF estimate of job creation in the opening section of this essay was derived from the Bureau of Economic Analysis's RIMS II model: a linear model linking science investments to economic outcomes. The basis is an input-output model of spending flows (*14*) in which spending on the RIMS II category of "scientific research, equipment, and facilities" directly generates scientific and construction jobs and indirectly generates jobs in service areas such as restaurants through a multiplier effect. This approach functionally equates the impact of science to that of building a football stadium or an airport: The impact is derived from the demand side and depends on the amount of spending on bricks, mortar, and workers.

Although this set of estimates was based on the most readily available and widely used models at hand, it is unlikely to do full justice to the long-term impact of science investments. Deeper insights can be derived from using a production function framework in which economic value is determined by the amount of physical capital, labor, materials (including land), and energy devoted to producing a good and to the efficiency with which these factors are combined (see chart, page 1273). Early work by Robert Solow, for which he received the 1987 Nobel Prize, described how these factors combine to generate productivity growth and increase welfare. Later work by Jorgenson and others (*10*) used an enhanced production function approach to decompose the sources of productivity growth: The source of the finding that information-technology–related increases in total factor productivity (i.e., innovation) explained more than three-quarters of the post-1995 increase in U.S. productivity growth. And a production function framework also provides the insight that the impact of science investment on jobs is more likely to create jobs for skilled than for unskilled workers, because skilled workers in the production function are complements for technological advances; unskilled workers are substitutes (*15*).

It is difficult to expand the production function framework to encompass the nonlinear and complex nature of value creation in the knowledge economy. Innovation is nonlinear because the demand side and the supply side of ideas are inextricably intertwined. Innovation also involves the interrelationships of human beings and social structures and processes. Thus, the term "the ecology of innovation" is often used to emphasize the nonlinear set of relationships at the micro, meso, and macro levels (see figure, above).

A good illustration of why it is critical to understand the complex nature of innovation when making science investments is provided by NIH's initial approach to funding biopharmaceutical research, particularly monoclonal antibodies and antisense technologies. NIH invested heavily in a research base, assuming that the resulting knowledge would draw entrepreneurs and venture capital and produce new drugs. However, as in many applications, technology has separate components, including a generic technology base, supporting infratechnologies, and proprietary market applications. Investment can occur at any of these points. Because this particular technology demanded substantial "proof-of-concept" (alternatively, "generic") technology research and such a technology platform was not initially provided, the results of the initial investments were disappointing. In the case of antisense (a subset of RNA technology), first-generation chemistry yielded only one small-market drug over a 15-year period. Subsequent investments have been much more fruitful (*16*). This anecdote illustrates that understanding how the venture capital component of our national innovation system is organized and works can be critical to ensuring that science investments achieve their full impact.

Understanding the ecology of innovation is important for answering the questions outlined in the introduction. The recovery part of ARRA was, by its nature, intended to have a short-term stimulative effect on job creation, but describing the impact of the reinvestment part of the stimulus is likely to take much longer. Research suggests that the time lags from initial investment to discovery, as well as the lag from patent to implementation, can take many years, or even decades. In other words, the science investment needs to generate an "aha" moment or an idea that has value; structuring that investment so that the ideas move beyond the initial research project is difficult (*17*). Translating that "aha" moment into an innovation also might require a well-functioning team or organization (*18*, *19*), a well-functioning patent system (*20*), a well-developed firm ecosystem (*21*), or appropriate university links to industry (*22*). The time lags can be substantial. Recent productivity growth in agriculture, for example, was based on research investments in the 1800s (*23*). Biotechnology commercialization was based on scientific findings dating from the 1950s. The Internet revolution that bore fruit in the 1990s was based on scientific investments in the 1970s and 1980s.

And, of course, a focus on economic value alone may also understate the true returns of investments in science. Indeed, one strand of research is attempting to develop a public value mapping of science outcomes: outcomes that are public, nonsubstitutable, and oriented to future generations and that capture dimensions such as competitiveness, equity, safety, security, infrastructure, and environment. The research is based on key ideas: (i) It is possible to identify public values, including ones not well captured by economic constructs; (ii) just as one can assess market failure, "public value failure" occurs when neither the market nor the public sector provides goods and services required to achieve designated public values; and (iii) innovation can be characterized not only in terms of contributions to economic growth and productivity but also in terms of the public values achieved (*24*).

Answering the Questions

Although there is a global interest in answering the questions, a recent Science of Science Policy roadmap, as well as researchers at a recent Science of Science Policy workshop concluded that the United States needs a major intellectual investment to permit further deep analysis of the impact of science investments (*25*). Some illustrations of those investments are identified below.

The passage of the ARRA and similar legislation in other countries provides one such opportunity for analysis. NSF's Science of Science and Innovation Program issued a RAPID (www.nsf.gov/pubs/2009/nsf09034/nsf09034.jsp) call for proposals to mobilize the research community to assess the effects of ARRA both on the ecology of innovation and on the science and engineering enterprise. The portfolio of funded research from that call should provide new insights into many of the scientific questions posed above as the research is completed.

Other examples of major investments also exist. The roadmap noted that the U.S. scientific data infrastructure is oriented toward program administration rather than empirical analysis. It currently does not allow science investments to be coupled with the associated scientific and technological, social, and economic outcomes (*25*). A number of U.S. research awards have been made to develop a pilot data infrastructure that provides information about where and to what purpose science tax dollars are spent. Some of these awards go beyond the use of administrative and survey data and both use and develop cyber tools to capture data on and about scientists, their interactions, and the related scientific and economic outcomes.

In addition, there is the potential to expand the current science data infrastructure, which has some of the elements necessary to fully inform the analysis of science investments. Grants.gov provides a unified portal to find and apply for federal government grants. Research.gov and science.gov provide information about research and development results associated with specific grants, and a consortium of federal agencies provides R&D summaries (www.osti.gov/fedrnd). Open.gov and data.gov are being implemented to promote citizen participation in government decision-making by making government data available online, in keeping with President Obama's vision (*26*). A mechanism that built on these and other initiatives could couple science investments with outcomes in a systematic fashion. It could also engage the scientific community and the public in an ongoing dialogue to describe and amplify knowledge about these outcomes.

Of course, the answer to the questions about the return on investments in science will not be contained in one number. A related intellectual investment is to advance understanding of how to convey complex answers about the impact of science investments to the public. Emerging visualization techniques seem to be more effective than tables and digital slide presentations at communicating the ways in which science investments bear fruit across a range of topics and disciplines. However, although visual representations are intuitively appealing, it is not clear what they convey: The scientific foundations upon which they are based are not fully developed. U.S.–funded research is thus moving beyond the science of simple mapping to leverage the science of visual analytics which has hitherto been used to "make sense" and describe the impact of terrorist, rather than scientific, networks. Just as John Snow used maps in 1854 to identify the waterborne source of cholera, researchers in the field are combining "the art of human intuition and the science of mathematical deduction to perceive patterns and derive knowledge and insight from them" (*27*).

Conclusion

The ARRA was intended to both promote recovery and make new investments in the American economy. Answering questions about the impact of the stimulus has two parts: short term and long term. Short-term estimates of the recovery aspect of the "science stimulus" do not properly convey the complexity of the process. And although the reinvestment aspect reflects a long-term bet that investments in science will bear more fruit than investments in stadia, and science still has a long way to go to provide full clarity in what those outcomes will be, a number of steps are being taken to ensure better answers in 2 year's time.

References and Notes

1. J. Mervis, *Science* **323**, 1274 (2009).
2. E. Hand, *Nature*; published online 26 February 2009, 10.1038/news.2009.126.
3. D. Goldston, *Nature* **458**, 21 (2009).
4. A. Leshner, *Science* **324**, 313 (2009).
5. Department for Innovation, Universities, and Skills (DIUS), *Innovation Nation*, *White Paper* (DIUS, Runcorn, UK, 2008).
6. OECD, "OECD innovation strategy" (OECD, Paris, 2009) www.oecd.org/pages/0,3417,en_41462537_41454856_1_1_1_1_1,00.html.
7. King Saud Univeristy, www.ksu.edu.sa/.
8. Japan Science and Technology Agency, www.jst.go.jp/EN.
9. L. Branscomb, in *SciSIP listserv* 25 March 2009.
10. D. W. Jorgenson, M. S. Ho, K. J. Stiroh, *J. Econ. Perspect.* **22**, 3 (2008).
11. Directorate for Science, Technology, and industry, OECD, *A Forward-Looking Response to the Crisis: Fostering an Innovation-Led, Sustainable Recovery* (OECD, Paris, 2009); www.ioe-emp.org/fileadmin/user_upload/documents_pdf/globaljobscrisis/generaldocs/Fostering_an_Innovation-led_and_Sustainable_Recovery.pdf.
12. S. J. Davis, M. Henrekson, *NBER Working Paper W12768* (2006); www.nber.org/papers.
13. J. J. Heckman, *NBER working paper 7288* (1999); www.nber.org/papers.
14. U.S. Bureau of Economic Analysis (Washington, DC), www.bea.gov/regional/rims.
15. R. Ehrenberg, R. Smith, *Modern Labor Economics Theory and Public Policy* (Pearson Addison-Wesley, Boston, MA, ed. 9, 2005).
16. G. Tassey, *Econ. Innov. N. Technol.* **17**, 617 (2008).
17. S. Scotchmer, NSF grant 0830186 (2008).
18. S. Kiesler, J. Cummings, NSF grant 0830306 (2008).
19. C. Schunn, NSF grant 0830210 (2008).
20. L. Branstetter, NSF grant 0830233 (2008).
21. E. Fuchs, NSF grant 0830354 (2008).
22. A. Link, D. Siegel, NSF grant 0827976 (2008).
23. K. Fuglie *et al.*, *Agricultural Research and Development: Public and Private Investments Under Alternative Markets and Institutions* (AER735, Economic Research Service, USDA, Washington, DC, 1996).
24. B. Bozeman, D. Sarewitz, NSF grant 0738203 (2007).
25. Office of Science and Technology Policy, Science of Science Policy, scienceofsciencepolicy.net.
26. B. H. Obama, *Barack Obama: Connecting and Empowering All Americans Through Technology and Innovation* (Obama '08, 9 September 2008).
27. J. Thomas, National Visualization and Analytics Center, http://nvac.pnl.gov/leadership.stm (2008).
28. http://en.wikipedia.org/wiki/Production_function#Production_function_as_a_graph
29. J. Hage, G. B. Jordan, J. Mote, *Sci. Public Policy* **34**, 731 (2007).
30. The opinions expressed are those of the author and may not reflect the policies of NSF.

10.1126/science.1175335

MATERIALS SCIENCE

Watching Nanocrystals Grow

In situ transmission electron microscopy has revealed unprecedented detail in the growth of platinum nanocrystals.

Christopher B. Murray

The ability to observe individual chemical reactions in real time is reshaping our understanding of molecular processes, revealing subtleties previously hidden in ensemble averages. For example, single-molecule fluorescence detection methods have revolutionized optical microscopy and in situ studies of chemical and biological systems (*1*). Liquid cell in situ transmission electron microscopy (TEM) is poised to write a new chapter in the solution synthesis and processing of materials. On page 1309 of this issue, Zheng *et al.* use a TEM liquid cell that allows liquids to be examined within the vacuum environment of a TEM in an elegant experiment that uncovers dynamic processes in the growth of platinum (Pt) nanocrystals (*2*).

In in situ TEM, samples can be thermally cycled, mechanically stressed, electrically probed, and even grown from the vapor phase in the microscope (*3*, *4*). This method has become an indispensable tool in "hard materials" research. The more recent development of liquid cell in situ TEM has enabled observation of real-time processes in liquid phases (*5*). This tool could transform colloidal nanocrystal synthesis by providing detailed mechanistic understanding. Colloidal synthesis and processing of semiconductor, metal and dielectric nanocrystals have advanced tremendously in the past two decades, but synthetic innovations have been largely empirical (*6*).

Pt nanocrystals are an ideal initial system for these studies because their high electron contrast allows liquid-cell TEM imaging of individual particles. The importance of colloidal Pt nanocrystals as heterogeneous catalysts has also generated many high-quality nanocrystal growth studies, some specifically asserting that growth through coalescence plays a critical role (*7*). These earlier studies provide some of the motivation for making direct in situ experiments (*7*).

The TEM liquid cell used by Zheng *et al.* (see the first figure) is microfabricated from a pair of 100-µm-thick silicon wafers, coated with 25 nm of silicon nitride, and sealed with a cover, similar to the design of Ross (*5*). Silicon is etched to create a central viewing chamber and a pair of microfabricated reservoirs containing the Pt reagents and surfactants. A 200-nm-thick indium gasket separates the two electron-transparent silicon nitride membrane windows.

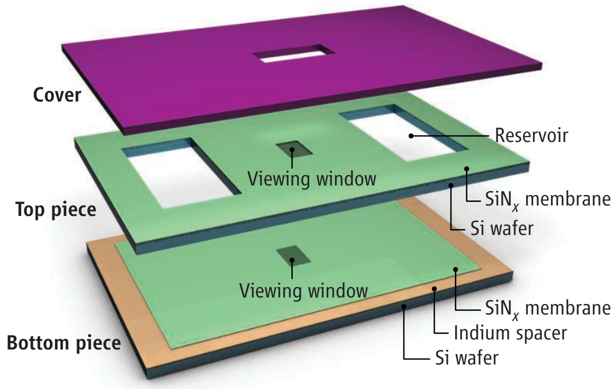

Windows on nanocrystal growth. A TEM cell that allows liquids to be studied is depicted.

Zheng *et al*. trigger nucleation and drive subsequent growth of the Pt nanocrystals by reducing Pt cations with the electron beam (*8*). Video-rate acquisition allows statistics of the growth trajectories of nanocrystals to be tracked from frame to frame (see the second figure). Zheng *et al.* observe that each nanocrystal has a finite probability of either growing steadily through the addition of metal-containing monomers from solution or merging with another nanocrystal in random coalescence events and thereby jumping ahead in the growth race. This subtle interplay of growth modes would be impossible to distinguish even with advanced in situ x-ray techniques (*9*), which are complementary to in situ TEM techniques in that they average over large ensembles of particles.

The steady bombardment of these nanocrystals by electrons likely leaves them highly negatively charged, because they are ungrounded and can float to high potential. Although it is somewhat unintuitive, Linse has established that highly charged colloid "macroions" with like charges can experience a net attractive force rather than the repulsion anticipated for simple point charges (*10*).

Perhaps the most intriguing observation of Zheng *et al.* is that coalescence events are often not epitaxial (which would create a single crystalline particle), nor do they initially produce compact, low-surface energy structures (*2*). After the "merger" of the nanocrystals (see panel B of the second figure), the composite particle appears to undergo a reorganization. After such mergers, many particles appear to take a hiatus from growth, and even slim down slightly. The merged particle undergoes etching and annealing that eliminates high-energy defects and surface asperities to produce ultimately a single coherent nanocrystal of the type seen in the bottom panel of part B of the figure.

Reorganization after nanocrystal coalescence proceeds effectively, even at low temperature, to yield a single crystalline product. The nominal temperature of the solution is barely more than one-tenth of the bulk Pt melting temperature, but the process is presumably aided by the energy of the electron beam and the depressed nanocrystal melting point. The relaxation periods that occurred during coalescence growth allow particles like particle 2 (see the second figure, panels D through F), which grow by the steady addition of monomer from solution, to catch up in size.

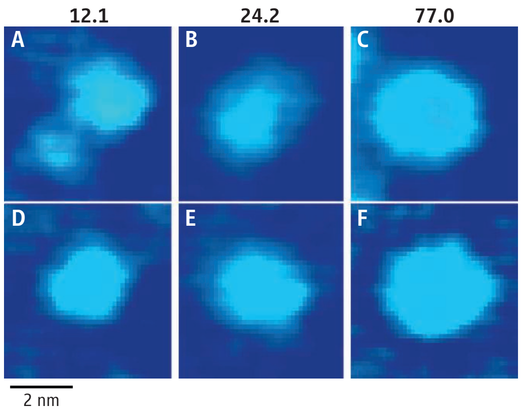

Contrasting growth modes. A series of video frames captured at 12.1, 24.2, and 77.0 s in the liquid-cell TEM for (**A**, **B**, and **C**) a particle growing by coalescence with a smaller particle and (**D**, **E**, and **F**) a particle growing through steady accretion of atoms.

CREDIT: (TOP) ADAPTED BY P. HUEY/*SCIENCE*

Department of Chemistry and Department of Materials Science and Engineering, University of Pennsylvania, Philadelphia, PA 19104, USA. E-mail: cbmurray@sas.upenn.edu

Despite the protracted period of nucleation and the different growth modes, Zheng *et al.* report that nanocrystals on average reach approximately the same size.

The approach developed by Zheng *et al.* should open the way to single-particle studies of the mechanism of oriented attachment. In this process, discrete nanocrystal building blocks fuse or polymerize after crystal faces contact to yield extended, single-crystalline nanostructures (*11*), but a definitive mechanism underlying this process has remained elusive (*12*). Direct comparisons could be made with molecular dynamics simulations and ex situ characterization of materials from conventional syntheses (*13*).

These initial studies suggest many related in situ nanocrystal growth experiments, which could be as simple as studying the effect of introducing preformed monodisperse seed nanocrystals into the reservoirs. More complex studies may be able to separate nucleation steps from growth processes. If a series of stabilizers with different chain lengths or head-group chemistry could assessed effectiveness in preventing or promoting coalescence, the results would be immediately useful. Integrating temperature control or adapting the system for continuous flow would further expand the scope of these experiments.

This approach to nanoscale structural characterization is also perfectly aligned with advances in the development of microreactors for the microfluidic production of nanocrystals (*14*). Nanocrystal microreactors have been demonstrated with complex mixing, heating, and online optical monitoring, and have even allowed isolation of products in segmented plug flow (*15*). The mechanistic insights for these studies should quickly influence nanocrystal synthesis, whether researchers are pushing tailored nanoscale materials toward large-scale "bulk" production or exploring highly customizable point-of-use fabrication in lab-on-a-chip approaches.

References and Notes

1. W. E. Moerner, D. P. Fromm, *Rev. Sci. Instrum.* **74**, 3597 (2003).
2. H. Zheng *et al.*, *Science* **324**, 1309 (2009).
3. P. J. Ferreira, K. Mitsuishi, E. A. Stach, *MRS Bull.* **33**, 83 (2008).
4. The special themes issue in which (*3*) appears provides a series of overviews of current in situ TEM investigations.
5. M. J. Williams *et al.*, *Nat. Mater.* **2**, 532 (2003).
6. C. B. Murray, C. R. Kagan, M. G. Bawendi, *Annu. Rev. Mater. Sci*. **30**, 545 (2000).
7. E. E. Finney, R. G. Finke, *J. Colloid Interface Sci.* **317**, 351 (2007).
8. J. Belloni, *Catalysis Today* **113**, 141 (2006).
9. B. Abecassis *et al.*, *Nano Lett.* **7**, 1723 (2007).
10. P. Linse, *J. Phys. Condens. Mater.* **14**, 13449 (2002).
11. R. L. Penn, J. F. Banfield, *Science* **281**, 969 (1998).
12. K. S. Cho *et al.*, *J. Am. Chem. Soc.* **127**, 7140 (2005).
13. M. J. Solomon, *Nat. Mater.* **6**, 557 (2007).
14. B. K. Yen *et al.*, *Adv. Mater*. **15**, 1858 (2003).
15. I. Shestopalov, J. D. Tice, R. F. Ismagilov, *Lab Chip* **4**, 316 (2004).

10.1126/science.1174666

PHYSICS

Dealing with Decoherence

For quantum computers to be a reality, the effects of interactions of qubits with their environment must be minimized.

Jan Fischer and Daniel Loss

The dream of building computers that work according to the rules of quantum mechanics has strongly driven research over the past decade in many fields of basic and applied sciences, including physics, chemistry, and computer science. About 10 years ago, it was shown mathematically that the direct use of quantum phenomena such as interference and entanglement could crucially speed up data searching and prime factorization for encryption. To turn quantum computers into reality, however, many issues in engineering and in basic physics need to be addressed.

One issue of central importance is the physical implementation of the qubit—the quantum analog of the information bit processed by today's computers. Whereas conventional bits can be set to either of the distinct states 0 or 1, qubits can also be in a coherent superposition of these two states: both 0 and 1. In principle, any quantum mechanical system with two distinct states, which can be put into such a superposition, could be used to encode quantum information. Thus, a large variety of candidate qubit systems have been proposed. We discuss one of the leading candidates, the solid-state implementation of spin qubits in quantum dots; however, the same fundamental challenges are shared by all candidate systems.

Department of Physics, University of Basel, Klingelbergstrasse 82, 4056 Basel, Switzerland. E-mail: jan.fischer@unibas.ch; daniel.loss@unibas.ch

The major problem in the realization of quantum computers is the short decoherence time. The qubit interacts with its environment, and the unavoidable coupling between the two causes a decay of qubit-state superpositions (see the figure, inset). The decoherence times are typically in the nano- to microsecond range for solid-state systems. However, they can easily vary over many orders of magnitude when the physical parameters (temperature, gate potentials, magnetic fields, material or isotope composition, confinement geometry, etc.) change.

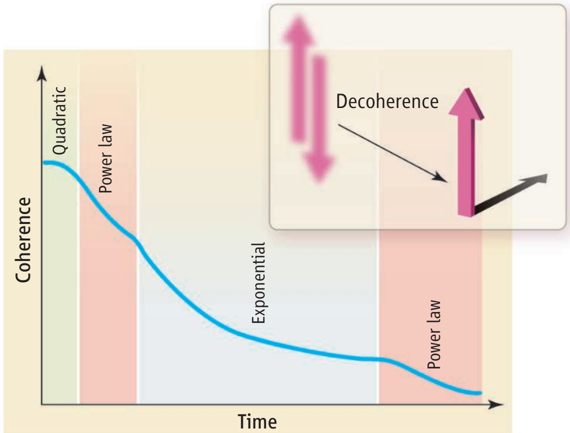

Losing it. A sketch of the decoherence of a spin qubit (electron in quantum dot) caused by a million nuclear spins that have been prepared in a noise-reduced state with a narrowed distribution. An initial quadratic decay is followed by a short-time power law, an intermediate-time exponential, and a long-time power-law decay. (**Inset**) Decoherence is the decay of quantum mechanical superpositions: The state evolves from "↑ and ↓" to either "↑" or "↓" as a result of interactions with the environment.

Building a quantum computer is therefore not simply an engineering problem with predictable progress. Instead, it is a complex problem involving many unwanted interactions with the outside world, raising the principal question of whether these interactions will ever allow sufficiently long coherence on a larger scale.

Decoherence is not of a "generic type" but is system-specific. Thus, the devil is in the details, and only understanding those details can reveal strategies to deal with decoherence. For instance, quantum error-correction schemes, which are essential for scalable quantum computation, almost exclusively assume a decoherence model characterized by a single-exponential decay time. However, we under-

Published by AAAS

stand now that there can be an entire "zoo of decoherence laws," even in the same system—with a time decay that can proceed through several different stages (see the figure).

The qubit in a quantum dot consists of a single electron whose spin states ↓ ("down") and ↑ ("up") represent the logical states 0 and 1 (*1*, *2*). These electrons can be initialized in either spin state, the state can be read out, and two neighboring spins can be coupled and decoupled. Thus, all the prerequisites for universal quantum computation are fulfilled. An attractive feature of this qubit system is that it can be operated in an all-electrical way, thus allowing the use of standard microelectronic technologies, which are flexible, fast, and scalable. The desired size would be a "quantum chip" containing about 10,000 qubits. Currently, however, only two-qubit quantum dots have been implemented.

The focus so far has been on GaAs-based (and also InAs-based) semiconductors, mainly because of the advanced nanofabrication techniques available (*2*). In these materials, decoherence at millikelvin temperatures arises from nuclear spins. There are typically a million of them inside a quantum dot, and they all couple to the single electron spin via the hyperfine interaction (*3*). This spin bath creates a random magnetic field, which leads to fluctuations in the electron spin precession and thus to decoherence. This happens fast, typically within tens of nanoseconds. In contrast, the flip of the electron spin due to lattice vibrations can be extremely slow, even exceeding seconds (*4*). For quantum computation to be viable, the coherence of a single qubit must be long enough to allow around 10,000 qubit operations. Although two-qubit operations to generate entanglement have already been demonstrated on a remarkably short time scale of about 0.2 ns (*5*), the decoherence time relative to this duration is still too fast.

Several strategies have been proposed and implemented to deal with this problem. One method to extend coherence, borrowed from nuclear magnetic resonance, is to apply magnetic field pulses (spin-echo sequences), which partly reverse the electron spin dynamics, thereby prolonging its coherence, even up to microseconds (*6*). Another idea is to prepare the nuclear spin bath in some less noisy state with a narrowed distribution width (*3*). Such state preparations have already been successfully implemented (*7*, *8*). Another strategy is to polarize the nuclear spins, either by electrical currents (*9*) or by cooling to ultralow temperatures, with the goal of freezing out the nuclear spins. It also may be possible to induce a magnetic phase transition in the nuclear spin system, resulting in a strong suppression of the harmful fluctuations of the spin bath (*10*).

An alternative approach is to use a hole—a missing electron in the valence band. The spin state of holes can be surprisingly long-lived (*11*). In contrast to electrons, their hyperfine interaction is weaker and, most important, highly anisotropic in GaAs dots, thus prolonging their decoherence time to tens of microseconds (*12*). Although the decoherence time has not yet been measured, initializing and reading out single-hole spins in quantum dots has been demonstrated (*13*).

Although the presence of nuclear spins is a nuisance, they can also be used to advantage. Manipulating the nuclear spins allows control over the electron spin, and the necessary coupling between two qubits can even be mediated by nuclear spins (*5*). Moreover, the nuclear-spin system itself is suitable for information storage, as it is more robust against perturbations from the environment because of its weaker magnetic coupling.

New materials may also be worth exploring. Quantum dots in carbon-based materials such as nanotubes, graphene, or diamond, or in other type IV semiconductors (especially silicon-germanium nanowires), have been investigated recently with a view toward spin qubits. These materials have the advantage of low abundances of spin-carrying nuclear isotopes, thus exhibiting weaker nuclear-spin interactions of the confined electron. For instance, natural carbon consists of 99% nuclei with zero spin. Coherent dynamics of single spins in diamond have already been reported (*14*), and coherence times on the order of microseconds have been measured (*15*). Finally, many proposals for hybrid systems have recently been made, suggesting the coupling of spins to photons in cavities. This opens up the possibility of storing the quantum information in one qubit type and processing the information in another one.

There is still a long way to go before a practical quantum computer will be reality. Nevertheless, the steady progress over the past decade is encouraging, and many workers in the field are cautiously optimistic that the goal can be reached.

References

1. D. Loss, D. P. DiVincenzo, *Phys. Rev. A* **57**, 120 (1998).
2. R. Hanson *et al.*, *Rev. Mod. Phys.* **79**, 1217 (2007).
3. W. A. Coish, D. Loss, *Phys. Rev. B* **70**, 195340 (2004).
4. S. Amasha *et al.*, *Phys. Rev. Lett.* **100**, 046803 (2008).
5. J. R. Petta *et al.*, *Science* **309**, 2180 (2005).
6. F. H. L. Koppens, K. C. Nowack, L. M. K. Vandersypen, *Phys. Rev. Lett.* **100**, 236802 (2008).
7. D. J. Reilly *et al.*, *Science* **321**, 817 (2008).
8. A. Greilich *et al.*, *Science* **317**, 1896 (2007).
9. K. Ono, S. Tarucha, *Phys. Rev. Lett.* **92**, 256803 (2004).
10. B. Braunecker, P. Simon, D. Loss, *Phys. Rev. Lett.* **102**, 116403 (2009).
11. D. Heiss *et al.*, *Phys. Rev. B* **76**, 241306 (2007).
12. J. Fischer *et al.*, *Phys. Rev. B* **78**, 155329 (2008).
13. B. D. Gerardot *et al.*, *Nature* **451**, 441 (2008).
14. R. Hanson *et al.*, *Science* **320**, 352 (2008).
15. F. Jelezko *et al.*, *Phys. Rev. Lett.* **92**, 076401 (2004).

10.1126/science.1169554

BIOCHEMISTRY

Force Signaling in Biology

J. Christof M. Gebhardt[1] and Matthias Rief[1,2]

Single-molecule studies are revealing the biomolecular processes initiated when biological systems sense mechanical forces.

Many processes in our body, like muscle contraction, cell locomotion and division, or transport processes, need force-producing actuators such as molecular motors. In turn, biological systems can also sense mechanical forces. Examples are the sense of touch, hearing, and the strengthening of muscle tissues upon physical exercise. In these cases, force triggers a biochemical signal cascade, but the mechanisms by which forces affect biomolecular conformation and biochemical signaling have long remained elusive. The development of ultrasensitive instruments for nanomanipulation—such as atomic force microscopy and optical and magnetic tweezers—has allowed the effect of forces on protein conformation and function to be probed at the single-molecule level (*1*–*4*).

On page 1330 of this issue, Zhang *et al.* use optical tweezers to clarify the role that mechanical forces play in the regulation of primary hemostasis in blood clotting (*5*). A key player in this process is von Willebrand factor (VWF), a large protein complex in

[1]Physik Department E22, Technische Universität München, James-Franck-Strasse, 85748 München, Germany. E-mail: mrief@ph.tum.de [2]Munich Center for Integrated Protein Science CIPSM, 81377 München, Germany.

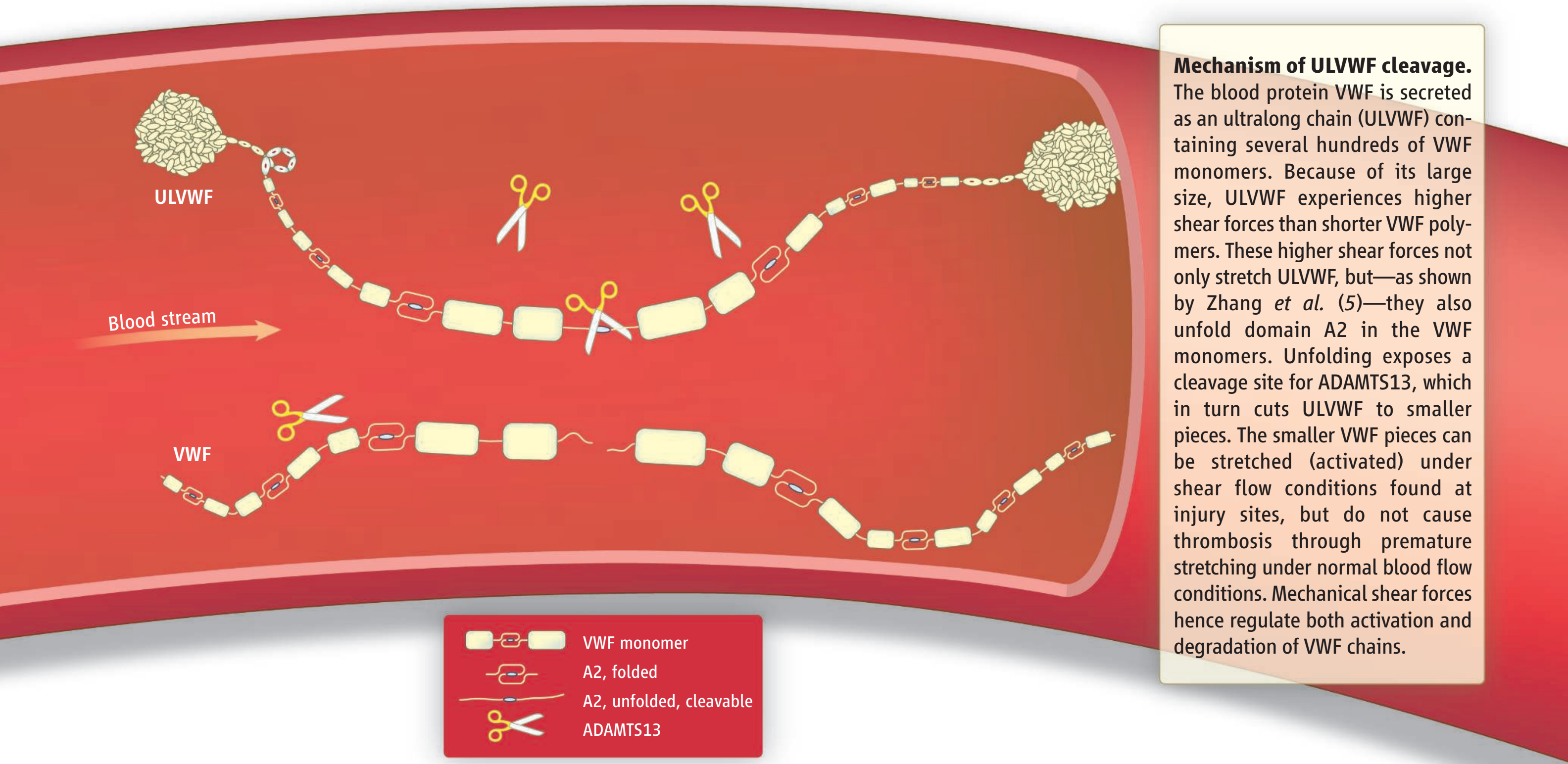

Mechanism of ULVWF cleavage. The blood protein VWF is secreted as an ultralong chain (ULVWF) containing several hundreds of VWF monomers. Because of its large size, ULVWF experiences higher shear forces than shorter VWF polymers. These higher shear forces not only stretch ULVWF, but—as shown by Zhang *et al.* (*5*)—they also unfold domain A2 in the VWF monomers. Unfolding exposes a cleavage site for ADAMTS13, which in turn cuts ULVWF to smaller pieces. The smaller VWF pieces can be stretched (activated) under shear flow conditions found at injury sites, but do not cause thrombosis through premature stretching under normal blood flow conditions. Mechanical shear forces hence regulate both activation and degradation of VWF chains.

which hundreds of large protein monomers are linked together to form a long chain (see the figure) (*6*). Under conditions of normal blood flow, VWF chains are in a collapsed state that cannot induce blood clotting. High shear forces at injury sites elongate VWF chains, resulting in the exposure of platelet-binding motifs that aggregate platelets and stop bleeding in small blood vessels (*7*).

VWF is initially secreted in a highly active ultralong form (ULVWF). Because hydrodynamic forces act along the whole contour of a molecule, the long ULVWF chains are more easily stretched in shear flow. However, this increases the risk of causing thrombosis through premature aggregation of platelets. The body must therefore counteract and regulate uncontrolled activation of ULVWF. This regulation is also mediated by shear flow forces. If stretched, ULVWF can be cleaved at its domain A2 by the metalloprotease ADAMTS13 (*8*). Tsai has speculated that domain A2 in the VWF monomer unfolds upon shear force–induced stretching of ULVWF, exposing an otherwise buried cleavage site for ADAMTS13 (*9*). ADAMTS13 can then cleave ULVWF.

Zhang *et al*. now provide direct evidence for force-induced unfolding and cleavage of A2. Using optical tweezers, they directly tested the activation mechanism of ADAMTS13-mediated cleavage of A2 on the single-molecule level. They found that an individual A2 domain unfolds at forces of ~11 pN when stretched mechanically. When relaxed to lower forces, A2 remains unfolded for about 2 s before it refolds. In their assay, cleavage of A2 by ADAMTS13 occurs only in the unfolded configuration; A2 is not cleaved if the applied force remains below the unfolding threshold. Mechanical force thus acts as a cofactor for ADAMTS13.

At first sight, the rather broad force distribution observed for the unfolding of A2 in the single-molecule assay seems to contradict the well-defined upper length limit observed for VWF chains in vivo. Obviously, a mechanism must exist that creates a sharp cutoff such that long ULVWF polymers get cleaved but shorter VWF polymers escape cleavage. Zhang *et al*. provide an explanation for this sharp cutoff: The force in the center of a VWF polymer depends on the square of its length. This quadratic dependence separates longer polymers from shorter ones. Using the 11 pN unfolding force, Zhang *et al.* calculate an upper length limit for VWF of 200 monomers at physiological shear rates. This number agrees well with the upper length limit of VWF chains observed in vivo.

Exposition of buried binding sites under the influence of mechanical load may be a general working principle of biological mechanosensors. Recently, Puchner *et al.* discovered a force-induced activation mechanism of the strain sensing kinase of the giant muscle protein titin (*2*). Using single-molecule force spectroscopy and molecular dynamics simulations, they found that mechanical force unfolds the C-terminal autoinhibitory tail of titin kinase, thus activating the enzyme. After force activation, adenosine triphosphate (ATP) can bind to the enzyme, phosphorylation can proceed, and force adaptation processes in muscle can be effected. Unfolding under mechanical shear stress also seems likely for many cytoskeletal proteins (*10*). In a recent study, del Rio *et al.* identified talin as a mechanosensor for the reorganization of the actin cytoskeleton (*4*). Talin couples the cytoskeleton to the extracellular matrix and contains several encrypted binding sites for vinculin. Signaling is activated upon vinculin binding. However, the binding sites are only exposed after talin is stretched mechanically and has partially unfolded. Hence, this molecule can also sense forces through mechanical unfolding.

Our understanding of forces as signals in living systems is still far from complete, and a picture of the primary molecular mechanisms for mechanosensing and mechanosignaling is just emerging. Even nonmechanical processes like cell differentiation can strongly depend on mechanical signals (*11*). How these mechanical signals are further processed and how they affect responses on the supramolecular, cellular, and even multicellular level remain important questions for the future.

References and Notes

1. C. Cecconi, E. A. Shank, C. Bustamante, S. Marqusee, *Science* **309**, 2057 (2005).
2. E. M. Puchner *et al.*, *Proc. Natl. Acad. Sci. U.S.A.* **105**, 13385 (2008).
3. J. P. Junker, F. Ziegler, M. Rief, *Science* **323**, 633 (2009).
4. A. del Rio *et al.*, *Science* **323**, 638 (2009).
5. X. Zhang *et al.*, *Science* **324**, 1330 (2009).
6. J. E. Sadler, *Annu. Rev. Biochem.* **67**, 395 (1998).
7. S. W. Schneider *et al.*, *Proc. Natl. Acad. Sci. U.S.A.* **104**, 7899 (2007).
8. G. G. Levy *et al.*, *Nature* **413**, 488 (2001).
9. H. M. Tsai, *Blood* **87**, 4235 (1996).
10. C. P. Johnson, H. Y. Tang, C. Carag, D. W. Speicher, D. E. Discher, *Science* **317**, 663 (2007).
11. A. J. Engler, S. Sen, H. L. Sweeney, D. E. Discher, *Cell* **126**, 677 (2006).
12. We thank A. Bausch and R. Netz for helpful comments on the manuscript. We acknowledge funding through Deutsche Forschungsgemeinschaft grant SFB 486 B9.

10.1126/science.1175874

ANTHROPOLOGY

On Becoming Modern

Ruth Mace

Human social evolution is determined by demography.

Unlike other animals, humans cooperate with nonrelatives in coordinated actions, decorate their bodies, build complex artefacts (useful or otherwise), talk, and divide themselves into linguistic groups. To understand the evolutionary basis of such behaviors, anthropologists must consider not only issues connected to social evolution in animals, but also the implications of the possible coevolution of genes and culture. Two articles in this issue examine aspects of human social evolution: On page 1293, Bowles (*1*) investigates the origins of altruism toward one's own social group, while on page 1298, Powell *et al.* (*2*) study the emergence of cultural complexity. Based on empirical evidence and modeling, both studies suggest that the demographic structure of our ancestral populations determined how social evolution proceeded.

If, like me, you were brought up on *The Selfish Gene* (*3*), you learned that selection acts on individuals or genes, and you are trained to be wary of group selectionist explanations for behavior. Group selection is generally rejected as unimportant because even a tiny amount of migration between groups quickly destroys the genetic differences needed for group selection to act. But recent literature on social evolution has reopened the debate, arguing that in some circumstances group selection might be important, especially in a cultural species like humans. Genetic and cultural traits are both heritable and subject to evolutionary processes, but cultural traits are not transmitted in a Mendelian way; they can be inherited from almost anyone, including people who may not share your genetic interests. This could lead to evolutionary outcomes not seen in other animals (*4*).

Perhaps the central difference between genetic and cultural transmission is that we can change our cultural phenotype during our lives—for example, to conform to group norms. Cultural differences between groups might be easier to maintain than are genetic ones, due to processes such as conformist social learning and punishment; several models show that if these processes occur, cultural group selection could explain the evolution of prosocial or altruistic behavior (*5*).

Bowles now makes a more radical claim: that the demographic structure of hunter-gatherer populations allowed group-selected genetic traits to evolve in humans. He argues that lethal warfare was endemic and that altruistic, group-beneficial behaviors that hurt the survival chances of individuals but improved the likelihood for groups to win conflicts could emerge by group selection. This argument was originally espoused by Darwin, but few formal tests of it have been done.

In his model, Bowles identifies two key determinants of whether group selection can favor altruistic behavior: the individual and group costs and benefits of altruism in warfare, and the extent of genetic differentiation among groups. An array of ethnographic and archaeological evidence shows that hunter-gatherers certainly did kill each other. How much of this killing was within or between groups is tricky to ascertain (especially from archaeological data) and varies among sites, but on average, 14% of adult deaths appear to have been due to warfare. The extent of prehistoric genetic differentiation is also difficult to estimate, but based on genetic studies of extant hunter-gatherers, the model shows that a realistic level of inbreeding within groups allows group benefits to offset fitness costs of roughly 3% associated with being an "altruistic warrior" relative to nonaltruists. Ironically, lethal hostility toward other groups could thus underpin cooperation and support within human communities.

Technological and cultural complexity. Sophisticated tools such as these harpoons began to emerge in the upper Paleolithic (between ca 40,000 and 10,000 years ago).

The model does not account for sex differences, which might matter, because females did not fight in wars, were likely to join and reproduce with the victorious group after conflict [they may well have been the objective of the conflict in the first place (*6*)], and were more likely, even in peacetime, to migrate out of their natal group to breed. The inheritance of the altruistic traits is assumed to be vertical and asexual, so the model could work for a cultural trait (possibly even better than for a genetic one). It is also possible that the measures of inbreeding observed are maintained by cultural processes, such as language differences between groups. Nonetheless, Bowles suggests that the model could theoretically apply to other social animals. Zoologists, whose limited tolerance of group selection rarely extends beyond the human species, will find this statement controversial; but it is certainly not without the bounds of scientific possibility to test.

Powell *et al.* address the evolution of technological and cultural complexity—human behaviors that have left clear traces in the archaeological record. Traits such as the creation of abstract art, improvements in stone and other tools, long-distance "trading," and the manufacture of musical instruments mark the emergence of modern humans who behaved much as we do (see the figure). These material expressions of the modern condition emerged much later than did anatomically modern humans. Some aspects of behavioral modernity first appeared in southern Africa, possibly as early as 90,000 years ago, only to disappear again and reappear in Eurasia ~45,000 years ago. The timing of these events makes a biological change in cognitive capacity a somewhat unlikely explanation.

Department of Anthropology, University College London, Taviton Street, London WC1H 0BW, UK. E-mail: r.mace@ucl.ac.uk

Powell *et al.* now argue that changes in population size and structure can explain the patterns of acquisition (and loss) of culturally inherited skills. The authors build on a model by Henrich (*7*), who showed that small populations were more likely to lose complex skills. Powell *et al.* examine a more realistically structured population, in which individuals live in groups (subpopulations) and inherit (learn) skills from others in the group or by contact due to migration between groups. The results show that the time since first occupation of a region is a far less reliable predictor of the accumulation of cultural skills than is the density of subpopulations and the degree of migration between them.

The authors then use coalescent models (a statistical approach assuming neutral traits which are subject to drift) of genetic variation in mitochondrial DNA to estimate prehistoric population densities at various sites. The resulting population density estimates are compatible with those necessary to prompt the onset of behavioral modernity at the appropriate time in sub-Saharan Africa, and then later in the Middle East. The genetic evidence cannot really help to explain the subsequent disappearance of these traits in sub-Saharan Africa, but there is some archaeological evidence (*8*) that depopulation may have occurred at the relevant time (around 70,000 to 60,000 years ago).

The model of Powell *et al.* only includes selection on cultural traits, not on individuals or populations. In the model, skills are assumed to be transmitted because they are beneficial. It is therefore possible that the advantages of cultural skill acquisition caused population density to increase, rather than emerged as a response to it. This is an area for further modeling. And, of course, Powell *et al.* argue that the cognitive ability to learn these skills was already present in all. Researchers seeking genes involved in cognitive ability would thus be unwise to base their evidence on correlating geographic patterns of candidate genes with geographic patterns of the emergence of culturally acquired skills—at least not without paying careful attention to demographic differences.

The two models (*1*, *2*) paint rather different pictures of Pleistocene life. Were early modern humans in frequent contact with neighboring groups to exchange cultural innovations, or were they inward looking, unwilling to travel, and constantly engaging their neighbors in lethal conflict? Probably both, at different times and in different places (although it may be possible to steal someone's cultural innovations and kill them too). Neither study claims that its model provides the unequivocal explanation. Indeed, there are many alternative explanations both for altruistic behavior in human groups and for the emergence of cultural modernity. Some alternative explanations may be more due to semantics than real differences in evolutionary processes (*9*), and some may work in addition to the processes proposed here. But by combining models with data, both studies put their hypotheses firmly up the list of possibilities to be taken seriously.

References

1. S. Bowles, *Science* **324**, 1293 (2009).
2. A. Powell, S. Shennan, M. G. Thomas, *Science* **324**, 1298 (2009).
3. R. Dawkins, *The Selfish Gene* (Oxford Univ. Press, Oxford, 1976).
4. P. J. Richerson, R. Boyd, *Not by Genes Alone: How Culture Transformed Human Evolution* (Univ. of Chicago Press, Chicago/London, 2005).
5. R. Andrés Guzmán, C. Rodriguez-Sickert, R. Rowthorn, *Evol. Hum. Behav.* **28**, 112 (2007).
6. N. Chagnon, *Yanomamo: The Fierce People* (Holt, Rinehart & Winston, New York, 1983).
7. J. Henrich, *Am. Antiq.* **69**, 197 (2004).
8. S. H. Ambrose, *J. Hum. Evol.* **34**, 623 (1998).
9. S. A. West, A. S. Griffin, A. Gardner, *J. Evol. Biol.* **21**, 374 (2008).

10.1126/science.1175383

CELL BIOLOGY

Hypoxic Hookup

The range of protective effects that a sirtuin deacetylase affords to cells and organisms under stressful conditions continues to grow.

Leonard Guarente

Hypoxia-inducible factors HIF-1α and HIF-2α are homologous transcription factors that activate an adaptive response in mammalian cells to low concentrations of environmental oxygen (*1*, *2*). HIF-activated genes protect against damaging reactive oxygen molecules generated by mitochondria in response to hypoxia, and also stimulate erythrocyte proliferation and blood vessel formation to enhance organism survival. Under normal oxygen conditions, HIF-1α and HIF-2α are hydroxylated on key prolines, which promotes their degradation. However, under hypoxic conditions, the HIF proteins are stabilized and accumulate in cells. On page 1289 of this issue, Dioum *et al.* show that during hypoxia, HIF-2α is deacetylated and thereby activated by SIRT1, a nicotinamide adenine dinucleotide (NAD)–dependent deacetylase (*3*). This finding extends the reach of SIRT1 as a cell and tissue maintenance and anti-aging factor to include resistance to hypoxic stress. SIRT1 has already been shown to protect against metabolic, genotoxic, and heat stress by deacetylating other key transcription factors that respond to those stressors (*4*–*8*) (see the figure).

Dioum *et al.* show that in cultured mammalian cells, SIRT1 bound to and deacetylated HIF-2α and activated the HIF-2α target genes *Sod2* (superoxide dismutase 2), *VegfA* (vascular endothelial growth factor A), and *Epo* (erythropoietin). A catalytically inactive form of SIRT1 was unable to alter HIF-2α activity, indicating the importance of HIF-2α deacetylation in the activation mechanism. Mutating three lysines of HIF-2α, which are acetylated, did not completely abolish activation by SIRT1. This indicates that other, unidentified lysines are important for HIF-2α regulation. It is not yet clear whether additional deacetylases (histone deacetylases or SIRTs 2 to 7) also play important roles in HIF-2α activation. However, depletion of SIRT1 alone increased the amount of acetylated HIF-2α during hypoxia, suggesting that SIRT1 is the primary HIF-2α deacetylase.

The relationship between SIRT1 and HIF-2α was also shown in biological settings. The liver is the chief source of erythropoietin production during mid-gestation in mice. Embryos lacking either Sirt1 or HIF-2α showed a defect in erythropoietin expression in the liver during this gestational period. Tail vein injection of adenoviral expression vectors containing Sirt1-encoding DNA along with vectors encoding either HIF protein demonstrated the potential of Sirt1 to activate HIF-2α, but not HIF-1α, in the adult liver. And a viral vector that triggered RNA interference of endogenous Sirt1 reduced expression of the liver *Epo* gene.

Because HIF-2α is only stable under hypoxic conditions in the studies described, Dioum *et al.* do not address whether SIRT1 itself is activated by hypoxia. This issue is extremely relevant to possible roles for sirtuin

Paul F. Glenn Lab and Department of Biology, Massachusetts Institute of Technology, Cambridge, MA 02139, USA. E-mail: leng@mit.edu

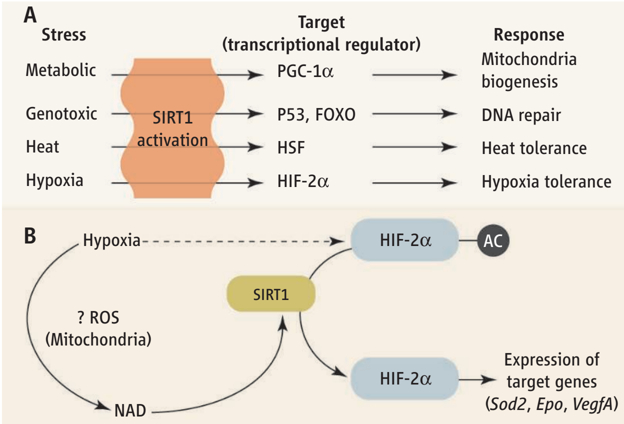

HIF-2α hijacks SIRT1. (**A**) SIRT1 responds to different stressors. PGC-1α, peroxisome proliferator–activated receptor γ coactivator 1α; HSF, heat-shock factor. (**B**) During hypoxia, HIF-2α protein is stabilized and then deacetylated by SIRT1 to increase its potential to activate target genes. SIRT1 may itself be activated by hypoxia via an increase in NAD rendered by reactive oxygen species produced by mitochondria, although this has not yet been demonstrated.

CREDIT: N. KEVITIYAGALA/SCIENCE

proteins in episodes of ischemia, during which vital organs such as the heart and brain are deprived of oxygen. At first glance, it might appear that the cellular redox environment would be more reducing during oxygen scarcity, thereby reducing NAD (a substrate of SIRT1) to the inactive NADH form, and decreasing sirtuin activity. However, SIRT1 is highly protective in mouse models of ischemia (*9*), which suggests that its activity under hypoxic conditions is actually high. One possible explanation for this paradox is that the increased production of reactive oxygen species by mitochondria under hypoxic conditions actually drives the redox state of the nucleus and cytoplasm toward oxidizing conditions, thereby increasing available NAD and sirtuin activity (see the figure).

Why does SIRT1 affect HIF-2α—which is present only in vertebrates—but not HIF-1α? The biology of the SIRT1–HIF-2α interaction is likely to be specific to higher organisms. One biochemical distinction between HIF-1α and HIF-2α that is observed in cell culture is that the latter is activated by a moderate reduction in oxygen availability, whereas the former requires a more severe reduction (*2*). Perhaps SIRT1 has evolved in vertebrates to function during a spectrum of hypoxic conditions, such as facilitating cell division and tissue modeling in response to physiological hypoxia (during normal development) and tissue repair and remodeling in response to pathological hypoxia (in adults).

Solid tumors can survive hypoxic conditions (the high cell density of a tumor limits the availability of oxygen to cells) by using protective mechanisms of healthy cells, including the activation of HIF-1α and HIF-2α. In this setting, HIF-dependent expression of the growth-promoting factor VEGF and other target genes can promote tumor growth by facilitating angiogenesis and other tumorigenic processes. Hence, HIF inhibitors are currently under development as anticancer drugs. Does this mean that SIRT1 inhibitors will also possess antitumor properties? Perhaps, but SIRT1 evolved to promote organism survival in response to stress. Thus, this sirtuin may have elaborated additional tumor suppressor mechanisms to offset any tumorigenic effects due to HIF-2α activation. Of note, one of the transcriptional programs activated by HIF-2α (but not HIF-1α) under hypoxia is driven by the proto-oncogene c-*myc* (*10*). However, c-myc is also deacetylated (thus destabilized) by SIRT1 (*11*), potentially countering any c-myc activation by SIRT1–HIF-2α. It is reasonable to infer that the integrated effects of SIRT1 in a solid tumor are not tumorigenic and might even restrain tumor growth.

The myriad of SIRT1 protective effects raises the question of why evolution has not maximized SIRT1 activity. By coupling SIRT1 activity to NAD and metabolism, an organism can up- or down-regulate its activity in accord with prevailing conditions to set its near-term strategy for either maintenance (during stressful conditions) or reproduction (during favorable conditions). Given that dietary and other environmental stressors have waned in the developed world, aging itself arguably poses the greatest stressor we must face. The challenge then is to boost the protective effects of sirtuins pharmacologically to counter the stress of normal aging and to mitigate aging-dependent diseases and disability.

References

1. E. L. Bell, N. S. Chandel, *Essays Biochem.* **43**, 17 (2007).
2. S. A. Patel, M. C. Simon, *Cell Death Differ.* **15**, 628 (2008).
3. E. M. Dioum *et al.*, *Science* **324**, 1289 (2009).
4. J. T. Rodgers *et al.*, *Nature* **434**, 113 (2005).
5. J. Luo *et al.*, *Cell* **107**, 137 (2001).
6. A. Brunet *et al.*, *Science* **303**, 2011 (2004); published online 19 February 2004 (10.1126/science.1094637).
7. M. Motta *et al.*, *Cell* **116**, 551 (2004).
8. S. D. Westerheide *et al.*, *Science* **323**, 1063 (2009).
9. D. Della-Morte *et al.*, *Neuroscience* **159**, 993 (2009).
10. J. D. Gordan *et al.*, *Cancer Cell* **11**, 335 (2007).
11. J. Yuan, K. Minter-Dykhouse, Z. Lou, *J. Cell Biol.* **185**, 203 (2009).

10.1126/science.1175679

IMMUNOLOGY

Amino Acid Addiction

J. Magarian Blander[1] and Derk Amsen[2]

Signaling pathways that control cellular responses to stress may also specify T cell differentiation.

Arguably the most exciting cell in the immune system these days is the T helper 17 (T_H17) cell. Much of the interest stems from its prominent role in autoimmune-related pathologies, such as multiple sclerosis, inflammatory bowel disease, and psoriasis (*1*). On page 1334 of this issue, Sundrud *et al.* report that a small molecule called halofuginone specifically inhibits the generation of T_H17 cells, without affecting other $CD4^+$ T cell types (*2*). The mechanism involved has potentially important implications for understanding how the immune system prevents untoward generation of harmful T_H17 cell responses.

[1]Immunology Institute, Department of Medicine, Mount Sinai School of Medicine, New York, NY 10029, USA. [2]Department of Cell Biology, Academic Medical Center, Amsterdam, Netherlands. E-mail: julie.blander@mssm.edu; d.amsen@amc.nl

Several lineages of $CD4^+$ T helper cells are generated by the mammalian immune system. T_H1 and T_H2 cells produce cytokines that activate immune responses against intracellular bacteria and helminth parasites, respectively. Regulatory T helper cells (T_{reg}) prevent other T cells from assaulting the body itself. T_H17 cells obviously did not evolve to cause autoimmunity, but mediate immune responses to certain bacteria and fungi by producing the proinflammatory cytokine interleukin-17 (IL-17) (*1*, *3*). T_H1, T_H2, and T_H17 cells arise from a common precursor cell type, directed by signals that inform about the nature of the infectious threat encountered. For T_H17 cells, differentiation is instructed by the cytokines transforming growth factor–β (TGF-β) and IL-6 (*1*).

Given the prominent involvement of T_H17 cells in autoimmunity, there is great interest in identifying drugs that inhibit these cells, ide-

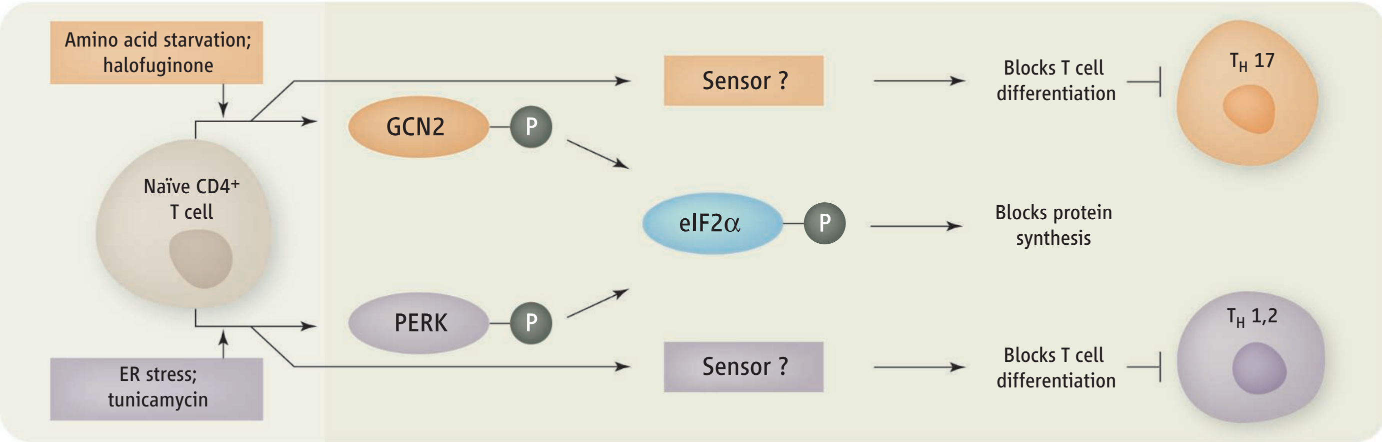

Stress and differentiation. Despite sharing a common signaling pathway that halts protein expression and induces protective genes, various stress conditions also mobilize separate pathways that differentially target T cell development. PERK, pancreatic endoplasmic reticulum eIF2α kinase.

ally without interfering with the function of the other T helper cell lineages. Halofuginone is an analog of the active compound found in *Dichroa febrifuga*, a plant used in traditional Chinese medicine to reduce malarial fever (*4*). In Western medicine, halofuginone has been used to treat fibrotic diseases such as scleroderma. Halofuginone inhibits collagen deposition, presumably by interfering with TGF-β–stimulated production of collagen by fibroblasts (*4*).

Sundrud *et al.* now report that halofuginone inhibits the development of both mouse and human T_H17 cells at concentrations that do not prevent general T cell activation or development of T_H1, T_H2, or T_{reg} cells. Systemic administration of halofuginone was also protective against autoimmunity in a mouse model for multiple sclerosis. In this model, disease can be manipulated experimentally to be driven by either T_H1 or T_H17 cells (*5*, *6*). Halofuginone only inhibited the disease promoted by T_H17 cells.

Whether halofuginone will be a therapeutic agent against autoimmune diseases remains to be determined. One caveat is that halofuginone inhibits differentiation, but not the effector function of already developed T_H17 cells. This might limit its potential, considering that clinical manifestations of autoimmune disorders usually occur after the autoaggressive T cells have developed. Furthermore, T_H17 cells produce cytokines (IL-10 and IL-22) that function in immune tolerance and tissue repair (*1*). Total blockade of T_H17 cell differentiation may thus cause undesired side effects.

Nonetheless, the findings by Sundrud *et al.* reveal an intriguing concept in T helper cell differentiation. Inhibition of T_H17 cell differentiation by halofuginone appears unrelated to its effect on signaling by the TGF-β receptor. Treatment of cultured T cells with halofuginone increased the expression of genes associated with the amino acid starvation response (see the figure). Mammalian cells are unable to synthesize several essential amino acids and must acquire them from the extracellular milieu. When amino acids are limiting, a protective starvation response program is initiated in which translation of most RNAs into proteins is blocked and the expression of a selective set of protective genes is induced (*7*–*9*). This response involves activation of an enzyme called general control nonderepressible–2 (GCN2) kinase. GCN2 then phosphorylates and thereby inactivates the eukaryotic translation initiation factor 2α (eIF2α). Consequently, translation of most RNAs is turned off. However, these conditions favor translation of RNA encoding the activating transcription factor 4 (ATF4), which induces expression of specific protective genes (*7*–*9*). Treatment of $CD4^+$ T cells with halofuginone resulted in phosphorylation of GCN2 and eIF2α as well as expression of ATF4 and its target genes. Inhibition of T_H17 cell differentiation by halofuginone could be overcome by treating cells with excess amino acids. Similarly, low availability of essential amino acids prevented differentiation of T_H17 cells, but not of T_H1 or T_H2 cells. This "addiction" of T_H17 cells to amino acids is reminiscent of earlier findings that certain aromatic amino acids are critical for synthesizing ligands for the aryl hydrocarbon receptor, a transcription factor required for generating IL-22–producing T_H17 cells (*10*).

What makes T_H17 cell differentiation uniquely sensitive to the starvation response, and how does this protective response prevent T_H17 cell differentiation? Activation of the eIF2α-ATF4 pathway may not be solely responsible because the drug tunicamycin, which induces stress in the endoplasmic reticulum (ER), also activates the eIF2α-ATF4 pathway (*11*), but does not inhibit T_H17 cell differentiation. Surprisingly, tunicamycin inhibits differentiation of T_H1 and T_H2 cells, instead. This suggests that sensors unique to each stress response pathway may differentially control individual T helper cell lineages.

Perhaps the most intriguing question is whether there is any evolutionary advantage afforded by the sensitivity of T_H17 cell differentiation to the amino acid starvation response. Could it have evolved to prevent untoward generation of these potentially dangerous cells? Indeed, the availability of certain amino acids in the tissue microenvironment can be diminished by various immunosuppressive enzymes (*12*). TGF-β, a major suppressive cytokine for other T helper cell lineages, promotes rather than inhibits differentiation of T_H17 cells (*1*), leaving a hole in the protective armament against rogue T_H17 responses. The existence of an alternative mechanism to hold T_H17 cells in check, through particular dependence on amino acids, is therefore an attractive idea.

References

1. T. Korn, E. Bettelli, M. Oukka, V. K. Kuchroo, *Annu. Rev. Immunol.* **27**, 485 (2009).
2. M. S. Sundrud *et al.*, *Science* **324**, 1334 (2009).
3. M. B. Torchinsky, J. Garaude, A. P. Martin, J. M. Blander, *Nature* **458**, 78 (2009).
4. M. Pines, D. Snyder, S. Yarkoni, A. Nagler, *Biol. Blood Marrow Transplant.* **9**, 417 (2003).
5. C. L. Langrish *et al.*, *J. Exp. Med.* **201**, 233 (2005).
6. H. Waldner, M. Collins, V. K. Kuchroo, *J. Clin. Invest.* **113**, 990 (2004).
7. C. Deval *et al.*, *FEBS J.* **276**, 707 (2009).
8. H. P. Harding *et al.*, *Mol. Cell* **6**, 1099 (2000).
9. R. C. Wek, H. Y. Jiang, T. G. Anthony, *Biochem. Soc. Trans.* **34**, 7 (2006).
10. M. Veldhoen, K. Hirota, J. Christensen, A. O'Garra, B. Stockinger, *J. Exp. Med.* **206**, 43 (2009).
11. H. P. Harding *et al.*, *Mol. Cell* **11**, 619 (2003).
12. A. L. Mellor, D. H. Munn, *Nat. Rev. Immunol.* **8**, 74 (2008).

10.1126/science.1175678

CREDIT: N. KEVITIYAGALA/SCIENCE

Disulfide Formation in the ER and Mitochondria: Two Solutions to a Common Process

Jan Riemer,[1] Neil Bulleid,[2] Johannes M. Herrmann[1]*

The endoplasmic reticulum (ER) was long considered to be the only compartment of the eukaryotic cell in which protein folding is accompanied by enzyme-catalyzed disulfide bond formation. However, it has recently become evident that cells harbor a second oxidizing compartment, the mitochondrial intermembrane space, where disulfide formation facilitates protein translocation from the cytosol. Moreover, protein oxidation has been implicated in many mitochondria-associated processes central for human health such as apoptosis, aging, and regulation of the respiratory chain. Whereas the machineries of ER and mitochondria both form disulfides between cysteine residues, they do not share evolutionary origins and exhibit distinct mechanistic properties. Here, we summarize the current knowledge of these oxidation systems and discuss their functional similarities and differences.

The production of functional proteins in the cell involves at least two steps: the synthesis of nascent polypeptides on cytosolic ribosomes, followed by the folding of these polypeptides into their functional conformation. Both processes can occur simultaneously, and ribosomes specifically recruit a variety of dedicated chaperone systems to their polypeptide exit tunnels to facilitate efficient folding of nascent chains. In the case of oxidative protein folding, synthesis and folding generally occur in temporally and spatially distinct reactions (Fig. 1A). Protein synthesis occurs in the cytosol where a very high concentration (10 to 14 mM) of reduced glutathione together with numerous reducing enzymes counteracts the formation of disulfide bonds (*1*). Thus, oxidative folding normally takes place only after translocation to a different compartment in which disulfide formation is favored. This spatial separation of synthesis and folding contributes to compartmentalization of the cell, ensuring that newly synthesized proteins become active only after successful delivery to their correct destination. Moreover, disulfide bonds provide increased stability, which is especially important for secreted and cell-surface proteins because they are not under the surveillance of the cellular chaperone machinery. In addition, redox regulation by the reversible formation of disulfide bonds can be used to adapt protein activity directly to the redox conditions in a given environment. In most cases, disulfide formation is an enzymatically catalyzed process that occurs in the periplasm of prokaryotes and in the ER and mitochondrial intermembrane space (IMS) of eukaryotes (Fig. 1B). We will focus specifically on the two eukaryotic oxidation machineries and compare their structural and mechanistic properties.

[1]Cell Biology, University of Kaiserslautern, Erwin Schrödinger Strasse 13, 67663 Kaiserslautern, Germany. [2]Faculty of Life Sciences, The Michael Smith Building, University of Manchester, Oxford Road, Manchester M13 9PT, UK.

*To whom correspondence should be addressed. E-mail: hannes.herrmann@biologie.uni-kl.de

Common Principles of Disulfide Bond Formation

The formation of disulfides in substrate proteins is a reversible reaction in which the thiol groups of two cysteine residues are oxidized to form a covalently linked disulfide. This can be achieved by thiol-disulfide exchange in which a disulfide bond present in an electron acceptor is reduced. Alternatively, the transfer of electrons to molecular oxygen leads to de novo disulfide bond formation (Fig. 1C). Despite the thermodynamically favorable nature of the oxygen-dependent protein oxidation, this reaction typically requires catalysts such as transition metals or the redox cofactor flavin adenine dinucleotide (FAD) to overcome the kinetic barrier caused by the incompatibility of one- and two-electron transfer processes.

The Mitochondrial Disulfide Relay

Recently, it was discovered that proteins with structural disulfides are commonly present in the IMS of mitochondria (*2*). Since then, the critical players in mitochondrial protein oxidation have been identified and their functions characterized (*2*–*7*). The mitochondrial disulfide relay system (Fig. 2A) facilitates disulfide bond formation in substrate proteins and plays a crucial role in the transport of newly synthesized IMS proteins across the outer mitochondrial membrane. Two proteins are of central importance for this process: Mia40 and Erv1. Mia40 is a conserved IMS protein, which is soluble in mammals and plants and membrane-anchored in fungi (*5*, *7*). Mia40 contains an essential redox-active disulfide bond in a cysteine-proline-cysteine signature that oxidizes cysteine residues of incoming polypeptide chains (*8*). The Mia40-dependent oxidation of incoming proteins locks them in a stably folded state in which

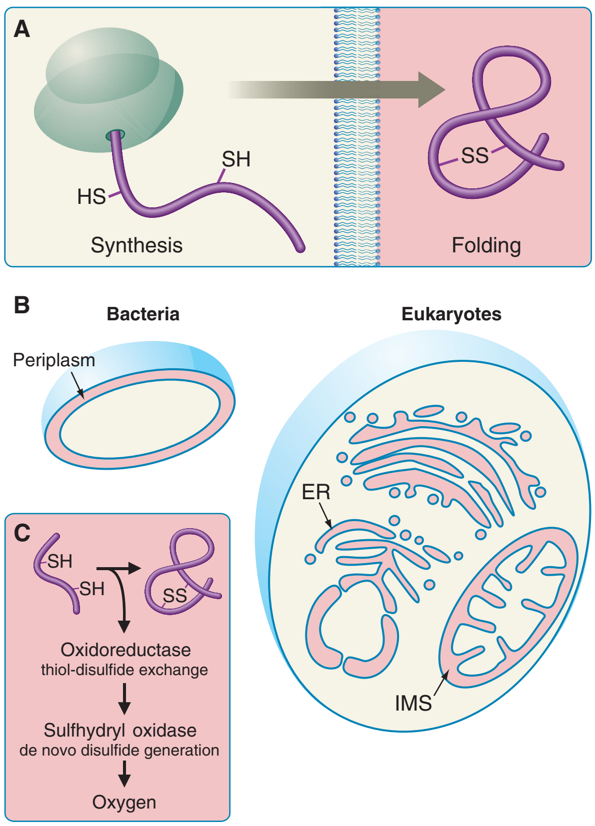

Fig. 1. Protein synthesis and oxidation occur in distinct cellular compartments. (**A**) In vivo, the sites of disulfide bond formation and protein synthesis are separated by a membrane. (**B**) Proteins are maintained in a reduced state in compartments in which protein synthesis takes place. These locations are separated by membranes from compartments harboring machineries for protein oxidation such as the bacterial periplasm, the ER, or the IMS of mitochondria. This spatial separation of protein synthesis and oxidation contributes decisively to the compartmental identity of cells. (**C**) Protein oxidation generally follows the same principles. First, proteins are oxidized by oxidoreductases that merely shuttle disulfide bonds that are initially generated by sulfhydryl oxidases. The oxidizing power for the entire process is provided by oxygen.

they are unable to traverse the outer membrane, thereby leading to a directed transport of Mia40 substrates into the mitochondrial IMS (*9*). Mia40 is reoxidized by Erv1, which belongs to a family of FAD-containing sulfhydryl oxidases (*2*). Members of this family are present in the secretory pathway (Erv2, quiescin-sulfhydryl oxidase) or expressed by certain viruses (e.g., E10R) (*10*). Erv1 contains two essential redox-active cysteine-x-x-cysteine pairs (where x indicates any amino acid), which shuttle electrons from Mia40 to FAD. In vitro, Erv1 can be directly reoxidized by oxygen in a reaction that yields hydrogen peroxide (H_2O_2). However, in vivo Erv1 is oxidized by cytochrome c, which in turn passes its electrons via cytochrome c oxidase to molecular oxygen to produce water (*11*, *12*). The connection to the respiratory chain increases the efficiency by which Erv1 is reoxidized, and also prevents the generation of H_2O_2 in the IMS. The small metal-binding protein Hot13 is an additional factor of the mitochondrial oxidation machinery. It improves the electron transfer between Mia40 and Erv1 by maintaining Mia40 in a zinc-free state that can be efficiently oxidized by Erv1 (*3*).

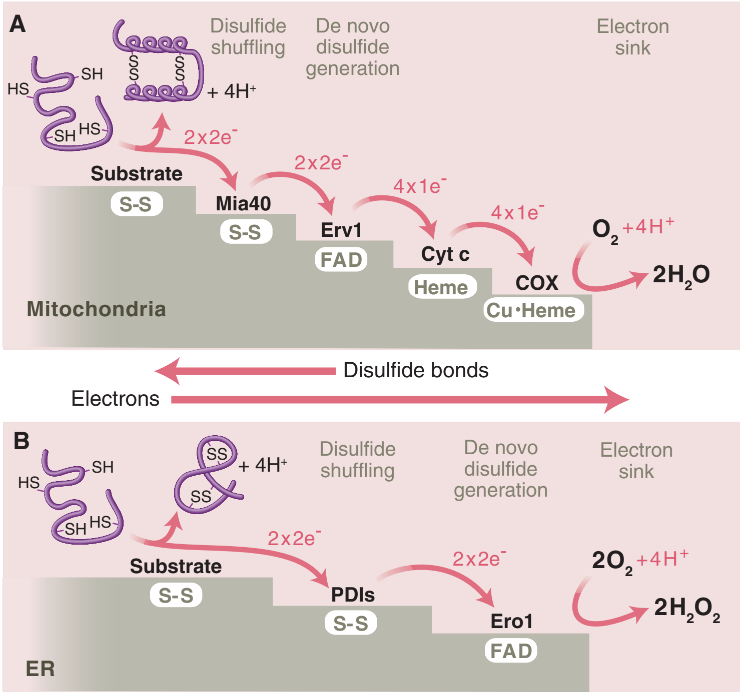

Fig. 2. The disulfide relay machineries of the IMS and the ER. (**A**) After their synthesis in the cytosol, IMS proteins are translocated across the outer membrane of mitochondria in an unfolded, reduced conformation. Oxidized Mia40 interacts with these proteins and facilitates their stable folding by the introduction of disulfide bonds. A cascade of redox-active proteins transfers electrons from Mia40 to cytochrome c oxidase, which converts oxygen to water. The flavoprotein Erv1 mediates the switch from two-electron to one-electron transfer. (**B**) Already during their translocation into the ER lumen, proteins are oxidized by PDIs. The PDIs are maintained in an oxidized state by the flavoprotein Ero1, which transfers electrons directly onto oxygen, thereby generating H_2O_2. Thus, protein oxidation in the ER and in mitochondria relies on distinct components, but the biochemical principles of the transfer cascades are similar.

The Oxidation Machinery of the ER

Disulfide bond formation in the ER typically occurs concomitantly with protein translocation, albeit without any functional coupling of both processes. In a first thiol-disulfide exchange reaction, electrons are shuttled from reduced substrate proteins to oxidized members of the protein disulfide isomerase family (PDIs; Fig. 2B). This results in the reduction of conserved cysteine-x-x-cysteine motifs in these PDIs. Subsequently, the PDIs are reoxidized by the flavoenzyme Ero1, which transfers electrons via FAD onto oxygen (*13*–*15*). To allow proteins to fold to their native states, disulfides sometimes have to be reshuffled by isomerization or repeatedly broken and reformed by cycles of reduction and oxidation. Both reactions are efficiently catalyzed by members of the PDI family. Reduced glutathione, which is transported from the cytosol to the ER lumen by an unknown mechanism, serves as reductant in this PDI-mediated folding reaction (*16*). The ER contains several PDIs, which differ considerably in size, redox potential, and substrate spectrum. Structurally, PDIs are characterized by one or several a- or b-type thioredoxin-like domains. Thioredoxin folds of the a-type are redox-active and comprise cysteine-x-x-cysteine motifs. The two residues that separate the cysteines substantially modulate the redox potential and, hence, influence the physiological function of the particular PDI protein (*17*, *18*). Noncatalytic b-type thioredoxin-like domains lack redox-active cysteine residues and presumably participate in peptide-binding and/or chaperone-like activities (*19*). Whereas PDIs shuffle disulfide bonds, Ero1 generates disulfide bonds de novo by the transfer of electrons from protein substrates to its FAD cofactor. This is achieved by a stepwise intracellular transfer reaction: a redox-active cysteine-x_4-cysteine motif in a flexible loop in Ero1 receives electrons from PDIs and passes them on to a redox-active cysteine-x-x-cysteine pair in the catalytic core of the protein, which consists of a four-helix bundle structure surrounding the FAD cofactor (*20*). Finally, electrons are shuttled via the redox-active isoalloxazine moiety of FAD to molecular oxygen, giving rise to the production of H_2O_2 (*15*, *20*).

Mechanistic Differences in the Eukaryotic Oxidation Machineries

A much greater diversity of substrates are oxidized by the ER machinery than by the mitochondrial machinery. In eukaryotic cells, thousands of different proteins are transported into the ER and along the secretory pathway (*21*). These proteins adopt different folds and can form complex oligomers often linked by intra- and intermolecular disulfides. In contrast, the mitochondrial IMS contains a rather small number of proteins. Moreover, most substrates of the mitochondrial disulfide relay system are of low molecular mass (7 to 15 kD) and show one type of fold: helix-turn-helix conformations in which the helices are connected by two parallel disulfide bonds. Depending on whether the cysteine pairs are separated by three or nine amino acid residues, these specific arrangements are named "twin Cx_3C" or "twin Cx_9C" motifs. Proteins with twin Cx_3C motifs constitute the group of small Tim proteins, which represent soluble chaperones that usher hydrophobic inner-membrane proteins across the IMS (*22*). Most proteins with twin Cx_9C motifs are involved in the biogenesis of respiratory chain complexes and are particularly important for the incorporation of copper into cytochrome c oxidase (*23*). In addition, the mitochondrial disulfide relay system is, directly or indirectly, implicated in the import of IMS proteins with other cysteine arrangements, such as Erv1, copper-zinc superoxide dismutase (Sod1), and copper chaperone for Sod1 (*24*, *25*). However, the precise role of Mia40 and Erv1 in the import and folding of these proteins is not known.

Multiple PDIs—One Mia40. Presumably as a consequence of the large diversity of substrate proteins, the ER contains numerous PDIs that ensure the oxidative folding of secreted proteins by performing oxidation, isomerization, and reduction reactions, and all contain one or more thioredoxin-like domains (Fig. 3A). However, except for certain PDIs such as ERp57 (*26*), the respective subset of endogenous substrates remains unknown. In contrast, Mia40 is the only protein known that directly oxidizes substrates in the IMS. However, Mia40 has a completely different structure than PDIs (Fig. 3A) and so far, it is not clear whether it has chaperone and/or isomerase activity.

Ero1 and Erv1 are unrelated twins. De novo disulfide bond formation in the IMS and the ER is driven by the sulfhydryl oxidases Erv1 and Ero1, respectively. Although evolutionarily unrelated, both proteins contain the same core structure: a four-helix bundle that coordinates the

FAD cofactor and positions it adjacent to a pair of cysteines (Fig. 3B) (*20*, *27*). These cysteines directly interact with FAD as well as with a second cysteine pair in a flexible region of the protein that swings in and out of the core to interact with either PDIs (in the case of Ero1) or Mia40 (in the case of Erv1). Given the different amino acid sequences of the proteins, the similarity of their three-dimensional structures and mechanism is surprising and a beautiful example of convergent evolution.

Spatial organization of disulfide bond formation. It has been proposed that disulfide bond formation in the ER as well as in the IMS proceed via a relay system, i.e., the oxidoreductases (Mia40 or PDIs) oscillate between substrates and their respective sulfhydryl oxidases. However, recently, a ternary complex between substrate, Mia40, and Erv1 has been observed (*28*). It was proposed that this substrate-Mia40-Erv1 complex persists during substrate oxidation. Whether such a tight spatial organization of the oxidation pathway in the ER exists is unclear.

Mitochondria avoid the production of H_2O_2. Ero1 transfers its electrons directly to molecular oxygen, giving rise to the production of H_2O_2 (*15*). To avoid damage to cellular components, this reactive compound has to be detoxified in close proximity to its site of generation. How this detoxification is facilitated is unclear. In the IMS, the production of H_2O_2 is avoided by coupling Erv1 directly to the respiratory chain, giving rise to the production of water. This coupling not only prevents the release of reactive oxygen species (ROS) but also increases the efficiency of Erv1 reoxidation (*11*, *12*).

The ER is more "oxidizing." The IMS is connected to the cytosol by porins in the outer membrane of mitochondria that allow the diffusion of small ions such as glutathione. Consequently, the IMS has a higher ratio of reduced to oxidized glutathione than the ER lumen (*29*, *30*). Nevertheless, the IMS is clearly more "oxidizing" than the cytosol or the mitochondrial matrix. Whether the higher concentration of oxidized glutathione in the IMS is due to the activity of Erv1 or to the production of ROS in this compartment remains to be clarified. However, the chemical environment does not necessarily dictate the redox state of proteins as the introduction of disulfide bonds is often enzymatically controlled. Hence, as has been shown for the ER, reduction and oxidation processes can occur in parallel in the same compartment.

The oxidation machinery in the ER is redox-regulated. Because the action of the oxidative machinery in the ER yields one molecule of H_2O_2 per de novo–generated disulfide bond, it has to be tightly controlled to counteract hyperoxidizing conditions and reactive oxygen damage. Recently, an elegant feedback regulation control system was identified that keeps a check on Ero1 activity (*31*–*33*): Ero1 contains several noncatalytic cysteine residues that form intramolecular disulfide bonds under hyperoxidizing conditions, which attenuate its oxidase activity.

Protein oxidation as regulator of protein function. The adaptation of Ero1 activity to the respective redox conditions in the ER is a wonderful example of redox control by disulfide formation. In the ER, several processes are regulated by the reversible formation of disulfide bonds. One example is the calcium homeostasis of the ER lumen where the uptake of calcium by the sarco(endo)plasmic reticulum calcium (SERCA) pump as well as the release by the inositol 1,4,5-trisphosphate (IP_3) receptor are controlled by redox regulation of cysteine residues (*34*, *35*). A redox control of Erv1 comparable to that of Ero1 has not been observed so far. However, the activity of Erv1 depends on the cellular oxygen concentration through its coupling to the respiratory chain. Thus, it appears conceivable that Erv1 could be involved in the adaptation of mitochondrial activities to the local oxygen concentration by introducing regulatory disulfide bonds (*36*). Although experimental evidence for a regulatory function of Erv1 in vivo is still missing, it is striking that many IMS proteins contain conserved cysteine residues in motifs deviating from the ones found in typical import substrates (Fig. 4). Potentially, processes such as the import of proteins into mitochondria, the biogenesis of the respiratory chain, respiratory activity, and apoptosis could be modulated by thiol-dependent redox processes, and it will be exciting to identify the relevance of these cysteine residues.

Protein Oxidation in Health and Disease

The oxidative folding of proteins in the ER is vital for cellular functionality. Dysfunctions in protein oxidation contribute to a variety of diseases (*37*–*39*), and the ER redox machinery plays

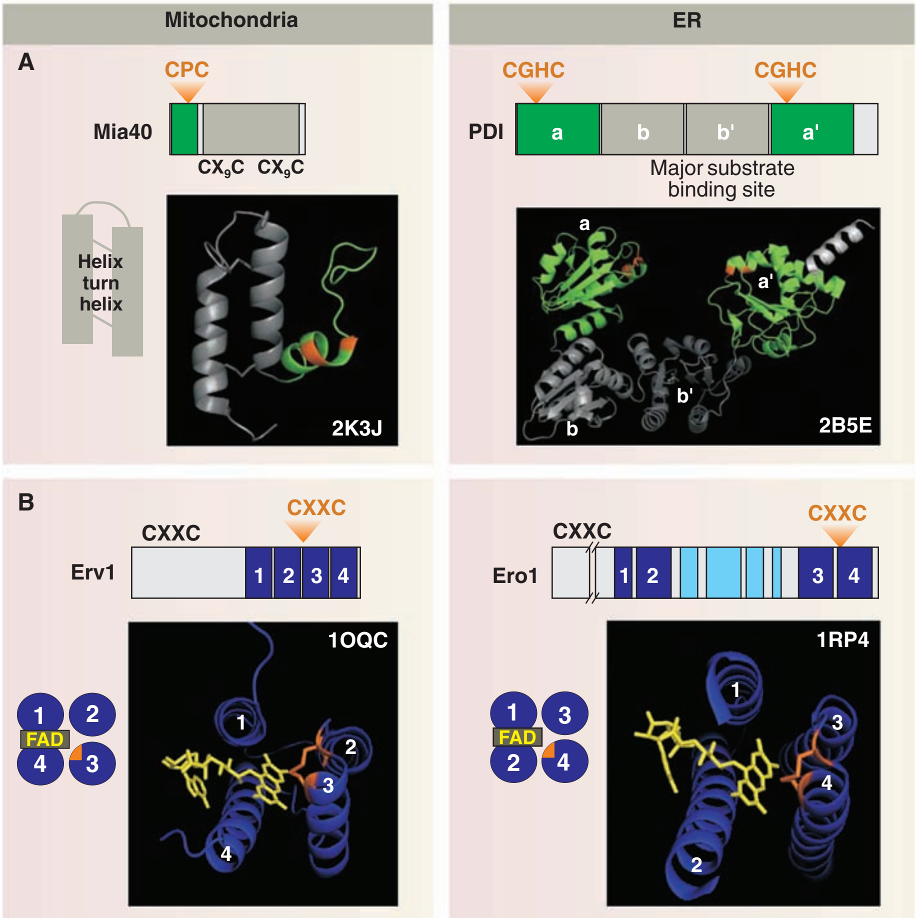

Fig. 3. The key components for eukaryotic protein oxidation. (**A**) Structures of the oxidoreductases Mia40 (*48*) and PDI (*49*). Presumably due to their interaction with a variety of reduced and unfolded substrates, both proteins consist of two modules to exhibit a redox function (green) mediated by a CPC (Mia40) or a CGHC (PDI) motif and a chaperone/peptide-binding function (gray). Although the chaperone function has been shown for the b/b′ thioredoxin-like domains of PDI, it has only been proposed for the helix-turn-helix motif of Mia40. (**B**) Structures of the sulfhydryl oxidases Erv1 (*27*) and Ero1 (*20*). Both proteins facilitate the de novo generation of disulfide bonds via a four-helix-bundle structure (dark blue, helices 1 to 4) positioning a FAD cofactor (yellow) in proximity to a cysteine pair (orange). Both proteins show an almost identical architecture, although the primary sequence and the order of the helices are completely different. For example, in Ero1 additional intervening helices (light blue) loop out from the helix bundle and do not contribute to the formation of the FAD-binding site. The Protein Database accession numbers are presented in white next to the structures.

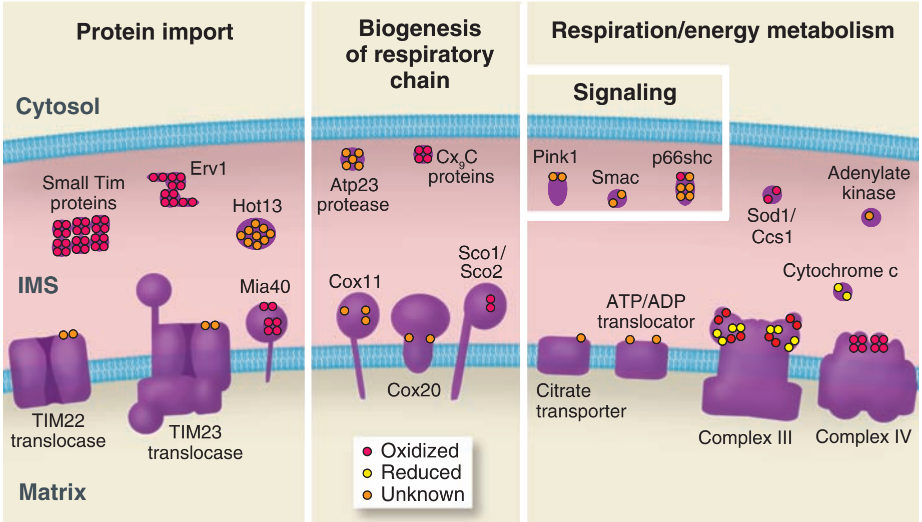

Fig. 4. IMS proteins with conserved cysteines. Numerous IMS proteins contain cysteine residues (indicated as dots) that are conserved among metazoa (p66shc, Pink1, Smac) or even among metazoa and fungi (all other proteins). Some of these cysteine residues coordinate cofactors such as heme groups or metal ions and therefore are maintained in a reduced state (yellow dots). In many cases, the presence of disulfide bonds between these residues has been proved (red dots). Further studies are needed to address the physiological relevance of thiol groups in the IMS, especially of those not characterized so far (orange dots).

a crucial role for the infection process of many viruses [for reviews, see, e.g., (*40*)]. The physiological relevance of mitochondrial protein oxidation is less understood. Mitochondria are a major source of cellular ROS production, particularly under pathological conditions. The oxidative stress caused by mitochondrial dysfunctions is intimately linked to the pathology of many neurodegenerative diseases such as Alzheimer's, Parkinson's, or Huntington's disease (*41*–*43*). However, it remains difficult to determine whether oxidative stress leads to, or is a consequence of, neurodegenerative processes.

Even under physiological conditions, the accumulating oxidative damage of mitochondrially produced ROS presumably contributes directly to the aging process of animals (*44*). ROS levels certainly influence the redox states of protein thiols, but it is not clear whether the aging effect of ROS is due to the increased formation of disulfide bonds in proteins or is caused by more pleiotropic oxidative damage. Recently, it was shown that the mitochondrial redox relay is critical for the translocation of Sod1 into mitochondria (*2*, *25*). Because this enzyme counteracts mitochondrial ROS, Erv1 activity might be directly linked to the protection from ROS. Mutations in Sod1 are a well-described cause of amyotrophic lateral sclerosis, a progressive, fatal neurodegenerative disease caused by the degeneration of motor neurons. Most mutations interfere with the folding of Sod1, which, at least for some mutations, leads to an accumulation of the mutated Sod1 in mitochondria (*45*). A dynamic redox-dependent distribution of proteins between the cytosol and the IMS was also observed for other proteins such as p66Shc. This critical determinant of individual life span (*46*) is translocated under stress conditions from the cytosol into the IMS of mitochondria in an oxidation-mediated manner (*47*). Critical for this translocation reaction is a cysteine-dependent homodimerization of the protein. It is not known how this oxidation is catalyzed, but it was suggested that p66Shc is oxidized by the mitochondrial disulfide relay system in order to trap it in the IMS (*47*).

Outlook

The formation of disulfide bonds in and between proteins is an efficient way to stabilize protein structures and to regulate protein activity in a redox-dependent manner. Recent studies on the oxidation machineries in the ER and in mitochondria have clarified the structures and mechanisms of both disulfide relay systems. Nevertheless, we only have a limited understanding of the physiological and pathological relevance, as well as of the regulatory functions, of these systems. This is particularly true for the mitochondrial disulfide relay. However, the large number of conserved cysteines in proteins of the IMS points to a critical role of thiol groups in this cellular compartment.

References and Notes

1. H. Ostergaard, C. Tachibana, J. R. Winther, *J. Cell Biol.* **166**, 337 (2004).
2. N. Mesecke *et al.*, *Cell* **121**, 1059 (2005).
3. N. Mesecke *et al.*, *EMBO Rep.* **9**, 1107 (2008).
4. S. Allen, V. Balabanidou, D. P. Sideris, T. Lisowsky, K. Tokatlidis, *J. Mol. Biol.* **353**, 937 (2005).
5. A. Chacinska *et al.*, *EMBO J.* **23**, 3735 (2004).
6. M. Rissler *et al.*, *J. Mol. Biol.* **353**, 485 (2005).
7. M. Naoe *et al.*, *J. Biol. Chem.* **279**, 47815 (2004).
8. N. Terziyska, B. Grumbt, C. Kozany, K. Hell, *J. Biol. Chem.* **284**, 1353 (2009).
9. H. Lu, S. Allen, L. Wardleworth, P. Savory, K. Tokatlidis, *J. Biol. Chem.* **279**, 18952 (2004).
10. D. L. Coppock, C. Thorpe, *Antioxid. Redox Signal.* **8**, 300 (2006).
11. K. Bihlmaier *et al.*, *J. Cell Biol.* **179**, 389 (2007).
12. D. V. Dabir *et al.*, *EMBO J.* **26**, 4801 (2007).
13. C. S. Sevier, J. W. Cuozzo, A. Vala, F. Aslund, C. A. Kaiser, *Nat. Cell Biol.* **3**, 874 (2001).
14. B. P. Tu, S. C. Ho-Schleyer, K. J. Travers, J. S. Weissman, *Science* **290**, 1571 (2000).
15. E. Gross *et al.*, *Proc. Natl. Acad. Sci. U.S.A.* **103**, 299 (2006).
16. S. Chakravarthi, C. E. Jessop, N. J. Bulleid, *EMBO Rep.* **7**, 271 (2006).
17. U. Grauschopf *et al.*, *Cell* **83**, 947 (1995).
18. T. Kortemme, N. J. Darby, T. E. Creighton, *Biochemistry* **35**, 14503 (1996).
19. P. Klappa, L. W. Ruddock, N. J. Darby, R. B. Freedman, *EMBO J.* **17**, 927 (1998).
20. E. Gross, D. B. Kastner, C. A. Kaiser, D. Fass, *Cell* **117**, 601 (2004).
21. S. Ghaemmaghami *et al.*, *Nature* **425**, 737 (2003).
22. C. M. Koehler, *Trends Biochem. Sci.* **29**, 1 (2004).
23. O. Khalimonchuk, D. R. Winge, *Biochim. Biophys. Acta* **1783**, 618 (2008).
24. K. Gabriel *et al.*, *J. Mol. Biol.* **365**, 612 (2007).
25. S. Reddehase, B. Grumbt, W. Neupert, K. Hell, *J. Mol. Biol.* **385**, 331 (2009).
26. C. E. Jessop *et al.*, *EMBO J.* **26**, 28 (2007).
27. C. K. Wu, T. A. Dailey, H. A. Dailey, B. C. Wang, J. P. Rose, *Protein Sci.* **12**, 1109 (2003).
28. D. Stojanovski *et al.*, *J. Cell Biol.* **183**, 195 (2008).
29. J. Hu, L. Dong, C. E. Outten, *J. Biol. Chem.* **283**, 29126 (2008).
30. P. I. Merksamer, A. Trusina, F. R. Papa, *Cell* **135**, 933 (2008).
31. C. S. Sevier *et al.*, *Cell* **129**, 333 (2007).
32. C. Appenzeller-Herzog, J. Riemer, B. Christensen, E. S. Sorensen, L. Ellgaard, *EMBO J.* **27**, 2977 (2008).
33. K. M. Baker *et al.*, *EMBO J.* **27**, 2988 (2008).
34. T. Higo *et al.*, *Cell* **120**, 85 (2005).
35. Y. Li, P. Camacho, *J. Cell Biol.* **164**, 35 (2004).
36. K. Bihlmaier, N. Mesecke, C. Kloeppel, J. M. Herrmann, *Ann. N. Y. Acad. Sci.* **1147**, 293 (2008).
37. P. A. Wearsch, P. Cresswell, *Curr. Opin. Cell Biol.* **20**, 624 (2008).
38. R. Sitia, I. Braakman, *Nature* **426**, 891 (2003).
39. L. Ellgaard, A. Helenius, *Nat. Rev. Mol. Cell Biol.* **4**, 181 (2003).
40. B. N. Lilley, H. L. Ploegh, *Immunol. Rev.* **207**, 126 (2005).
41. Q. Shi, G. E. Gibson, *Alzheimer Dis. Assoc. Disord.* **21**, 276 (2007).
42. N. Y. Calingasan *et al.*, *Neuroscience* **153**, 986 (2008).
43. C. Henchcliffe, M. F. Beal, *Nat. Clin. Pract. Neurol.* **4**, 600 (2008).
44. D. C. Wallace, *Annu. Rev. Genet.* **39**, 359 (2005).
45. J. Liu *et al.*, *Neuron* **43**, 5 (2004).
46. E. Migliaccio *et al.*, *Nature* **402**, 309 (1999).
47. M. Gertz, F. Fischer, D. Wolters, C. Steegborn, *Proc. Natl. Acad. Sci. U.S.A.* **105**, 5705 (2008).
48. L. Banci *et al.*, *Nat. Struct. Mol. Biol.* **16**, 198 (2009).
49. G. Tian, S. Xiang, R. Noiva, W. J. Lennarz, H. Schindelin, *Cell* **124**, 61 (2006).

50. We thank B. Anstett for help with Fig. 4 and M. Bien and L. Ellgaard for critical reading of the manuscript. Research in the author's laboratories is supported by fellowships of the Deutsche Forschungsgemeinschaft and the Stiftung fur Innovation in Rheinland-Pfalz.

10.1126/science.1170653

Anthropogenic Impacts on Nitrogen Isotopes of Ice-Core Nitrate

M. G. Hastings,[1]* J. C. Jarvis,[2] E. J. Steig[2]

The biogeochemical cycling of nitrogen has fundamentally changed in the past 150 years with the addition of nitrogen oxide emissions (NO_x = NO + NO_2) from fossil fuel combustion and the fixation of atmospheric nitrogen to create fertilizer (*1*). Nitrate deposition (as HNO_3 or NO_3^-) is the main sink for NO_x, so NO_x sources must influence the nitrogen isotope composition [$\delta^{15}N$ (*2*)] of atmospheric nitrate. Quantifying this influence is complicated by the lack of available data on $\delta^{15}N$ of NO_x sources, which include lightning, biomass burning, biogenic processes in soils, and fossil fuel combustion. Chemistry, transport, and postdepositional processes (e.g., evaporation or biological fixation) may also influence the $\delta^{15}N$ of nitrate deposition.

To determine whether the ice core record of nitrate offers a means to track changes in NO_x sources through time, we analyzed the $\delta^{15}N$ of nitrate in a 100-m-long ice core from Summit, Greenland (72.5°N, 38.4°W) spanning the past 300 years (*3*). The data reveal a clear trend in $\delta^{15}N$, which decreases from preindustrial values near 11 per mil (‰) to significantly lower values (–1‰) in the past decade (Fig. 1). This decrease in $\delta^{15}N$ is strongly correlated with fossil fuel emissions estimates since 1750 (r = –0.92, P < 0.01) (*4*). The nitrate concentration record shows a clear rise since ~1890, in good agreement with several higher-resolution records from Greenland (*5*). In contrast to nitrate concentration, the $\delta^{15}N$ shows a noticeable change as early as ~1850.

Impurities in Greenland ice primarily result from transport of Northern Hemisphere (N.H.) pollutants, and the isotopic composition of nitrate appears to reflect this (*6*, *7*). The trend in $\delta^{15}N$ of nitrate over the past 300 years is difficult to explain except as the result of variations in NO_x sources. Although isotopic fractionation associated with chemistry, transport, accumulation rate, and/or postdepositional processing of nitrate may affect the $\delta^{15}N$ of nitrate preserved in ice (*6*, *7*), none of these processes is expected to follow such a trend. To test this, we investigated seasonality in $\delta^{15}N$ in recent and preindustrial ice (fig. S1). Recent accumulation shows seasonality in $\delta^{15}N$, with summer values higher than winter. In contrast, preindustrial ice shows no seasonal difference in $\delta^{15}N$. Importantly, although the $\delta^{15}N$ of nitrate deposited in both seasons has decreased over time, a greater decrease is apparent in winter. If chemical and/or physical processes were of primary importance, we would not expect a significant change in $\delta^{15}N$ seasonality over time. Furthermore, the observed change suggests that the seasonality observed in modern snow is due primarily to variations in NO_x source emissions and/or their geographic distribution rather than local photochemistry (*7*).

Assuming that the observed change in $\delta^{15}N$ since 1850 is caused by NO_x sources alone, we can calculate, by mass balance, that the average $\delta^{15}N$ of NO_x is –12.8‰ (±2.4‰), with use of a pre-1850 $\delta^{15}N$ and nitrate mean (±SD) of 11.4‰ (±1.3‰) and 73.3 parts per billion (ppb) (±11.9 ppb), respectively, and 0.5‰ (±2.4‰) and 133.0 ppb (±25.5 ppb) post-1950. The greatest rate of change in $\delta^{15}N$ occurs between 1950 and 1980, coincident with a rapid increase in fossil fuel emissions. The significant coherence between emissions estimates and $\delta^{15}N$ suggests that this source is largely responsible for the trend in $\delta^{15}N$ (Fig. 1 and fig. S2). A negative $\delta^{15}N$ for fossil fuel NO_x implies that nitrate deposition to Greenland arising from preindustrial sources has an overall positive $\delta^{15}N$, although this contrasts with our present, limited knowledge of the $\delta^{15}N$ of NO_x sources (*8*). Qualitatively, a negative $\delta^{15}N$ associated with fossil fuel emissions and an overall positive $\delta^{15}N$ associated with other N.H. sources may explain the recent changes in $\delta^{15}N$ (fig. S2). For example, from 1980 to 1990 both $\delta^{15}N$ and nitrate concentration increased. Compared with the previous several decades, the rate of NO_x emissions from fossil fuel combustion slowed between 1980 and 1990, whereas both biomass burning and agricultural emissions of NO_x increased (*9*).

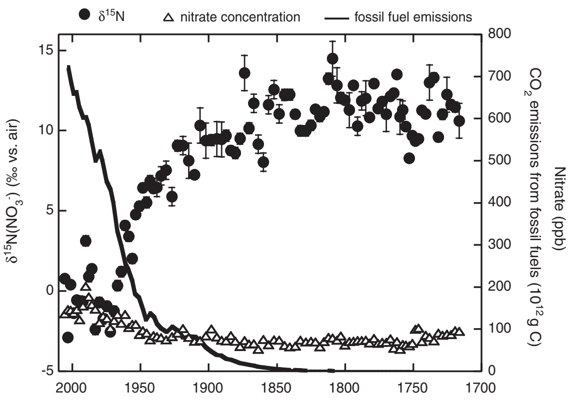

Fig. 1. $\delta^{15}N$ of nitrate (solid circles) and nitrate concentration (open triangles) in a 100-m ice core from Summit, Greenland, spanning ~1718 to 2006. Each data point represents ~2 to 3 years of accumulation. The $\delta^{15}N$ of nitrate was determined by using the denitrifier method; nitrate concentrations were determined by using standard ion chromatography (*3*). The error bars on $\delta^{15}N$ symbols indicate ±1 standard error of the mean based on multiple analyses of the same sample; error bars for nitrate concentration are smaller than the symbol size. Also shown is an estimate of global CO_2 emissions from fossil fuels since 1750 (solid black line; right axis) (*4*).

Our results suggest that it should be possible to quantitatively reconstruct the influence of different NO_x sources on preserved nitrate. Obtaining quantitative results will require source-specific isotopic measurements of NO_x, as well as a better understanding of possible fractionations associated with chemistry and transport. The variability in $\delta^{15}N$ of nitrate in the recent past, as well as on longer time scales (*10*), has implications for the interpretation of $\delta^{15}N$ of total nitrogen found in lake and ocean sediments and in tree rings (*11*). Further measurements of $\delta^{15}N$ of nitrate will contribute to understanding the influence of climate on natural sources of NO_x.

References and Notes

1. J. N. Galloway *et al.*, *Science* **320**, 889 (2008).
2. $\delta^{15}N$ (‰) = ($R_{sample}/R_{standard}$ – 1) × 1000‰, where R = $^{15}N/^{14}N$ and the standard is atmospheric N_2.
3. Materials and methods are available as supporting material on *Science* Online.
4. G. Marland, T. A. Boden, R. J. Andres, *Trends: A Compendium of Data on Global Change* (Oak Ridge National Laboratory, U.S. Department of Energy, Oak Ridge, TN, 2008).
5. J. F. Burkhart, R. C. Bales, J. R. McConnell, M. A. Hutterli, *J. Geophys. Res.* **111**, D22309 (2006); and references therein.
6. S. Morin *et al.*, *Science* **322**, 730 (2008).
7. J. C. Jarvis, E. J. Steig, M. G. Hastings, *Geophys. Res. Lett.* **35**, L21804 (2008); and references therein.
8. C. Kendall, E. M. Elliott, S. D. Wankel, in *Stable Isotopes in Ecology and Environmental Science*, R. Michener, K. Lajtha, Eds. (Wiley-Blackwell, Hoboken, NJ, 2007), pp. 375–449; and references therein.
9. J. A. van Aardenne, F. J. Detener, J. G. J. Olivier, C. G. M. Lein Goldewijk, J. Lelieveld, *Global Biogeochem. Cycles* **15**, 909 (2001).
10. M. G. Hastings, D. M. Sigman, E. J. Steig, *Global Biogeochem. Cycles* **19**, GB4024 (2005).
11. For example, A. P. Wolfe, C. A. Cooke, W. O. Hobbs, *Arct. Antarct. Alp. Res.* **38**, 465 (2006).
12. We acknowledge financial support from NSF (OPP 0454803) and the Joint Institute for the Study of the Atmosphere and Ocean (JISAO) under National Oceanic and Atmospheric Administration (NOAA) cooperative agreement no. NA17RJ1232 (JISAO Contribution no. 1747); logistical support from VECO Polar Resources and Ice Coring and Drilling Services (ICDS); and analytical and technical support from D. Gleason, S. Kunasek, P. Neff, J. Wettstein, and A. Schauer.

Supporting Online Material

www.sciencemag.org/cgi/content/full/324/5932/1288/DC1
Materials and Methods
Figs. S1 and S2
Table S1

5 January 2009; accepted 16 April 2009
10.1126/science.1170510

[1]Department of Geological Sciences and Environmental Change Initiative, Brown University, Providence, RI 02912, USA. [2]Department of Earth and Space Sciences, University of Washington, Seattle, WA 98195, USA.

*To whom correspondence should be addressed. E-mail: meredith_hastings@brown.edu

Regulation of Hypoxia-Inducible Factor 2α Signaling by the Stress-Responsive Deacetylase Sirtuin 1

Elhadji M. Dioum,[1,2]* Rui Chen,[1,2]* Matthew S. Alexander,[2] Quiyang Zhang,[2] Richard T. Hogg,[2] Robert D. Gerard,[2,3] Joseph A. Garcia[1,2]†

To survive in hostile environments, organisms activate stress-responsive transcriptional regulators that coordinately increase production of protective factors. Hypoxia changes cellular metabolism and thus activates redox-sensitive as well as oxygen-dependent signal transducers. We demonstrate that Sirtuin 1 (Sirt1), a redox-sensing deacetylase, selectively stimulates activity of the transcription factor hypoxia-inducible factor 2 alpha (HIF-2α) during hypoxia. The effect of Sirt1 on HIF-2α required direct interaction of the proteins and intact deacetylase activity of Sirt1. Select lysine residues in HIF-2α that are acetylated during hypoxia confer repression of Sirt1 augmentation by small-molecule inhibitors. In cultured cells and mice, decreasing or increasing Sirt1 activity or levels affected expression of the HIF-2α target gene erythropoietin accordingly. Thus, Sirt1 promotes HIF-2 signaling during hypoxia and likely other environmental stresses.

Hypoxia-inducible factors (HIFs) are transcriptional regulators that control genes induced during hypoxia and other stresses (*1*). Activation of the founding HIF member, HIF-1α, is increased when oxygen concentrations are reduced. The second HIF alpha member, endothelial PAS domain protein 1 (EPAS1) (*2*), also known as HIF-2α, is closely related to HIF-1α in structure and is likewise activated during hypoxia (*3*). HIF-2α target genes identified from mouse knockout studies include *Sod2* encoding the mitochondrial-localized major antioxidant enzyme manganese superoxide dismutase (*4*), *VegfA* encoding the proangiogenic regulator vascular endothelial growth factor A (*5*), and *Epo* encoding the cytokine erythropoietin (*6*, *7*).

The activity of HIF members is in part regulated by oxygen concentrations. When oxygen levels are normal, HIF-1α and HIF-2α undergo posttranslational modifications by oxygen-dependent prolyl (*8*, *9*) and asparaginyl (*10*) hydroxylases that decrease HIF-α protein stability and activity, respectively. When oxygen levels are low, oxygen-dependent hydroxylases are inactive and HIF-α signaling increases. Although they are subject to similar oxygen-dependent modifications, HIF-1α and HIF-2α differ in other details of their regulation.

HIF-1α, but not HIF-2α, is transcriptionally regulated during hypoxia, and the activity of HIF-1α is proportional to its abundance (*3*, *11*, *12*). Amounts of HIF-2α protein increase modestly during hypoxia, but HIF-2α–dependent transactivation increases markedly, which suggests that additional posttranslational mechanisms besides oxygen-dependent hydroxylation regulate HIF-2α activity (*13*). Hypoxia alters cellular redox state in vivo (*14*, *15*). Redox-sensitive

[1]Veterans Affairs North Texas Health Care System, Department of Medicine, 4500 South Lancaster Road, Dallas, TX 75216, USA. [2]University of Texas Southwestern Medical Center at Dallas, Department of Internal Medicine, 5323 Harry Hines Boulevard, Dallas, TX 75390–8573, USA. [3]University of Texas Southwestern Medical Center at Dallas, Department of Molecular Biology, 5323 Harry Hines Boulevard, Dallas, TX 75390–8573, USA.

*These authors contributed equally to this work.
†To whom correspondence should be addressed. E-mail: joseph.garcia@utsouthwestern.edu

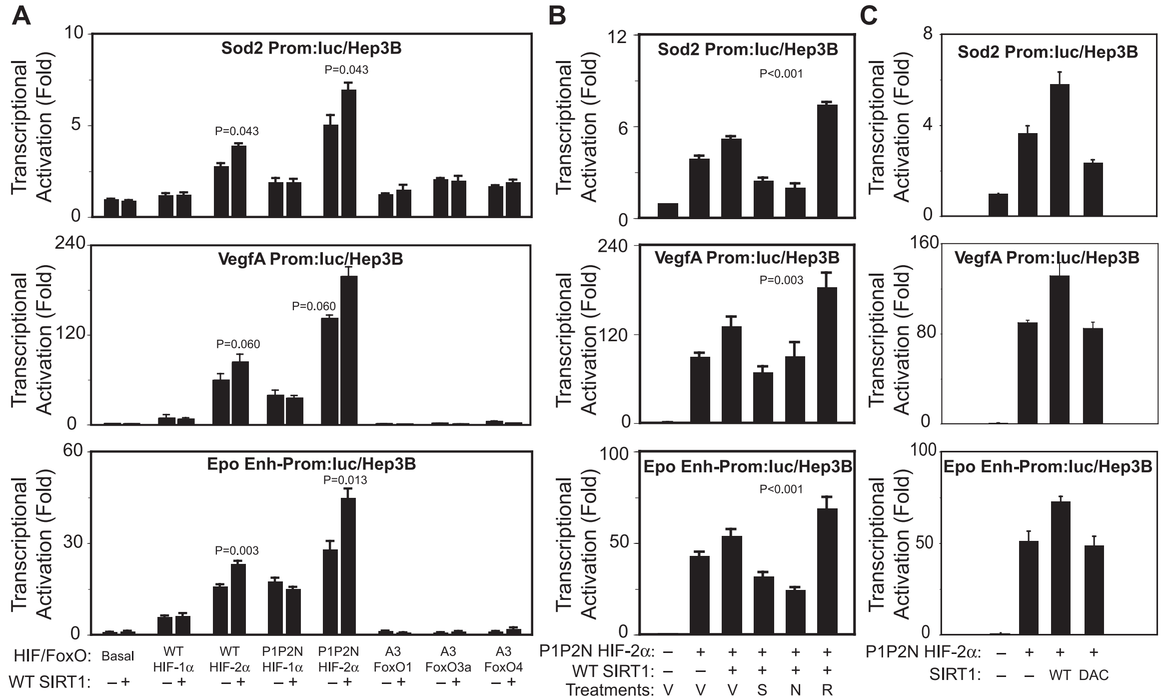

Fig. 1. Augmentation of HIF-2 signaling by Sirt1. (**A**) Activation of transcription from a mouse *Sod2* promoter (Sod2 Prom:luc), *VegfA* promoter (VegfA Prom:luc), or *Epo* enhancer-promoter (Epo Enh-Prom:luc) reporter by exogenous SIRT1 in human hepatoma Hep3B cells expressing WT or constitutively active (P1P2N) HIF-1α or HIF-2α, or constitutively active (A3) FoxO1, FoxO3a, or FoxO4. Statistical significance (Student's *t* test) of transcription factor plus SIRT1, relative to transcription factor alone, is indicated. (**B**) Effects of treatment with vehicle (V), the Sirt1 inhibitor sirtinol (S), the end-product inhibitor nicotinamide (N), or the activator resveratrol (R) on augmentation by exogenous SIRT1 of transcription from the Sod2 Prom:luc, VegfA Prom:luc, or Epo Enh-Prom:luc reporters in Hep3B cells expressing P1P2N HIF-2α. Statistical significance [analysis of variance (ANOVA)] of P1P2N HIF-2α plus SIRT1 with pharmacological treatment relative to P1P2N HIF-2α plus SIRT1 with vehicle is indicated. (**C**) Transcriptional effects of exogenous WT or deacetylase mutant (DAC) SIRT1 expressed with P1P2N HIF-2α on transcription from the Sod2 Prom:luc, VegfA Prom:luc, or Epo Enh-Prom:luc reporters in Hep3B cells. The bars in (A) to (C) represent the mean ± SEM of three independent transfections, with each transfection performed in triplicate.

modifications of HIF-α proteins are one potential mechanism whereby HIF-α activity could be controlled.

Silent information regulator 2 (Sir2) is a redox-sensitive, class III histone deacetylase (HDAC) initially identified from studies of aging in yeast (*16*). Homologs of the Sir2 protein in higher eukaryotic organisms are known as Sirtuin (Sirt) proteins, with Sirt1 being most closely related to Sir2 (*17*). In cultured mammalian cells, Sirt1 is activated in response to growth factor deprivation and increased oxidative stress. Changes in the cellular redox state as reflected by pyridine nucleotide homeostasis, specifically concentrations of oxidized nicotinamide adenine dinucleotide (NAD+) or the ratio of the concentration of NAD+ and its reduced form NADH, control the deacetylase activity of Sir2 and its homologs (*18*).

Sirt1 augments HIF-2 signaling. Because hypoxia affects the cellular redox state, we reasoned that Sirt1 could be activated during hypoxia and could participate in HIF signaling. We investigated whether HIF-responsive regulatory regions responded to Sirt1 overexpression. In human hepatoma Hep3B cells, overexpression of wild-type (WT) HIF-2α activated the isolated mouse *Sod2* promoter reporter, Sod2 Prom:luc, also activated by HIF-2α in human embryonic kidney (HEK) 293 cells (*4*). Overexpression of Sirt1 further augmented transcriptional activity of this reporter induced by WT HIF-2α (Fig. 1A). Sirt1 also augmented WT HIF-2α–activated transcription of isolated mouse *VegfA* and *Epo* regulatory regions (Fig. 1A). In contrast, Sirt1 did not augment transcription of Sod2 Prom:luc, Vegf Prom:luc, or Epo Enh-Prom:luc mediated by WT HIF-1α (Fig. 1A).

We examined whether activation of HIF-2α signaling by Sirt1 was independent of known oxygen-dependent modifications of HIF-α proteins. Alanine substitutions of the proline (P) and asparagine (N) residues that are hydroxylated under normal oxygen conditions result in mutant HIF-α proteins, referred to as P1P2N HIF-1α or P1P2N HIF-2α, that are equally active when oxygen conditions are normal (normoxia) as when they are reduced (hypoxia). Sirt1 augmented transcription of the Sod2 Prom:luc, Vegf Prom:luc, or Epo Enh-Prom:luc reporter by P1P2N HIF-2α, but not by P1P2N HIF-1α (Fig. 1A). Sirt1 augmentation of P1P2N HIF-2α signaling was similar or exceeded that of WT HIF-2α signaling for all three reporters.

Sirt1 deacetylation of FoxO transcription factors results in enhanced transcription of genes encoding prosurvival factors including *Sod2* (*19*), also a target for HIF-2α (*4*). FoxO members also participate in the hypoxia response (*20*). We determined whether Sirt1 augmentation of HIF-2α signaling involves signaling through FoxO proteins. In comparison with HIF-2α, constitutively active FoxO, expressed in the absence or presence of Sirt1, modestly activated transcription of Sod2 Prom:luc and had no effect on transcription of Vegf Prom:luc or Epo Enh-Prom:luc (Fig. 1A). The synthetic HIF-responsive reporter 3xHRE-tk Prom:luc, consisting of three HIF-responsive elements (HREs) upstream of a minimal thymidine kinase (tk) promoter, was activated to a comparable extent by P1P2N HIF-1α or P1P2N HIF-2α, but Sirt1 only augmented HIF-2α–activated transcrip-

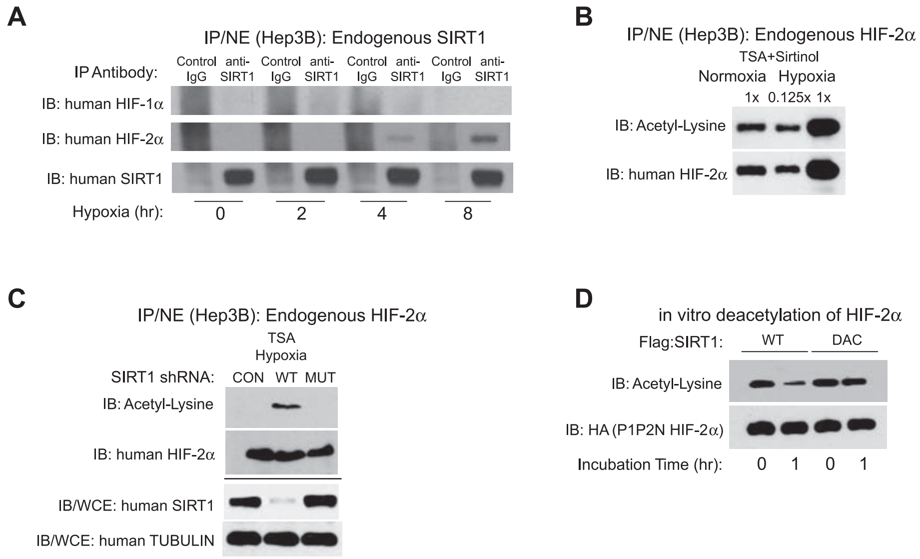

Fig. 2. Regulation of HIF-2α acetylation by Sirt1. (**A**) Association of endogenous SIRT1 and HIF-2α during hypoxia. SIRT1 was immunoprecipitated (IP) from nuclear extracts (NE) of Hep3B cells at the indicated time points. Association of HIF-1α or HIF-2α was detected by immunoblotting (IB). (**B**) Acetylation of endogenous HIF-2α during hypoxia. HIF-2α was immunoprecipitated (IP) from nuclear extracts (NE) prepared from Hep3B cells maintained under normal oxygen conditions (normoxia) or reduced oxygen conditions (hypoxia) and treated with trichostatin A (TSA) plus sirtinol. Equivalent amounts (1x) of the normoxia and hypoxia immunoprecipitated HIF-2α samples, as well as an adjusted amount (0.125x) of the hypoxia HIF-2α sample, were examined for acetylated and total HIF-2α by immunoblotting (IB). (**C**) Depletion of SIRT1 and acetylation of endogenous HIF-2α during hypoxia. Acetylation of endogenous HIF-2α was detected by immunoblotting (IB) nuclear extracts (NE) prepared with TSA from hypoxia-exposed Hep3B cells expressing control (CON), WT, or MUT Sirt1 shRNA. Depletion of SIRT1 was confirmed by immunoblotting of whole-cell extracts (WCE). (**D**) In vitro deacetylation of acetylated P1P2N HIF-2α by WT or DAC SIRT1. After 1 hour, amounts of acetylated and total P1P2N HIF-2α were assessed by IB.

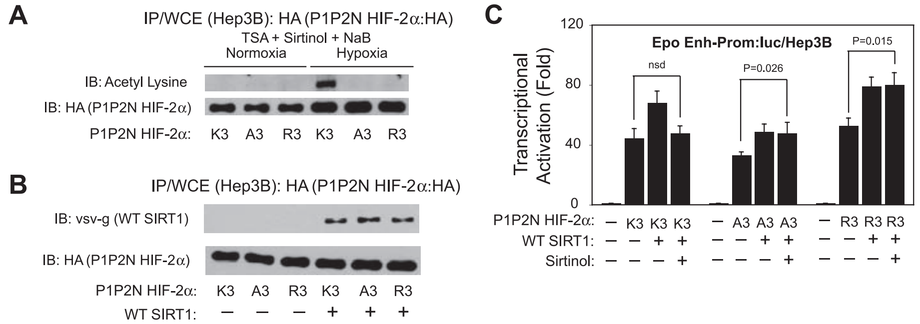

Fig. 3. Regulatory roles of HIF-2α carboxy terminal acetylated lysines. (**A**) Acetylation of P1P2N HIF-2α containing intact lysine (K3), alanine-substituted (A3), or arginine-substituted (R3) amino acids in the carboxy terminus expressed in Hep3B cells and maintained under normal oxygen conditions (normoxia) or under reduced oxygen conditions (hypoxia). P1P2N HIF-2α was immunoprecipitated (IP) from WCE prepared with TSA, sirtinol, and sodium butyrate (NaB). Acetylated or total HIF-2α in immunoprecipitated samples was assessed by IB. (**B**) Association of Sirt1 with HIF-2α lysine substitution mutants. P1P2N HIF-2α with intact carboxy terminal acetylated lysine residues (K3) or with alanine (A3) or arginine (R3) substitutions expressed in Hep3B cells and immunoprecipitated from WCE. Amounts of HIF-2α and associated exogenous SIRT1 were detected by IB. (**C**) Transcriptional activation of HIF-2α lysine substitution mutants by Sirt1. Transcription of the Epo Enh-Prom:luc reporter by exogenous SIRT1 in Hep3B cells in which parental (K3), alanine-substituted (A3), or arginine-substituted (R3) P1P2N HIF-2α was expressed in either the absence or presence of the Sirt1 inhibitor sirtinol. Statistical significance (Student's *t* test) of P1P2N HIF-2α plus SIRT1 in the presence of Sirtinol, relative to P1P2N HIF-2α alone, for each P1P2N HIF-2α form is indicated. The data represent the mean ± SEM of three independent transfections, with each transfection performed in triplicate.

tion (fig. S1A). The synthetic FoxO-responsive reporter 8xFBE-tk Prom:luc, containing eight FoxO binding elements (FBEs) upstream of the minimal tk promoter, responded only to constitutively nuclear FoxO members and not to HIF-α overexpression with or without Sirt1 (fig. S1A).

We examined whether Sirt1 augmentation of HIF-2 signaling was affected by pharmacological modulation of Sirt1 activity. Nicotinamide (NAM), a pyridine nucleotide end product generated after Sir2- or Sirt1-mediated deacetylation, inhibits Sir2 or Sirt1 action (*21*), as does the synthetic compound sirtinol (*22*), whereas the natural polyphenol resveratrol stimulates activity of Sir2 or Sirt1 (*23*). NAM or sirtinol reduced, and resveratrol increased, the ability of Sirt1 to augment HIF-2α transactivation of the *Sod2, VegfA,* and *Epo* reporters (Fig. 1B) (*24*). In comparison, NAM, sirtinol, and resveratrol had no effect on transcription of these reporters by HIF-1α (fig. S1B).

Nuclear-localized Sirt1 modulates the activity of coactivator proteins (*25*, *26*), represses select transcription factors (*27*–*29*), and activates other transcription factors (*19*, *30*–*34*) through its deacetylase activity. We examined whether genetic modulation of Sirt1 deacetylase activity affected augmentation of HIF-2 signaling by Sirt1. A site-directed point mutation that inhibits Sirt1 deacetylase activity (DAC) eliminated the Sirt1 stimulatory effect on expression of all three reporters (Fig. 1C).

HIF-2α acetylation during hypoxia is reversed by Sirt1. Augmentation of HIF-2α signaling by Sirt1 required an intact deacetylase function of Sirt1. We determined whether endogenous HIF-2α can bind to and act as an acetylated substrate for Sirt1 in Hep3B cells. Endogenous HIF-2α, but not HIF-1α, associated with Sirt1 during hypoxia (Fig. 2A). When isolated from hypoxia-exposed Hep3B cells in the presence of the HDAC I/II inhibitor trichostatin A (TSA) and the HDAC III (Sirt1) inhibitor sirtinol, HIF-2α was acetylated (Fig. 2B). After depletion of endogenous Sirt1, acetylated HIF-2α was detected in extracts from hypoxia-exposed Hep3B cells prepared in the absence of pharmacological inhibitors of Sirt1 (Fig. 2C). Acetylated HIF-2α was directly deacetylated by WT Sirt1 but not by DAC Sirt1, as assessed by in vitro deacetylation assays (Fig. 2D).

We next examined whether augmentation of HIF-2α signaling by Sirt1 was restricted to Hep3B cells. Amounts of P1P2N HIF-1α and P1P2N HIF-2α protein in Hep3B and HEK293 cells were similar and were not affected by Sirt1 overexpression (figs. S1C and S3C). Augmentation of HIF-2α signaling by Sirt1 for isolated reporters was observed in HEK293 cells and responded similarly to pharmacological modulation of Sirt1 activity (fig. S2 and S3) (*24*). Sirt1 associated with exogenous P1P2N HIF-2α, but not with exogenous P1P2N HIF-1α, in HEK293 cells maintained under normal atmospheric oxygen concentrations and occurred irrespective of whether class I/II (TSA) or class I/II+III (TSA + NAM) HDAC inhibitors were present (fig. S4A). Acetylation of exogenous P1P2N HIF-2α protein isolated from HEK293 cells exposed to hypoxia was not observed with effective concentrations of TSA (fig. S4B) but was observed when treated with TSA and sirtinol (fig. S4C). Acetylation and amounts of endogenous HIF-2α protein increased during hypoxia in HEK293 cells (fig. S4D). Exogenous as well as endogenous HIF-2α was acetylated during hypoxia when endogenous Sirt1 in HEK293 cells was depleted in the absence of Sirt1 inhibitors (fig. S4, E and F).

Sirt1 augmentation localizes to the HIF-2α carboxy terminus. We tested whether a specific region of HIF-2α binds to and confers augmentation by Sirt1. We expressed truncated forms of P1P2N HIF-2α in HEK293 cells along with Sirt1 and analyzed immunoprecipitated proteins. The carboxy terminus (C terminus) of HIF-2α, encompassing amino acids 350 to 870, was sufficient to form a stable complex with Sirt1 (fig. S5, A and B). In vitro stable and direct binding of WT Sirt1, but not DAC Sirt1, to the HIF-2α C terminus was detected using bacterial-produced HIF-2α (fig. S5C). Sirt1 augmentation of HIF-2α transcription from reporters occurred in both Hep3B and HEK293 cells, with hybrid HIF proteins containing the C terminus of HIF-2α (figs. S6A and S7A). Activation of a mammalian two-hybrid reporter occurred when WT Sirt1 and the C terminus of HIF-2α were coexpressed as hybrid constructs in either Hep3B or HEK293 cells (figs. S6B and S7B).

We asked whether specific acetylated lysine residues in the C terminus of HIF-2α could play a regulatory role in HIF-2 signaling. Mass spectrometry revealed acetylation of exogenous P1P2N HIF-2α during hypoxia at three lysine residues (K385, K685, and K741) within the HIF-2α C terminus (fig. S8, A to C). Substitution mutants of the three acetylated lysines in the C terminus of HIF-2α, with alanine (A3) or arginine (R3) residues, were not acetylated during hypoxia (Fig. 3A and fig. S9A) but retained interaction with Sirt1 (Fig. 3B and fig. S9B).

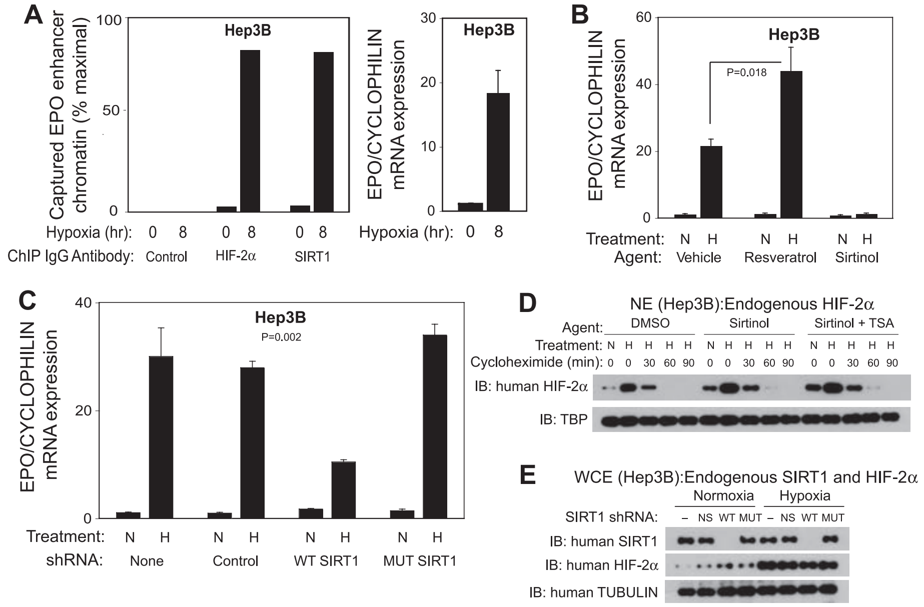

Fig. 4. Modulation of *Epo* gene expression by Sirt1 in cell culture. (**A**) Association of endogenous SIRT1 and HIF-2α to the *EPO* enhancer during hypoxia. Using extracts prepared from Hep3B cells after hypoxia exposure, chromatin immunoprecipitation (ChIP) assays were done with antibodies to SIRT1, HIF-1α, or HIF-2α and with primers encompassing the human *EPO* enhancer. *EPO* mRNA expression was assessed by real-time reverse transcription polymerase chain reaction (rtRT-PCR) for parallel samples and was normalized to expression of the housekeeping gene *cyclophilin B* (CYCLOPHILIN). (**B**) Pharmacological manipulations of Sirt1 activity and *EPO* expression during hypoxia. After vehicle, resveratrol, or sirtinol treatment, *EPO* expression was measured by rtRT-PCR in Hep3B cells maintained under normal (normoxia, N) or reduced (hypoxia, H) oxygen conditions. Statistical significance (Student's *t* test) is indicated. The data represent the mean ± SEM of triplicates for each treatment. (**C**) SIRT1 depletion and *EPO* expression during hypoxia. *EPO* gene expression was measured by rtRT-PCR in Hep3B cells expressing control, WT SIRT1 shRNA, or MUT SIRT1 shRNA and maintained under normoxia (N) or hypoxia (H) conditions. Statistical significance (ANOVA) for hypoxia samples is indicated. The data represent the mean ± SEM of triplicates for each transfection. (**D**) Pharmacological inhibition of Sirt1 activity and endogenous HIF-2α stability. Nuclear extracts (NE) from hypoxia-exposed Hep3B cells treated with dimethyl sulfoxide, sirtinol, or sirtinol plus TSA followed by cycloheximide-mediated protein inhibition were prepared and immunoblotted (IB) with antibodies recognizing human HIF-2α or the normalization control TATA-binding protein (TBP). (**E**) Sirt1 depletion and endogenous HIF-2α amounts. WCE of normoxia- or hypoxia-exposed Hep3B cells treated with control, WT SIRT1 shRNA, or MUT SIRT1 shRNA were immunoblotted (IB) with antibodies recognizing human SIRT1, HIF-2α, or the normalization control α-tubulin (TUBULIN).

Similar to findings observed with lysine substitution mutants of PPAR gamma coactivator 1α (PGC-1α), also a target for Sirt1-mediated deacetylation and augmentation (*35*), transcriptional activities of the HIF-2α lysine substitution mutants were augmented by Sirt1 but were not repressed by a small molecule inhibitor of Sirt1 (Fig. 3C and fig. S9C).

Sirt1 regulates Epo expression in cell culture. We next assessed whether Sirt1 participated in regulation of endogenous HIF-2α target genes in cells. Chromatin immunoprecipitation experiments revealed increased recruitment of Sirt1 and HIF-2α to the *Epo* enhancer region in Hep3B cells during hypoxia (Fig. 4A). Pharmacological manipulations of Sirt1 activity resulted in increased abundance of *Epo* mRNA with agents that stimulate Sirt1 deacetylase activity and decreased *Epo* mRNA concentrations with agents that inhibit Sirt1 deacetylase activity (Fig. 4B). Depletion of Sirt1 resulted in reduced induction of *Epo* mRNA (Fig. 4C). Neither pharmacological manipulations nor genetic inhibition of Sirt1 affected amounts of endogenous HIF-2α protein (Fig. 4, D and E).

Sirt1 contributes to Epo regulation in mice. If inhibiting Sirt1 deacetylase activity blunts HIF-2α signaling in cells, then reduced Sirt1 gene dosage should affect in vivo HIF-2α signaling. We determined whether Sirt1 signaling is physiologically relevant to regulation of the HIF-2α selective target gene *Epo*. During mouse development, the liver is a major source of *Epo* at the mid- to late-gestational stages. At embryonic day 14.5 (E14.5), when HIF-2α deficiency results in lower *Epo* mRNA concentrations in the fetal liver, $Sirt1^{-/-}$ embryos had significantly lower amounts of *Epo* mRNA compared with $Sirt1^{+/+}$ mice (Fig. 5A). In contrast, at E12.5, when HIF-2α deficiency has no effect on *Epo* mRNA concentrations in the fetal liver, $Sirt1^{-/-}$ embryos had similar amounts of *Epo* mRNA as $Sirt1^{+/+}$ mice (fig. S10).

$Sirt1^{-/-}$ mice exhibit substantial prenatal and perinatal lethality as well as marked postnatal pathology (*36*). $Sirt1^{+/-}$ mice, in comparison, lack gross abnormalities or gestational lethality. To assess whether partial Sirt1 deficiency affects in vivo HIF-2α signaling, we tested whether renal *Epo* gene expression differed between $Sirt1^{+/-}$ and $Sirt1^{+/+}$ mice exposed to hypoxia (6% oxygen). $Sirt1^{+/-}$ mice had blunted induction of renal *Epo* mRNA relative to $Sirt1^{+/+}$ mice after hypoxia exposure (Fig. 5B). Both groups of mice had similar amounts of renal *Epo* mRNA under ambient oxygen conditions (21% oxygen, room air).

Congenital Sirt1 deficiency affects fetal and adult *Epo* gene expression in mice. We asked whether acute alterations in Sirt1 could modulate *Epo* gene expression in adult mice. Adenoviruses encoding P1P2N HIF-1α, P1P2N HIF-2α, or WT Sirt1 were injected into tail veins of adult mice; hepatic *Epo* mRNA levels and hematocrits were measured 1 week later. Sirt1 alone had no significant effect on hepatic *Epo* mRNA levels and hematocrits (fig. S11). Ectopic P1P2N HIF-2α, but not P1P2N HIF-1α, expression markedly increased hepatic *Epo* mRNA levels as well as hematocrits; these physiological parameters were further augmented when WT Sirt1 was coexpressed with P1P2N HIF-2α (Fig. 5C).

We determined whether Sirt1 deacetylase activity was required to augment *Epo* gene expression by ectopic P1P2N HIF-2α in adult mice. Adenoviruses encoding P1P2N HIF-1α, P1P2N HIF-2α, WT Sirt1, or DAC Sirt1 were injected into adult mice; hepatic *Epo* mRNA levels and hematocrits were measured 1 week later. Ectopic P1P2N HIF-2α, but not P1P2N HIF-1α, markedly increased hepatic *Epo* mRNA levels (Fig. 5C) and spleen weights, the latter indicative of a dramatic increase in circulating red blood cell mass (fig. S12A). Combined overexpression of P1P2N HIF-2α and WT, but not DAC, Sirt1 further augmented *Epo* mRNA levels (Fig. 5C) and hematocrits (fig. S12B).

Although overexpression of Sirt1 alone does not affect *Epo* gene expression in the liver, endogenous Sirt1 could contribute to HIF-2 signaling in the liver when HIF-2 signaling is active. We examined whether an acute reduction in Sirt1 levels affected hepatic *Epo* gene expression induced by ectopic P1P2N HIF-2α expression. Adenovirus encoding short hairpin RNA (shRNA) against Sirt1 were injected into mice to deplete Sirt1 in livers. The rise in hepatic *Epo* mRNA concentrations (Fig. 5D) and hematocrits (fig. S13) induced by ectopic P1P2N HIF-2α were blunted in mice expressing WT, but not mutant (MUT), Sirt1 shRNA.

Discussion. We reasoned that during hypoxic stress, redox changes would activate Sirt1 and that activated Sirt1 would regulate HIF signaling. Our molecular and biochemical findings support this hypothesis. Furthermore, our cell culture and animal data extend the biological action for Sirt1, beyond its previously defined roles in aging and caloric restriction, to a functional role in hypoxic signaling. Specifically, we demonstrate that Sirt1 augments HIF-2α signaling and consequently participates in regulation of the HIF-2α target gene *Epo*. Erythropoietin, generally considered an erythrogenic growth factor, is also a potent prosurvival factor that protects developing stem cell and progenitor cells in a variety of organs (*37*). Activation of Sirt1 may facilitate HIF-2α–directed production of erythropoietin in cellular niches characterized by hypoxic and possibly other environmental stresses.

In developing mice, hepatic *Epo* gene expression is normally induced by physiological hypoxia induced by growth. Sirt1 deficiency affects embryonic hepatic *Epo* gene expression at the same developmental time point when HIF-2α deficiency exerts its consequence. In adult mice, hypoxia-induced increases in renal *Epo* gene expression are blunted in Sirt1 haploinsufficient mice, similar to that observed with adult HIF-2α haploinsufficient mice (*7*). As further evidence of Sirt1/HIF-2α signaling regulating *Epo* gene expression in vivo, acute Sirt1 knockdown in adult liver

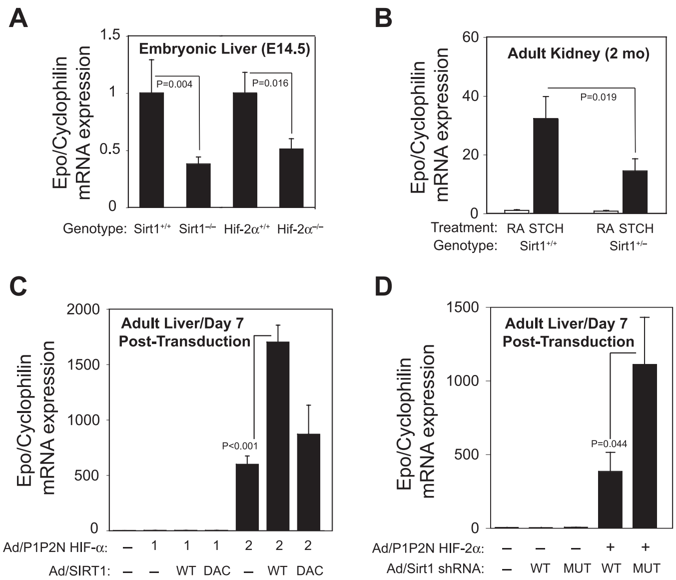

Fig. 5. Modulation of *Epo* gene expression by Sirt1 in animals. (**A**) Hepatic *Epo* expression at E14.5 during development in Sirt1- or HIF-2α–deficient mice. Amounts of *Epo* mRNA expressed in livers of $Sirt1^{+/+}$, $Sirt1^{-/-}$, $HIF\text{-}2\alpha^{+/+}$, and $HIF\text{-}2\alpha^{-/-}$ embryos. Statistical significance (Student's *t* test) is indicated. The bars represent the mean ± SD of five embryos of each genotype. (**B**) Renal *Epo* expression during hypoxia in animals with Sirt1 haploinsufficiency. Amounts of *Epo* mRNA expressed in kidneys of 2-month-old $Sirt1^{+/+}$ or $Sirt1^{+/-}$ mice exposed to short-term continuous hypoxia (STCH). Statistical significance (Z-test) is indicated. The bars represent the mean ± SD of six ($Sirt1^{+/+}$) or eight ($Sirt1^{+/-}$) mice. (**C**) Hepatic *Epo* expression in animals expressing ectopic Sirt1 and HIF-2α. Amounts of *Epo* mRNA expressed in liver at day 7 after injection in adult mice of adenovirus encoding mock, P1P2N HIF-1α, P1P2N HIF-2α, WT Sirt1, or DAC Sirt1, as indicated. Statistical significance (Student's *t* test) is indicated. The bars represent the mean ± SD of five mice per treatment group. (**D**) Hepatic *Epo* expression in animals depleted in Sirt1 and expressing ectopic HIF-2α. Amounts of *Epo* mRNA expressed in liver at day 7 after injection in adult mice of adenovirus encoding mock, Sirt1 WT shRNA, Sirt1 MUT shRNA, or P1P2N HIF-2α, as indicated. Statistical significance (Student's *t* test) is indicated. The bars represent the mean ± SD of five mice per treatment group. For (A) to (D), amounts of *Epo* mRNA were measured by rtRT-PCR and were normalized to amounts of *cyclophilin B* (cyclophilin) mRNA, a housekeeping gene whose expression levels are similar between the different groups.

blunts ectopic HIF-2α–induced increases in hepatic *Epo* gene expression, whereas concomitant Sirt1 and HIF-2α overexpression further augments hepatic *Epo* gene expression in normoxic mice compared with ectopic HIF-2α overexpression alone.

Although Sirt1 overexpression augments HIF-2α–induced *Epo* expression, increased Sirt1 activity alone is not sufficient to induce hepatic *Epo* gene expression in mice. Interestingly, HIF signaling and Sirt1 activity in the liver are inversely regulated during caloric restriction. Whereas caloric restriction of aged rats results in reduced HIF-1 signaling and blunted expression of HIF target genes in the liver, including *Epo* (*38*), caloric restriction is associated with increased hepatic Sirt1 activity (*39*), which indicates that Sirt1 or HIF-2α signaling pathways can be controlled independent of each other in a stress-dependent manner. In addition to repressing HIF-1α signaling, caloric restriction may directly repress HIF signaling induced by HIF-2α. Alternatively, caloric restriction may induce expression of a repressor of *Epo* gene expression that suppresses Sirt1/HIF-2α signaling in a dominant fashion.

Our data integrate Sirt1-HIF-2α signaling with other stress-responsive, prosurvival signal transduction pathways that are modulated by Sirt1 in mammals. HIF-2α is only present in vertebrates and regulates expression of prosurvival factors under hypoxia and other adverse environmental conditions (*2*). HIF-2 signaling, regulated in part by hypoxia-induced acetylation, and Sirt1 augmentation of HIF-2 signaling, conferred through Sirt1/HIF-2α complex formation as well as by Sirt1-mediated deacetylation of acetylated HIF-2α, likely have a specialized role in higher metazoans. Signaling from Sirt1 to HIF-2α could be induced by other environmental stresses besides hypoxia that alter pyridine nucleotide homeostasis and activate HIF-2α signaling. Identifying the relevant environmental stressors that induce Sirt1/HIF-2α signaling and defining the role of Sirt1/HIF-2α signaling in the regulation of protective cellular mechanisms in mammals may provide novel therapeutic opportunities for human disease states.

References and Notes

1. G. L. Semenza, *Biochem. Pharmacol.* **59**, 47 (2000).
2. H. Tian, S. L. McKnight, D. W. Russell, *Genes Dev.* **11**, 72 (1997).
3. G. L. Wang, B. H. Jiang, E. A. Rue, G. L. Semenza, *Proc. Natl. Acad. Sci. U.S.A.* **92**, 5510 (1995).
4. M. Scortegagna *et al.*, *Nat. Genet.* **35**, 331 (2003).
5. E. M. Dioum, S. L. Clarke, K. Ding, J. J. Repa, J. A. Garcia, *Invest. Ophthalmol. Vis. Sci.* **49**, 2714 (2008).
6. M. Morita *et al.*, *EMBO J.* **22**, 1134 (2003).
7. M. Scortegagna *et al.*, *Blood* **105**, 3133 (2005).
8. R. K. Bruick, S. L. McKnight, *Science* **294**, 1337 (2001).
9. A. C. Epstein *et al.*, *Cell* **107**, 43 (2001).
10. P. C. Mahon, K. Hirota, G. L. Semenza, *Genes Dev.* **15**, 2675 (2001).
11. J. Rius *et al.*, *Nature* **453**, 807 (2008).
12. S. Sperandio *et al.*, *Mol. Carcinog.* **48**, 38 (2008).
13. J. F. O'Rourke, Y. M. Tian, P. J. Ratcliffe, C. W. Pugh, *J. Biol. Chem.* **274**, 2060 (1999).
14. O. Garofalo, D. W. Cox, H. S. Bachelard, *J. Neurochem.* **51**, 172 (1988).
15. R. C. Vannucci, R. M. Brucklacher, *Brain Res.* **653**, 141 (1994).
16. H. A. Tissenbaum, L. Guarente, *Nature* **410**, 227 (2001).
17. E. Michishita, J. Y. Park, J. M. Burneskis, J. C. Barrett, I. Horikawa, *Mol. Biol. Cell* **16**, 4623 (2005).
18. J. M. Denu, *Trends Biochem. Sci.* **28**, 41 (2003).
19. A. Brunet *et al.*, *Science* **303**, 2011 (2004).
20. W. J. Bakker, I. S. Harris, T. W. Mak, *Mol. Cell* **28**, 941 (2007).
21. K. J. Bitterman, R. M. Anderson, H. Y. Cohen, M. Latorre-Esteves, D. A. Sinclair, *J. Biol. Chem.* **277**, 45099 (2002).
22. C. M. Grozinger, E. D. Chao, H. E. Blackwell, D. Moazed, S. L. Schreiber, *J. Biol. Chem.* **276**, 38837 (2001).
23. K. T. Howitz *et al.*, *Nature* **425**, 191 (2003).
24. Pairwise comparisons between P1P2N HIF-2α plus WT SIRT1 with vehicle and P1P2N HIF-2α plus WT SIRT1 with the indicated pharmacological treatment (sirtinol, NAM, or resveratrol) were significant for all three reporters at $P < 0.050$ using Student's t test with the Bonferroni correction.
25. M. Fulco *et al.*, *Mol. Cell* **12**, 51 (2003).
26. T. Bouras *et al.*, *J. Biol. Chem.* **280**, 10264 (2005).
27. H. Vaziri *et al.*, *Cell* **107**, 149 (2001).
28. E. Langley *et al.*, *EMBO J.* **21**, 2383 (2002).
29. J. Luo *et al.*, *Cell* **107**, 137 (2001).
30. A. van der Horst *et al.*, *J. Biol. Chem.* **279**, 28873 (2004).
31. J. W. Liu *et al.*, *Oncogene* **24**, 2020 (2005).
32. Y. Kobayashi *et al.*, *Int. J. Mol. Med.* **16**, 237 (2005).
33. H. Daitoku *et al.*, *Proc. Natl. Acad. Sci. U.S.A.* **101**, 10042 (2004).
34. K. F. Chua *et al.*, *Cell Metab.* **2**, 67 (2005).
35. J. T. Rodgers *et al.*, *Nature* **434**, 113 (2005).
36. H. L. Cheng *et al.*, *Proc. Natl. Acad. Sci. U.S.A.* **100**, 10794 (2003).
37. C. T. Noguchi, P. Asavaritikrai, R. Teng, Y. Jia, *Crit. Rev. Oncol. Hematol.* **64**, 159 (2007).
38. M. J. Kang *et al.*, *Biogerontology* **6**, 27 (2005).
39. H. Y. Cohen *et al.*, *Science* **305**, 390 (2004).

40. We acknowledge A. Das, N. Wang, and K. Ding for technical assistance. We thank members of the laboratory of F. Alt for generously providing Sirt1 knockout mice, R. Hammer for assistance with mouse husbandry, Y. Li and H. Ball in the University of Texas Southwestern Medical Center Protein Chemistry Technology Center for mass spectrometry, and C. Xing for suggestions for statistical analyses. These studies were supported by funds provided by Amgen, American Heart Association, and Department of Veterans Affairs.

Supporting Online Material

www.sciencemag.org/cgi/content/full/324/5932/1289/DC1
Materials and Methods
Figs. S1 to S13
References

18 December 2008; accepted 21 April 2009
10.1126/science.1169956

Did Warfare Among Ancestral Hunter-Gatherers Affect the Evolution of Human Social Behaviors?

Samuel Bowles[1,2]

Since Darwin, intergroup hostilities have figured prominently in explanations of the evolution of human social behavior. Yet whether ancestral humans were largely "peaceful" or "warlike" remains controversial. I ask a more precise question: If more cooperative groups were more likely to prevail in conflicts with other groups, was the level of intergroup violence sufficient to influence the evolution of human social behavior? Using a model of the evolutionary impact of between-group competition and a new data set that combines archaeological evidence on causes of death during the Late Pleistocene and early Holocene with ethnographic and historical reports on hunter-gatherer populations, I find that the estimated level of mortality in intergroup conflicts would have had substantial effects, allowing the proliferation of group-beneficial behaviors that were quite costly to the individual altruist.

Intergroup hostilities figure prominently in a number of explanations of the evolution of human social behavior, starting with Darwin (*1*). The underlying mechanism is that (as Darwin put it) groups with "a greater number of courageous, sympathetic and faithful members, who were always ready to warn each other of danger, to aid and defend each other…would spread and be victorious over other tribes" [(*1*), p. 156]. An implication is that if intergroup conflict is frequent and lethal, then more altruistic group-beneficial behaviors—those entailing greater costs to the individual altruist—will be able to proliferate.

Notwithstanding a number of insightful recent studies (*2*–*4*), however, lethal intergroup conflict among hunter-gatherers during the Late Pleistocene and early Holocene remains a controversial subject, with little agreement on either its extent or consequences (*5*, *6*). Among the empirical challenges are the lack of written accounts, the difficulty in making inferences from hunter-gatherers in the ethnographic record about conditions before the domestication of plants and animals and the emergence of states, and the fact that most foragers made little use of fortifications and killed each other with the same weapons that they used to hunt other animals, thus leaving few distinctive archaeological traces other than skeletal remains.

In light of the available archaeological and ethnographic evidence, could war among ances-

[1]Santa Fe Institute, 1399 Hyde Park Road, Santa Fe, NM 87501, USA. [2]University of Siena, Siena 53100, Italy. E-mail: samuel.bowles@gmail.com

tral humans have had substantial effects on the evolution of altruistic behavior? To answer the question, I draw upon recent models of human evolution in which competition between groups plays a prominent role (*7–14*) to quantify the relation between the frequency and intensity of warfare and the selective pressures operating on altruistic behaviors. I use a variant of these models along with a new set of empirical estimates of the extent of war among both prehistoric and historic hunter-gatherers to derive an explicit measure of the importance of warfare in the evolution of human social behavior. This measure is the maximum degree of altruistic behavior—namely c^*, the greatest cost borne by individuals in order to benefit fellow group members—that could have proliferated given the empirically likely extent of warfare during the Late Pleistocene and early Holocene.

The absence of archaeological evidence of persistent economic and political differentiation between families before about 24,000 years ago (*15*) indicates that the most informative data for understanding Late Pleistocene humans pertain to hunting and gathering populations without formal political structures (chiefs, "big men," or states). I exclude populations making substantial use of domesticated plants and animals, namely, pastoral, horticultural, agricultural, and equestrian hunting populations. Because hunter-gatherer populations occupying resource-rich areas in the Late Pleistocene and early Holocene were probably sedentary (at least seasonally), I have included wars involving settled as well as purely mobile populations.

Table 1. Fraction of total mortality due to warfare (δ): summary statistics. Complete sources, methods, and other details for this and Table 2 are in (*17*). Weights are the square root of the total number of deaths.

	Weighted mean	Arithmetic mean	Median
Archaeological	0.12	0.14	0.12
Ethnographic	0.16	0.14	0.13–0.15
All	0.14	0.14	0.12

By "wars" I mean events in which coalitions of members of a group seek to inflict bodily harm on one or more members of another group. The term is not ideal for the ambushes, revenge murders, and other kinds of hostilities likely to have occurred between ancestral groups of humans. Most hostile intergroup contact among hunter-gatherers was probably ongoing or intermittent, with occasional casualties, more akin to boundary conflicts among chimpanzees (*16*) than to the pitched battles of modern warfare.

Using these definitions and selection criteria, I studied all available archaeological and ethnographic sources that present (or are cited as presenting) relevant data. Of these 34 sources, 14 were found to present data that were unrepresentative (for example, when warfare was primarily with modern agricultural populations), unreliable, or inadequate. In three cases, re-estimation of the critical information was possible. Skeletal evidence from sites with fewer than 10 individuals was also excluded. Possible biases in this data set are discussed below. The 8 ethnographic and 15 archaeological sources included yield similar results (Table 1), consistent with the view that prehistoric warfare was frequent and lethal, but somewhat less so than estimates based on data in the standard source for these estimates (*6*). The populations studied appear in Fig. 1. [Details and additional caveats concerning these and the data to follow appear in (*17*).]

Intergroup conflict and the evolution of social behaviors. Although both genetic and cultural transmission are probably involved in the evolution of altruistic behaviors, I model only the former, not because it is more important but because it presents greater challenges. (I comment on extensions to cultural transmission below.)

The primary behaviors thought to have been spread by war are what Darwin termed the "social and moral qualities" and other forms of altruism. This paradoxical role of war arises because, in the absence of within-group positive assortment, altruism will suffer adverse within-group selection. But it might be sustained by the between-group selection pressures that warfare introduces if altruists willingly fight on behalf of others in their group so that otherwise comparable groups with many altruists tend to prevail in intergroup contests. In game theoretic terms, defense or predation is a public good (participating is an n-person prisoner's dilemma) in which those who participate confer benefits on their fellow group members at a cost to themselves. While I treat the case of the altruist as warrior as paradigmatic, willingness to take mortal risks as a fighter is not the only form of altruism that contributes to prevailing in intergroup contests; more altruistic and hence more cooperative groups may be more productive and sustain healthier, stronger, or more numerous members, for example, or make more effective use of information.

The two key determinants of the effect of warfare on the evolution of social behaviors are the extent of genetic differences between the winners and losers of conflicts and the effect of the number of altruists in a group on group members' average fitness. Warfare affects the second by making the presence of altruists in a group critical to the members' survival (and hence their fitness). There are two ways in which the outcome of a conflict may affect the average fitness of its members. The first is that members of losing groups are more likely to perish, and those who die may either produce no offspring or leave children who

Fig. 1. Sources of archaeological (filled squares) and ethnographic (filled dots) evidence on warfare and genetic (open dots) data on between-group differences.

suffer high mortality due to inadequate parental care. The second is that, as with chimpanzees (*18*), weaker groups cede territory, thereby redistributing fitness-relevant resources between the groups.

I consider a large population made up of subpopulations that periodically engage in hostile contests and study an altruistic behavior that is costly to the individual and has no beneficial effects for group members other than increasing the group's probability of prevailing in intergroup contests. Groups are sufficiently large that the increased probability of group success in conflict that is associated with an additional altruistic member does not compensate the individual for the cost of the behavior in question. Thus, adopting the altruistic behavior decreases the expected fitness of an individual (by comparison to an individual eschewing the behavior) while increasing the expected fitness of other group members (*19*). For simplicity, I represent the altruistic behavior in question as the expression of a single allele and let individuals reproduce asexually; the model is readily extended to any form of vertical transmission, including cultural.

Modeling warfare and conditions under which altruism may evolve. Following (*12*), suppose that in every generation with probability κ, a group is paired for a contest with another group and survives with probability λ, which is increasing in the fraction of altruists in the group. Groups are the same size (normalized to 1), except that groups that have won a contest are momentarily of size 2 (the other group is eliminated). The surviving group divides, forming two daughter groups of equal size. The size of group j in the next generation is thus 1, 2, or 0 with probabilities $(1-\kappa)$, $\kappa\lambda$, and $\kappa(1-\lambda)$, respectively, so the expected size is $w_j = 1 - \kappa + 2\kappa\lambda$. The effect of the prevalence of altruists on the expected size of the group in the next generation is the likelihood of a contest (κ), times the effect on group size of surviving or not (2), times the effect of the prevalence of altruists on the probability of a group surviving should a contest occur (λ_A), that is, $\kappa 2\lambda_A$.

Let $p_{ij} = 1$ if individual i in group j is an altruist, with $p_{ij} = 0$ otherwise. Let p_j be the fraction

Table 2. Archaeological and ethnographic evidence on the fraction (δ) of adult mortality due to warfare. "Before present" indicates before 2008.

Site	Archaeological evidence Approx. date (years before present)	Author (date)	δ
British Columbia (30 sites)	5500–334	Cybulski (1994)	0.23
Nubia (site 117)	14–12000	Wendoff (1968)	0.46
Nubia (near site 117)	14–12000	Wendoff (1968)	0.03
Vasiliv'ka III, Ukraine	11000	Telegin (1961)	0.21
Volos'ke, Ukraine	"Epipalaeolithic"	Danilenko (1955)	0.22
S. California (28 sites)	5500–628	Lambert (1997)	0.06
Central California	3500–500	Moratto (1984)	0.05
Sweden (Skateholm I)	6100	Price (1985)	0.07
Central California	2415–1773	Andrushko *et al*. (2005)	0.08
Sarai Nahar Rai, N.India	3140–2854	Sharma (1973)	0.30
Central California (2 sites)	2240–238	Jurmain (2001)	0.04
Gobero, Niger	16,000–8200	Sereno *et al*. (2008)	0.00
Calumnata, Algeria	8300–7300	Chamla *et al*. (1970)	0.04
Ile Teviec, France	6600	Newall *et al*. (1979)	0.12
Bogebakken, Denmark	6300–5800	Newall *et al*. (1979)	0.12
Population, region	*Ethnographic evidence* **Dates**	**Author (date)**	δ
Ache, Eastern Paraguay*	Precontact (1970)	Hill and Hurtado (1996)	0.30
Hiwi, Venezuela-Colombia*	Precontact (1960)	Hill *et al*. (2007)	0.17
Murngin, NE Australia*†	1910–1930	Warner (1931)	0.21
Ayoreo, Bolivia-Paraguay‡	1920–1979	Bugos (1985)	0.15
Tiwi, N. Australia§	1893–1903	Pilling (1968)	0.10
Modoc, N. California§	"Aboriginal times"	Ray (1963)	0.13
Casiguran Agta, Philippines*	1936–1950	Headland (1989)	0.05
Anbara, N. Australia*†‖	1940–1960	Hiatt (1965)	0.04

*Foragers. †Maritime. ‡Seasonal forager-horticulturalists. §Sedentary hunter-gatherers. ‖Recently settled.

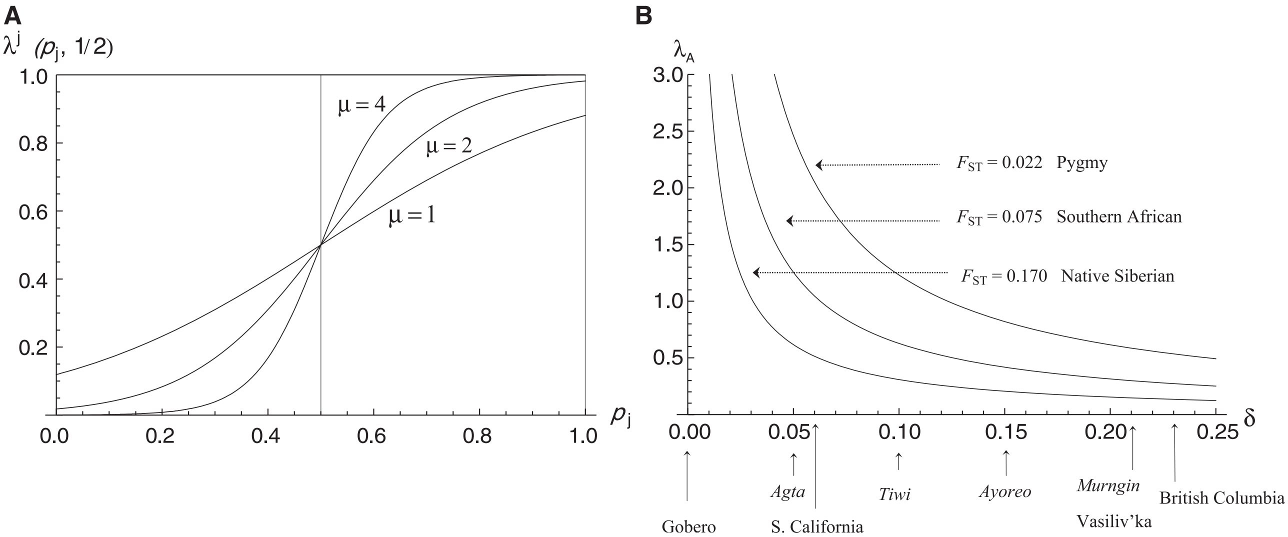

Fig. 2. (**A**) Contest success probabilities [$\lambda^j (p_j, p) = \lambda^j (p_j, ½)$] for group j if half of the opposing group are altruists. The parameter μ determines the slope of the function (λ_A) at $p_j = 0.5$. This success function differs from that of the Lanchester model (*45*) in which the group with more combatants wins with certainty and the rate of losses of the two groups per unit of time depends on the square of the number of fighters in each. The implied Lanchester model survival function in the figure would be a step function with the step at one-half, which would imply much stronger effects of warfare on the evolution of social behavior (*8*). (**B**) Wartime mortality (δ) and the effect of altruism on success in conflicts (λ_A) sufficient for the proliferation of an altruistic trait with $c = 0.03$ for three estimates of the extent of genetic differentiation among groups (F_{ST}). Shown are the values of c^* consistent with Eq. 6 for the estimated F values from (*12*) [see also (*17*)]. The representative values of δ are from Table 2. Populations on the horizontal axis in italics are from the ethnographic sample; the rest are from the archaeological sample.

of group j's membership that are altruists, p and p' be the altruist-fraction of the metapopulation in a given and subsequent generation, respectively, and $\Delta p \equiv p' - p$. Then, using the Price equation (*20*) and assuming a constant metapopulation size, the evolution of altruism (summarized by Δp) can be expressed as a between-group effect plus a within-group effect:

$$\Delta p = \mathrm{var}(p_j)\beta_G + E\{\mathrm{var}(p_{ij})\}\beta_i \qquad (1)$$

The terms $\mathrm{var}(p_j)$ and $E\{\mathrm{var}(p_{ij})\}$ are, respectively, the between-group and within-group genetic variance. ($E\{\}$ indicates a size-weighted average over groups.) The coefficient β_G is the effect of variation in p_j on the average fitness of members of group j (w_j), which (see above) is

$$\beta_G \equiv dw_j/dp_j = \kappa 2\lambda_A \qquad (2)$$

The coefficient β_i is the effect of variation in p_{ij} (namely, switching from a nonaltruist to an altruist) on the fitness of an individual in group j (w_{ij}):

$$\beta_i \equiv dw_{ij}/dp_{ij} = -c + \kappa 2\lambda_A/n \qquad (3)$$

where $-c$ is the direct fitness effect of adopting the altruistic behavior and the second term is the indirect positive effect on the individual's fitness that results from the group's greater probability of prevailing in a contest. This indirect effect is $(dw_j/dp_j)(dp_j/dp_{ij})$ and is derived using Eq. 2 and $dp_j/dp_{ij} = 1/n$, where n is group size (number of individuals in a single reproducing generation in the absence of reproductive skew, fluctuations in group size, and nonrandom migration).

Wright's inbreeding coefficient F_{ST} is the ratio of between-group to total genetic variance [$\equiv \mathrm{var}(p_j)/(\mathrm{var}(p_j) + E\{\mathrm{var}(p_{ij})]$, so one can rearrange Eq. 1 to give a condition for the proliferation of the altruistic trait (namely, $\Delta p > 0$):

$$F_{ST}/(1 - F_{ST}) > -\beta_i/\beta_G \qquad (4)$$

which says that the extent of genetic differentiation among groups must be greater than the ratio of the costs of the altruistic behavior (the within-group selection pressure) to the benefits (the between-group selection pressures). Equation 4 is a multilevel selection analog to Hamilton's rule for the proliferation of altruism by kin selection.

With these results, the condition for an altruistic allele to proliferate (Eq. 4) can be written as

$$F_{ST}/(1 - F_{ST}) > c/\kappa 2\lambda_A - 1/n \qquad (5)$$

Rearranging Eq. 5, I define the critical value c^* as the maximum cost of the altruistic behavior consistent with its proliferating in the population:

$$c^* = \kappa 2\lambda_A \{F_{ST}/(1 - F_{ST}) + 1/n\} \qquad (6)$$

To estimate c^*, one needs to know how frequent and how lethal intergroup conflicts were. The richest source is the skeletal evidence studied by archaeologists.

Archaeological evidence. As with all archaeological data, it is difficult to establish if the sites that have been studied are representative of Late Pleistocene and early Holocene conditions. As these sites involve burials, they are almost certainly not representative in one respect: Simple disposal of the dead (rather than burial) appears to be typical of the archetypal so-called immediate return foraging group (*21*). There may be more than accidental bias in the burials studied for signs of violence, given that evidence of violent deaths may be deemed more interesting or worthy of publication than the absence of such evidence. Evidence on given individuals is also incomplete, leading to the opposite bias. Most skeletal remains are never found, and those that are range from intact to fragmentary or poorly preserved, often consisting of just a few of the 100 or so bones in an adult human (excluding the small bones of the hands and feet). The remains of 2185 prehistoric people from Californian sites are accessible to researchers in a museum collection that totals only 12,044 bones (excluding hands and feet); more than 90% of the individuals' bones are absent (*22*).

Moreover, although some osteological evidence is indicative of ongoing intergroup violence (simultaneous burials, severed limbs, and other evidence of trophy taking, for example), one cannot always distinguish between deaths due to intergroup violence and that occurring within groups. Other biases may lead to underestimates. Many deaths in warfare do not leave projectile points embedded in bone or other traces of violent death: "an analysis that included only projectile points embedded in bone would miss over half of the projectiles…and 75 percent of what was in all probability the actual number of projectile wounds" (*23*). Studies of arrow wounds treated by U.S. Army surgeons during the Indian Wars found that fewer than a third of the arrows struck bone (*24*) and that 61% of fatal arrow wounds were to the abdomen (*25*). Finally, fatalities during combat may fall far short of the total effect of warfare when account is taken of the mortality and reduced reproductive success occasioned by the displacement of the surviving losers. Table 2 gives the resulting estimates.

Ethnographic evidence. Most ethnographic studies of premodern war have concerned populations whose unusually bellicose relations among groups may not reflect conditions of Late Pleistocene hunter-gatherers: horticultural peoples in the highlands of Papua New Guinea and parts of lowland South America, or equestrian hunters or sedentary horticulturalists in North America. Among nonequestrian foragers, detailed accounts provide examples of intergroup conflict of exceptional brutality among Aboriginal Australians, Eskimos, and other groups (*3*, *26*, *27*), but most do not allow quantitative estimates of the resulting mortality. In other groups, war is entirely absent from the ethnographic record, but in some of these cases, like the !Kung and other Southern African groups, this absence may be the result of recent state interventions (*28*, *29*). For eight populations, ethnographic studies allow estimates of the deaths due to warfare as a fraction of total mortality (summarized in Table 2). As in the case of archaeological studies, selection bias may lead to an exaggeration of the extent of warfare mortality. Moreover, some populations are not entirely representative of foragers during the Late Pleistocene due to the impact of non–hunter-gatherer influences.

Calibrating the model with hunter-gatherer data. To estimate c^*—the maximal direct individual cost of a group-beneficial behavior that could have proliferated—I translate our estimated per-generation mortality rates into an equivalent frequency of decisive conflicts in which the entire territory of a group is taken by the winners, and the losing population is eliminated. This allows me to treat the territorial losses and mortality in a consistent way, and to maintain a constant group size, greatly simplifying the analysis. The data on mortality provide an estimate of κ, the per-generation probability of such a a decisive conflict.

Table 3. Largest cost (c^*) for an altruistic trait to proliferate given estimates of genetic differentiation and mortality in intergroup hostilities (δ) among three Arnhem Land, Australian hunter-gatherer populations. The entries are given by Eq. 6, where $\kappa = 2\delta$. Genetic differentiation ($F_{ST} = 0.040$) is among seven groups [including Tiwi and Murngin (see Fig. 3)] and is from (*34*) [see also (*17*)]; δ is from Table 2; $\lambda_A = 2$; $n = 26$, the size of a single generation in a coalition of three groups of the census size considered to be typical of nonequestrian, non-Arctic foragers during the Late Pleistocene (*44*).

	Murngin $\delta = 0.207$	Tiwi $\delta = 0.100$	Anbara $\delta = 0.045$
$n = 26$	0.133	0.064	0.029
$n = \infty$	0.069	0.033	0.015

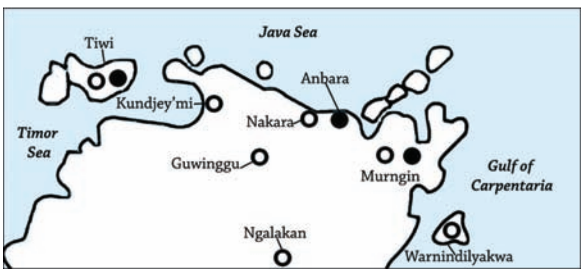

Fig. 3. Data sources in Arnhem Land, Australia, for ethnographic evidence on warfare (filled dots) and genetic differentiation (open dots). [Source: Table 2 and (*34*)] The maximum distance between pairs of groups shown is about 600 km.

Mortality results when a group loses a conflict, occurring with probability $\kappa(1 - \lambda)$. If war does not occur or if the group engages in war but prevails, then all deaths are from other causes, so $\kappa(1 - \lambda)$ is estimated by δ, the fraction of mortality due to war. Averaging across groups, $\lambda = \frac{1}{2}$; so $\delta = \frac{1}{2}\kappa$, giving $\kappa = 2\delta$.

We need two additional pieces of information: the effect of additional altruists on the probability of group survival (λ_A) and the extent of genetic differentiation among groups (F_{ST}). There is no way to estimate λ_A empirically for hunter-gatherers, and it may vary depending on the degree of imbalance between the warring groups, the available weapons, and the nature of the conflict (ambush, pitched battle) and the terrain (open plains, mountain pass). The intuitive meaning of alternative functions is illustrated in Fig. 2A. For the contest success functions illustrated, the assumption that the success function is approximately linear (λ_A is a constant) works as long as the groups are not very imbalanced. Because I use a probabilistic (rather than deterministic) function, even groups with substantial fractions of altruists on average suffer significant mortality. For example, if the difference between two groups in the fraction of altruists is 10% and $\lambda_A = 2$, then should a conflict occur, the expected mortality of the group with fewer altruists is just 1.50 times the mortality in the more altruistic group (*17*). (For the mortality in the less altruistic group to be double that of the more altruistic group, $\lambda_A = 3.3$ would be required.) Even with very frequent conflicts, e.g., $\kappa = 0.2$ (and $\lambda_A = 2$), the difference in the expected size (next generation) of these two groups is only 0.04.

Available estimates of F_{ST} for hunter-gatherer populations measure the extent of genetic differentiation both among subpopulations in a given ethno-linguistic group (e.g., among the !Kung in Botswana) and among subpopulations in more than one ethno-linguistic group (e.g., among 18 ethnic groups in Southern Africa). Because prehistoric warfare probably was most common on the boundaries of an expanding ethno-linguistic unit, the latter measure may be the more appropriate one for this study. Excluding those populations that currently live at such a distance from another that it is unlikely that they interacted in the distant past and those that are not at least somewhat reproductively isolated from non–hunter-gatherer populations, there is a total of 18 estimates among hunter-gatherer groups (*17*). The mean F_{ST} of the 18 estimates is 0.074, whereas that for the 15 estimates between ethno-linguistic groups is 0.078. The median for both sets is 0.075. Differences in the genetic material and statistical methods on which these estimates are based make direct comparisons difficult [the Pygmy and Arnhem Land estimates are based on microsatellite data and as a result are likely to be underestimates (*30*, *31*)]. In the illustrative calculations below, I use the median and range of the estimates for between–ethno-linguistic group differentiation.

Results. I can now answer the question with which I began: What is the maximum cost of altruism (c^*) such that the group benefits would offset the within-group selection pressures against the altruists? To decide whether the resulting values of c^* are "large" or "small," note that $c^* = 0.03$, for example, is a quite substantial cost, one that in the absence of intergroup competition would lead the fraction of altruists in a group to fall from 0.9 to 0.1 in just 150 generations. An illustration more directly related to the question of warfare is the following. Suppose that in every generation, a group is engaged in a war with probability $\kappa = 2\delta$ and that an altruistic "warrior" will die with certainty in a lost war and with probability 0.20 in a war in which the group prevails, while nonaltruistic members also die with certainty in lost wars but do not die in won wars. (These mortality assumptions are extremely unfavorable for the altruists.) Assuming the altruists have no reproductive advantages during peacetime, then $c = 0.2\delta$, or (using the mean estimate of δ from Table 1) $c = 0.028$.

To study the evolutionary consequences of warfare under Pleistocene conditions using recent data, one would ideally use estimates of both genetic differentiation and wartime mortality from hunter-gatherer populations living in close proximity with one another but having little contact with farmers or herders. Such groups exist in Arnhem Land, Australia, the continent thought by many to be the best laboratory of likely Late Pleistocene and early Holocene conditions among foragers (*32*). Depictions of warriors and battles in the rock art of Arnhem Land populations date from as early as 10,000 years ago (*33*). The availability of archaeological, ethnographic, and genetic data for this region makes it a remarkable laboratory for this investigation (Fig. 3).

Table 3 presents data on the extent of wartime mortality in three nearby groups of foragers—the Anbara, Murngin, and Tiwi—along with estimates of genetic differentiation among seven Aboriginal groups (including the Tiwi and Murngin) in that relatively small area (*34*). The estimates of c^* for these populations (assuming $\lambda_A = 2$) make it clear that if groups were as differentiated as these populations and as warlike as the Murngin, between-group competition could overcome very strong within-group selection against altruistic behavior. Even for groups similar to the more peaceful Anbara, quite costly forms of altruism could proliferate by this mechanism ($c^* = 0.029$). The second line in the table gives the values of c^* for very large (strictly infinite) groups, that is, ignoring the term $1/n$ in Eq. 6 and thus eliminating the direct benefit accruing to the altruist.

To explore the importance of variations in λ_A, Fig. 2B uses the extreme F_{ST} values for differentiation between ethno-linguistic groups (Native Siberian and Pygmy) and the median of these values (South African) to show the combinations values of λ_A and δ such that the between-group selection would offset a $c^* = 0.03$. Figure 2B indicates that for plausible values of the effect of altruistic behaviors on a group's chances of prevailing in contests (λ_A), the levels of warfare mortality observed in many populations would offset substantial costs of altruism.

Discussion. The mortality data summarized in Table 1 are consistent with what is known about the Late Pleistocene from more indirect data. Frequent lethal intergroup encounters may reconcile two otherwise anomalous facts about hunter-gatherer demographics. Human population grew extraordinarily slowly or not at all for the 100,000 years prior to 20,000 years before the present (*35*, *36*), yet under peaceful conditions foraging populations are capable of growth rates exceeding 2% per annum (*37*, *38*).

Further, the extraordinary volatility of climate during the Late Pleistocene (*39*) must have resulted in natural disasters and periodic resource scarcities, known strong predictors of intergroup conflict among hunter-gatherers in the historical record (*40*), and undoubtedly forced long-distance migrations and occasioned frequent encounters between groups having no established political relations. The mortality data from Southern California (*23*) and Nubia (*41*) are consistent with this hypothesis.

The evidence that intergroup conflict may have contributed significantly to the proliferation of a genetic predisposition to behave altruistically does not mean that it did, or that the mechanism I have described explains the evolution of human altruism. The model applies with even greater force to behaviors transmitted culturally rather than genetically, in part because between-group differentiation is considerably greater and hence the evolutionary impact of differential group success in contests is stronger.

One cannot say with certainty which of these data should be the basis for our conclusions concerning the evolutionary impact of lethal intergroup competition during the Late Pleistocene and early Holocene. Even though periods of climatic volatility would bring even quite distant groups into contact during migrations, the far-flung settlements of the circumpolar regions, desert Southern Africa, and Western Australia would be far less likely to be in contact—either conflictual or beneficial—than groups living in closer proximity such as those in coastal Arnhem Land and lowland New Guinea. Moreover, the more populated coastal and riverine areas contributed disproportionately to the gene pool of subsequent generations. But taking all of the evidence into account, it seems likely that, for many groups and for substantial periods of human prehistory, lethal group conflict may have been frequent enough to support the proliferation of quite costly forms of altruism.

This might help explain why altruism often does not extend across group boundaries, and how this kind of "parochial altruism" may have evolved in humans (*13*) and perhaps even other animals. Because humans are far from unique in the extent of lethal intergroup conflicts (*42*) and because genetic differentiation among populations of some other "warlike" animals may not be very different from that among humans (*43*), there remains the as-yet unexplored possibility that a similar evolutionary dynamic may occur in other animals.

References and Notes

1. C. Darwin, *The Descent of Man* (D. Appleton & Co., New York, 1873).
2. A. Gat, *War in Human Civilization* (Oxford Univ. Press, Oxford, 2006).
3. E. S. Burch, *Alliance and Conflict: The World System of the Unupiaq Eskimos* (Univ. of Nebraska Press, Lincoln, NE, 2005).
4. S. A. LeBlanc, *Constant Battles* (St. Martins Press, New York, 2003).
5. B. Ferguson, in *Troubled Times: Violence and Warfare in the Past*, D. L. Martin, D. W. Frayer, Eds. (Gordon & Breach, Amsterdam, 1997), pp. 321–354.
6. L. Keeley, *War Before Civilization* (Oxford Univ. Press, New York, 1996).
7. K. Aoki, *Evolution* **36**, 832 (1982).
8. S. A. Boorman, P. R. Levitt, *Theor. Popul. Biol.* **4**, 85 (1973).
9. R. Andrés Guzmán, C. Rodríguez-Sickert, R. Rowthorn, *Evol. Hum. Behav.* **28**, 112 (2007).
10. S. Bowles, J.-K. Choi, A. Hopfensitz, *J. Theor. Biol.* **223**, 135 (2003).
11. O. Smirnov, H. Arrow, D. J. Kennett, J. Orbell, *J. Polit.* **69**, 927 (2007).
12. S. Bowles, *Science* **314**, 1569 (2006).
13. J.-K. Choi, S. Bowles, *Science* **318**, 636 (2007).
14. L. Lehmann, M. Feldman, *Proc. R. Soc. London Ser. B. Biol. Sci.* **275**, 2877 (2008).
15. V. Formicola, *Curr. Anthropol*. **48**, 446 (2007).
16. J. H. Manson, R. W. Wrangham, *Curr. Anthropol.* **32**, 369 (1991).
17. Methods and other supporting materials are available on *Science* Online.
18. J. Williams, G. Oehlert, J. Carlis, A. E. Pusey, *Anim. Behav.* **68**, 523 (2004).
19. B. Kerr, P. Godfrey-Smith, M. Feldman, *Trends Ecol. Evol.* **19**, 135 (2004).
20. G. R. Price, *Nature* **227**, 520 (1970).
21. J. Woodburn, in *Death and the Regeneration of Life*, M. Bloch, J. Parry, Eds. (Cambridge Univ. Press, Cambridge, 1982), pp. 187–210.
22. J. M. Tenney, *Hum. Evol.* **5**, 397 (1990).
23. P. Lambert, in *Troubled Times: Violence and Warfare in the Past*, D. L. Martin, D. W. Frayer, Eds. (Gordon & Breach, Amsterdam, 1997), pp. 77–109.
24. G. Milner, *Am. Antiq.* **70**, 144 (2005).
25. J. H. Bill, *Am. J. Med. Sci.* **40**, 365 (1862).
26. J. Morgan, *The Life and Adventures of William Buckley: Thirty-Two Years a Wanderer Amongst the Aborigines* [Australia National Univ. Press (first published 1852), Canberra, 1979].
27. J. Melbye, S. Fairgrieve, *Arctic Anthropol.* **31**, 57 (1994).
28. I. Schapera, *The Khoisan Peoples of South Africa* (Routledge & Kegan Paul, London, 1930).
29. C. Campbell, *World Archaeol.* **18**, 255 (1986).
30. L. Jost, *Mol. Ecol.* **17**, 4015 (2008).
31. P. W. Hedrick, *Evolution* **59**, 1633 (2005).
32. H. Lourandos, *Continent of Hunter-Gatherers* (Cambridge Univ. Press, Cambridge, 1997).
33. P. Tacon, C. Chippendale, *Camb. Archaeol. J.* **4**, 211 (1994).
34. S. J. Walsh, R. J. Mitchell, N. Watson, J. S. Buckleton. *J. Hum. Genet.* **52**, 712 (2007).
35. J.-P. Bocquet-Appel, P.-Y. Demars, L. Noiret, D. Dobrowsky, *J. Archaeol. Sci.* **32**, 1656 (2005).
36. M. N. Cohen, in *Biosocial Mechanisms of Population Regulation*, M. N. Cohen, R. S. Malpass, H. G. Klein, Eds. (Yale Univ. Press, New Haven, CT, 1980), pp. 275–303.
37. F. A. Hassan, in *Biosocial Mechanisms of Population Regulation*, M. N. Cohen, R. S. Malpass, H. G. Klein, Eds. (Yale Univ. Press, New Haven, CT, 1980), pp. 305–319.
38. S. R. Johansson, S. R. Horowitz, *Am. J. Phys. Anthropol.* **71**, 233 (1986).
39. North Greenland Ice Core Project members, *Nature* **431**, 147 (2004).
40. C. Ember, M. Ember, *J. Conflict Resolut.* **36**, 242 (1992).
41. F. Wendorf, *Prehistory of Nubia* (Southern Methodist Univ. Press, Dallas, TX, 1968).
42. R. W. Wrangham, M. L. Wilson, M. N. Muller, *Primates* **47**, 14 (2006).
43. T. L. Goldberg, L, M. Ruvolo. *Mol. Biol. Evol.* **14**, 976 (1997).
44. F. Marlowe, *Evol. Anthropol.* **14**, 54 (2005).
45. F. W. Lanchester, *Aircraft in Warfare, the Dawn of the Fourth Arm* (Constable & Co., Ltd., Tiptee, UK, 1916), p. 222.
46. Thanks to I. Levina and A. Verashchagina for translating the Russian and Ukrainian archaeological materials; P. Lambert and K. Kennedy for assistance with the Californian and Indian archaeological evidence; M. Alexander, K. Ames, B. Bertram, L. Luigi Cavalli-Sforza, T. Clutton-Brock, W. Cote, E. Einhorn, D. Wood Gordon, H. Kaplan, K. Hill, K. Howard, S.-H. Hwang, K. Langergraber, S. Le Blanc, J. Mitani, C. Resnicke, R. Rowthorn, P. Seabright, E. Alden Smith, T. Taylor, D. Ulibarri, L. Vigilant, E. Wood, and R. Wrangham for valuable contributions; and the Behavioral Sciences Program of the Santa Fe Institute, the U.S. National Science Foundation, the European Science Foundation, and the University of Siena for support of this work. The author declares no competing interests.

Supporting Online Material
www.sciencemag.org/cgi/content/full/324/5932/1293/DC1
Materials and Methods
Tables S1 to S5
References and Notes

5 November 2008; accepted 10 April 2009
10.1126/science.1168112

REPORTS

Late Pleistocene Demography and the Appearance of Modern Human Behavior

Adam Powell,[1,3] Stephen Shennan,[2,3] Mark G. Thomas[1,3]*

The origins of modern human behavior are marked by increased symbolic and technological complexity in the archaeological record. In western Eurasia this transition, the Upper Paleolithic, occurred about 45,000 years ago, but many of its features appear transiently in southern Africa about 45,000 years earlier. We show that demography is a major determinant in the maintenance of cultural complexity and that variation in regional subpopulation density and/or migratory activity results in spatial structuring of cultural skill accumulation. Genetic estimates of regional population size over time show that densities in early Upper Paleolithic Europe were similar to those in sub-Saharan Africa when modern behavior first appeared. Demographic factors can thus explain geographic variation in the timing of the first appearance of modern behavior without invoking increased cognitive capacity.

The Upper Paleolithic (UP) transition, which occurred in Europe and western Asia about 45 thousand years ago (ka) (*1*, *2*), and later in southern and eastern Asia (*3*, *4*), Australia (*5*, *6*), and Africa (*7*), is seen by many as marking the origins of modern human behavior. UP material culture, usually referred to as the Late Stone Age (LSA) in Africa, is characterized by a substantial increase in technological and cultural complexity, including the first consistent presence of symbolic behavior, such as abstract and realistic art and body decoration (e.g., threaded shell beads, teeth, ivory, ostrich egg shells, ochre, and tattoo kits); systematically produced microlithic stone tools (especially blades and burins); functional and ritual bone, antler, and ivory artifacts; grinding and pounding stone tools; improved hunting and trapping technology (e.g., spear throwers, bows, boomerangs, and nets); an increase in the long-distance transfer of raw materials; and musical instruments, in the form of bone pipes (*1*, *2*, *5*, *7*–*9*).

In Europe and western Asia, the UP transition happened relatively rapidly, with most of the characteristic features listed above appearing (the "full package"), and is thought to coincide with the appearance of anatomically modern humans (AMH) in a region previously occupied by Neandertals (*10*). In southern Siberia and northeast Asia, microlithic technology appears between 43 and 27 ka (*11*), but a fuller UP package is not evident until ~22 ka (*12*). The evidence from south and southeast Asia and Australia also points to a more gradual accumulation of modern behavioral traits (ornamentation, use of ochre, and possibly rock art) (*3*–*6*). These are thought to first appear soon after the initial expansions of AMH into the regions but only become widespread later on, ~30 ka (*4*) and ~20 ka, if not later (*5*), in south Asia and Australia, respectively. In Africa, the idea of a single transition has been

[1]Research Department of Genetics, Evolution, and Environment, University College London, Wolfson House, 4 Stephenson Way, London NW1 2HE, UK. [2]Institute of Archaeology, University College London, 31–34 Gordon Square, London WC1H 0PY, UK. [3]Arts and Humanities Research Council (AHRC) Centre for the Evolution of Cultural Diversity, Institute of Archaeology, University College London, 31–34 Gordon Square, London WC1H 0PY, UK.

*To whom correspondence should be addressed. E-mail: m.thomas@ucl.ac.uk

contested (*9*) because there is strong evidence for the sporadic appearance of many markers of modern behavior at multiple sites as early as 70 to 90 ka (*2*, *9*, *13*), and possibly as far back as 160 ka (*14*). The African Middle Stone Age (MSA) sites of Katanda, Democratic Republic of Congo (~90 ka) (*9*); Klasies River mouth (Howieson's Poort and Still Bay industries), South Africa (~65 to 70 ka) (*9*, *15*); and, in particular, Blombos Cave, South Africa (~75 ka) (*10*, *13*) present a striking array of modern traits, including the earliest evidence of abstract art (*8*, *13*), as well as geometric blades, barbed bone harpoon points (*9*), bone awls, and marine shell personal ornaments (*10*). However, these markers are intermittent and disappear between ~75 and 60 ka before making a more stable and widespread reappearance in the LSA starting ~40 ka (*7*, *10*, *13*).

Notwithstanding the oversimplifications made in the above outline, any adequate account of the emergence of modern behavior would need to explain not only the transition itself but also its heterogeneous spatial and temporal structuring (*2*) and earlier transient appearance in sub-Saharan Africa (*9*, *10*, *13*). It is now widely accepted that AMH evolved in Africa ~160 to 200 ka (*9*, *16*–*18*) and expanded into most habitable parts of the Old World between 90 and 40 ka (*19*–*21*). If, as some have suggested (*22*–*24*), the main cause of behavioral modernity is heritable biological change just before the UP/LSA, then any such mutation(s) would have had to rise to substantial frequencies after human populations had dispersed out of Africa; implying either their rapid spread around the world in the past 45,000 years or, potentially, geographic structuring of cognitive capacity. Furthermore, it is difficult to account for the southern African evidence with a late, biologically determined cognitive advance. Many authors have argued that AMH (*1*, *9*, *10*, *17*, *20*), and possibly even Neandertals (*8*, *10*), possessed the requisite capacities long before the UP/LSA. This raises the further question of why there was a delay of some 100,000 years between anatomical modernity and perceived behavioral modernity (*1*, *17*). A number of mechanisms triggering the expression of modern behavior have been proposed, many of which invoke demographic change as a causal factor. These include expansion into new environments necessitating the invention of new technologies (*25*), increased subpopulation density escalating intergroup resource competition (*1*, *25*) or social organization (*1*), increased intergroup interaction requiring various cultural signaling mechanisms (*6*, *25*, *26*), and increased stimulus for exoteric language (*23*, *27*, *28*). Two recent cultural evolutionary models (*29*, *30*), which explicitly demonstrate the positive effect of increasing population size on the accumulation of beneficial culturally inherited skills, have been proposed as an integral explanatory component of the appearance of modern behavior [see also (*17*)]. Here, we adapt and extend Henrich's transmission model (*30*) into a more realistic structured metapopulation, which reflects plausible late Pleistocene conditions, to investigate the effects of demographic factors on the accumulation (or loss) of cultural complexity.

Henrich's model (*30*) demonstrates that under certain critical conditions, directly biased transmission can lead to cumulative adaptation of a culturally inherited skill, even when the transmission process is inaccurate. Each individual in a population of size *N* has a *z* value, z_i, that measures their level of ability at

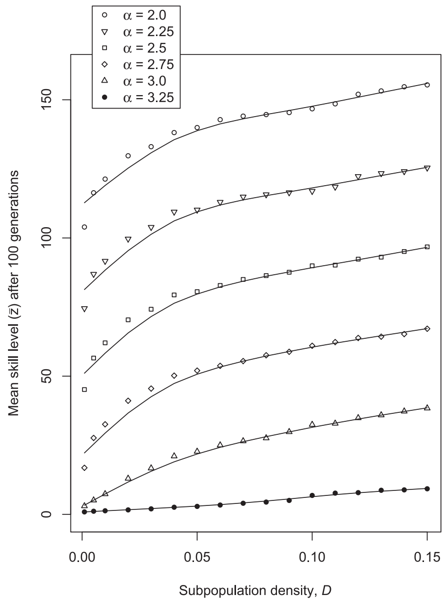

Fig. 1. Mean *z* values in the final (100th) generation, averaged over 100 iterations, for a range of values of skill complexity α and subpopulation density *D*.

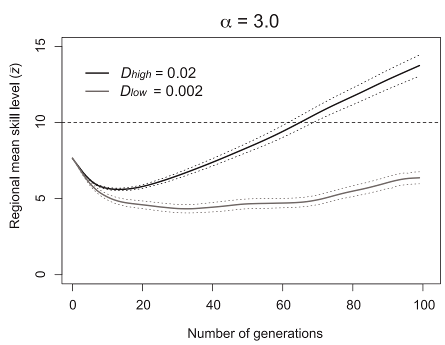

Fig. 2. Regional mean *z* values (averaged over 100 iterations) over 100 generations in a heterogeneous subpopulation density world. The 95% confidence intervals for each region are given as dotted lines.

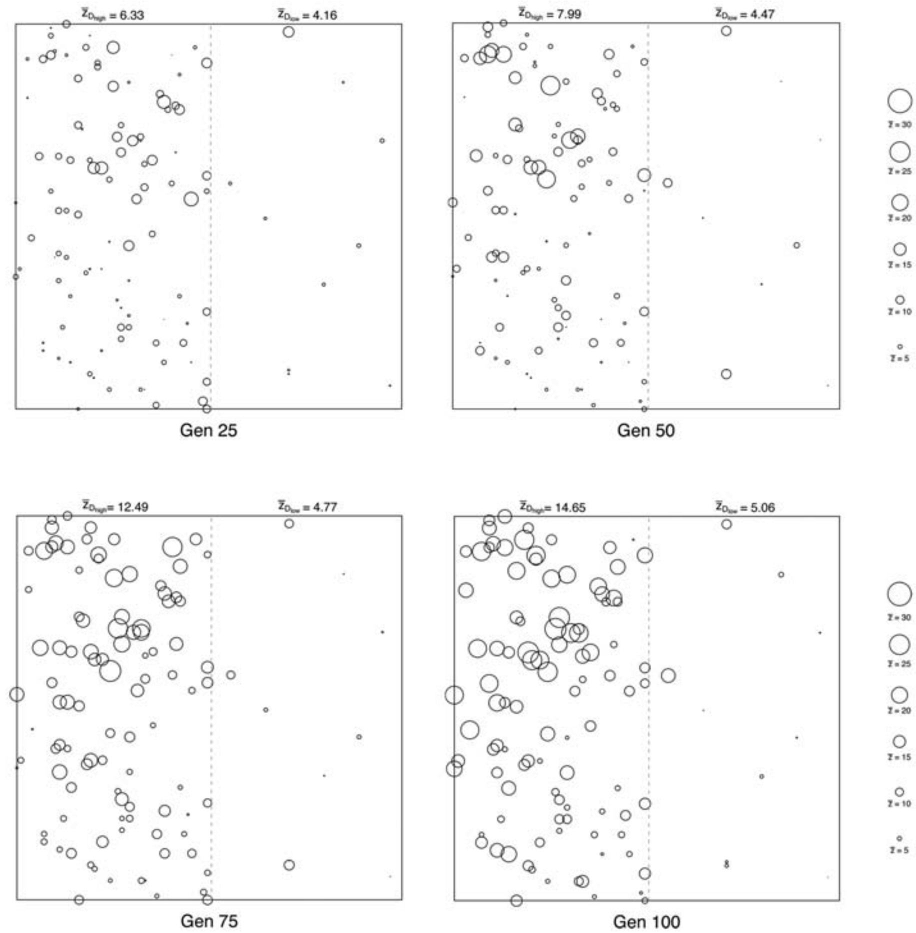

Fig. 3. An illustration, from a single iteration and shown at 25-generation intervals, of the spatial structuring of skill accumulation in a heterogeneous subpopulation density world. The left side of each subplot is populated at density D_{high} (0.02) and the right side at density D_{low} (0.002). Each subpopulation is marked by a circle, centered on the spatial location of the group and with diameter proportional to its mean *z* value. Regional mean *z* values are also given at the top of each subplot.

some cultural skill or in some cultural domain. Members of this population attempt to learn from the maximally skilled individual (i.e., direct bias), but an imperfect learning process leads on average to a loss of skill (a reduction in z value), determined by the parameter α. However, individual errors or "inaccurate inferences" during transmission (the extent of which are governed by a parameter β) occasionally allow some learners to acquire a z value greater than that of their model. Henrich shows that as population size, N, increases, the more likely it is that the positive combined effect of these occasional inaccurate inferences and the selective choice of cultural model to copy will outweigh the degrading effect of low-fidelity transmission. This results in an increase in the mean level of skill in the population, $\bar{z}$. He terms this "cumulative adaptive evolution" and derives the critical population size necessary, N^*, for this to occur for specific ratios of α and β (*30*, *31*).

We introduce a stochastic transmission model analogous to the one presented by Henrich that incorporates both vertical and skill-level dependent oblique learning processes. We place individuals in G subpopulations, each of size N, in a simulated world at density D. These subpopulations are connected by Gaussian random-walk migratory activity, with standard deviation M_{SD}, such that the mean global migration rate approximates the subpopulation density D (*31*). Where possible, we use parameter values from ethnographic and comparative behavioral studies that approximate presumed late Pleistocene demography (*31*). We initialize simulations by giving all adults in all subpopulations a z value of 10.0 and run forward for 100 generations. The mean level of cultural skill accumulation, $\bar{z}$, is measured by averaging z values across all individuals in all subpopulations. If the mean z value in the final generation is greater than 10.0 (i.e., $\Delta\bar{z} > 0$), then the result was deemed "cumulatively adaptive." To account for stochastic variation in simulation outcomes, we performed 100 iterations and averaged the results across these.

We first explored the effects of varying the number of subpopulations in our simulated world, G, on the mean level of cultural skill accumulated, $\bar{z}$. For values of $G > \sim 50$, the $\bar{z}$ value did not increase much further across the entire range of subpopulation densities D and skill complexities α (fig. S1). Figure 1 illustrates that the degree of skill accumulation increased with increasing subpopulation density and decreasing skill complexity. These results indicate that the accumulation, or maintenance, of culturally inherited skill is not dependent on the absolute metapopulation size, but rather on the degree of interaction of the constituent subpopulations, given population substructure and that $G > \sim 50$. However, when $G < \sim 50$, skill accumulation will, to an extent, be dependent on G, and thus the size of the metapopulation. This result may have some bearing on debate concerning the erosion of cultural complexity in Holocene Tasmania (*30*, *32*, *33*). As a conservative measure, we fixed G at 100 in all subsequent simulations.

A key feature of the UP is the geographic heterogeneity in apparent onset times, despite different regions being mutually accessible with modest migration activity. To investigate whether skill accumulation can be spatially structured as a result of different subpopulation densities, we partitioned our simulated world into two regions differing in density by an order of magnitude, D_{high} and D_{low}. We retained M_{SD} at 1.0, but as a proportion of the mean nearest neighbor distance, $\bar{r}_E$, in the lower density region (*31*). This ensured that sufficient subpopulations were connected by migratory activity—including across the partition—for the migration rate to approximate the density in each region. We set $D_{high} = 0.02$ and $D_{low} = 0.002$ and simulated a range of α values (2.0 to 4.0). For all α values, we found that skill accumulation is consistently higher in the D_{high} region even though the two regions were contiguous. As an example, when we fixed $\alpha = 3.0$, this difference in mean regional z values, averaged over 100 iterations, was maintained over the entire duration of the simulation (Fig. 2). Figure 3 and movie S1 provide an illustration from a single iteration of the spatial structuring of skill accumulation.

We would also expect heterogeneity in migratory range during the late Pleistocene due to, for example, differing terrains, vegetation, or subsistence strategies (*4*). To investigate whether this could result in spatial structuring of skill accumulation, we populated the simulated world at a constant subpopulation density $D = 0.01$ and partitioned it into two regions with differing M_{SD} values (*31*); $M_{SD,high} = 1.0$ and $M_{SD,low} = 0.1$, allowing migratory activity across the partition. Similarly to the heterogeneous density world, we find that skill accumulation was consistently higher in the well-connected $M_{SD,high}$ region across all α values simulated (2.0 to 4.0). An example, with $D = 0.01$ and $\alpha = 2.9$, is given in fig. S2, with mean regional z values averaged over 100 iterations. Fig. S3 and movie S2 provide a spatial illustration from a single iteration.

From the above results, it is clear that migratory activity among a set of subpopulations can have the same effect on skill accumulation as increasing the size of a single population (*30*). This is because it increases the within-group variance in skill levels, z_i, which feeds the selective directly biased transmission process and offsets the eroding effect of low-fidelity transmission. We therefore sought to quantify the effect of increasing migration activity in terms of the effective number of adult individuals available as transmission models within each subpopulation. To achieve this, we inverted the previous simulation process; for given values of α and D, we simulated widely over N to find the minimum number of adults, N_{min}, needed in each subpopulation for adaptive cumulative evolution to occur (Fig. 4). We repeated this process for the same range of α, but with no migratory process operating, to obtain the minimum number of adults required for skill accumulation in an isolated subpopulation, N_0, for each value of α (Fig. 4) [this is directly equivalent to Henrich's analytical result (*30*) but uses the extended transmission process presented in our study]. We then calculated the effective increase in N due to migratory activity by finding the difference between the N_{min} we expect for given values of α and D, and the N_0 we expect for the same value of α. As can be seen from Fig. 4, not only does increasing migratory activity have the same effect as increasing the size of an isolated population (*30*), but also this effect is greater for higher skill complexities, α.

Our simulation results demonstrate that the influence of demography on cultural transmission

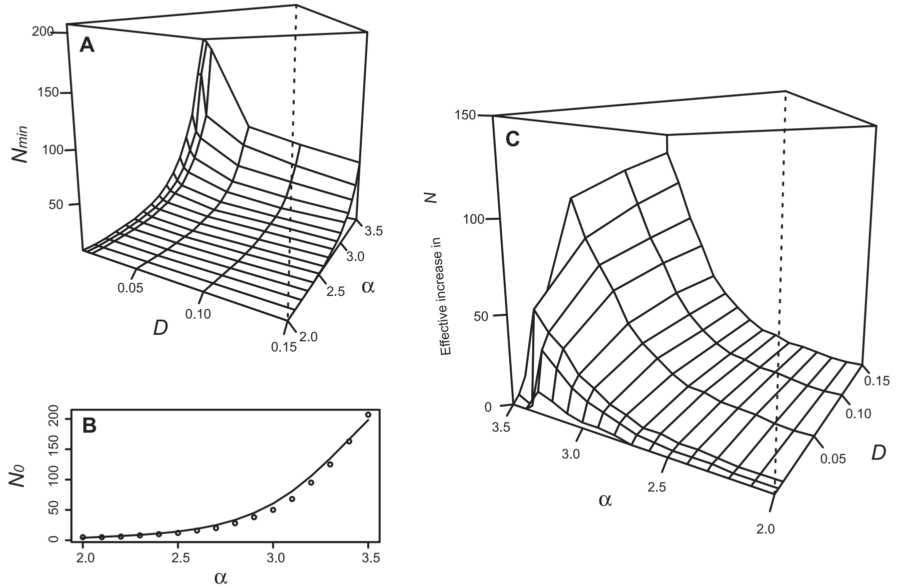

Fig. 4. The effective increase in adult subpopulation size due to migratory activity. (**A**) The minimum number of adults required for adaptive cumulative evolution to occur, N_{min}, for a range of values for subpopulation density D and skill complexity α. (**B**) The minimum number of adults needed in a single isolated population N_0 for the same range of α values. (**C**) The effective increase in adult subpopulation size N due to migratory activity for this range of D and α, calculated by subtracting surface (A) from curve (B) extended along the D axis. The axes of (C) have been rotated for display purposes.

processes provides a mechanism to explain three key features of the emergence of modern behavior in the archaeological record: the early appearance, and subsequent disappearance, of many modern traits in Southern Africa 90 to 70 ka; geographical heterogeneity in the timing of the UP outside Africa; and the delay between the emergence of AMH as a species and the material expression of modern behavioral traits. If, as proposed here, demographic factors are fundamental in shaping the evolution of human behavior, then well-supported estimates of late Pleistocene regional population densities will be crucial to understanding the UP/LSA. Recent estimates of population size changes in the late Pleistocene—based on a Bayesian coalescent inference method with a global data set of coding-region mitochondrial DNA (mtDNA) sequences (*34*)—permit some comparisons of relative effective population densities in different regions of the world and at different times.

By setting the UP transition in Europe at 45 ka (*1*, *2*), we can infer the critical effective population size, and therefore density, necessary for the accumulation of markers of modern behavior. Although this transition is closely associated with the initial colonization by AMH, the rapid rise in skill levels under favorable demographic conditions that we observe in our simulations indicates that cultural intensification would be largely insensitive to the time since first occupation. We assume that the habitable area of Europe would not have included most of Scandinavia, resulting in an estimated area of 8.883 million km^2. The median effective population size estimate in Europe at ~45 ka is 2905 [with 95% highest posterior density interval of 280.4 to 15,933.9], giving an effective population density of $\sim 3.2714 \times 10^{-4} km^{-2}$. The time at which this density would have been reached in sub-Saharan Africa (estimated area ~24.270 million km^2) is ~101 ka. Although this is a relatively crude date estimate, and ignores the importance of the likely large heterogeneity in population densities at the local level, it does correspond well with the first appearance of modern behavioral traits in the region (*9*, *13*). Furthermore, applying this estimation method to the Middle East and North Africa region (estimated area ~13.588 million km^2) gives a date of ~40 ka at which the critical density is reached, relatively consistent with the first evidence of modern behavior in the Levant and northeast Africa (*2*, *7*).

In southern Asia, our predicted time for the UP transition (~52 ka) considerably predates the first archaeological evidence for modern behavior at ~30 ka (*3*). Similarly, the date estimate for northern and central Asia (~40 ka) predates that of the first full UP site found at ~22 ka (*12*). One possible explanation lies in the choice of the regions used in the analysis presented by Atkinson *et al*. (*34*). An important assumption of the ancestral population size estimation method used is that samples are taken from unstructured (i.e., randomly mating) populations. Although multiple loci clustering analysis (*35*, *36*) broadly supports this assumption for most of the other regions, it clearly does not for either the southern Asian or the north and central Asian geographic regions (*34*). Performing Bayesian coalescent inference (*34*) on such structured data sets is likely to have resulted in an overestimation of the effective population size and the time at which population expansion took place. In addition, coalescence date estimates for major mtDNA haplogroups in southern Asia have been interpreted as reflecting an initial phase of population growth somewhat later (*37*). A second possible explanation for this anomalous result is that, although population density may have been sufficiently high for behaviorally modern traits to otherwise accumulate, the migratory range may have been insufficient to allow wide-scale interaction between subpopulations. This may have been the case in southern Asia during the later Pleistocene (*4*).

Although the inferred population densities (*34*) could account for the early appearance of behaviorally modern traits in sub-Saharan Africa and the Middle East—given our demographic model of cultural skill accumulation—they cannot explain the subsequent absence of these features between 70 and ~40 ka because no population size reduction during this period is inferred [see figure 1 in (*34*)]. However, the method of coalescent inference used (Bayesian skyline analysis) may be unable to accurately reconstruct more complex demographic histories when using sequences sampled from a single locus (*38*), so repeated bottlenecks and/or expansions, which would have an important bearing on the accumulation of culturally inherited skills (*17*), may not be recaptured. Paleoclimatic data does indicate worsening conditions during oxygen isotope stage 4 (~75 to 60 ka) (*21*)—possibly leading to population decline, fragmentation, and range contractions—during this period (*20*, *21*). Lahr and Foley (*20*) suggest that continent-wide secondary population bottlenecks may have occurred ~70 ka, and there is some evidence that the sites of the South African Howieson's Poort industries became effectively depopulated by ~60 ka (*15*, *20*).

We would expect a degree of positive feedback on population density after the accumulation of culturally inherited skills; the development of more advanced technologies, and possibly social organization, would likely lead to population growth. Furthermore, we would expect to see more artifactual evidence of behavioral modernity in higher population density contexts through increased deposition. Although the model we have presented does not accommodate these processes or explain the necessary cognitive developments that make possible the invention or improvement of complex behavioral traits, it does provide a demographic mechanism for limiting the degree to which early human populations would have accumulated these culturally inherited skills over time. Our model provides a plausible explanation for the spatial and temporal structuring of the markers of modern behavior in the paleoanthropological record, even if all AMH had the requisite biologically determined cognitive capacities from the time of origin some 160 to 200 ka.

References and Notes

1. P. Mellars, *Evol. Anthropol.* **14**, 12 (2005).
2. O. Bar-Yosef, *Annu. Rev. Anthropol.* **31**, 363 (2002).
3. M. D. Petraglia, in *Rethinking the Human Revolution,* P. Mellars, K. Boyle, O. Bar-Yosef, C. Stringer, Eds. (McDonald Institute for Archaeological Research, Univ. of Cambridge, Cambridge, 2007), pp. 383–394.
4. H. V. A. James, M. D. Petraglia, *Curr. Anthropol.* **46**, (suppl.), 3 (2005).
5. A. Brumm, M. W. Moore, *Camb. Archaeol. J.* **15**, 157 (2005).
6. J. F. O'Connell, J. Allen, in *Rethinking the Human Revolution,* P. Mellars, K. Boyle, O. Bar-Yosef, C. Stringer, Eds. (McDonald Institute for Archaeological Research, Univ. of Cambridge, Cambridge, 2007), pp. 395–410.
7. S. H. Ambrose, *J. Archaeol. Sci.* **25**, 377 (1998).
8. F. d'Errico *et al*., *J. World Prehist.* **17**, 1 (2003).
9. S. McBrearty, A. S. Brooks, *J. Hum. Evol.* **39**, 453 (2000).
10. J. Zilhão, *J. Archaeol. Res.* **15**, 1 (2007).
11. P. J. Brantingham, A. I. Krivoshapkin, L. Jinzeng, Y. Tserendagva, *Curr. Anthropol.* **42**, 735 (2001).
12. P. J. Brantingham, K. W. Kerry, A. I. Krivoshapkin, Y. V. Kuzmin, in *Entering America: Northeast Asia and Beringia Before the Last Glacial Maximum,* D. B. Madsen, Ed. (Univ. of Utah Press, Salt Lake City, UT, 2004), pp. 255–283.
13. C. S. Henshilwood *et al*., *Science* **295**, 1278 (2002).
14. C. W. Marean *et al*., *Nature* **449**, 905 (2007).
15. Z. Jacobs *et al*., *Science* **322**, 733 (2008).
16. I. McDougall, F. H. Brown, J. G. Fleagle, *Nature* **433**, 733 (2005).
17. C. Stringer, in *Rethinking the Human Revolution,* P. Mellars, K. Boyle, O. Bar-Yosef, C. Stringer, Eds. (McDonald Institute for Archaeological Research, Univ. of Cambridge, Cambridge, 2007), pp. 15–20.
18. T. D. White *et al*., *Nature* **423**, 742 (2003).
19. N. Ray, M. Currat, P. Berthier, L. Excoffier, *Genome Res.* **15**, 1161 (2005).
20. M. M. Lahr, R. A. Foley, *Am. J. Phys. Anthropol.* Suppl. **27**, 137 (1998).
21. S. H. Ambrose, *J. Hum. Evol.* **34**, 623 (1998).
22. R. G. Klein, *Evol. Anthropol.* **9**, 17 (2000).
23. N. Chomsky, *Linguistic Enquiry* **36**, 1 (2005).
24. S. J. Mithen, *The Prehistory of the Mind: A Search for the Origins of Art, Religion, and Science* (Thames & Hudson, London, 1996).
25. M. C. Stiner, S. L. Kuhn, *Hum. Ecol.* **34**, 693 (2006).
26. M. Vanhaeren, in *From Tools to Symbols from Early Hominids to Humans,* F. d'Errico, L. Blackwell, Eds. (Wits Univ. Press, Johannesburg, 2005), pp. 525–553.
27. J. Bolender, *Biol. Philos.* **22**, 383 (2007).
28. D. Everett, *Curr. Anthropol.* **46**, 621 (2005).
29. S. J. Shennan, *Camb. Archaeol. J.* **11**, 5 (2001).
30. J. Henrich, *Am. Antiq.* **69**, 197 (2004).
31. Materials and methods are available as supporting material on *Science* Online.
32. D. Read, *Am. Antiq.* **71**, 164 (2006).
33. J. Henrich, *Am. Antiq.* **71**, 771 (2006).
34. Q. D. Atkinson, R. D. Gray, A. J. Drummond, *Mol. Biol. Evol.* **25**, 468 (2008).
35. N. A. Rosenberg *et al*., *Science* **298**, 2381 (2002).
36. J. Z. Li *et al*., *Science* **319**, 1100 (2008).
37. C. Sun *et al*., *Mol. Biol. Evol.* **23**, 683 (2006).
38. A. J. Drummond, "Reconstructing evolutionary bottlenecks using the coalescent," http://bioinf.cs.auckland.ac.nz/index.php/2008/03/02/the-coalescent-for-bottlenecks (2008).

39. We thank J. Henrich, P. Richerson, K. Laland, A. Bentley, T. Kivisild, T. Sumner, F. d'Errico, and C. Stringer for discussion, and Q. Atkinson for making data available. This work was supported by an AHRC Centre for the Evolution of Cultural Diversity studentship awarded to A.P. and a Wissenschaftskolleg zu Berlin fellowship awarded to M.G.T.

Supporting Online Material

www.sciencemag.org/cgi/content/full/324/5932/1298/DC1
Materials and Methods
Figs. S1 to S3
Movies S1 and S2
References

23 December 2008; accepted 21 April 2009
10.1126/science.1170165

Pd-Pt Bimetallic Nanodendrites with High Activity for Oxygen Reduction

Byungkwon Lim,[1] Majiong Jiang,[2] Pedro H. C. Camargo,[1] Eun Chul Cho,[1] Jing Tao,[3] Xianmao Lu,[1] Yimei Zhu,[3] Younan Xia[1]*

Controlling the morphology of Pt nanostructures can provide a great opportunity to improve their catalytic properties and increase their activity on a mass basis. We synthesized Pd-Pt bimetallic nanodendrites consisting of a dense array of Pt branches on a Pd core by reducing K_2PtCl_4 with L-ascorbic acid in the presence of uniform Pd nanocrystal seeds in an aqueous solution. The Pt branches supported on faceted Pd nanocrystals exhibited relatively large surface areas and particularly active facets toward the oxygen reduction reaction (ORR), the rate-determining step in a proton-exchange membrane fuel cell. The Pd-Pt nanodendrites were two and a half times more active on the basis of equivalent Pt mass for the ORR than the state-of-the-art Pt/C catalyst and five times more active than the first-generation supportless Pt-black catalyst.

Platinum (Pt) is the most effective catalyst to facilitate both hydrogen oxidation and oxygen reduction in a proton-exchange membrane (PEM) fuel cell (*1*–*4*), but several critical issues still need to be addressed before such cells can be commercialized for automotive applications: For example, the oxygen reduction reaction (ORR) is kinetically limited at the cathode (*5*–*8*), and the scale of the Pt crystallites leads to high costs for Pt-based electrocatalysts with sufficient surface area and activity (*9*). In order to overcome these barriers, it is necessary to maximize the activity of a Pt-based catalyst by engineering its morphology and/or composition.

During the last decade, a number of strategies have been proposed for improving the performance of an electrocatalyst for the ORR that involved alloying Pt with other transition metals at high temperatures (800 to 1000°C) (*10*, *11*) or depositing a monolayer of Pt electrochemically onto fine particles of other metals immobilized on an electrode (*12*). Although these bimetallic catalysts have shown great improvements in activity, the lack of procedures for controlled large-scale synthesis has limited their use in commercial devices. In addition, the structural complexities of these systems have also made it difficult to decipher underlying mechanisms. For these reasons, the most commonly used electrocatalysts for the ORR are still based on fine particles of Pt supported on porous carbon materials (Pt/C). The catalytic activity of Pt nanoparticles can be drastically enhanced by maximizing the expression of certain facets that are intrinsically more active toward a specific reaction (*13*–*16*). However, it is rather difficult to synthesize Pt nanoparticles that combine both high surface area and the desired highly active facets on their surfaces because Pt nanoparticles of <5 nm in size tend to exist as truncated octahedrons covered by a mix of {100} and {111} facets in an effort to minimize the total interfacial free energy (*16*, *17*).

Most recently, seeded growth has emerged for precisely controlling the morphology and composition of metallic nanostructures that are prepared using solution-phase methods (*18*–*20*). This technique has also enabled the preparation of bimetallic nanostructures with an unconventional morphology that cannot be achieved otherwise (*20*). Here we describe a facile, aqueous-phase route to synthesize bimetallic nanodendrites consisting of a dense array of Pt branches on a core of palladium (Pd) nanocrystal (NC). In this approach, truncated octahedral NCs of Pd with an average size of 9 nm were used as seeds so as to direct the dendritic growth of Pt upon the reduction of K_2PtCl_4 by L-ascorbic acid in an aqueous solution. Using this simple approach, we routinely produced Pd-Pt bimetallic nanodendrites with high surface areas and the particularly active facets for the ORR in high yields. These Pd-Pt nanodendrites displayed substantially enhanced ORR activity as compared with

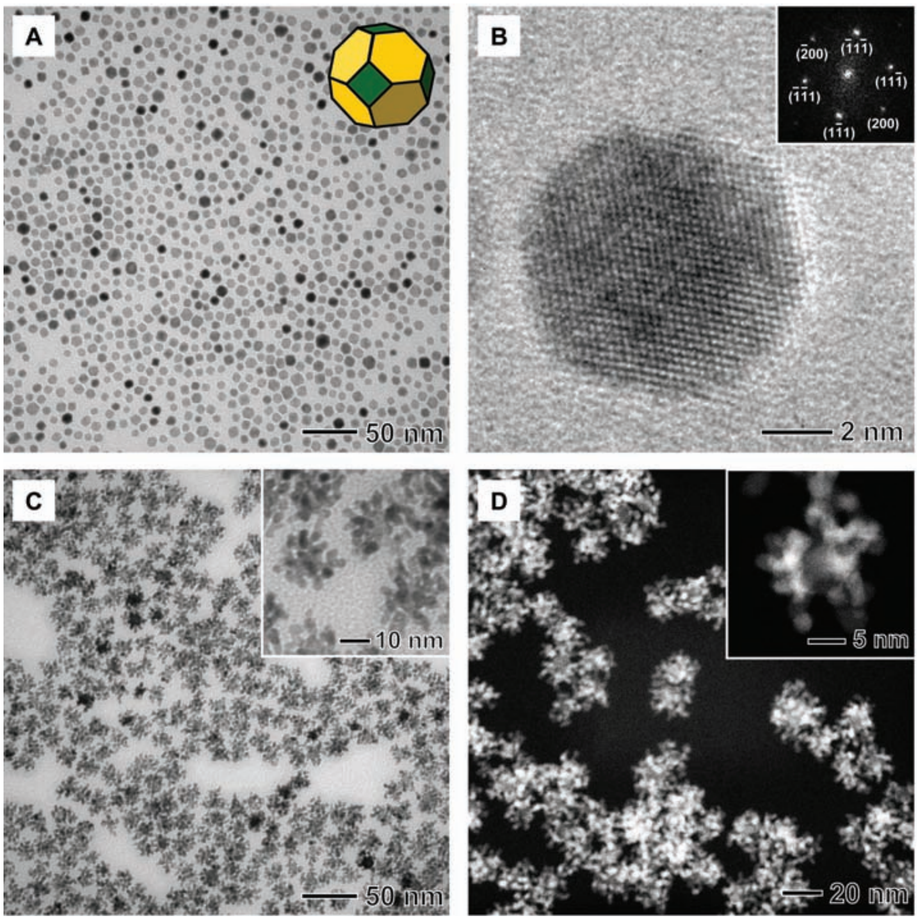

Fig. 1. (**A**) TEM image of truncated octahedral Pd NCs synthesized by reducing Na_2PdCl_4 with L-ascorbic acid in an aqueous solution. The inset shows a geometrical model of the truncated octahedron, where the green and yellow colors denote the {100} and {111} facets, respectively. (**B**) HRTEM image of a single truncated octahedron of Pd recorded along the [011] zone axis and the corresponding FT pattern (inset). (**C**) TEM image of Pd-Pt nanodendrites synthesized by reducing K_2PtCl_4 with L-ascorbic acid in the presence of truncated octahedral Pd NC seeds in an aqueous solution. (**D**) HAADF-STEM image of Pd-Pt nanodendrites.

[1]Department of Biomedical Engineering, Washington University, St. Louis, MO 63130, USA. [2]Department of Chemistry, Washington University, St. Louis, MO 63130, USA. [3]Condensed Matter Physics and Materials Science Department, Brookhaven National Laboratory, Upton, NY 11973, USA.

*To whom correspondence should be addressed. E-mail: xia@biomed.wustl.edu

that of commercial Pt/C and Pt-black catalysts. This synthesis also provides a convenient and environmentally benign route to large-scale production because it does not require high temperature, organic solvent, or electrochemical deposition.

In the first step, we synthesized uniform, truncated octahedral NCs of Pd by reducing Na_2PdCl_4 with L-ascorbic acid in an aqueous solution (*21*). A transmission electron microscopy (TEM) image of the as-prepared Pd NCs is shown in Fig. 1A. The NCs were nearly 100% in truncated octahedral shape and had an average size of 9.1 nm (fig. S1) (*21*). A high-resolution TEM (HRTEM) image of a single Pd NC and the corresponding Fourier-transform (FT) pattern indicate that it was indeed a piece of single crystal with its surface being enclosed by both {111} and {100} facets (Fig. 1B). The fringe orientation in the HRTEM image also confirms its shape as a truncated octahedron encased by eight {111} and six {100} facets (fig. S2) (*21*).

These Pd NCs were then used as seeds for the formation of Pd-Pt bimetallic nanodendrites (*21*). A typical TEM image of the product revealed that a number of Pt branches had grown from a Pd core into dendritic tendrils, although single-arm branching was also observed (Fig. 1C). The Pd-Pt nanodendrites had an average size of 23.5 nm (fig. S3) (*21*). The energy-dispersive x-ray spectroscopy (EDS) line scanning analysis showed the bimetallic nanostructure consisting of a core rich in Pd and many arms rich in Pt (fig. S4) (*21*). The high-angle annular dark-field scanning TEM (HAADF-STEM) image in Fig. 1D shows the intense contrast between the core and the surrounding branches of a nanodendrite, demonstrating a three-dimensional dendritic morphology. Both TEM and STEM analyses confirmed the absence of isolated Pt nanoparticles in the product. The overall weight percentage of Pt in the Pd-Pt nanodendrites was 85% as determined by inductively coupled plasma mass spectrometry (ICP-MS) measurements.

We further characterized the Pd-Pt nanodendrites by means of HRTEM. Figure 2A gives an HRTEM image of a single Pd-Pt nanodendrite, which clearly shows overgrowth of Pt branches at multiple sites on the Pd seed. The nucleation sites for Pt appear to be distributed over the entire surface of the truncated octahedral Pd seed and do not overlap extensively. For the Pt branches, the average diameter was ~3 nm. The HRTEM image in Fig. 2B reveals the continuous lattice fringes from the Pd core to the Pt branches, indicating that the Pt branches were grown epitaxially on the Pd seed [Pd and Pt have a lattice mismatch of only 0.77% (*20*)]. HRTEM images of individual Pt branches (Fig. 2, C to F) show their single crystalline structure with a highly ordered continuous fringe pattern, and most of the exposed facets were found to be {111}, although some {110} and high-index {311} facets could also be identified in addition to a small fraction of {100}. The identical FT patterns associated with the same crystal orientations (Fig. 2, insets) are also indicative of the

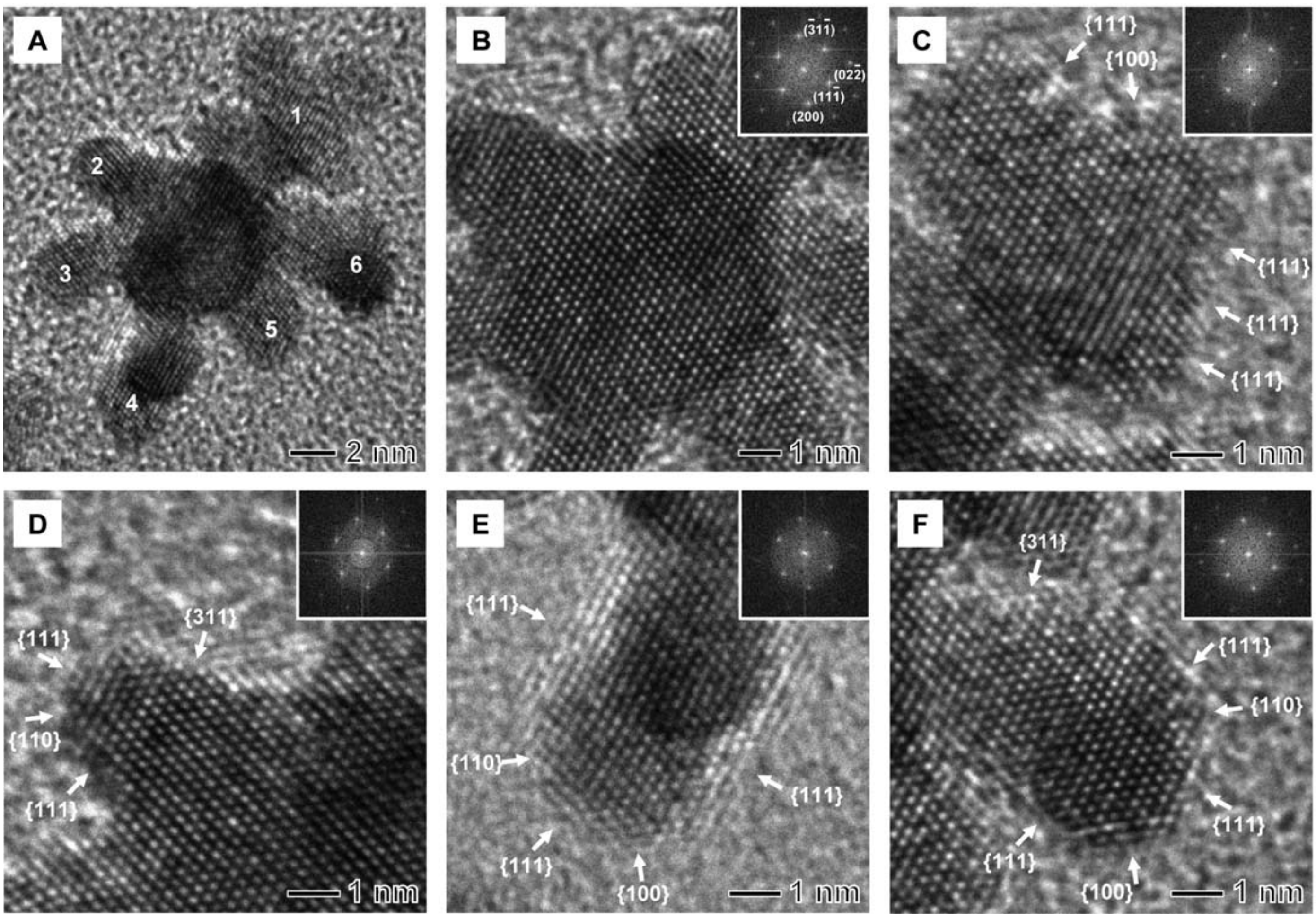

Fig. 2. (**A**) HRTEM image of a single Pd-Pt nanodendrite. (**B**) HRTEM image recorded from the center of the Pd-Pt nanodendrite shown in (A). The image clearly shows the continuous lattice fringes from the Pd core to the Pt branches, demonstrating the epitaxial relation between Pd and Pt. (**C** to **F**) HRTEM images recorded from Pt branches 1, 2, 4, and 6 marked in (A), respectively. The images reveal that most of the exposed facets on the Pt branches were {111} planes. Some {110} and high-index {311} facets can also be identified in addition to a small fraction of {100} facets. The identical FT patterns shown in the insets indicate that the Pt branches have the same lattice orientation as the Pd core regardless of their different growth directions.

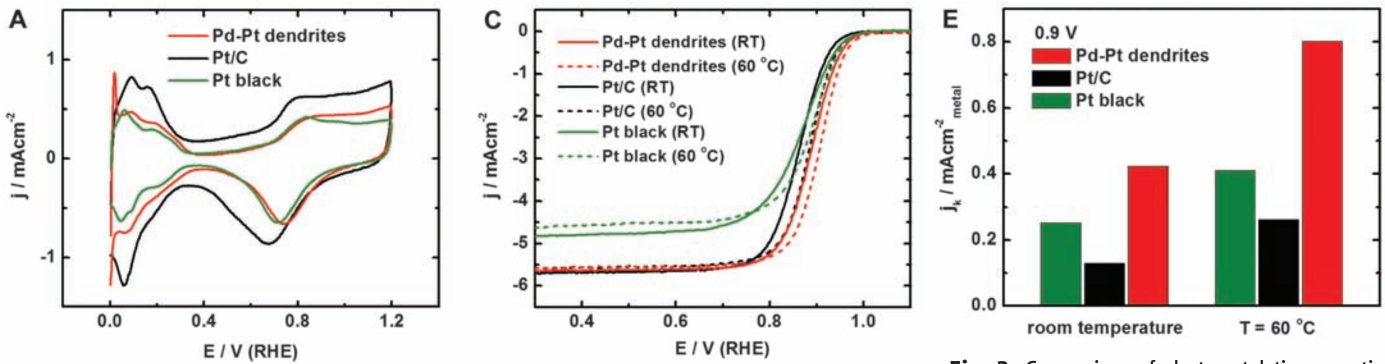

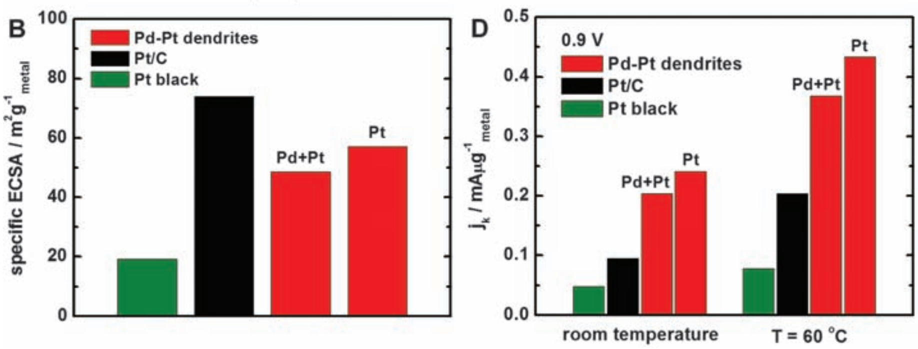

Fig. 3. Comparison of electrocatalytic properties of the Pd-Pt nanodendrites, Pt/C catalyst (E-TEK) (20% by weight of 3.2-nm Pt nanoparticles on carbon support), and Pt black (Aldrich) (fuel cell grade). (**A**) CV curves recorded at room temperature in an Ar-purged 0.1 M $HClO_4$ solution with a sweep rate of 50 mV/s. (**B**) Specific ECSAs for the Pd-Pt nanodendrites, Pt/C catalyst, and Pt black. (**C**) ORR polarization curves for the Pd-Pt nanodendrites, Pt/C catalyst, and Pt black recorded at room temperature and 60°C in an O_2-saturated 0.1 M $HClO_4$ solution with a sweep rate of 10 mV/s and a rotation rate of 1600 rpm. (**D**) Mass activity and (**E**) specific activity at 0.9 V versus RHE for these three catalysts. Mass and specific activities are given as kinetic current densities (j_k) normalized in reference to the loading amount and ECSA of metal, respectively. For the Pd-Pt nanodendrites or Pt/C catalyst, the metal loading on a RDE was 15.3 μg/cm^2, whereas the metal loading was 40.8 μg/cm^2 for the Pt black. In (A) and (C), current densities were normalized in reference to the geometric area of a RDE (0.196 cm^2).

epitaxial relation between the Pd core and the Pt branches. The epitaxial overgrowth of single-crystal Pt branches suggests that they were formed via direct nucleation on the Pd NC seed rather than random aggregation of Pt nuclei that might be formed through homogeneous nucleation in the solution.

The observed dendritic growth of Pt branches can probably be attributed to the high rate of Pt reduction as mediated by an autocatalytic process (*22*), which has been used to account for the formation of porous and other branched nanostructures of Pt (*23–26*). In the present system, once Pt has nucleated on the surface of a Pd NC upon reduction by L-ascorbic acid, the Pt nuclei can serve as catalytic sites for further reduction of the Pt precursor and create favorable sites for atomic addition. Growth occurs preferentially on the Pt nuclei, and deposition proceeds along the developing Pt branches, rather than conformally on the Pd seed. We also observed branching via autocatalytic reduction of the Pt precursor in the absence of Pd seeds. In this case, however, the final product was dominated by a spherical, foamlike morphology with overall sizes of 20 to 35 nm (fig. S5) (*21*). This morphology might be caused by extensive overlap and possible fusion between adjacent branches during the growth process. The truncated octahedral Pd seeds provide multiple nucleation sites for Pt that are spatially separated from each other in order to avoid overlap and fusion and allow the formation of Pt branches with an open dendritic structure.

We benchmarked the electrocatalytic properties of the Pd-Pt nanodendrites toward the ORR against both commercial Pt/C catalyst (E-TEK, Somerset, NJ) (20% by wt. of 3.2-nm Pt nanoparticles on Vulcan XC-72 carbon support) and Pt black (Aldrich, St. Louis, MO) (fuel cell grade). Figure 3A shows cyclic voltammetry (CV) curves of these three catalysts recorded at room temperature in Ar-purged 0.1 M $HClO_4$ solutions at a sweep rate of 50 mV/s. The CV curves exhibited two distinctive potential regions associated with H_{upd} adsorption/desorption processes ($H^+ + e^- = H_{upd}$) between $0 < E < 0.37$ V and the formation of a OH_{ad} layer ($2H_2O = OH_{ad} + H_3O^+ + e^-$) beyond ~0.6 V, where H_{upd} and OH_{ad} refer to the underpotentially deposited hydrogen and the adsorbed hydroxyl species, respectively. The electrochemically active surface area (ECSA) was calculated by measuring the charge collected in the H_{upd} adsorption/desorption region after double-layer correction and assuming a value of 210 μC/cm^2 for the adsorption of a hydrogen monolayer (*21*, *27*). The specific ECSA (the ECSA per unit weight of metal) of the Pd-Pt nanodendrites (48.5 m^2/g$_{Pd+Pt}$) was found to be 66% of the Pt/C catalyst (74.0 m^2/g$_{Pt}$) (Fig. 3B). Based on the Pt mass, the specific ECSA of the Pd-Pt nanodendrites (57.1 m^2/g$_{Pt}$) was 77% of the Pt/C catalyst. In contrast, the Pt black exhibited a small specific ECSA (19.1 m^2/g$_{Pt}$) mainly because of extensive agglomeration in the sample (fig. S6) (*21*). The highly branched structure of our Pd-Pt nanodendrites provides a reasonably high surface area despite their relatively large overall particle size.

The ORR measurements were performed in O_2-saturated 0.1 M $HClO_4$ solutions by using a glassy carbon rotating disk electrode (RDE) at both room temperature and 60°C. For the Pd-Pt nanodendrites and Pt/C catalyst, the metal loading on a RDE was 15.3 μg/cm^2, whereas the loading was increased to 40.8 μg/cm^2 for the Pt black so as to avoid a substantial drop of the diffusion-limiting currents that occurs at relatively low loadings for low-specific-surface-area catalysts (fig. S7) (*21*, *28*). Polarization curves for the ORR on these three catalysts are shown in Fig. 3C. For all of these catalysts, the diffusion-limiting currents were obtained in the potential region below 0.6 V, whereas a mixed kinetic-diffusion control region occurs between 0.7 and 1.0 V. The kinetic current was calculated from the ORR polarization curve by using mass-transport correction and normalized to the loading amount of metal in order to compare the mass activity of different catalysts (*21*). At room temperature, the Pd-Pt nanodendrites exhibited a mass activity of 0.204 mA/μg$_{Pd+Pt}$ on the basis of the total mass of Pd and Pt at 0.9 V versus a reversible hydrogen electrode (RHE), which was 2.1 and 4.3 times greater than that of the Pt/C

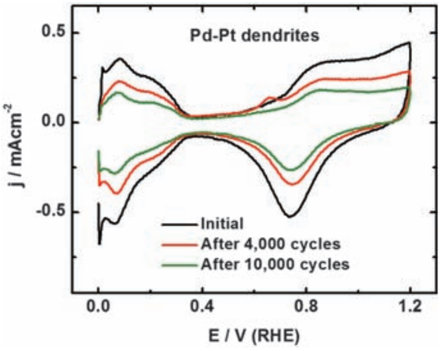

Fig. 4. CV curves for the Pd-Pt nanodendrites before and after accelerated durability test. The durability test was carried out for the same sample at room temperature in an O_2-saturated 0.1 M $HClO_4$ solution with the cyclic potential sweeping between 0.6 and 1.1 V at a sweep rate of 50 mV/s. The metal loading on a RDE was 15.3 μg/cm^2 and current densities were normalized in reference to the geometric area of a RDE (0.196 cm^2).

catalyst (0.095 mA/μg$_{Pt}$) and the Pt black (0.048 mA/μg$_{Pt}$), respectively (Fig. 3D, left). If the Pt mass was solely taken into account, the mass activity of the Pd-Pt nanodendrites (0.241 mA/μg$_{Pt}$) was 2.5 times that of the state-of-the-art Pt/C catalyst for PEM fuel cells and 5.0 times that of the first-generation supportless Pt-black catalyst. At 60°C, the Pt mass activity of the Pd-Pt nanodendrites (0.433 mA/μg$_{Pt}$) was still greater than that of the Pt/C catalyst (0.204 mA/μg$_{Pt}$) and the Pt black (0.078 mA/μg$_{Pt}$) (Fig. 3D, right) and almost meets the performance targets for ORR fuel cell catalysts (0.44 mA/μg$_{Pt}$ at 0.9 V versus RHE and 80°C) set by the U.S. Department of Energy (DOE) (*9*). In this study, the measured activities of the commercial Pt catalysts are in good agreement with the reported or predicted values in literature (*9*).

For a better understanding of the observed difference in ORR activity, we normalized the kinetic current against the ECSA of each catalyst. The Pd-Pt nanodendrites had a specific activity (i.e., kinetic current per unit surface area of catalyst) of 3.1 to 3.4 times that of the Pt/C catalyst and 1.7 to 2.0 times that of the Pt black depending on the temperature (Fig. 3E and table S1) (*21*), demonstrating the accelerated ORR kinetics on the surfaces of the Pd-Pt nanodendrites. The ORR activity on low-index crystallographic facets of Pt in a nonadsorbing electrolyte such as perchloric acid is known to increase on the order of Pt(100) << Pt(111) < Pt(110), with the difference in activity between Pt(111) and Pt(110) being minor (*7*, *29*, *30*). This difference in ORR activity most likely arises from the structure-sensitive inhibiting effect of OH_{ad} species on Pt(*hkl*), which blocks the active site for O_2 adsorption and thus retards the ORR kinetics. In addition, the high-index stepped Pt surfaces have exhibited slightly greater ORR activities than the low-index planes in acidic solutions (*31*), which could be attributed to the favorable adsorption of O_2 molecules on the stepped surfaces (*32*, *33*). The higher specific activity of the Pd-Pt nanodendrites might be related to the preferential exposure of {111} facets along with some {110} and high-index {311} facets on the Pt branches as compared with those of small Pt nanoparticles on Pt/C catalyst, which usually take the shape of a truncated octahedron and are thus enclosed by a mix of {100} and {111} facets (fig. S8) (*21*). As expected, the Pt black samples showed an irregular morphology with poorly defined facets. We can conclude that the observed high activity based on Pt mass for the Pd-Pt nanodendrites results from the reasonably high surface area intrinsic to the dendritic morphology and the exposure of particularly active facets toward the ORR on the Pt branches.

We also performed accelerated durability tests by applying linear potential sweeps between 0.6 and 1.1 V at 50 mV/s in O_2-saturated 0.1 M $HClO_4$ solutions at room temperature. After 4000 cycles, the CV measurements showed a loss of 30% in ECSA for the Pd-Pt nanodendrites, 36% for the Pt/C catalyst, and 33% for the Pt black (Fig. 4 and fig. S9) (*21*), suggesting that the Pd-Pt nanodendrites had durability slightly better than the Pt/C catalyst and the Pt black. After 10,000 cycles, the Pd-Pt nanodendrites showed a loss of 50% in ECSA. It might be possible to improve the durability of the Pd-Pt nanodendrites for the ORR by incorporating Au. Zhang *et al.* have recently demonstrated the stabilization of Pt ORR catalysts against Pt dissolution by modifying them with Au clusters, which were deposited onto the carbon-supported Pt nanoparticles through a galvanic replacement reaction (*34*). Their Au/Pt/C catalyst showed a negligible loss of 4% in ECSA after 30,000 cycles of the durability test. Additionally, enhancement of the ORR activity is expected through the optimization of both composition and dimension of the Pd-Pt nanodendrites by varying the ratio of Pt precursor to Pd seeds involved in a synthesis. By taking advantage of this controllable solution-phase synthesis, our approach provides a promising route to the development of next-generation catalysts with substantial reduction in Pt loading while retaining high ORR activity. The Pd-Pt bimetallic nanodendrites may also find use as catalysts beyond fuel cell applications.

References and Notes

1. T. E. Mallouk, *Nature* **343**, 515 (1990).
2. B. C. H. Steele, A. Heinzel, *Nature* **414**, 345 (2001).
3. M. L. Perry, T. F. Fuller, *J. Electrochem. Soc.* **149**, S59 (2002).
4. W. Vielstich, A. Lamm, H. A. Gasteiger, *Handbook of Fuel Cells: Fundamentals, Technology, and Applications* (Wiley, West Sussex, UK, ed. 1, 2003).
5. E. Yeager, *Electrochim. Acta* **29**, 1527 (1984).
6. N. M. Marković, T. J. Schmidt, V. Stamenković, P. N. Ross, *Fuel Cells (Weinh.)* **1**, 105 (2001).
7. N. M. Marković, P. N. Ross, *Surf. Sci. Rep.* **45**, 117 (2002).
8. W. Chen, J. Kim, S. Sun, S. Chen, *J. Phys. Chem. C* **112**, 3891 (2008).
9. H. A. Gasteiger, S. S. Kocha, B. Sompalli, F. T. Wagner, *Appl. Catal. B* **56**, 9 (2005).
10. S. Mukerjee, S. Srinivasan, *J. Electroanal. Chem.* **357**, 201 (1993).
11. S. Mukerjee, S. Srinivasan, M. P. Soriaga, J. McBreen, *J. Electrochem. Soc.* **142**, 1409 (1995).
12. R. R. Adzic *et al.*, *Top. Catal.* **46**, 249 (2007).
13. R. Narayanan, M. A. El-Sayed, *Nano Lett.* **4**, 1343 (2004).
14. N. Tian, Z.-Y. Zhou, S.-G. Sun, Y. Ding, Z. L. Wang, *Science* **316**, 732 (2007).
15. K. M. Bratlie, H. Lee, K. Komvopoulos, P. Yang, G. A. Somorjai, *Nano Lett.* **7**, 3097 (2007).
16. C. Wang, H. Daimon, T. Onodera, T. Koda, S. Sun, *Angew. Chem. Int. Ed.* **47**, 3588 (2008).
17. H. Song, F. Kim, S. Connor, G. A. Somorjai, P. Yang, *J. Phys. Chem. B* **109**, 188 (2005).
18. S. E. Habas, H. Lee, V. Radmilovic, G. A. Somorjai, P. Yang, *Nat. Mater.* **6**, 692 (2007).
19. H. Lee, S. E. Habas, G. A. Somorjai, P. Yang, *J. Am. Chem. Soc.* **130**, 5406 (2008).
20. B. Lim *et al.*, *Nano Lett.* **8**, 2535 (2008).
21. Materials and methods are available as supporting material on *Science* Online.
22. L. C. Ciacchi, W. Pompe, A. D. Vita, *J. Phys. Chem. B* **107**, 1755 (2003).
23. Y. Song *et al.*, *J. Am. Chem. Soc.* **126**, 635 (2004).
24. J. Chen, T. Herricks, Y. Xia, *Angew. Chem. Int. Ed.* **44**, 2589 (2005).
25. X. Teng, X. Liang, S. Maksimuk, H. Yang, *Small* **2**, 249 (2006).
26. B. Lim *et al.*, *Nano Lett.* **8**, 4043 (2008).
27. T. J. Schmidt *et al.*, *J. Electrochem. Soc.* **145**, 2354 (1998).
28. K. J. J. Mayrhofer *et al.*, *Electrochim. Acta* **53**, 3181 (2008).
29. N. Markovic, H. Gasteiger, P. N. Ross, *J. Electrochem. Soc.* **144**, 1591 (1997).
30. V. R. Stamenkovic *et al.*, *Science* **315**, 493 (2007).
31. A. Kuzume, E. Herrero, J. M. Feliu, *J. Electroanal. Chem.* **599**, 333 (2007).
32. D. W. Blakely, G. A. Somorjai, *Surf. Sci.* **65**, 419 (1977).
33. N. M. Marković, R. R. Adžić, B. D. Cahan, E. B. Yeager, *J. Electroanal. Chem.* **377**, 249 (1994).
34. J. Zhang, K. Sasaki, E. Sutter, R. R. Adzic, *Science* **315**, 220 (2007).

35. This work was supported by startup funds from Washington University in St. Louis. B.L. was also partially supported by postdoctoral fellowships from the Korea Research Foundation funded by the Korean Government (KRF-2006-352-D00067). P.H.C.C. was also supported in part by the Fulbright Program and the Brazilian Ministry of Education (Coordenação de Aperfeiçoamento de Pessoal de Nível Superior). E.C.C. was also partially supported by postdoctoral fellowships from the Korea Research Foundation funded by the Korean Government (KRF-2007-357-D00070). J.T. and Y.Z. were supported by the U.S. DOE/Basic Energy Sciences (DEAC02-98CH10886). We thank H. Yang for technical assistance with the electrochemical measurements.

Supporting Online Material

www.sciencemag.org/cgi/content/full/1170377/DC1
Materials and Methods
Figs. S1 to S9
Table S1

30 December 2008; accepted 9 April 2009
Published online 14 May 2009;
10.1126/science.1170377
Include this information when citing this paper.

Natural Quasicrystals

Luca Bindi,[1] Paul J. Steinhardt,[2]* Nan Yao,[3] Peter J. Lu[4]

Quasicrystals are solids whose atomic arrangements have symmetries that are forbidden for periodic crystals, including configurations with fivefold symmetry. All examples identified to date have been synthesized in the laboratory under controlled conditions. Here we present evidence of a naturally occurring icosahedral quasicrystal that includes six distinct fivefold symmetry axes. The mineral, an alloy of aluminum, copper, and iron, occurs as micrometer-sized grains associated with crystalline khatyrkite and cupalite in samples reported to have come from the Koryak Mountains in Russia. The results suggest that quasicrystals can form and remain stable under geologic conditions, although there remain open questions as to how this mineral formed naturally.

Solids, including naturally forming minerals, are classified according to the order and rotational symmetry of their atomic arrangements. Glasses and amorphous solids have disordered arrangements with no exact rotational symmetry. Crystals have atomic structures with long-range periodic order that can be described by a single atom or atomic cluster that repeats at regular intervals. According to the well-known theorems of crystallography derived nearly two centuries ago, the rotational symmetries of crystals are highly restricted: Two-, three-, four-, and sixfold symmetry axes are allowed, but five-, seven-, and all higher-fold symmetry axes are forbidden. Quasicrystals (*1*, *2*) (short for quasiperiodic crystals) have a more subtle kind of long-range order. In a quasiperiodic structure, the atomic positions along each symmetry axis are described by a sum of two or more periodic functions whose wavelengths have an irrational ratio (inexpressible as a ratio of integers). This difference exempts quasicrystals from the crystallographic restrictions: They can exhibit all the rotational symmetries forbidden to crystals, including fivefold symmetry. Just as square or hexagonal tilings are commonly used as geometric analogs for periodic crystals, the Penrose tiling (*3*) is used as an analog for quasicrystals. The fivefold symmetric tiling consists of acute and obtuse rhombic tiles that repeat along each symmetry direction with frequencies whose quotient is $\tau = \frac{1+\sqrt{5}}{2} = 1.618$, the golden ratio.

The concept of quasicrystals was introduced 25 years ago (*1*), and the first example observed was a rapidly quenched alloy of Al and Mn with icosahedral symmetry (*2*). Since then, over 100 examples have been identified (*4*), but all have been synthetic alloys produced in the laboratory under controlled conditions, ranging from fast to moderately slow quenching (*5*). A substantial number have icosahedral symmetry, but other crystallographically forbidden symmetries have been observed as well (*1*, *4*). Among the most carefully studied is the icosahedral phase of AlCuFe (i-AlCuFe), reported by Tsai *et al*. (*6*) and subsequently examined over a range of stoichiometries, temperatures, and quench conditions (*5*). The optimal composition, $Al_{63}Cu_{24}Fe_{13}$, is known to be stable over the temperature range from 500° to 870°C at atmospheric pressure, but its stability under wider ranges of temperature and pressure has not been fully explored.

To search for quasicrystals beyond the chemical families in which they are already known to occur, a scheme to identify quasicrystals based on powder diffraction data was developed and applied (*7*) to a collection of over 80,000 patterns published as the "powder diffraction file" by the International Center for Diffraction Data (ICDD-PDF). The ICDD-PDF includes some 9000 mineral patterns in addition to synthetic phases. Figures of merit were identified to rank the observed powder patterns according to how they compared with those of ideal quasicrystals. Known quasicrystals in the ICDD-PDF were successfully identified by this procedure. Among other materials, samples of the 50 most highly ranked were obtained and explored with transmission electron microscopy (TEM) and powder x-ray diffraction (XRD), but no new quasicrystals, synthetic or natural, were found (*7*). As a result, the search turned to possibilities outside the existing catalog, beginning with minerals with compositions similar to those of known quasicrystals synthesized in the laboratory.

Many synthetic quasicrystals are metallic alloys, often including Al, which led to the consideration of the mineral khatyrkite, with a nominal composition of $(Cu,Zn)Al_2$. Khatyrkite (*8*, *9*) was originally found in a metal placer, reported as coming from a Triassic (200 million years old) ultramafic (silicon-poor) zone (*10*) of the Koryak Mountains, northeast of the Kamchatka Peninsula in Russia. Cupalite, nominally (Cu,Zn)Al, is reported to form in close association with khatyrkite and is orthorhombic (*8*, *9*). The only reported samples of khatyrkite were described as roughly 30-μm grains found in association with weathered serpentinite and located near the Listvenitovyi Stream in the Chetkinvaiam tectonic melange (*9*, *10*).

We examined a khatyrkite-bearing sample from the collection of the Museo di Storia Naturale of the Università degli Studi di Firenze (catalog number 46407/G) that was acquired in 1990 and cataloged as coming from the Koryak region, although we have no direct evidence that our sample originated from the same location as the type specimen. Instead of a metal placer, the sample includes an assemblage (Fig. 1A) of spinel, augite, and forsteritic olivine. We made polished thin sections and examined the microstructure using backscattered electron (BSE) imaging in the scanning electron microscope (*11*). To quantify the stoichiometry of these phases, we examined samples using wavelength-dispersive x-ray analysis in an electron microprobe (*12*).

The study revealed a number of Al-rich grains consistent with khatyrkite and cupalite, though with only traces of Zn as compared with the reported composition (*8*, *9*). These grains were intergrown with forsteritic olivine (Fig. 2A) and an unknown mineral, AlCuFe, corresponding to the β phase (*5*) in the synthetic Al-Cu-Fe alloy (Fig. 2B). The complex assemblage of mineral phases shown in Figs. 1 and 2 provides evidence

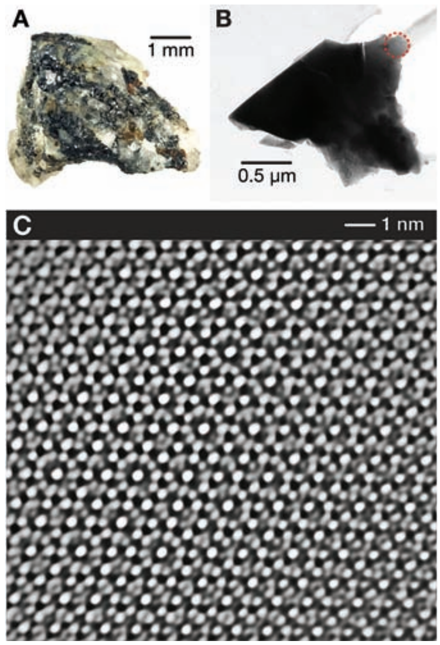

Fig. 1. (**A**) The original khatyrkite-bearing sample used in the study. The lighter-colored material on the exterior contains a mixture of spinel, augite, and olivine. The dark material consists predominantly of khatyrkite ($CuAl_2$) and cupalite (CuAl) but also includes granules, like the one in (**B**), with composition $Al_{63}Cu_{24}Fe_{13}$. The diffraction patterns in Fig. 4 were obtained from the thin region of this granule indicated by the red dashed circle, an area 0.1 μm across. (**C**) The inverted Fourier transform of the HRTEM image taken from a subregion about 15 nm across displays a homogeneous, quasiperiodically ordered, fivefold symmetric, real space pattern characteristic of quasicrystals.

[1]Museo di Storia Naturale, Sezione di Mineralogia, Università degli Studi di Firenze, Firenze I-50121, Italy. [2]Princeton Center for Theoretical Science, and Joseph Henry Laboratories, Department of Physics, Princeton University, Princeton, NJ 08544, USA. [3]Princeton Institute for the Science and Technology of Materials, Princeton University, Princeton, NJ 08544, USA. [4]Department of Physics and School of Engineering and Applied Sciences, Harvard University, Cambridge, MA 02138, USA.

*To whom correspondence should be addressed. E-mail: steinh@princeton.edu

Table 1. Best fit of the powder XRD pattern from the mineral sample to an ideal FCI quasicrystal, using the automated scheme in (*7*). The first two columns show the magnitude of the scattering vector $|\mathbf{Q}|$ for the real and ideal patterns, and column three shows the difference between these two values. The fourth column is the relative intensity (100 is the most intense). The fifth column is the best-fit index assignment (integer linear combinations of the six vectors $\{\mathbf{g}_k, \mathbf{g}_5\}$), and the last column is an equivalent two-integer index introduced by Janot (*4*) (eqs. 3.20 to 3.26) and used in Fig. 3A, in which $\mathbf{Q} = \frac{\sqrt{N+\tau M}}{d}$ with distance d = 34 Å and six-dimensional lattice parameter $a_6 \equiv \frac{d}{\sqrt{2(2+\tau)}} = 12.64$ Å.

$\lvert Q_{real} \rvert$ (Å^{-1})	$\lvert Q_{ideal} \rvert$ (Å^{-1})	Δ	I_{rel}	n_i	(N,M)
0.1116	0.1120	0.32%	2	200000	(8,4)
0.1808	0.1812	0.20%	5	$11\bar{1}\bar{1}11$	(12,16)
0.2668	0.2670	0.06%	20	200022	(24,36)
0.2931	0.2932	0.03%	25	$31\bar{1}\bar{1}11$	(28,44)
0.3082	0.3083	0.03%	20	220022	(32,48)
0.3571	0.3576	0.12%	5	$31\bar{1}\bar{1}31$	(44,64)
0.4080	0.4078	0.05%	10	420022	(56,84)
0.4255	0.4254	0.02%	5	$31\bar{1}\bar{1}33$	(60,92)
0.4744	0.4744	0.00%	90	$42\bar{2}\bar{2}22$	(72,116)
0.4985	0.4988	0.06%	100	$40\bar{2}042$	(80,128)
0.5787	0.5786	0.02%	5	$53\bar{1}\bar{1}33$	(108,172)
0.6887	0.6884	0.05%	15	$62\bar{2}044$	(152,244)
0.7052	0.7054	0.03%	5	$62\bar{2}\bar{2}44$	(160,256)
0.8078	0.8071	0.08%	30	$60\bar{4}064$	(208,336)

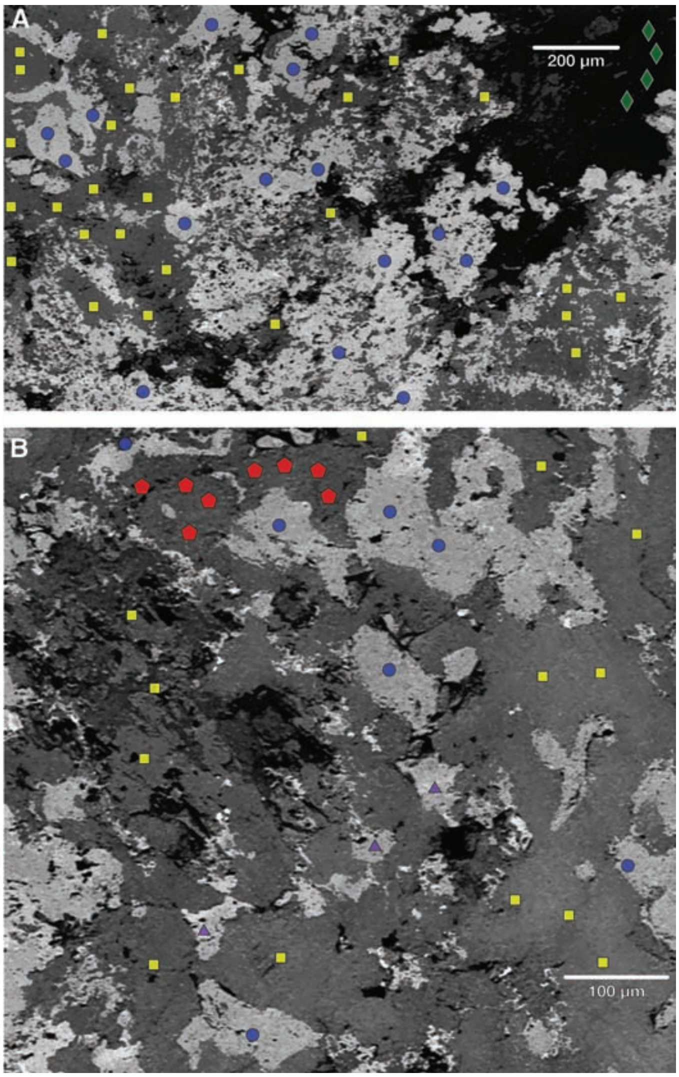

Fig. 2. (**A** and **B**) BSE images of two thin polished slices of the khatyrkite sample shown in Fig. 1. At least one microprobe analysis was made at each location marked with a symbol, corresponding to the following phases: khatyrkite ($CuAl_2$), yellow squares; cupalite (CuAl), blue circles; unknown mineral (AlCuFe), corresponding to β phase (*5*, *12*) in the synthetic alloy, purple triangles; forsteritic olivine [$(Mg_{0.95}Fe_{0.05})_2SiO_4$], intimately associated with khatyrkite, green diamonds; and natural quasicrystal with approximate composition $Al_{63}Cu_{24}Fe_{13}$, red pentagons.

that all the phases were formed naturally by geologic processes and are unlikely to have been introduced by human activity; however, elucidating the mechanisms responsible for this heterogeneous morphology and for the low oxygen fugacity implied by the existence of metallic Al remains a serious and fascinating challenge. In addition to these phases, we observed within the sample a grain about 90 to 120 µm across that, based on 18 microprobe analyses, is approximately $Al_{65}Cu_{20}Fe_{15}$, with an uncertainty of less than 0.1 atomic %. This is close to the optimal stoichiometry of synthetic i-AlCuFe (*5*). Over 200 microprobe samplings show that the chemical composition in each of the metallic phases shown in Fig. 2 has a fairly uniform composition. Extensive studies of AlCuFe alloy formation in the laboratory do not show the same assemblage of metal alloys found in this sample (*13*).

To investigate the atomic structure of this possible i-AlCuFe phase, we removed grains from the polished thin sections, mounted them on glass fibers, and collected powder XRD patterns with a diffractometer (*14*). The powder XRD pattern gives direct information about the atomic structure that can indicate whether it is a quasicrystal, using the scheme in (*7*). For an icosahedral quasicrystal, the diffraction scattering intensity in Fourier space at scattering wave vector $\mathbf{q}$ is $I(\mathbf{q}) = \sum|\rho_\mathbf{Q}|^2\delta_{\mathbf{q},\mathbf{Q}}$, where $\rho_\mathbf{Q}$ is complex, and the sum is over a discrete lattice of reciprocal vectors $\mathbf{G}$, expressible as integer linear combinations of the six fundamental wave vectors $\mathbf{g}_k = \left[\sin\beta\cos\left(\frac{2\pi k}{5}\right), \sin\beta\sin\left(\frac{2\pi k}{5}\right), \cos\beta\right]$ for $k = 0,\ldots,4$ and $\cos\beta = \frac{1}{\sqrt{5}}$ and g_5 = (0,0,1). The vectors $\{\mathbf{g}_k, \mathbf{g}_5\}$ are oriented along the six fivefold symmetry axes of an icosahedron (*15*). The icosahedron (which has the symmetry of a soccer ball) also has 10 threefold symmetry axes and 15 twofold symmetry axes. Associated with each peak $\mathbf{Q}$ is a complementary wave vector $\overline{\mathbf{Q}}$, obtained by using the same six integers to construct the corresponding linear combinations of $\overline{\mathbf{g}}_k = \mathbf{g}_{2k \bmod 5}$ and $\overline{\mathbf{g}}_5 = -\mathbf{g}_5$. The diffraction scattering intensity at peak $\mathbf{Q}$ tends to decrease as $|\overline{\mathbf{Q}}|$ increases. Synthetic i-AlCuFe is a face-centered icosahedral (FCI) quasicrystal (*5*); in these structures, Bragg peaks occur only at integer linear combinations of $\{\mathbf{g}_k, \mathbf{g}_5\}$ where the sum of the integers is even. Applying the automated indexing program in (*7*), we compared the powder XRD pattern of our AlCuFe mineral grains to that of an ideal FCI structure and found that all of the major peaks (Fig. 3A) match closely with Bragg reflections in the ideal structure, as shown in Table 1. We also quantified the degree of conformity, using figures of merit corresponding to $\overline{\Delta}$, the intensity-weighted average of the absolute deviation of each $\mathbf{Q}$ from its closest-matching FCI peak (column three in Table 1), and the intensity-weighted average of $\overline{\mathbf{Q}}$, as discussed in (*7*); Fig. 3B shows that the sample ranked extremely high.

To explore the atomic structure, several granules, each a few micrometers across (such as the one shown in Fig. 1B), were removed from the glass fiber and examined with TEM (*16*). On the submicrometer length scale, the grains are mostly homogeneous but contain some smaller domains with slightly different compositions. Some of these regions were found with energy-dispersive x-ray analysis to be $Al_{63 \pm 1}Cu_{24 \pm 1}Fe_{13 \pm 1}$, within an error equal to the known composition of synthetic i-AlCuFe. (This suggests that the electron microprobe analysis, which averages over larger domains, included regions with different compositions.) The diffraction patterns from these regions, obtained by tilting the sample at various angles, are shown in Fig. 4. These patterns, consisting of sharp peaks arranged in an incommensurate lattice with five-, three-, and twofold symmetry, are the characteristic signature of an icosahedral quasicrystal (*1*, *5*). In addition, the angles between the symmetry planes shown in Fig. 4 are consistent with icosahedral symmetry. For example, the angle between the two- and fivefold symmetry planes was measured to be 31.6° ± 0.5°, which agrees with the ideal rotation angle between the twofold and fivefold axes of an icosahedron (arctan $\frac{1}{\tau} \approx 31.7°$). The inverted Fourier transform of the high-resolution TEM (HRTEM) image shown in Fig. 1C shows that the real space structure consists of a homogeneous, quasiperiodic, and fivefold symmetric pattern. Together, these TEM results provide conclusive evidence of crystallographically forbidden icosahedral symmetry in a naturally occurring phase.

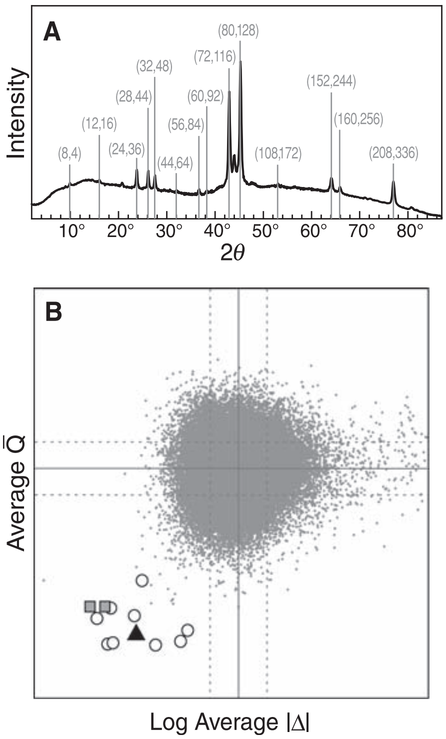

Fig. 3. (**A**) Powder XRD pattern for the natural sample, with major peaks indexed by the automated scheme in (*7*). The narrow sharp peaks indicate a high degree of translational order. (**B**) The distribution of two figures of merit introduced in (*7*) to separate quasicrystals from among a large collection of powder patterns in the ICDD-PDF: (i) the logarithm of the intensity-weighted average $|\Delta|$, where Δ is the absolute deviation of each **Q** from the closest-matching FCI peak (column three in Table 1); and (ii) the intensity-weighted average of $\overline{\mathbf{Q}}$. Known synthetic FCI quasicrystals are indicated with gray squares (AlCuFe) and white circles (other examples). They cluster far from ordinary crystalline minerals (gray dots), whose average and standard deviation are indicated by solid and dashed lines, respectively. The natural sample, marked with the black triangle, is several standard deviations away from the average and well within the cluster of known FCI quasicrystals.

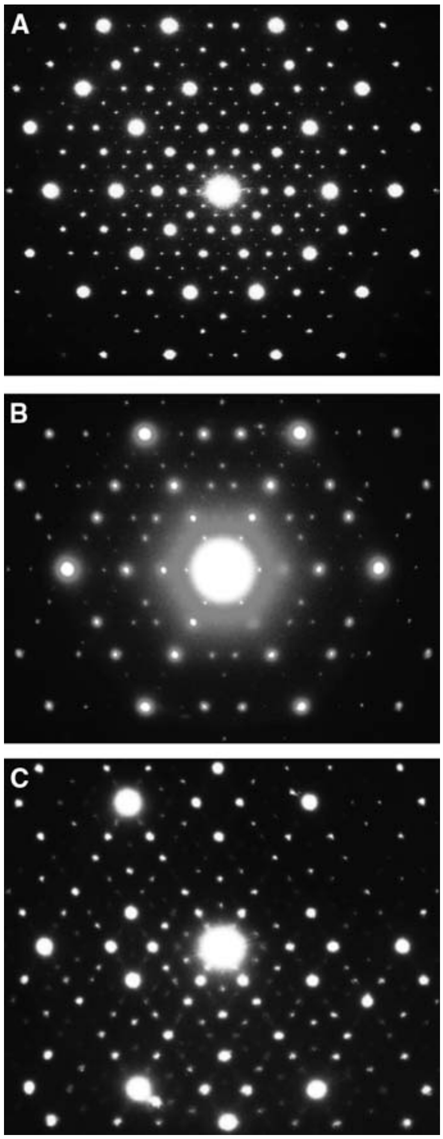

Fig. 4. The fivefold (**A**), threefold (**B**), and twofold (**C**) diffraction patterns obtained from a region (red dashed circle) of the granule in Fig. 1B match those predicted for a FCI quasicrystal, as do the angles that separate the symmetry axes.

TEM and XRD also demonstrated the high degree of structural perfection in the mineral quasicrystal. In the electron diffraction patterns in Fig. 4, there is no visible distortion. Quasicrystals produced by rapid quenching or embedded in a matrix of another phase often exhibit measurable deviations from the ideal pattern due to phason strains (*15, 17*). An experimental signature is a shift in Bragg peak positions relative to the ideal by an amount proportional to $\overline{\mathbf{Q}}$, corresponding to larger shifts for peaks with smaller intensity. If the diffraction pattern is held at a grazing angle and viewed down rows of peaks, the phason strain can be observed as deviations of the dimmer peaks from straight rows (*15*). The diffraction patterns in Fig. 4 display no discernible evidence of phason strain. This qualitative observation is quantified by the XRD data in column three of Table 1, which demonstrate that the natural quasicrystal has a degree of structural perfection comparable to that of the best laboratory specimens (Fig. 3B). Either the mineral samples formed without phason strain in the first place, or subsequent annealing was sufficient for phason strains to relax away.

A nearly structurally perfect natural quasicrystal that formed under geologic conditions would have several implications for geology and condensed-matter physics. The definition of a mineral, which previously included periodic crystals, incommensurate structures (*18*, *19*), and amorphous phases, would henceforth include quasicrystals, expanding the catalog of structures formed by nature and raising an interesting challenge to explain how they formed naturally. Finally, the study of natural quasicrystals may provide insights about the formation and stability of quasicrystals at temperatures and pressures not studied in the laboratory previously, and perhaps an avenue for discovering new quasicrystals with compositions not yet synthesized.

References and Notes

1. D. Levine, P. J. Steinhardt, *Phys. Rev. Lett.* **53**, 2477 (1984).
2. D. Shechtman, I. Blech, D. Gratias, J. W. Cahn, *Phys. Rev. Lett.* **53**, 1951 (1984).
3. R. Penrose, *Bull. Inst. Math. Appl.* **10**, 266 (1974).
4. C. Janot, *Quasicrystals: A Primer* (Oxford Univ. Press, Oxford, 1994).
5. P. A. Bancel, *Quasicrystals: The State of the Art*, D. DiVincenzo, P. J. Steinhardt, Eds. (World Scientific, Singapore, 1991), pp. 17–56.
6. A. P. Tsai, A. Inoue, T. Masumoto, *Jpn. J. Appl. Phys.* **26**, L1505 (1987).
7. P. J. Lu, K. Deffeyes, P. J. Steinhardt, N. Yao, *Phys. Rev. Lett.* **87**, 275507 (2001).
8. L. V. Razin, N. S. Rudashevskij, L. N. Vyalsov, *Zapiski Vses. Mineralog. Obshch.* **114**, 90 (1985).
9. F. C. Hawthorne *et al.*, *Am. Mineral.* **71**, 1277 (1986).
10. N. I. Filatova, V. S. Vishnevskaya, *Tectonophysics* **269**, 131 (1997).
11. The instrument was a Zeiss-EVO MA15 scanning electron microscope coupled with an Oxford INCA250 energy-dispersive spectrometer, operated with 25-kV accelerating voltage, 500-pA probe current, 2500 counts per second as average count rate on the whole spectrum, and counting time of 100 s. Samples were sputtered with 30-nm-thick carbon film.
12. The instrument was a JEOL JXA-8600 electron microprobe, using a 20-kV accelerating voltage; 40-nA

beam current; 30-s counting time; and Al-Kα, Cu-Kα, and Fe-Kα lines.
13. L. Zhang, R. Lück, *Z. Metallkd.* **94**, 774 (2003).
14. The instrument was an Oxford Diffraction Excalibur PX Ultra diffractometer with a 165-mm diagonal Onyx charge-coupled device detector at 2.5:1 demagnification. The program *Crysalis* RED (Oxford Diffraction 2006) was used to convert the observed diffraction rings into a conventional XRD pattern.
15. T. C. Lubensky, J. E. S. Socolar, P. J. Steinhardt, P. A. Bancel, P. A. Heiney, *Phys. Rev. Lett.* **57**, 1440 (1986).
16. The instrument was a Philips CM200-FEG TEM configured with a super-twin lens. The instrument was operated at 200 kV with a vacuum pressure of ~2×10^{-7} torr; the electron beam size ranged from 50 nm to 0.3 μm.
17. D. Levine, T. C. Lubensky, S. Ostlund, S. Ramaswamy, P. J. Steinhardt, J. Toner, *Phys. Rev. Lett.* **54**, 1520 (1985).
18. B. Dam, A. Janner, J. D. H. Donnay, *Phys. Rev. Lett.* **55**, 2301 (1985).
19. E. Makovicky, B. G. Hyde, *Struct. Bonding* **46**, 101 (1981).
20. We are indebted to L. Hollister and G. MacPherson for their critical examination of the results, especially regarding the issue of natural origin. We also thank P. Bonazzi, K. Deffeyes, S. Menchetti, and P. Spry for useful discussions and S. Bambi at the Museo di Storia Naturale for the photograph of the original sample in Fig. 1A. L.B. thanks the Ministerio dell'Istruzione dell'Università e della Ricerca Programma di Ricerca Nazionale 2007 project "Complexity in minerals: modulation, phase transition, structural disorder," issued to S. Menchetti. This work was supported in part by U.S. Department of Energy grant DE-FG02-91ER40671 (P.J.S.), the NSF MRSEC program through New York University (grant DMR-0820341; P.J.S.), the Princeton Center for Complex Materials (grant DMR-0819860; N.Y.), and the New Jersey Commission of Science and Technology (N.Y.).

12 January 2009; accepted 23 March 2009
10.1126/science.1170827

Observation of Single Colloidal Platinum Nanocrystal Growth Trajectories

Haimei Zheng,[1,2,3] Rachel K. Smith,[3]* Young-wook Jun,[2,3]* Christian Kisielowski,[1,2] Ulrich Dahmen,[1,2]† A. Paul Alivisatos[2,3]†

Understanding of colloidal nanocrystal growth mechanisms is essential for the syntheses of nanocrystals with desired physical properties. The classical model for the growth of monodisperse nanocrystals assumes a discrete nucleation stage followed by growth via monomer attachment, but has overlooked particle-particle interactions. Recent studies have suggested that interactions between particles play an important role. Using in situ transmission electron microscopy, we show that platinum nanocrystals can grow either by monomer attachment from solution or by particle coalescence. Through the combination of these two processes, an initially broad size distribution can spontaneously narrow into a nearly monodisperse distribution. We suggest that colloidal nanocrystals take different pathways of growth based on their size- and morphology-dependent internal energies.

The growth of colloidal nanocrystals has advanced remarkably, and now it is possible to make colloidal nanocrystals of a wide range of solids, ranging from metals to semiconductors and insulators, with narrow size distributions (variations in diameter less than 5%) and high crystallinity (*1*–*5*). It is also possible to control their shapes, from spheres to disks or rods, as well as their topology (solid, hollow, nested) and their connectivity and branching patterns by adjusting the growth parameters, such as surfactant, concentration, or temperature (*6*–*11*). The current state of nanocrystal synthesis has been largely achieved empirically with some classical models (*12*–*14*) for particle growth serving as guides. Here, we demonstrate that it is possible to directly observe the growth trajectories of individual colloidal nanocrystals in solution by using a liquid cell that operates inside a transmission electron microscope (TEM), and that these trajectories reveal a set of pathways more complex than those previously envisioned.

Consider the simplest case of a narrow size distribution of nearly spherical colloidal nanoparticles. A model based on kinetics that can account for this size distribution was proposed by LaMer and Dinegar (*12*) and improved by Reiss (*13*). An abrupt increase in monomer concentration induces a burst of nucleation events followed by a period of rapid growth. The initial broad size distribution because of a spread in nucleation time or other variations such as mixing can be corrected with "size distribution focusing," in which small crystals "catch up" with larger ones because the growth rate of nanocrystals decreases as the size increases (*1*). Inhibition of particle aggregation is typically achieved by using surfactant ligands that stabilize the particle surface and provide a barrier to coalescence. The thinking underlying this approach has guided many syntheses (*1*, *2*, *4*). A second scenario for nanocrystal control employs an equilibrium approach. One devises a system in which the binding of surfactant to the nanoparticle surface is nearly as strong as the bonds within the crystal, strong enough then to thermodynamically drive the system toward a particular average size for a given concentration of surfactant and monomeric species (*15*–*17*). These two distinct models consider only the possibility of particle growth through the addition of monomeric species. However, there is substantial evidence that particle coalescence or even oriented attachment can also play a role in nanocrystal growth (*18*–*22*). The lack of consensus on the controlling mechanisms is mainly due to the lack of direct evidence for nanocrystal growth in solution. In situ observation of the dynamic growth process is expected to substantially advance our understanding of nanocrystal growth mechanisms,

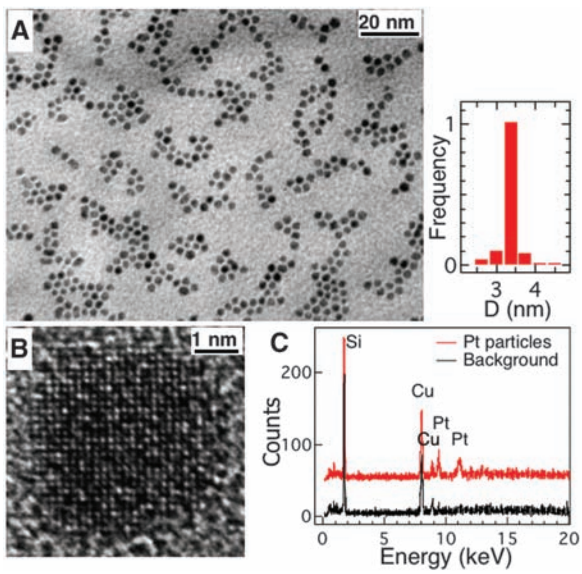

Fig. 1. TEM of Pt nanocrystals synthesized in a liquid cell. (**A**) Bright-field TEM image of Pt nanocrystals with a histogram of particle size distribution, obtained from measurements of 150 particles. (**B**) High-resolution TEM image of a Pt nanocrystal, which was recorded after the in situ experiment. (**C**) EDS spectra from Pt nanocrystals (red) and background (black) obtained ex situ from the same liquid cell. The observed Si and Cu signals are from the silicon nitride membrane window and the cover of the liquid cell, respectively.

[1]National Center for Electron Microcopy, Lawrence Berkeley National Laboratory, Berkeley, CA 94720, USA. [2]Materials Sciences Division, Lawrence Berkeley National Laboratory, Berkeley, CA 94720, USA. [3]Department of Chemistry, University of California, Berkeley, CA 94720, USA.

*These authors contributed equally to this paper.
†To whom correspondence should be addressed. E-mail: udahmen@lbl.gov (U.D.); alivis@berkeley.edu (A.P.A.)

although its application to specific syntheses will have to take into account factors such as the thermodynamic and geometric differences between microscopic in situ and macroscopic flask experiments.

In order to observe colloidal nanocrystal growth, one needs a technique that can image through liquids during the chemical reaction with nanometer resolution and in real time. Williams *et al.* have developed a liquid cell reactor that can be placed in a special TEM sample holder, which was used to image the dynamic growth of Cu clusters on a surface during electrochemical plating by using a TEM with a resolution of 5 nm (*23*) [see also other related techniques in (*24*–*26*)].We employed this TEM capability in a self-contained liquid cell with an improved resolution in the subnanometer range (fig. S1) (*27*). We used these disposable liquid cells to image platinum nanocrystal growth in solution in situ using a JEOL3010 microscope operated at 300 kV. Because the cells fit into a standard TEM sample holder, we also used CM300 and CM200 TEMs equipped with an x-ray detector for high-resolution TEM imaging and elemental analysis ex situ on the same cell. We prepared a stock solution for synthesis by dissolving Pt(acetylacetonate)$_2$ (10 mg/mL) in a mixture of *o*-dichlorobenzene and oleylamine (9:1 in volume ratio). We loaded about 100 nanoliters of the growth solution into the reservoir of a liquid cell, and the solution was drawn into the cell by capillary force. Subsequently, the cell was sealed and loaded into the microscope. Within the electron-transparent window, the reaction solution of about 200 nm in thickness was confined between two silicon nitride membranes (25 nm each).

A key feature of these experiments is the ability to use the electron beam to induce the nucleation of Pt nanocrystals. The growth of Pt nanocrystals in solution was initiated by the electron beam irradiation, and a constant beam intensity of 2×10^4 to 14×10^4 A/m^2 was maintained during the growth (*27*). The beam intensity varied briefly in the initial exposure to the electron beam (a few seconds) during the time required to focus for imaging. Nanocrystals nucleated and grew during this period of time. Under constant illumination, there was normally a subsequent round of nucleation followed by growth (movie S1; also see movie S2 for comparison). Figure 1A shows platinum nanocrystals obtained inside a liquid cell by the exposure of the growth solution to the electron beam for about 5 min. Nearly monodisperse nanoparticles with an average diameter of 3.4 nm and a SD of 8% were obtained (Fig. 1A, inset). The platinum nanoparticles were mostly single crystalline with a face-centered cubic structure (Fig. 1B) and a composition of pure Pt, as confirmed by energy-dispersive x-ray spectroscopy (EDS) (Fig. 1C).

In situ observation of the Pt nanoparticle growth provides details of the growth kinetics. Figure 2 shows a sequence of video images recorded at 0.0 s, 12.1 s, 24.2 s, and 77.0 s of exposure to electron beam radiation (movie S1). From the initial growth solution of Pt^{2+} precursor, a large number of Pt nanocrystals emerged, and new particles continued to appear. The nucleation under a constant electron beam irradiation spanned more than 10 s (see the number of particles as a function of time in Fig. 2B). Particle growth and nucleation occurred in parallel (see particles highlighted by arrows in Fig. 2A, indicating examples of growth). Along with the conventional particle growth by means of monomer addition from solution, frequent coalescence events between the particles were observed. At the early stage of the growth, the number of particles gradually increased and reached a maximum at 21.0 s. Subsequently, the number of particles dropped significantly and eventually settled at a constant value. Although some smaller particles were seen to dissolve completely, the decrease in the number of particles was mainly due to the coalescence events between individual particles (see the number of coalescence events as a function of time in Fig. 2B).

We examined the particles that have similar initial sizes but grow along different pathways. Figure 3A shows a sequence of video frames of two particles that were taken from the same field of view (fig. S2). The particle formed by means of simple growth shows a continuous increase of size and maintains a nearly spherical shape. In addition, mostly uniform diffraction contrast within the particle was observed, indicating single crystalline characteristics throughout the growth. However, the coalesced particle shows both shape changes and different diffraction contrast, indicating polycrystalline characteristics within the particle after the coalescence event. Eventually (about 16.0 s after the coalescence event) it forms a single crystalline particle with a nearly spherical shape. This is characteristic of punctuated growth, in which the growth of the coalesced particles pauses after coalescence during the period of structural relaxation. These pauses contribute to the situation in

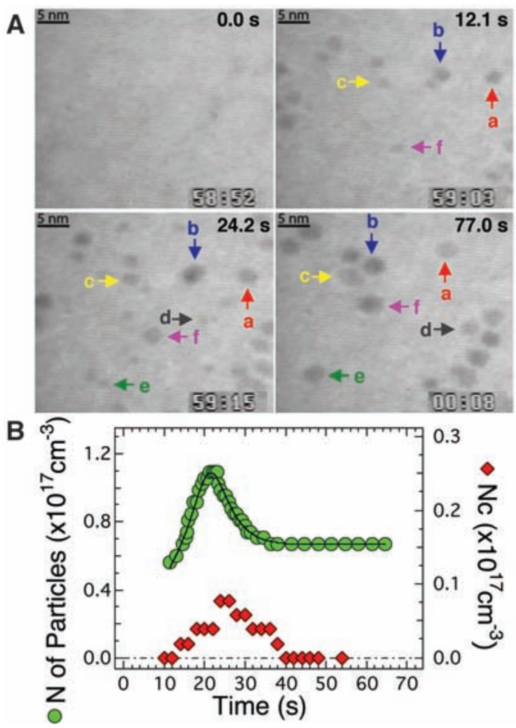

Fig. 2. Growth and coalescence of Pt nanocrystals. (**A**) Video images acquired at 0.0 s, 12.1 s, 24.2 s, and 77.0 s of exposure to the electron beam. Specific particles are labeled with arrows. The growth trajectories of these individual particles reveal the multiple pathways leading to size focusing. (**B**) Number of particles (left axis) and number of coalescence events (Nc, right axis) during an interval of 2.0 s versus time. Particles nucleate and grow during the adjustment of focus for imaging (0 to 10 s), the details of which were not available.

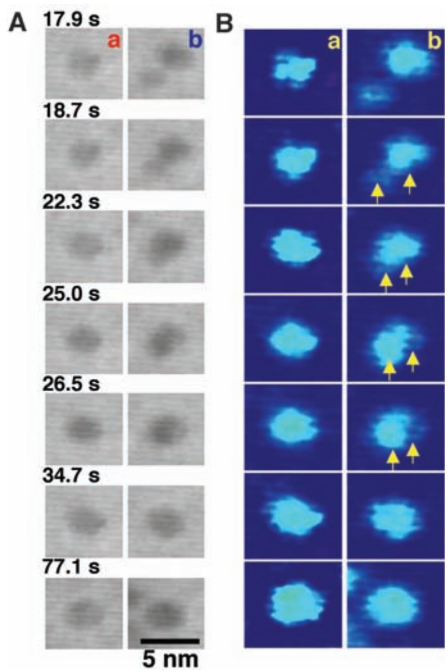

Fig. 3. Comparison of different growth trajectories. (**A**) Video images showing simple growth by means of monomer addition (left column) or growth by means of coalescence (right column). Particles are selected from the same field of view. (**B**) Enlarged (1.5 times) color images of (A). Distinct contrast changes are highlighted with arrows indicating recrystallization, which were observed in the coalesced particle but not in the case of simple growth.

which particles that are formed by the steady simple growth process in order to "catch up" so that the two types of particles show similar final sizes.

We considered the evolution of particle size distribution in light of the observed single-particle growth trajectories. Figure 4A shows the histograms of particle size distribution at different stages of growth (19.7 s, 24.2 s, 30.3 s, and 77.0 s; for each plot, we measured about 120 to 170 particles within an area of 50 nm by 60 nm and in intervals of 100 ms). At the early stages, particle size distributions are broad, because of the spread of nucleation events over time. At 24.2 s, we observed a bimodal distribution. At a later stage, the distribution has a single peak, and the initially broad distribution has spontaneously narrowed.

In order to understand this size-focusing behavior, we have examined the growth trajectories of each individual nanoparticle. Figure 4B shows particle size as a function of growth time for a few selected particles as examples (particles are highlighted by arrows in Fig. 2A), in which an effective size of $d = 2 \times \sqrt{A/\pi}$ was used, where A is the projected area of the particle in the video images. A particle evolving by means of simple growth shows a continuous increase of size until it reaches a saturation stage (particle a). However, particles resulting from coalescence events (particles b to e) show a jump of particle size after each coalescence event. A smaller particle can "catch up" to the size of a bigger particle through multiple coalescence events. The fact that multiple coalescence events are more commonly observed among the small particles is attributed to their higher energy due to a larger surface-to-volume ratio and an increased collision frequency resulting from a greater mobility. Such growth kinetics of individual nanoparticles deviates from the ensemble behavior, shown in Fig. 4C, which reflects the average particle size within an area of 50 nm by 60 nm as a function of time. The evolution of the mean particle size versus time resembles the trend predicted by classical growth models of a diffusion-controlled Ostwald ripening process (*2*) [the size of the particles (d) is proportional to growth time (t), $d^3 \sim t$]. This illustrates that direct observations of single-particle growth trajectories provide important insights into nanocrystal growth mechanisms, which are not accessible with a conventional analysis on the basis of the ensemble. For example, we found that there is a period of time after a coalescence event during which the coalesced particles cease to grow. After this relaxation period, the particle resumes growth through monomer addition. The combined effects of monomer addition, coalescence, and punctuated growth all contribute to the focusing of the size distribution.

During coalescence, the combined particle has a higher internal energy and chemical potential because of the appearance of grain boundaries and a higher surface energy per volume that is determined by its shape as compared with that of a spherical particle of the same size. Such higher-energy particles may lose monomers (dissolve) in the solution and/or change shape. Similar effects have been observed in the growth of Ge islands from a vapor phase (*28*). In our case, the combined nanoparticle changes shape, forming a spherical particle along with the recrystallization. During this relaxation period, there is a slight decrease of particle size. However, nanocrystals that evolve by means of simple growth show a continuous increase of particle size until reaching a saturation stage (Fig. 4B). We further found that the relaxation time (τ, highlighted in Fig. 4B, inset) increases with the particle size (d) following a power law relationship, $\tau \sim d^{3.3}$ (Fig. 4D). When considering the relaxation process as a recrystallization process in which monomeric species migrate on the two-dimensional nanocrystal surface, such a result is fairly reasonable. The relaxation time is proportional to the total surface area ($A = \frac{1}{4}\pi \times d^2$) and inversely proportional to the mobility (β) of monomers on the particle surface, $\beta \propto \frac{1}{d}$, where $1/d$ is the curvature of the particle. Therefore, the relationship between the relaxation time and the size of the coalesced particles is estimated by $\tau \sim d^3$, which is close to our experimentally observed value. However, this is only a rough estimate. Additional factors, such as variations in the nature of coalescence (oriented or random attachment) or details of size and shape of the coalesced particle need to be considered for more accurate evaluation (*29*).

Additionally, we found that oleylamine surfactants play a large role in the growth of monodisperse platinum nanocrystals. When the amount of oleylamine in the growth solution was decreased (0 to 3%), platinum crystal foils and dendrites were observed (fig. S3).

In summary, we have observed the dynamic growth of colloidal platinum nanocrystals in solution with subnanometer resolution by using a TEM. The evolution of monodisperse platinum nanocrystals involves complex growth trajectories, such as punctuated growth correlated with coalescence events, features that have not been considered in the classical models for nanocrystal growth. Considering coalescence as an alternative to simple growth by attachment of monomeric species, we expect that growth by particle attachment may also play an important role in the synthesis of nanocrystals with more complex shapes. More generally, we have shown that in situ TEM enables the visualization of single nanoparticles in solution with subnanometer resolution and offers great potential for addressing many fundamental issues in materials science, chemistry, and other fields of science.

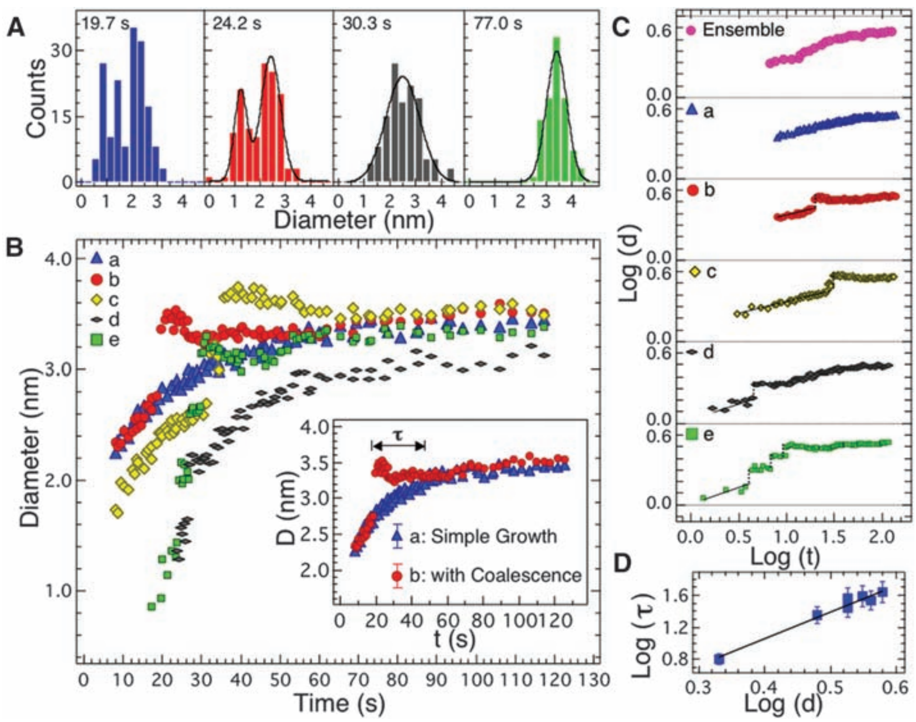

Fig. 4. Growth kinetics of Pt nanoparticles. (**A**) Histograms of particle size distribution at 19.7 s, 24.2 s, 30.3 s, and 77.0 s. Black curves are Gaussian fits. (**B**) Particle size versus growth time. These particles are highlighted in Fig. 2A. Inset shows two types of growth trajectories. A relaxation time (τ) was observed after a coalescence event. Error bars for particle diameter measurements are less than ± 0.18 nm. (**C**) Logarithmic relationship of particle size versus growth time for the ensemble and those individual particles in (B). Black lines are guides for the eye, and dashed lines show the coalescence events. (**D**) Logarithmic relationship of relaxation time versus the size of the coalesced particles. Black line shows linear fit.

References and Notes

1. X. G. Peng, J. Wickham, A. P. Alivisatos, *J. Am. Chem. Soc.* **120**, 5343 (1998).
2. C. B. Murray, C. R. Kagan, M. G. Bawendi, *Annu. Rev. Mater. Sci.* **30**, 545 (2000).

3. B. L. Cushing, V. L. Kolesnichenko, C. J. O'Connor, *Chem. Rev.* **104**, 3893 (2004).
4. Y. Yin, A. P. Alivisatos, *Nature* **437**, 664 (2005).
5. D. J. Norris, A. L. Efros, S. C. Erwin, *Science* **319**, 1776 (2008).
6. X. G. Peng *et al.*, *Nature* **404**, 59 (2000).
7. L. Manna, E. C. Scher, A. P. Alivisatos, *J. Am. Chem. Soc.* **122**, 12700 (2000).
8. V. F. Puntes, K. M. Krishnan, A. P. Alivisatos, *Science* **291**, 2115 (2001).
9. V. F. Puntes, D. Zanchet, C. K. Erdonmez, A. P. Alivisatos, *J. Am. Chem. Soc.* **124**, 12874 (2002).
10. D. J. Milliron *et al.*, *Nature* **430**, 190 (2004).
11. Y. D. Yin *et al.*, *Science* **304**, 711 (2004).
12. V. K. LaMer, R. H. Dinergar, *J. Am. Chem. Soc.* **72**, 4847 (1950).
13. H. Reiss, *J. Chem. Phys.* **19**, 482 (1951).
14. T. Sugimoto, *Adv. Colloid Interface Sci.* **28**, 65 (1987).
15. D. V. Leff, P. C. Ohara, J. R. Heath, W. M. Gelbart, *J. Phys. Chem. B* **99**, 7036 (1995).
16. Y. Chen, E. Johnson, X. Peng, *J. Am. Chem. Soc.* **129**, 10937 (2007).
17. Y. A. Yang, H. M. Wu, K. R. Williams, Y. C. Cao, *Angew. Chem. Int. Ed.* **44**, 6712 (2005).
18. J. F. Banfield, S. A. Welch, H. Z. Zhang, T. T. Ebert, R. L. Penn, *Science* **289**, 751 (2000).
19. C. Pacholski, A. Kornowski, H. Weller, *Angew. Chem. Int. Ed.* **41**, 1188 (2002).
20. J. H. Yu *et al.*, *J. Am. Chem. Soc.* **127**, 5662 (2005).
21. M. Niederberger, H. Colfen, *Phys. Chem. Chem. Phys.* **8**, 3271 (2006).
22. M. A. Watzky, E. E. Finney, R. G. Finke, *J. Am. Chem. Soc.* **130**, 11959 (2008).
23. M. J. Williamson, R. M. Tromp, P. M. Vereecken, R. Hull, F. M. Ross, *Nat. Mater.* **2**, 532 (2003).
24. P. L. Gai, *Microsc. Microanal.* **8**, 21 (2002).
25. K. L. Liu *et al.*, *Lab Chip* **8**, 1915 (2008).
26. N. de Jonge, D. B. Peckys, G. J. Kremers, D. W. Piston, *Proc. Natl. Acad. Sci. U.S.A.* **106**, 2159 (2009).
27. Materials and methods are available as supporting material on *Science* Online.
28. F. M. Ross, J. Tersoff, R. M. Tromp, *Phys. Rev. Lett.* **80**, 984 (1998).
29. J. E. Burke, D. Turnbull, in *Progress in Metal Physics*, vol. 3 (Pergamon Press, London, 1952), pp. 220–292.

30. The authors would like to thank A. Minor and J. Turner for their help with the initial tests on the liquid cells. This project is supported by the Director, Office of Science, Office of Basic Energy Sciences, Materials Sciences and Engineering Division of the U.S. Department of Energy under contract DE-AC02-05CH11231.

Supporting Online Material
www.sciencemag.org/cgi/content/full/324/5932/1309/DC1
Materials and Methods
Figs. S1 to S3
Movies S1 and S2
References

10 February 2009; accepted 8 April 2009
10.1126/science.1172104

Large-Area Synthesis of High-Quality and Uniform Graphene Films on Copper Foils

Xuesong Li,[1] Weiwei Cai,[1] Jinho An,[1] Seyoung Kim,[2] Junghyo Nah,[2] Dongxing Yang,[1] Richard Piner,[1] Aruna Velamakanni,[1] Inhwa Jung,[1] Emanuel Tutuc,[2] Sanjay K. Banerjee,[2] Luigi Colombo,[3]* Rodney S. Ruoff[1]*

Graphene has been attracting great interest because of its distinctive band structure and physical properties. Today, graphene is limited to small sizes because it is produced mostly by exfoliating graphite. We grew large-area graphene films of the order of centimeters on copper substrates by chemical vapor deposition using methane. The films are predominantly single-layer graphene, with a small percentage (less than 5%) of the area having few layers, and are continuous across copper surface steps and grain boundaries. The low solubility of carbon in copper appears to help make this growth process self-limiting. We also developed graphene film transfer processes to arbitrary substrates, and dual-gated field-effect transistors fabricated on silicon/silicon dioxide substrates showed electron mobilities as high as 4050 square centimeters per volt per second at room temperature.

Graphene, a monolayer of sp^2-bonded carbon atoms, is a quasi–two-dimensional (2D) material. Graphene has been attracting great interest because of its distinctive band structure and physical properties (*1*). Today, the size of graphene films produced is limited to small sizes (usually <1000 μm^2) because the films are produced mostly by exfoliating graphite, which is not a scalable technique. Graphene has also been synthesized by the desorption of Si from SiC single-crystal surfaces, which yields a multilayered graphene structure that behaves like graphene (*2*, *3*), and by a surface precipitation process of carbon in some transition metals (*4*–*8*).

[1]Department of Mechanical Engineering and the Texas Materials Institute, 1 University Station C2200, The University of Texas at Austin, Austin, TX 78712–0292, USA. [2]Department of Electrical and Computer Engineering, Microelectronics Research Center, The University of Texas at Austin, Austin, TX 78758, USA. [3]Texas Instruments, Dallas, TX 75243, USA.

*To whom correspondence should be addressed. E-mail: colombo@ti.com (L.C.); r.ruoff@mail.utexas.edu (R.S.R.)

Electronic application will require high-quality large-area graphene that can be manipulated to make complex devices and integrated in silicon device flows. Field-effect transistors (FETs) fabricated with exfoliated graphite have shown promising electrical properties (*9*, *10*), but these devices will not meet the silicon device scaling requirements, especially those for power reduction and performance. One device that could meet the silicon roadmap requirements beyond the 15-nm node was proposed by S. K. Banerjee *et al.* (*11*). The device is a "BisFET" (bilayer pseudospin FET) that is made up of two graphene layers separated by a thin dielectric. The ability to create this device can be facilitated by the availability of large-area graphene. Making a transparent electrode, another promising application of graphene, also requires large films (*6*, *12*–*14*).

At this time, there is no pathway for the formation of a graphene layer that can be exfoliated from or transferred from the graphene synthesized on SiC, but there is a way to grow and transfer graphene grown on metal substrates (*5*–*7*). Although graphene has been grown on a number of metals, we still have the challenge of growing large-area graphene. For example, graphene grown on Ni seems to be limited by its small grain size, presence of multilayers at the grain boundaries, and the high solubility of carbon (*6*, *7*). We have developed a graphene chemical vapor deposition (CVD) growth process on copper foils (25 μm thick in our experiment). The films grow directly on the surface by a surface-catalyzed process, and the film is predominantly graphene with <5% of the area having two- and three-layer graphene flakes. Under our processing conditions, the two- and three-layer flakes do not grow larger with time. One of the major benefits of our process is that it can be used to grow graphene on 300-mm copper films on Si substrates (a standard process in Si technology). It is also well known that annealing of Cu can lead to very large grains.

As described in (*15*), we grew graphene on copper foils at temperatures up to 1000°C by CVD of carbon using a mixture of methane and hydrogen. Figure 1A shows a scanning electron microscopy (SEM) image of graphene on a copper substrate where the Cu grains are clearly visible. A higher-resolution image of graphene on Cu (Fig. 1B) shows the presence of Cu surface steps, graphene "wrinkles," and the presence of non-uniform dark flakes. The wrinkles associated with the thermal expansion coefficient difference between Cu and graphene are also found to cross Cu grain boundaries, indicating that the graphene film is continuous. The inset in Fig. 1B shows transmission electron microscopy (TEM) images of graphene and bilayer graphene. With the use of a process similar to that described in (*16*), the as-grown graphene can be easily transferred to alternative substrates, such as SiO_2/Si or glass (Fig. 1, C and D), for further evaluation and for various applications; a detailed transfer process is described (*15*). The process and method used to transfer graphene from Cu was the same for the SiO_2/Si substrate and the glass substrate. Although it is difficult to see the graphene on the SiO_2/Si substrate, a similar graphene film from another Cu substrate transferred on glass clearly shows that it is optically uniform.

We used Raman spectroscopy to evaluate the quality and uniformity of graphene on a SiO_2/Si substrate. Figure 2 shows SEM and optical images with the corresponding Raman spectra and maps of the D, G, and 2D bands providing information on the defect density and film thickness. The Raman spectra are from the spots marked with the corresponding colored circles shown in the other panels (in Fig. 2, A and B, green arrows are used instead of circles so as to show the trilayer region more clearly). The thickness and uniformity of the graphene films were evaluated via color contrast under optical microscope (*17*) and Raman spectra (*7*, *18*, *19*).

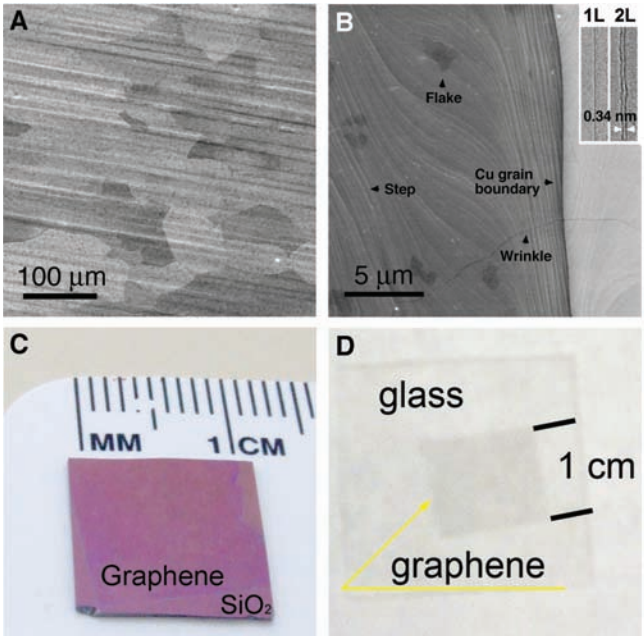

Fig. 1. (**A**) SEM image of graphene on a copper foil with a growth time of 30 min. (**B**) High-resolution SEM image showing a Cu grain boundary and steps, two- and three-layer graphene flakes, and graphene wrinkles. Inset in (B) shows TEM images of folded graphene edges. 1L, one layer; 2L, two layers. (**C** and **D**) Graphene films transferred onto a SiO_2/Si substrate and a glass plate, respectively.

The Raman spectrum from the lightest pink background in Fig. 2B shows typical features of monolayer graphene: (i) a ~0.5 G–to–2D intensity ratio and (ii) a symmetric 2D band centered at ~2680 cm^{-1} with a full width at half maximum of ~33 cm^{-1}. The second lightest pink flakes (blue circle) correspond to bilayer graphene, and the darkest one (green arrow) represents trilayer graphene. This thickness variation is more clearly shown in the SEM image in Fig. 2A. The D map in Fig. 2D, which has been associated with defects in graphene, is rather uniform and near the background level, except for regions where wrinkles are present and close to few-layer regions. The G and the 2D maps clearly show the presence of more than one layer in the flakes. In the wrinkled regions, there are peak height variations in both the G and 2D bands, and there is a broadening of the 2D band. An analysis of the intensity of the optical image over the whole sample (1 cm by 1 cm) showed that the area with the lightest pink color is more than 95%, and all 40 Raman spectra randomly collected from this area show monolayer graphene. There is only a small fraction of trilayer or few-layer (<10) graphene (<1%), and the rest is bilayer graphene (~3 to 4%).

We grew films on Cu as a function of time and Cu foil thickness under isothermal and isobaric conditions. Using the process flow described in (*15*), we found that graphene growth on Cu is self-limited; growth that proceeded for more than 60 min yielded a similar structure to growth runs performed for ~10 min. For times

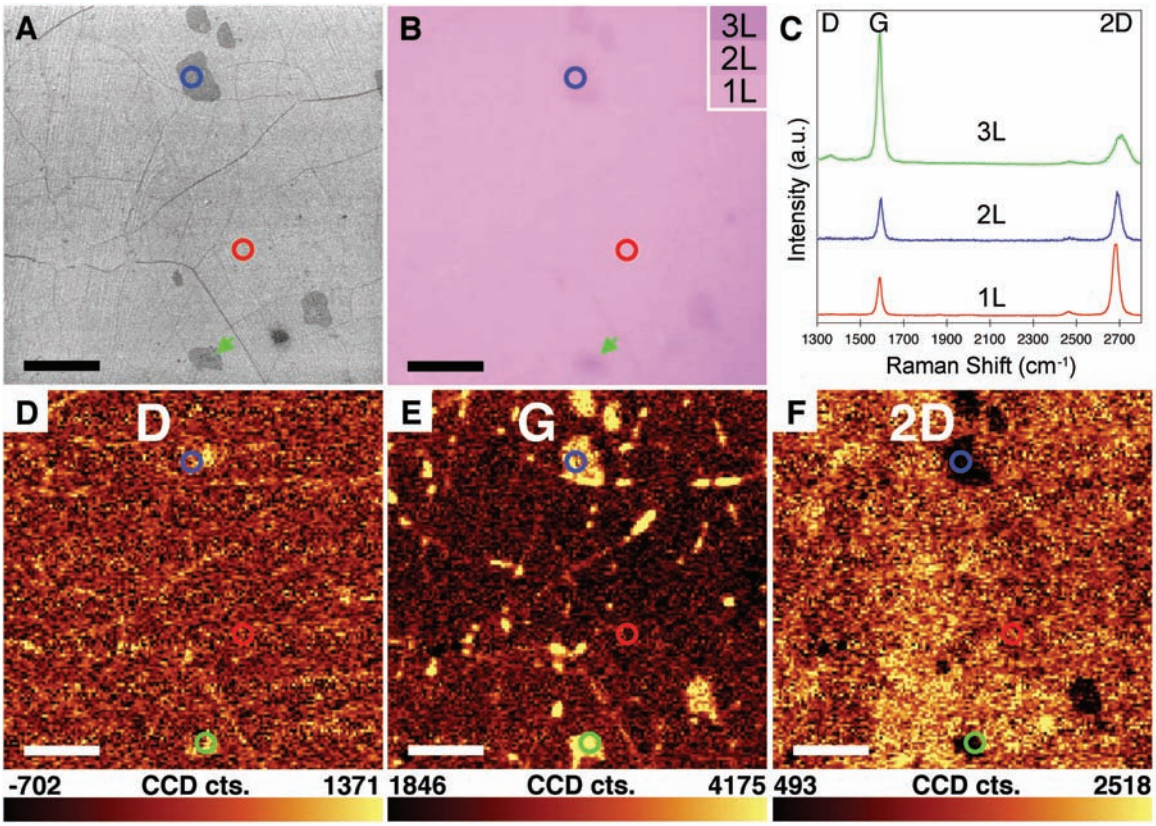

Fig. 2. (**A**) SEM image of graphene transferred on SiO_2/Si (285-nm-thick oxide layer) showing wrinkles, as well as two- and three-layer regions. (**B**) Optical microscope image of the same regions as in (A). (**C**) Raman spectra from the marked spots with corresponding colored circles or arrows showing the presence of one, two, and three layers of graphene. a.u., arbitrary units. (**D** to **F**) Raman maps of the D (1300 to 1400 cm^{-1}), G (1560 to 1620 cm^{-1}), and 2D (2660 to 2700 cm^{-1}) bands, respectively (WITec alpha300, λ_{laser} = 532 nm, ~500-nm spot size, 100× objector). CCD cts., charge-coupled device counts. Scale bars, 5 µm.

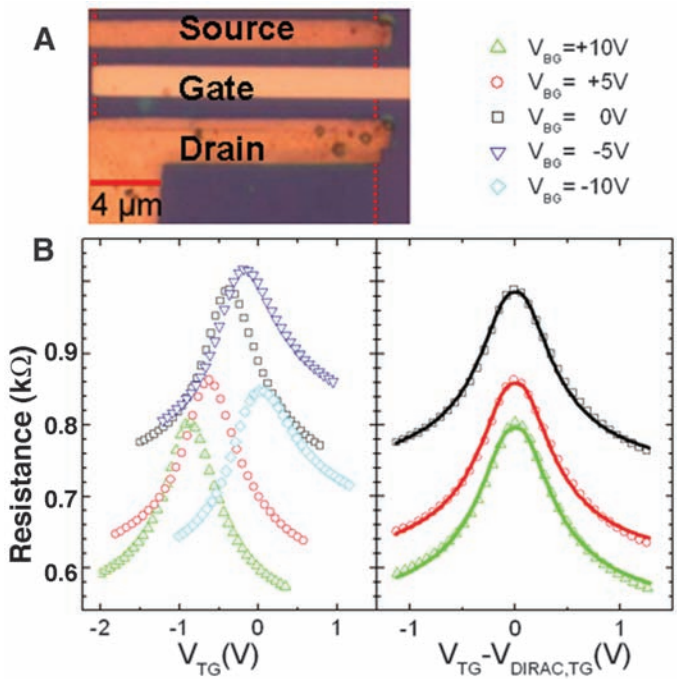

Fig. 3. (**A**) Optical microscope image of a graphene FET. (**B**) Device resistance versus top-gate voltage (V_{TG}), with different back-gate (V_{BG}) biases, and versus V_{TG}-$V_{Dirac,TG}$ (V_{TG} at the Dirac point), with a model fit (solid line).

much less than 10 min, the Cu surface is usually not fully covered [SEM images of graphene on Cu with different growth time are shown in fig. S3 (*15*)]. The growth of graphene on Cu foils of varying thickness (12.5, 25, and 50 μm) also yielded similar graphene structure with regions of double and triple flakes, but neither discontinuous monolayer graphene for thinner Cu foils nor continuous multilayer graphene for thicker Cu foils, as we would have expected based on the precipitation mechanism. According to these observations, we concluded that graphene is growing by a surface-catalyzed process rather than a precipitation process, as has been reported by others for Ni (*5–7*). Monolayer graphene formation caused by surface segregation or surface adsorption of carbon has also been observed on transition metals such as Ni and Co at elevated temperatures by Blakely and coauthors (*20–22*). However, when the metal substrates were cooled down to room temperature, thick graphite films were obtained because of precipitation of excess C from these metals, in which the solubility of C is relatively high.

In recent work, thin Ni films and a fast-cooling process have been used to suppress the amount of precipitated C. However, this process still yields films with a wide range of graphene layer thicknesses, from one to a few tens of layers and with defects associated with fast cooling (*5–7*). Our results suggest that the graphene growth process is not one of C precipitation but rather a CVD process. The precise mechanism will require additional experiments to understand in full, but very low C solubility in Cu (*23–25*) and poor C saturation as a result of graphene surface coverage may be playing a role in limiting or preventing the precipitation process altogether at high temperature, similar to the case of impeding of carburization of Ni (*26*). This provides a pathway for growing self-limited graphene films.

To evaluate the electrical quality of the synthesized graphene, we fabricated dual-gated FETs with Al_2O_3 as the gate dielectric and measured them at room temperature. Along with a device model that incorporates a finite density at the Dirac point, the dielectric, and the quantum capacitances (*9*), the data are shown in Fig. 3. The extracted carrier mobility for this device is ~4050 $cm^2 V^{-1} s^{-1}$, with the residual carrier concentration at the Dirac point of $n_0 = 3.2 \times 10^{11}$ cm^{-2}. These data suggest that the films are of reasonable quality, at least sufficient to continue improving the growth process to achieve a material quality equivalent to the exfoliated natural graphite.

References and Notes

1. A. K. Geim, K. S. Novoselov, *Nat. Mater.* **6**, 183 (2007).
2. C. Berger *et al.*, *Science* **312**, 1191 (2006); published online 12 April 2006 (10.1126/science.1125925).
3. K. V. Emtsev *et al.*, *Nat. Mater.* **8**, 203 (2009).
4. P. W. Sutter, J.-I. Flege, E. A. Sutter, *Nat. Mater.* **7**, 406 (2008).
5. Q. Yu *et al.*, *Appl. Phys. Lett.* **93**, 113103 (2008).
6. K. S. Kim *et al.*, *Nature* **457**, 706 (2009).
7. A. Reina *et al.*, *Nano Lett.* **9**, 30 (2009).
8. J. Coraux, A. T. N'Diaye, C. Busse, T. Michely, *Nano Lett.* **8**, 565 (2008).
9. S. Kim *et al.*, *Appl. Phys. Lett.* **94**, 062107 (2009).
10. M. C. Lemme *et al.*, *Solid-State Electron.* **52**, 514 (2008).
11. S. K. Banerjee, L. F. Register, E. Tutuc, D. Reddy, A. H. MacDonald, *IEEE Electron Device Lett.* **30**, 158 (2009).
12. P. Blake *et al.*, *Nano Lett.* **8**, 1704 (2008).
13. R. R. Nair *et al.*, *Science* **320**, 1308 (2008); published online 3 April 2008 (10.1126/science.1156965).
14. X. Wang, L. Zhi, K. Müllen, *Nano Lett.* **8**, 323 (2008).
15. See supporting material on *Science* Online.
16. A. Reina *et al.*, *J. Phys. Chem. C* **112**, 17741 (2008).
17. Z. H. Ni *et al.*, *Nano Lett.* **7**, 2758 (2007).
18. A. C. Ferrari *et al.*, *Phys. Rev. Lett.* **97**, 187401 (2006).
19. A. Das *et al.*, *Nat. Nanotechnol.* **3**, 210 (2008).
20. M. Eizenberg, J. M. Blakely, *Surf. Sci.* **82**, 228 (1979).
21. M. Eizenberg, J. M. Blakely, *J. Chem. Phys.* **71**, 3467 (1979).
22. J. C. Hamilton, J. M. Blakely, *Surf. Sci.* **91**, 199 (1980).
23. R. B. McLellan, *Scr. Metal.* **3**, 389 (1969).
24. G. Mathieu, S. Guiot, J. Carbané, *Scr. Metal.* **7**, 421 (1973).
25. G. A. López, E. J. Mittemeijer, *Scr. Mater.* **51**, 1 (2004).
26. R. Kikowatz, K. Flad, G. Horz, *J. Vac. Sci. Technol. A* **5**, 1009 (1987).
27. We thank the Nanoelectronic Research Initiative (NRI–Southwest Area Nanoelectronics Center, grant no. 2006-NE-1464), the Defense Advanced Research Projects Agency Carbon Electronics for RF Applications Center, and the University of Texas at Austin for support.

Supporting Online Material
www.sciencemag.org/cgi/content/full/1171245/DC1
Materials and Methods
Figs. S1 to S3

22 January 2009; accepted 9 April 2009
Published online 7 May 2009;
10.1126/science.1171245
Include this information when citing this paper.

Superconductivity at the Two-Dimensional Limit

Shengyong Qin, Jungdae Kim, Qian Niu, Chih-Kang Shih*

Superconductivity in the extreme two-dimensional limit is studied on ultrathin lead films down to two atomic layers, where only a single channel of quantum well states exists. Scanning tunneling spectroscopy reveals that local superconducting order remains robust until two atomic layers, where the transition temperature abruptly plunges to a lower value, depending sensitively on the exact atomic structure of the film. Our result shows that Cooper pairs can still form in the last two-dimensional channel of electron states, although their binding is strongly affected by the substrate.

Studies of two-dimensional (2D) superconductivities have been generally limited to the regime where the superconducting order parameter behaves as a 2D wave function but the underline electrons are still three-dimensional (*1–11*). Recent advancements in materials synthesis have enabled the growth of epitaxial superconductor thin films with unprecedented control in crystallinity, atomic smoothness, and film thickness, thus opening up new opportunities in investigations of 2D superconductivity (*7–16*). Studies of superconducting properties of ultrathin Pb films on Si or Ge substrates by transport, magnetic, and spectroscopic measurements have revealed several new aspects of 2D superconductivity (*7–11*), such as quantum oscillations of the superconducting order parameter as a function of the film thickness (*7*, *8*). Moreover, D. Eom *et al.* discovered that superconductivity remains surprisingly robust, even for films as thin as 5 monolayers (ML) (*8*). However, even in such thin films, there still exist several quantum well channels (*17*). It is unclear how much mixing between them occurs and how such mixing influences superconductivity. Consequently, some very interesting questions arise: Could it be possible to engineer a superconducting thin film with only one quantum well channel? Moreover, what will be the superconducting properties at this ultimate limit, and in particular, to what extent does the robustness of superconductivity remain at this limit?

The transition temperature (T_c) as a function of the film thickness (Fig. 1) shows oscillations for $L > 5$ (where L is the number of atomic layers) that have been reported previously, as well as new data for the thinnest films down to $L = 2$, which is the last Pb film that can be stable according to the quantum growth principle (*18*). More notably, $L = 2$ also corresponds to the single quantum channel regime: Along the (111) crystal direction, $k_F = 0.45\ \pi/d$, where k_F is the Fermi wave vector, and d is the spacing between lattice planes, giving rise to the condition of $k_F L \sim \pi$ for the existence of a single quantum well channel. As the film thickness decreases, one first observes an increase of the quantum oscillations of T_c, followed by a dramatic drop of T_c to substantially lower values at the ultimate limit of 2 ML. In addition, we find that there are two different types of $L = 2$ films, which differ in subtle atomic reconstructions but have a substantial difference in T_c.

The fabrication of pristine ultrathin films requires a careful preparation of the substrate, resulting in a Pb-Si reconstruction template containing a mixture of $\sqrt{3}\times\sqrt{3}$ and $\sqrt{7}\times\sqrt{3}$ structures (fig. S1) (*19–22*). This procedure results in a uniform 2-ML Pb film on the template (Fig. 2A). There are two types of 2-ML Pb films (labeled as type I and II); each type resides on an individual terrace. A zoom-in view shows that type I has an underlying 1 × 1 atomic structure with a moiré pattern periodicity of ~3.0 nm (Fig. 2B), whereas type II has an underlying $\sqrt{3} \times \sqrt{3}$ atomic structure (oriented 30° with respect to the 1 × 1 structure) with a moiré pattern periodicity of ~4.4 nm (Fig. 2C). Moreover, the underlying 1 × 1 structure in type I has the same surface lattice parameter (3.50 ± 0.10 Å) as the bulk Pb to within 3%, whereas the $\sqrt{3} \times \sqrt{3}$ structure in type II has a lattice parameter of 6.50 ± 0.15 Å, which is very close to that of the Si $\sqrt{3}\times\sqrt{3}$ structure, implying the existence of a pseudomorphic strain.

Although in this image, type I is more abundant, investigations over more than 100 terraces show that there is no preferential abundance of either type. Most notably, we never observe a mixed phase of type I and II on the same terrace. Often, type II contains small holes of 2- to 6-nm in diameter that extend down to the substrate. On type I film, however, holes are formed at the descending edge of the terrace. Such holes ex-

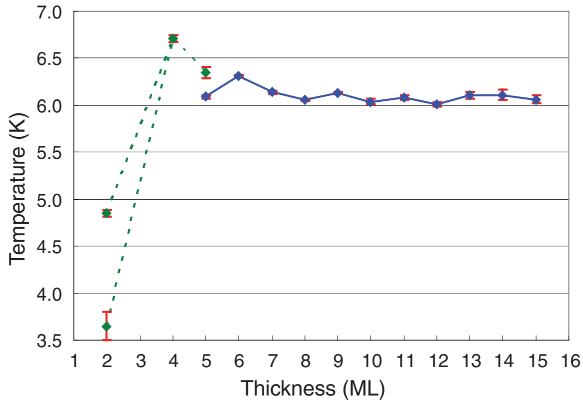

Fig. 1. Superconducting transition temperature (T_c) as a function of film thickness. As the film thickness decreases, an increase of the quantum oscillations of T_c was observed, followed by a dramatic drop of T_c to substantially lower values at the ultimate limit of 2 ML. At $L = 2$, two different kinds of films result in two different T_c values. The data point at $L = 3$ is absent because it is thermodynamically unstable to form a film of 3 ML. The old data (*8*) were acquired on films grown on Si(111) 7 × 7, whereas the new data (2, 4, and 5 ML) were acquired on films grown on a new Pb-Si(111) template. Determination of T_c and error bars are described in the supporting online material.

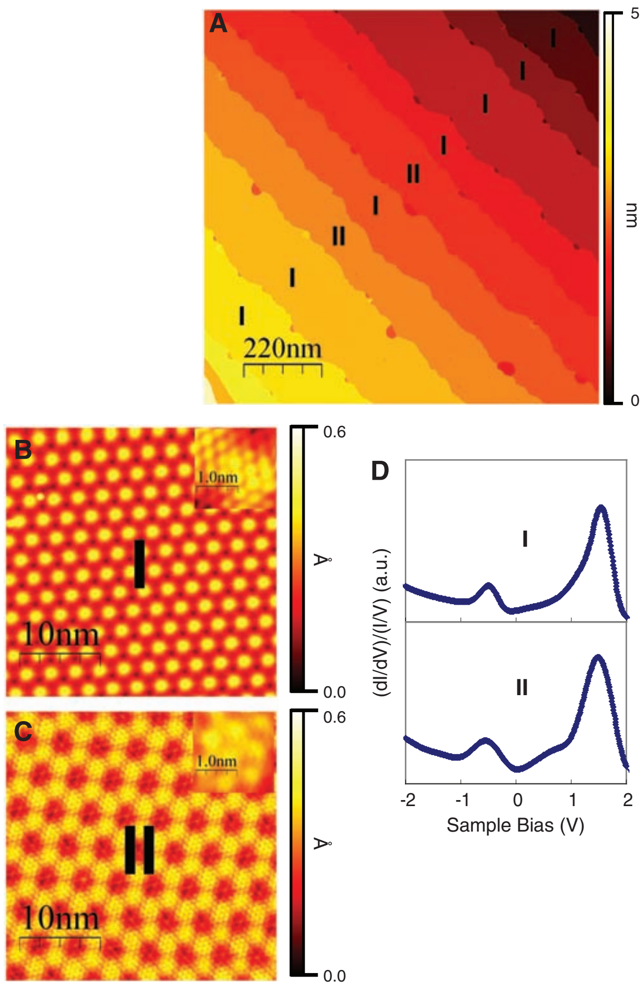

Fig. 2. (**A**) STM image of a uniform 2-ML Pb film. (**B** and **C**) STM images of two types of 2-ML Pb films (labeled as type I and II); each type resides on an individual terrace. Insets are zoom-in views, showing that type I has an underlying 1 × 1 atomic structure with a moiré pattern periodicity of ~3.0 nm (B), whereas type II has an underlying $\sqrt{3} \times \sqrt{3}$ atomic structure with a moiré pattern periodicity of ~4.4 nm (C). The orientation of the $\sqrt{3} \times \sqrt{3}$ atomic structure is rotated 30° with respect to the 1 × 1 structure. (**D**) Tunneling spectroscopy of QWS on two types of films, revealing the same level spacing and relative positions to E_F. a.u., arbitrary units.

Department of Physics, The University of Texas at Austin, Austin, TX 78712, USA.

*To whom correspondence should be addressed. E-mail: shih@physics.utexas.edu

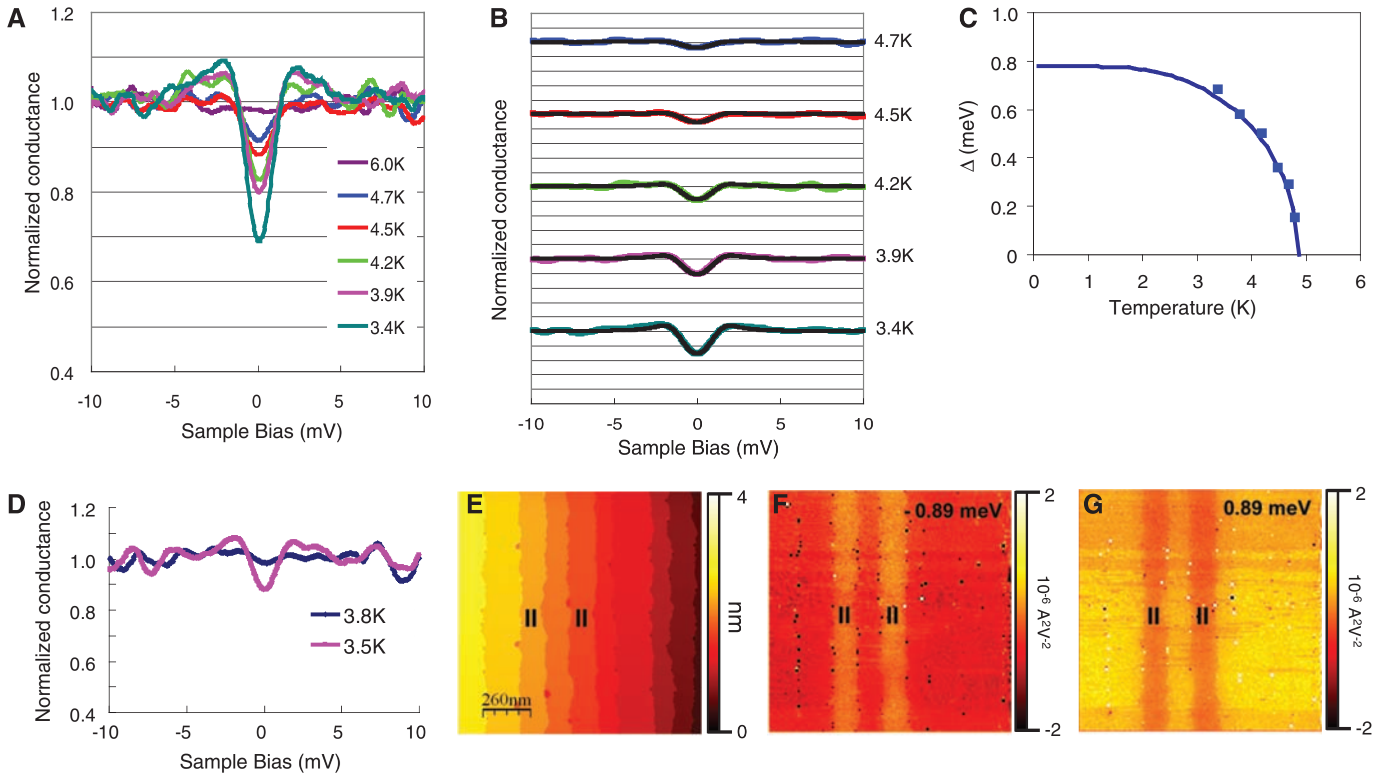

Fig. 3. (**A**) Normalized conductance spectra acquired at various temperatures for type I films. The superconducting gap is clearly visible at 3.4 K and gradually disappears as the temperature is raised to 6.0 K. (**B**) Normalized conductance spectra (nonblack colors) taken by STM were fitted using the BCS-like formula for the tunneling conductance (black). (**C**) The energy gaps (Δ) for several temperatures were obtained from (B) and plotted as blue squares. The blue curve is a fitting of these energy gap data using a BCS-like gap equation to obtain a T_c of ~4.9 K for the type I film. (**D**) Tunneling measurements of the type II 2-ML films. The superconducting gap did not show until the temperature dropped to 3.5 K. We estimated the T_c to be ~3.65 ± 0.15 K. (**E**) Large-area STM image of 2-ML Pb film. The two terraces labeled with "II" are type II films, and the rest of the terraces are type I. (**F** and **G**) d^2I/dV^2 mapping at 4.0 K (128 × 128 pixels with a pixel resolution of 10.1 nm) at sample biases of –0.89 and 0.89 mV, respectively. First, a large superconductivity contrast between type I and II films was revealed; next, the superconductivity on the same terrace was shown to be very uniform, with clear boundaries at the terrace edges.

pose the substrate template atomic structure, and they allow one to conveniently determine the thickness of the film.

Despite this structural difference, these two types of 2-ML films have almost identical electronic structure in the normal state (*23*). Tunneling spectroscopy (Fig. 2D) reveals the same quantum well states (QWS) level spacing and relative positions to the Fermi level (E_F). This result indicates that the electron density is similar for the two types of films, implying a similar atom density. However, such measurements are not sensitive enough to tell if there is a small difference (i.e., a few percent) in electron density between these two structures.

The superconducting properties of these two types of films, on the other hand, are different. Figure 3A shows tunneling spectra acquired at various temperatures for type I films. The superconducting gap is clearly visible at 3.4 K and gradually disappears as the temperature is raised to 6.0 K. These spectra can be fitted with the Bardeen-Cooper-Schrieffer (BCS)–like density of states (DOS) to obtain a temperature-dependent superconducting gap $\Delta(T)$, which allows us to obtain a T_c of ~4.9 K for the type I film (*19*, *24*). However, tunneling measurements of the type II film (Fig. 3C) did not show any superconducting gap until the temperature drops to 3.5 K, at which point a small gap is observed. Because the T_c is very close to the lower temperature limit of our scanning tunneling microscopy (STM), we did not measure enough temperature-dependent data points to fit for the T_c value. Nevertheless, we estimated the T_c to be ~3.65 ± 0.15 K.

To further illustrate spatial variation of the superconducting property, we plotted the 2D mapping of the second derivative of the current-voltage (*I-V*) curve near the steepest slope of the gap-opening regions. Figure 3E shows a large-area STM image, and Fig. 3, F and G, shows d^2I/dV^2 mapping at biases of –0.89 and 0.89 mV, respectively. Not only does such a second derivative spectroscopic image reveal the large superconductivity contrast between type I and II films, but also it further shows that superconductivity on the same terrace is very uniform, with clear boundaries at the terrace edges.

On such films, one can occasionally find a local region containing coexistence of 4 and 5 ML (Fig. 4A), which allows us to probe the transition region from the ultimate 2-ML limit to thicker regimes that have previously been investigated. On the same sample (and on several subsequently prepared samples), we were not able to find any region with 3-ML film. Even 4-ML regions are quite rare and only can be found when they are connected to 5-ML regions. We take these results as indication of thermodynamic instability at these film thicknesses due to quantum size effect, a subject of extensive investigation in recent years (*12*–*18*). The findings here are consistent with earlier studies, except that they are in an even thinner regime.

The temperature-dependent normalized conductance spectra acquired on 4- and 5-ML films (Fig. 4B) clearly show that the gap in 4-ML films is always deeper than that in 5-ML films at all temperatures. Using the same fitting method, we get the temperature-dependent gap $\Delta(T)$, which was fitted with BCS theory, and we were able to obtain a T_c value of 6.7 K for the 4-ML film and 6.3 K for the 5-ML film (Fig. 4C). The contrast in T_c between 4- and 5-ML films illustrates the continuation of the quantum oscillations in the superconducting gap reported earlier, except that here the oscillation amplitude is further enhanced in the thinner regime (Fig. 1).

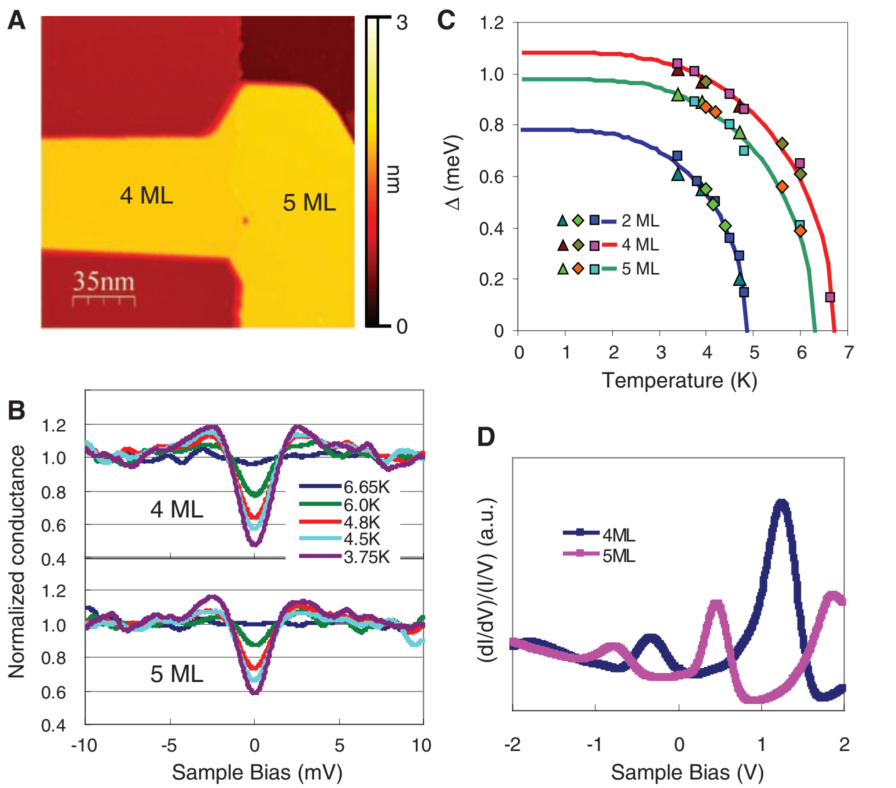

Fig. 4. (**A**) STM image of 4- and 5-ML films. (**B**) Temperature-dependent normalized conductance spectra acquired on 4- and 5-ML films. The gap in 4-ML film is always deeper than that of 5-ML film at all temperatures. (**C**) Fitting with BCS temperature-dependent superconducting gap Δ(T) for 4- and 5-ML and type I 2-ML films. The data consist of results from three independent runs and are labeled with different symbols. T_c values of 6.7 K for the 4-ML film and 6.3 K for the 5-ML film were obtained. (**D**) Tunneling spectra with a larger bias range acquired above T_c for 4- and 5-ML regions, showing QWS.

Consistent with this interpretation are the locations of the QWS of these two thicknesses (Fig. 4D), where one observes that 4-ML films contain a QWS peak closer to E_F.

Theoretically, a simple jellium model predicts that quantum oscillations of the DOS (and, thus, many electronic properties) would increase in amplitude toward thinner thicknesses (*17*). It is interesting to see that quantum oscillations of the T_c follow the same trend. This trend persists down to 4-ML films where two quantum channels still exist. However, such a robust superconducting behavior takes a substantial dive at 2 ML when only one quantum channel exists.

The observation of persistent superconductivity in all but the last stable film (2-ML film), as shown in Fig. 1, is in sharp contrast with results obtained from transport and magnetic susceptibility studies (*7*, *9*). Starting from large film thicknesses, T_c shows an overall decreasing trend with the thinning of film thickness. In these studies, phase coherence of the superconducting order parameter over large scales is required in manifestation of superconductivity, and such phase coherence can easily be affected by scatterings. The gradual degradation of superconductivity was attributed to scattering from roughness at interfaces with the substrate and the covering materials (these other studies were performed ex situ on films covered with a protective layer) (*7*, *9*). On the other hand, our probe is of local nature and is sensitive to the magnitude, rather than the phase, of the order parameter. Moreover, we take special care in the preparation of the substrate, and the Pb film surface is maintained intact in ultrahigh vacuum throughout the measurement stage.

Still, two key questions remain: Why does the T_c drop at 2 ML, and why are the T_c values different for type I and II? We believe that the answer might lie in the fact that even such a pristine film needs to be supported on a substrate. Film-substrate interactions can play an important role in influencing the superconductivity, especially in the 2-ML limit when there is only a single quantum channel of electronic states to support the formation of Cooper pairs or local superconducting ordering. As we described earlier, there are two different atomic arrangements for the 2-ML films: In type I, the underlying 1 × 1 atomic structure has the same lattice parameter as the bulk Pb, whereas in type II, the $\sqrt{3} \times \sqrt{3}$ atomic structure assumes a similar lattice constant as the Si $\sqrt{3} \times \sqrt{3}$ structure. This result indicates that the type II film is under tensile strain laterally. The phonon spectrum and the interaction of phonons with the electrons should be considerably different (*25*–*27*), resulting in a further reduction of T_c. For films of 4 ML or thicker, the atomic structure is close to the bulk atomic structure. With two or more quantum channels of electronic states to support the formation of Cooper pairs, the effect of substrate can be markedly reduced. If this conjecture is correct, one might be able to fine tune the strength of superconducting ordering in the single-channel limit by engineering the film/substrate interface.

References and Notes

1. M. Strongin, R. S. Thompson, O. F. Kammerer, J. E. Crow, *Phys. Rev. B* **1**, 1078 (1970).
2. G. J. Dolan, J. Silcox, *Phys. Rev. Lett.* **30**, 603 (1973).
3. B. G. Orr, H. M. Jaeger, A. M. Goldman, *Phys. Rev. Lett.* **53**, 2046 (1984).
4. R. C. Dynes, A. E. White, J. M. Graybeal, J. P. Garno, *Phys. Rev. Lett.* **57**, 2195 (1986).
5. D. B. Haviland, Y. Liu, A. M. Goldman, *Phys. Rev. Lett.* **62**, 2180 (1989).
6. A. Yazdani, A. Kapitulnik, *Phys. Rev. Lett.* **74**, 3037 (1995).
7. Y. Guo *et al.*, *Science* **306**, 1915 (2004).
8. D. Eom, S. Qin, M.-Y. Chou, C. K. Shih, *Phys. Rev. Lett.* **96**, 027005 (2006).
9. M. M. Özer, J. R. Thompson, H. H. Weitering, *Nat. Phys.* **2**, 173 (2006).
10. M. M. Özer, Y. Jia, Z. Zhang, J. R. Thompson, H. H. Weitering, *Science* **316**, 1594 (2007).
11. T. Nishio *et al.*, *Phys. Rev. Lett.* **101**, 167001 (2008).
12. A. R. Smith, K.-J. Chao, Q. Niu, C. K. Shih, *Science* **273**, 226 (1996).
13. I. B. Altfeder, K. A. Matveev, D. M. Chen, *Phys. Rev. Lett.* **78**, 2815 (1997).
14. V. Yeh, L. Berbil-Bautista, C. Z. Wang, K. M. Ho, M. C. Tringides, *Phys. Rev. Lett.* **85**, 5158 (2000).
15. W. B. Su *et al.*, *Phys. Rev. Lett.* **86**, 5116 (2001).
16. D.-A. Luh, T. Miller, J. J. Paggel, M. Y. Chou, T.-C. Chiang, *Science* **292**, 1131 (2001).
17. C. M. Wei, M. Y. Chou, *Phys. Rev. B* **66**, 233408 (2002).
18. Z. Zhang, Q. Niu, C. K. Shih, *Phys. Rev. Lett.* **80**, 5381 (1998).
19. Supporting material is available on *Science* Online.
20. E. Ganz, I. Hwang, F. Xiong, S. K. Theiss, J. Golovchenko, *Surf. Sci.* **257**, 259 (1991).
21. T. Schmidt, E. Bauer, *Phys. Rev. B* **62**, 15815 (2000).
22. M. Hupalo, J. Schmalian, M. C. Tringides, *Phys. Rev. Lett.* **90**, 216106 (2003).
23. S. M. Lu *et al.*, *Phys. Rev. B* **75**, 113402 (2007).
24. J. Bardeen, L. N. Cooper, J. R. Schrieffer, *Phys. Rev.* **108**, 1175 (1957).
25. D.-A. Luh, T. Miller, J. J. Paggel, T.-C. Chiang, *Phys. Rev. Lett.* **88**, 256802 (2002).
26. J. J. Paggel, D.-A. Luh, T. Miller, T.-C. Chiang, *Phys. Rev. Lett.* **92**, 186803 (2004).
27. F. Yndurain, M. P. Jigato, *Phys. Rev. Lett.* **100**, 205501 (2008).
28. This work was supported by NSF grant DMR-0606485, the Welch Foundation, and the Texas Advanced Research Program.

Supporting Online Material

www.sciencemag.org/cgi/content/full/1170775/DC1
SOM Text
Fig. S1
References

12 January 2009; accepted 16 April 2009
Published online 30 April 2009;
10.1126/science.1170775
Include this information when citing this paper.

Social Transmission of a Host Defense Against Cuckoo Parasitism

Nicholas B. Davies*† and Justin A. Welbergen

Coevolutionary arms races between brood parasites and hosts involve genetic adaptations and counter-adaptations. However, hosts sometimes acquire defenses too rapidly to reflect genetic change. Our field experiments show that observation of cuckoo (*Cuculus canorus*) mobbing by neighbors on adjacent territories induced reed warblers (*Acrocephalus scirpaceus*) to increase the mobbing of cuckoos but not of parrots (a harmless control) on their own territory. In contrast, observation of neighbors mobbing parrots had no effect on reed warblers' responses to either cuckoos or parrots. These results indicate that social learning provides a mechanism by which hosts rapidly increase their nest defense against brood parasites. Such enemy-specific social transmission enables hosts to track fine-scale spatiotemporal variation in parasitism and may influence the coevolutionary trajectories and population dynamics of brood parasites and hosts.

Darwin's concept of the "entangled bank" (*1*) captures an ecological world in which organisms evolve in response to changes not only in the physical environment but also in their competitors, predators, and parasites. Cuckoo-host interactions involve adaptations and counteradaptations in response to selection from the host and the parasite (*2*, *3*) and are a model for investigating the outcome of biotic changes involving coevolution. However, host defenses can be costly. Attacking and mobbing an adult cuckoo can reduce the chance that the host nest is parasitized, but may attract nest predators or other brood parasites and can put the mobbers themselves at risk (*4*). Egg rejection may redeem a host's reproductive investment but entails a risk in that the host could reject its own eggs rather than the parasite egg (*5*). Therefore, defenses are advantageous only above a threshold level of parasitism (*6*, *7*). A host population may experience conditions on either side of this parasitism threshold because of fine-scale spatial and temporal variation in the parasitism rate (*4*, *8*, *9*). Therefore, individual hosts would maximize their fitness by adjusting their defenses according to local cuckoo activity. As predicted, the propensity to mob adult cuckoos increases with local parasitism risk (*4*), and hosts are more likely to reject eggs or desert nests if they see a cuckoo at their nest (*5*, *10*, *11*). Phenotypically flexible host behavior is thus likely to explain small-scale geographical variation in host defenses, as well as result in rapid changes in defenses at a site within seasons and between years (*4*, *9*, *12*).

Host responses to adult cuckoos might involve learning, which would permit hosts to fine-tune defenses to the magnitude of the local threat (*13*). Hosts of the common cuckoo (*Cuculus canorus*) introduced from Britain to New Zealand some 130 years ago, and isolated from that brood parasite ever since, have retained the behavior of rejecting foreign eggs but, unlike their ancestral populations in Europe, do not mob a cuckoo mount (*14*). In general, birds isolated from predators are less responsive to nest enemies but can rapidly learn to increase their response, either from their own experience of predation or by observing others mobbing an enemy (*13*, *15*). This suggests that introduced birds might have lost their response to adult cuckoos through lack of experience with parasitism rather than genetic change (*14*). In central Japan, common cuckoos began to parasitize azure-winged magpies (*Cyanopica cyana*) 40 years ago (*16*). Initially, magpies showed little defense, but aggression toward cuckoos and egg rejection increased more rapidly than can be explained by a change in host genotypes. Instead, it suggests that these birds learned to respond to the cuckoo and to exhibit a preexisting, but phenotypically flexible, egg rejection behavior (*16*).

Hosts might learn to increase their defenses against adult cuckoos from direct experience. However, opportunities for individual learning are limited because cuckoos are very secretive when surveying prospective hosts, and their laying visits are often extremely short [~10 s (*3*)]. Furthermore, close inspection by hosts may be dangerous because cuckoos resemble potentially lethal sparrowhawks (*Accipiter nisus*) (*17*). It is also possible that hosts increase defenses through social learning. When individual learning is costly and environments are variable, models suggest that it is beneficial to use the behavior of others as a source of information about local conditions (*18*). Such information could be socially transmitted, enabling individuals to modify their behavior by observing others (*19*). Social learning could lead to rapid cultural transmission of

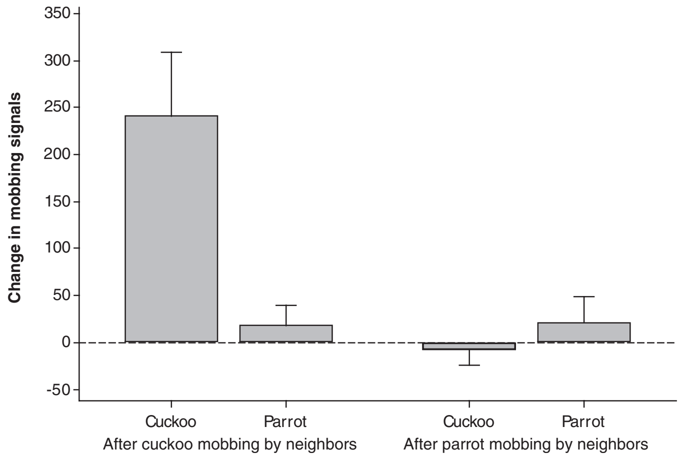

Fig. 1. Change in mobbing signals (number of rasp calls and mandible snaps per 5 min) given by focal pairs at their own nest to presentations of both a model cuckoo and a model parrot, after they had observed mobbing of either a cuckoo (n = 24 nests) or a parrot (n = 17 nests) at the nest on a neighboring territory. The figure plots mean change in response per 5 min (± SE) from trials before to trials after observation of neighbor mobbing (dashed line indicates no change). There was a significant interaction between the response to cuckoo versus parrot and the mobbing experience on the neighboring territory ($F_{1,55.1}$ = 8.84, P = 0.004).

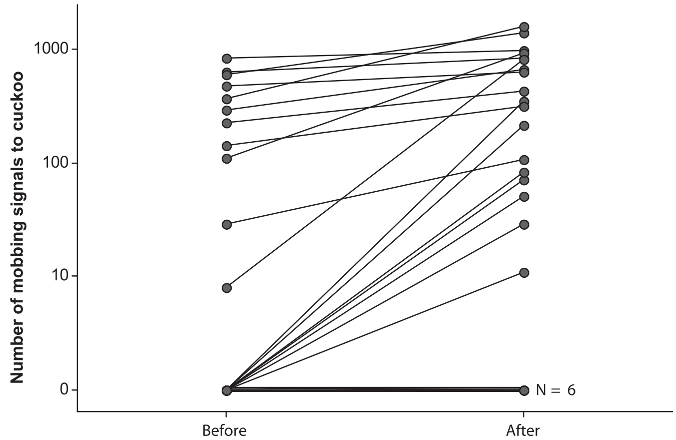

Fig. 2. Number of mobbing signals (rasp calls and mandible snaps per 5 min; log scale) given by focal pairs (n = 24) to a model cuckoo at their own nest, before and after their experience of cuckoo mobbing on the neighboring territory.

Department of Zoology, University of Cambridge, Downing Street, Cambridge CB2 3EJ, UK.

*To whom correspondence should be addressed. E-mail: n.b.davies@zoo.cam.ac.uk
†The authors contributed equally to this work.

defenses in local host populations if naïve birds learn to mob a novel enemy by observing a conspecific mobbing it, and then socially transmit the response to other individuals (*20*).

In fenland sites in Cambridgeshire, UK, where reed warblers (*Acrocephalus scirpaceus*) are the main cuckoo host (*5*), we found a striking dichotomy in reed warbler responses to cuckoo mounts placed next to their nests (*4*). At 48% of nests observed (n = 191), the warblers mobbed the mounts, most of them intensively, with threat postures, swoops, and direct attacks, accompanied by loud rasp calls and bill snaps. However, at 52% of nests, there was no mobbing response, and warblers retreated after a brief inspection of the mount. Part of this variation is related to the degree of parasitism risk. Reed warblers were more likely to risk close inspection and mob if their nest was more vulnerable to parasitism (*4*). However, even at high-risk sites, many reed warblers did not mob. These were more likely to be younger, inexperienced birds, because earlier breeders both mobbed more (*4*) and were likely to be older, returning breeders (*21*). Our previous experiments showed that a resident pair's mobbing calls often attracted birds from neighboring territories (*22*). It is unlikely that reed warblers produced mobbing calls in order to attract neighbors, because mobbing calls were given irrespective of whether other pairs were nesting nearby, and attracted neighbors were often chased away (*22*). Nevertheless, neighbors could eavesdrop on residents' mobbing behavior and thus learn about the danger of cuckoos.

In order to test whether reed warblers acquire or enhance their mobbing defense through social learning from experienced individuals, we examined the response to model cuckoos and parrots (parrots were chosen to represent a novel, harmless intruder) (*21*). At 41 focal nests, we first recorded the baseline response to models as the number of mobbing signals (rasp calls and mandible snaps) given within 5 min after the arrival of the first focal warbler to within 1 m of the model (*21*). Then, the focal pair was given an opportunity for social learning by the placement of either a model cuckoo or a model parrot next to the nest on the adjacent, neighboring territory. Therefore, each focal pair experienced neighbor mobbing of only one of the two models, either a cuckoo (n = 24 nests) or a parrot (n = 17 nests). To encourage a mobbing response from the neighbors and to attract the focal pair into the neighboring territory, a loudspeaker broadcast reed warbler mobbing signals near the model for 10 min (*21*). After this playback period, we recorded the mobbing signals of the neighboring birds for 1 min. Finally, we retested the focal pair with both a cuckoo and a parrot model at their own nest, and then again 3 to 6 days later. We predicted that if social learning was specific for the mobbing stimulus, then the focal pair's mobbing would increase only in response to the model mobbed on the neighboring territory.

Focal pairs were attracted to the models (to a distance of <2 m) at the neighbors' nest in the majority of cases [25 out of 27 (25/27); in 14/41 trials, the vegetation was too dense to record focal bird activity]. They were as likely to be attracted to the neighbors' nest during parrot trials (11/11) as during cuckoo trials (14/16; Fisher's exact test, P = 0.499). Reed warblers normally mob model cuckoos much more strongly than model parrots (*4*), but our data show that the playback stimulated equally strong neighbor mobbing of both models. Neighbors were as likely to mob the parrot (14/17) as the cuckoo model (19/24; P = 1.0) and gave as many mobbing signals to the parrot (mean ± 1 SE, 57.1 ± 17.9/min) as to the cuckoo (66.4 ± 14.9/min; t test, t_{34} = 0.40, P = 0.692). Therefore, parrot and cuckoo presentations on neighboring territories provided equal opportunities for social learning by the focal birds. The proportion of neighbors that mobbed the cuckoo after hearing the playbacks was significantly higher than the proportion of focal pairs that mobbed the cuckoo in baseline trials (19/24 versus 18/41; χ^2 = 7.68, df = 1, P = 0.006). Thus, not only does mobbing attract neighboring individuals (*22*), it can also be induced by mobbing signals [response facilitation (*19*)] and so is a likely candidate for social transmission.

Nevertheless, when a parrot was mobbed on the neighboring territory it had no effect on the mobbing of either parrots or cuckoos by focal pairs at their own nests. In contrast, neighbors mobbing a cuckoo led to a marked increase in focal pair mobbing, but only of cuckoos, not of parrots (Fig. 1). Therefore only cuckoo mobbing led to a response, and furthermore, observational conditioning (*19*) was specific to cuckoos. This result is not confounded by the fact that focal individuals that experienced cuckoo mobbing on a neighboring territory encountered a cuckoo three times during our experimental trials, whereas those that experienced parrot mobbing encountered cuckoos just twice (*21*).

After experiencing neighbor mobbing of a cuckoo, all 11 focal pairs that mobbed the cuckoo in their first, baseline trial increased their cuckoo mobbing, and 7/13 focal pairs that did not mob the cuckoo on the first trial now did so (Fig. 2). We were unable to explain why six of the pairs retained a nonmobbing response; the increase in mobbing by the focal pair was not related to whether we saw them attracted to the neighbors' nest ($F_{1,3.5}$ = 0.35, P = 0.581), nor to the magnitude of the neighbors' mobbing response ($F_{1,17.8}$ = 0.08, P = 0.776). Fourteen of the 24 focal pairs that experienced neighbor mobbing of cuckoos were retested with the cuckoo model 3 to 6 days later (*23*); their mobbing response was still significantly higher than on the first, baseline trial (paired t test, t_{13} = 2.55, P = 0.024) and as strong as on the previous post–social learning trial (t_{13} = –1.19, P = 0.255), indicating that any increased mobbing response was retained.

Cuckoo mobbing by neighbors alerted the focal pair, resulting in a relatively quicker inspection of both cuckoo and parrot mounts as compared to parrot mobbing (Fig. 3). This suggests that focal pair attention is directed at the neighbor responses toward specific enemies, not just at any intruder. This response to cuckoos is most likely adaptive because female cuckoos have laying territories (*5*), and cuckoo activity on a neighbor's territory signals an increased risk of parasitism (*4*). More rapid inspection of potential nest enemies is typical of reed warblers nesting in sites with a high risk of parasitism (*21*). The specific increase in cuckoo mobbing (Fig. 1) suggests that reed warblers may be predisposed to learn to target cuckoos. However, it is also possible that response intensity increased toward the cuckoo mounts because our procedures added to their stimulus salience because of prior experience with cuckoos, which could not have been the case for parrots. Predispositions to learn to respond to stimuli relevant to survival and reproduction have been demonstrated in rhesus macaques (*Macaca mulatta*), in which social learning readily leads to fear of snakes but not of harmless stimuli, such as flowers and rabbits (*24*).

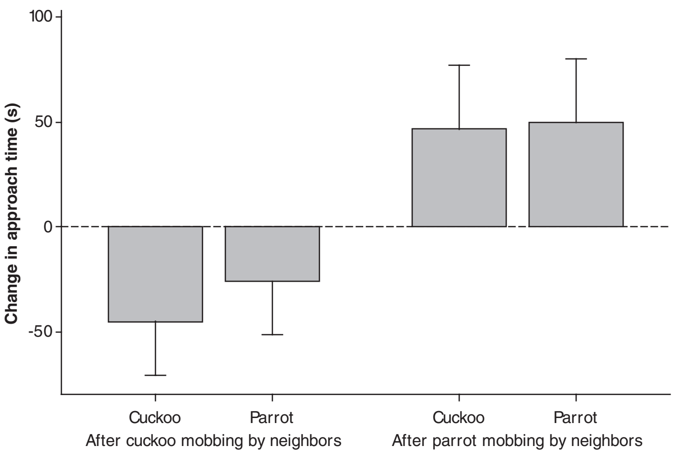

Fig. 3. Change in a focal pair's time to first approach to cuckoo and parrot models presented at their own nest, after experiencing mobbing of either a cuckoo (n = 24 nests) or a parrot (n = 17 nests) at a nest on a neighboring territory. The figure plots mean ± SE change in approach time from trials before to trials after observation of neighbor mobbing. There was an effect of mobbing experience on the neighboring territory ($F_{1,78.0}$ = 7.23, P = 0.009) but no effect of model type ($F_{1,78.0}$ = 0.11, P = 0.738) and no interaction between mobbing experience and model type ($F_{1,78.0}$ = 0.00, P = 0.966).

Reed warblers distinguish cuckoos from other nest enemies (*22*) and specifically adjust cuckoo mobbing to local parasitism risk (*4*). The specificity of social learning observed here provides evidence that mobbing is a phenotypically plastic trait, adaptive in the context of brood parasitism. We suggest that naïve individuals may learn from bolder birds or from those who, by chance, observed a cuckoo depredate or parasitize their nest. Further experiments are needed to test whether social learning leads only to a change in the perception of parasitism risk or also may involve the refining of a template for cuckoo recognition, akin to the genetic predispositions that guide learning in other contexts (*13*).

Social learning could trigger a marked increase in host defenses; by focusing on neighbors' responses to adult cuckoos, focal pairs not only increase cuckoo mobbing as a front line of defense (*4*) but are also alerted to increased vigilance (*11*) and egg rejection (*5*, *10*). Therefore, our results support the hypothesis that rapid changes in host defenses (*14*, *16*) may reflect social transmission of responses to adult cuckoos as nest enemies. Social learning has implications for the coevolutionary trajectories of brood parasites and hosts because it promotes phenotypic plasticity that can drive or impede genetic evolution (*25*). Furthermore, by influencing how rapidly hosts lose or gain defenses, social learning may affect the population dynamics of both brood parasites and hosts (*26*).

References and Notes

1. C. Darwin, *On the Origin of Species* (Murray, London, 1859).
2. S. I. Rothstein, S. K. Robinson, Eds., *Parasitic Birds and Their Hosts: Studies in Coevolution* (Oxford Univ. Press, Oxford, 1998).
3. N. B. Davies, *Cuckoos, Cowbirds and Other Cheats* (Poyser, London, 2000).
4. J. A. Welbergen, N. B. Davies, *Curr. Biol.* **19**, 235 (2009).
5. N. B. Davies, M. de L. Brooke, *Anim. Behav.* **36**, 262 (1988).
6. A. Lotem *et al.*, *Anim. Behav.* **49**, 1185 (1995).
7. N. B. Davies *et al.*, *Proc. R. Soc. London Ser. B* **263**, 925 (1996).
8. I. J. Øien *et al.*, *J. Anim. Ecol.* **65**, 147 (1996).
9. A. K. Lindholm, *J. Anim. Ecol.* **68**, 293 (1999).
10. A. Moksnes *et al.*, *Ibis* **142**, 247 (2000).
11. N. B. Davies *et al.*, *Anim. Behav.* **65**, 285 (2003).
12. M. de L. Brooke *et al.*, *Proc. R. Soc. London Ser. B* **265**, 1277 (1998).
13. A. S. Griffin, *Learn. Behav.* **32**, 131 (2004).
14. K. Hale, J. V. Briskie, *J. Avian Biol.* **38**, 198 (2007).
15. R. F. Maloney, I. G. MacLean, *Anim. Behav.* **50**, 1193 (1995).
16. H. Nakamura *et al.*, in *Parasitic Birds and Their Hosts: Studies in Coevolution*, S. I. Rothstein, S. K. Robinson, Eds. (Oxford Univ. Press, Oxford, 1998), pp. 94–112.
17. N. B. Davies, J. A. Welbergen, *Proc. R. Soc. London Ser. B* **275**, 1817 (2008).
18. R. Boyd, P. J. Richerson, *Lect. Math Life Sci.* **20**, 1 (1989).
19. W. Hoppitt, K. N. Laland, *Adv. Stud. Behav.* **38**, 105 (2008).
20. E. Curio *et al.*, *Science* **202**, 899 (1978).
21. See supporting material on *Science* Online for methods and additional text and data.
22. J. A. Welbergen, N. B. Davies, *Anim. Behav.* **76**, 811 (2008).
23. These tests included 5/11 that mobbed during the baseline trial, 5/7 that did not mob during the baseline trial but did so after social learning, and 4/6 that retained a nonmobbing response throughout.
24. M. Cook, S. Mineka, *J. Abnorm. Psychol.* **98**, 448 (1989).
25. T. D. Price *et al.*, *Proc. R. Soc. London Ser. B* **270**, 1433 (2003).
26. F. Takasu *et al.*, *Am. Nat.* **142**, 819 (1993).
27. We thank the Natural Environment Research Council; the National Trust, C. Thorne, and the Wicken Fen Group; English Nature; and M. Brooke, J. Davies, R. Kilner, O. Krüger, and the Behavioural Ecology Group at Cambridge.

Supporting Online Material
www.sciencemag.org/cgi/content/full/324/5932/1318/DC1
Materials and Methods
SOM Text
Fig. S1
References

12 February 2009; accepted 20 April 2009
10.1126/science.1172227

Epigenetic Temporal Control of Mouse *Hox* Genes in Vivo

Natalia Soshnikova[1] and Denis Duboule[1,2]*

During vertebrate development, the temporal control of *Hox* gene transcriptional activation follows the genomic order of the genes within the *Hox* clusters. Although it is recognized that this "*Hox* clock" serves to coordinate body patterning, the underlying mechanism remains elusive. We have shown that successive *Hox* gene activation in the mouse embryo is closely associated with a directional transition in chromatin status, as judged by the dynamic progression of transcription-competent modifications: Increases in activation marks correspond to decreases in repressive marks. Furthermore, using a mouse in which a *Hox* cluster was split into two pieces, we document the necessity to maintain a clustered organization to properly implement this process. These results suggest that chromatin modifications are important parameters in the temporal regulation of this gene family.

Hox genes, which are generally arranged in clusters at genomic loci, are essential for patterning the anterior to posterior animal body axis (*1*–*3*). In vertebrates, these genes are activated in a time sequence that follows their physical order within the cluster, a process referred to as temporal collinearity (*4*). This property is observed in animals developing their trunk via a rostral to caudal time sequence, yet the underlying molecular mechanism is elusive (*5*, *6*). A progressive transition in chromatin state was hypothesized (*7*, *8*), whereby an initially repressed configuration becomes open for transcription. The subsequent observation of chromatin decondensation at these loci when transcription is induced supported this hypothesis (*9*).

Hox genes are repressed by Polycomb group (PcG) proteins (*10*). Mutation of *PcG* genes induces ectopic *Hox* expression and results in posterior homeotic transformations (*11*, *12*). PcG proteins form large complexes with histone-modifying activities; for example, Polycomb Repressive Complex 2 (PRC2) trimethylates histone H3 at lysine 27 (H3K27me3) (*13*–*16*), an essential modification for long-term repression of target genes. In contrast, *Trithorax* group (TrxG) proteins antagonize *PcG* proteins and activate target gene expression (*10*). TRX complexes trimethylate histone H3 at lysine 4 (H3K4me3), a mark generally associated with active transcription (*17*). Genome-wide studies of both H3K27me3 and H3K4me3 modifications in embryonic stem cells (ESC) and other cultured cells have revealed specific profiles during the maintenance phase of *Hox* gene expression in vitro (*18*–*21*). We looked at the in vivo dynamics of chromatin marks during the sequential activation of *Hoxd* genes in developing murine tail buds.

We dissected out mouse tail buds during late somitogenesis when the last *Hox* genes become transcribed (*22*) and performed expression profiling at E8.5 (embryonic day 8.5), E9.0, and E9.5 (Fig. 1A) using tiling arrays covering 2 Mb of DNA containing the *HoxD* cluster. This highly syntenic region (*23*) also contains four ubiquitously expressed genes, *Atp5g3*, *Lnp*, *Mtx2,* and *Hnrpa3*, and two gene deserts (fig. S1). Transcription of *Hoxd1* to *Hoxd9* was active at all three time points (Fig. 1B), reflecting the onset of *Hox* gene transcription during early gastrulation. However, transcriptional progression was observed for more posterior genes, with *Hoxd10* and *Hoxd11* transcribed at E9.0 (Fig. 1B), whereas by E9.5 transcriptional activity had spread over *Hoxd12*, *Hoxd13*, and the nearby neighbor gene *Evx2* (Fig. 1B). Low transcript levels were detected for *Hoxd13* before activation of *Hoxd10* (Fig. 1B, arrow).

We mapped the sites occupied by RNA polymerase II using chromatin immunoprecipitation combined with hybridization on tiling array (ChIP-chip) (Fig. 1B and fig. S1). The Pol II profile corresponded to transcribed regions; whereas virtually no Pol II was scored centromeric to *Hoxd10* at E8.5, signals were detected for both *Hoxd10* and *Hoxd11* at E9.0. At E9.5, the whole centromeric part of the cluster was fully occupied by Pol II (Fig. 1B), indicating that it was recruited in a collinear manner too. In agreement with transcript profiling, a weak Pol II binding was scored at the *Hoxd13* locus at E8.5. Similarly, high levels of H3K9/K14 acetylation (AcH3) were found in

[1]National Research Centre Frontiers in Genetics, Department of Zoology and Animal Biology, University of Geneva, Sciences III, Quai Ernest-Ansermet 30, 1211 Geneva 4, Switzerland. [2]National Research Centre Frontiers in Genetics, School of Life Sciences, Federal Institute of Technology (EPFL), Lausanne, Switzerland.

*To whom correspondence should be addressed. E-mail: Denis.Duboule@unige.ch; Denis.Duboule@epfl.ch

E8.5 tail buds, covering from *Hoxd1* to *Hoxd9* (Fig. 1B). However, AcH3 marks were also scored over the silenced *Hoxd10* and *Hoxd11* (Fig. 1B, arrowheads). Along with the transcriptional activation of these two genes, the levels of AcH3 were expanded to cover the entire gene cluster by day 9.5, matching both the presence of Pol II and the robust transcription of the *Hoxd10* to *Hoxd13* interval. As for *Hox* genes, AcH3 modification appeared at the *Evx2* locus before Pol II binding was scored, consistent with a role for this modification in transcriptional initiation (*17*).

We next investigated the status of both H3K27 and H3K4 trimethylation. H3K27me3 levels were assessed in E8.5 and E9.5 tail buds and in ESC. In ESC, consistent with previous studies (*19*, *20*), H3K27me3 marks, associated with transcriptional repression, covered the entire gene cluster (Fig. 2). Accordingly, transcription of *Hoxd* genes was not detected in these cells (Fig. 2, RNA). During collinear activation in tail buds, a complete loss of H3K27me3 mark was progressively observed over the telomeric part of the cluster, initially from *Hoxd1* to *Hoxd4* at E8.5 and subsequently extending until *Hoxd11* at E9.5 (Fig. 2). Because H3K27me3 disappeared upon gene activation, we conclude that tail bud cells that do not express any *Hox* gene do not implement this repression. H3K27me3 marks slightly overlapped with transcriptionally active regions, for example, over the *Hoxd11-Hoxd12* loci at E9.5 (Fig. 2 and fig. S2), likely illustrating some temporal heterogeneity in the activation of *Hoxd* genes within neighboring cells. Also, samples may have included mixtures of cells expressing and cells not expressing a particular *Hox* gene because of the anterior-posterior extent of the dissected domains. Finally, the H3K27me3 signals were higher over the silenced part of the *Hox* gene cluster in E8.5 tail bud cells than in ESC, suggesting that a tighter repression is implemented during axial development.

We checked whether this progressive demethylation of H3K27 was paralleled by an increased trimethylation of H3K4. Consistent with previous results (*24*), we scored low levels of H3K4me3 over *HoxD* in ESC, with residual signals on CpG islands (Fig. 2). In E8.5 tail buds, however, H3K4me3 marks drastically increased and covered the telomeric part of the cluster up to both *Hoxd10* and *Hoxd11*, which are still silenced at this time point (Fig. 2). Therefore, as for AcH3, H3K4me3 marks were detected before Pol II binding and prelabeled future sites of transcription. At E9.5, elevated levels of H3K4 trimethylation over the *Hoxd12* and *Hoxd11* loci corresponded to their robust transcriptional activation (Fig. 2). Altogether, temporal collinearity in tail buds corresponds to chromatin dynamics, progressing along the cluster and involving the removal of H3K27me3 marks, the methylation of H3K4, and the acetylation of H3. Transcriptional activation along the gene cluster occurs within a region of transition between H3K27me3 and H3K4me3 marks, a window that shifts with time toward the centromeric extremity of the cluster (fig. S2).

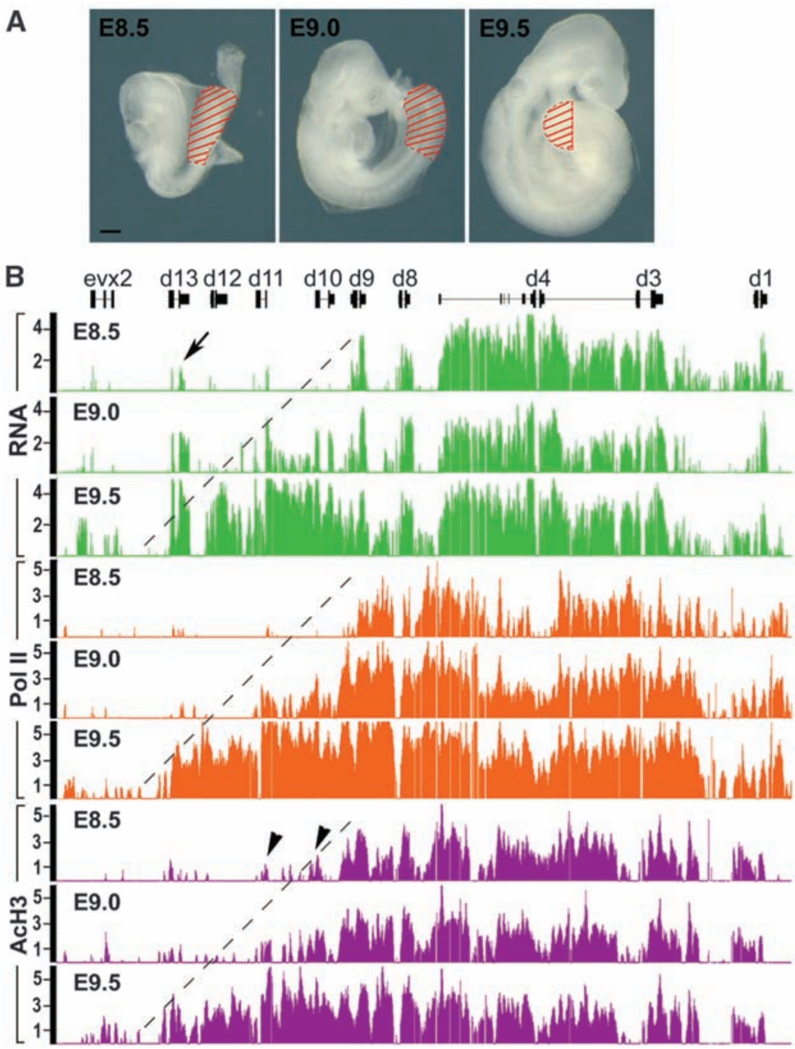

Fig. 1. Collinear activation of *Hoxd* genes during axial development. (**A**) E8.5, E9.0, and E9.5 embryos, with dissected samples indicated in red. Scale bar, 200 μm. (**B**) Transcript profiles on tiling arrays using reverse-transcribed total RNA (green). Bound RNA Pol II (orange) and the AcH3 pattern (magenta) are also displayed for the *HoxD* cluster. The *y* axis indicates the $\log_2$ ratio of cDNA/genomic DNA or ChIP-enriched/input signal intensity.

This collinear chromatin dynamic suggests a mechanism whereby modifications would spread from the telomeric extremity of the cluster to the opposite end. We assessed this possibility by using mice where the *HoxD* cluster is split into two pieces, separated by a 3-Mb inversion (*25*) (Fig. 3A). In this configuration, the *Hoxd11* to *Hoxd13* region becomes isolated from the rest of the cluster. This allows a test of whether early establishment and dynamic progression of both H3K27me3 and H3K4me3 marks require an integral gene cluster.

From *Hoxd1* to *Hoxd9*, the mutant (*inv*) transcript profile was as in wild type (Fig. 3B), demonstrating that cis regulations required to initiate transcription of these genes either lie within this segment of the cluster or are telomeric (*26*). However, differences were observed close to the break point. First, *Hoxd10* was transcribed at E8.5, whereas this gene is normally silent at this stage. Second, ectopic antisense transcripts were detected in the small posterior half-cluster (fig. S3A), likely triggered by the new genomic neighborhood. As in wild type, premature *Hoxd13* transcription was scored in *inv* mutants, indicating that this transcriptional activity does not require telomeric-located regulatory sequences controlling other genes of the cluster. This late-occurring leakage in temporal collinearity may reflect the spurious activity of enhancers located nearby and dedicated to strongly activate this gene in subsequent morphological contexts (*27*). In E9.5 *inv* tail buds, neither *Hoxd12* nor *Hoxd11* showed transcriptional increase (fig. S3B). Their expression was slightly elevated between E8.5 and E9.5 but remained very low when compared to the wild-type situation. On the other side of the breakpoint, *Hoxd10* transcription peaked as in wild type, whereas transcripts located upstream of *Hoxd10* and originating from the *Hoxd11* locus were reduced in amount due to the break (fig. S3B).

ChIP-chip analyses of H3K4me3 distribution in E8.5 homozygous *inv* tail buds showed enrichment over the *Hoxd12* to *Hoxd10* region, on both sides of the break point (Fig. 3C), whereas

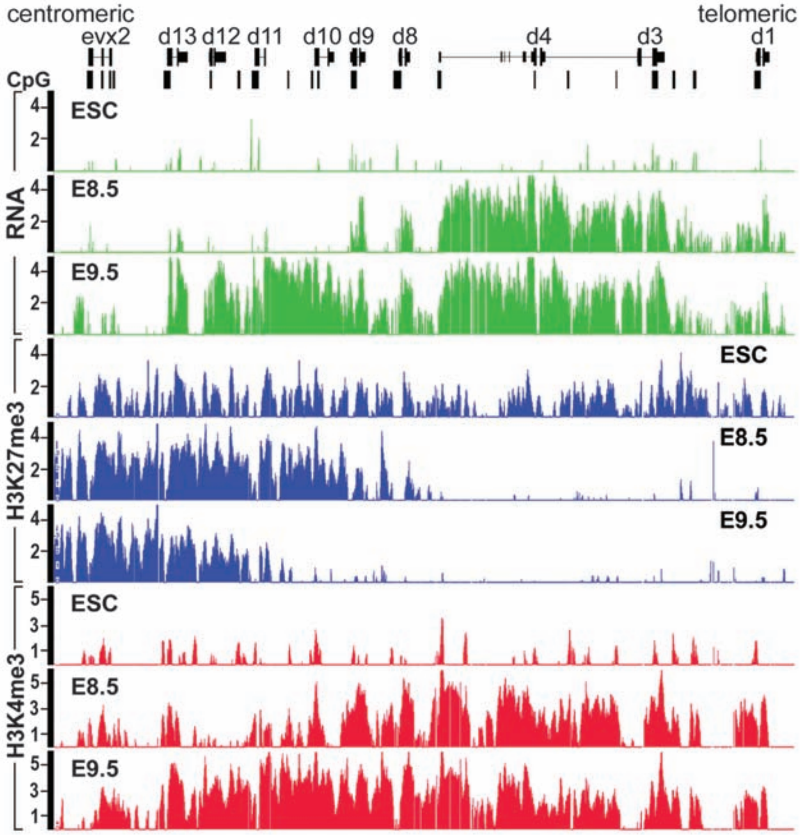

Fig. 2. Chromatin marks during temporal collinearity. Transcriptional activities (green) are shown in ESC and in E8.5 and E9.5 embryos. In ESC, a 120-kb domain is decorated by H3K27me3 (blue), yet at rather low density. In the embryo, H3K27me3 marks progressively retract from the telomeric to the centromeric extremity of the cluster. In addition, levels of H3K27me3 modifications found over silenced genes are higher than in ESC. Low enrichment ($\log_2 \leq 1$) for H3K4me3 (red) marks all CpG islands within *HoxD* in ESC, as opposed to the strong levels ($\log_2 = 4$) detected over *Hoxd1* to *Hoxd9* at E8.5. An increase ($\log_2 \leq 3$) in H3K4me3 marks was also detected at the silenced *Hoxd10*, *Hoxd11*, and *Evx2* loci at this early stage, in the absence of detectable transcripts.

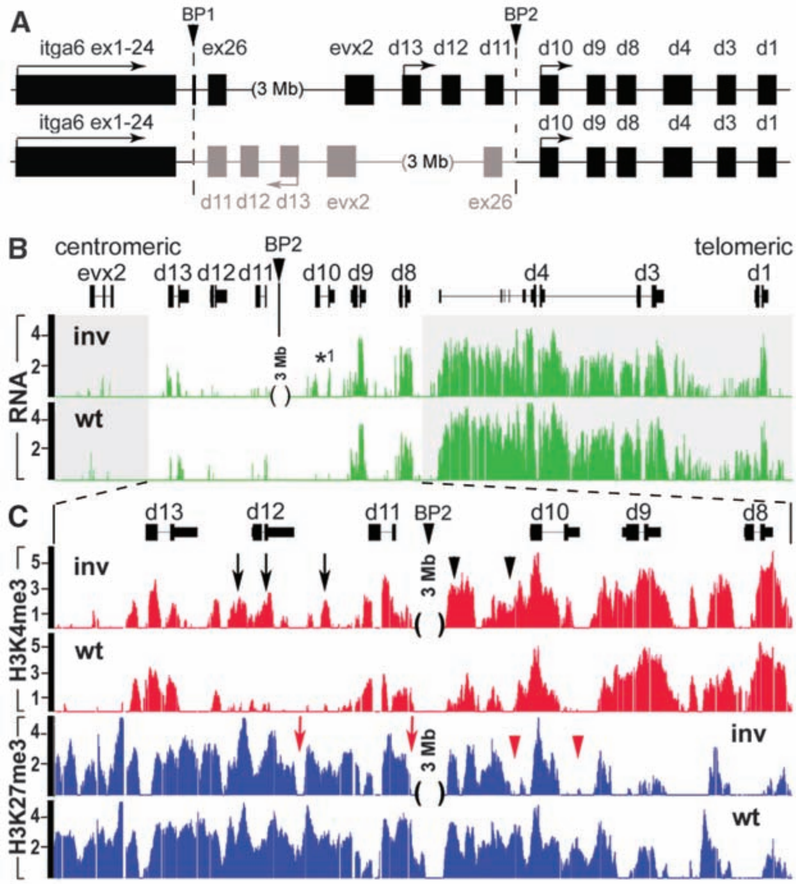

Fig. 3. Transcriptional activation in a split *HoxD* cluster. (**A**) Scheme of the *Integrin-alpha6* (*Itga6*)-*HoxD* inversion (in gray). Dashed lines and arrowheads indicate both breakpoints (BP1 and BP2), either between exons 24 and 26 of *Itga6* or between *Hoxd11* and *Hoxd10*. The inversion positions the centromeric *Hoxd13* to *Hoxd11* DNA segment 3 Mb away from the rest of the cluster. (**B**) Transcript profiles (green) in wild-type (wt) and mutant (*inv*) tail buds at E8.5. Animals with a split cluster activate *Hoxd10* prematurely (E8.5, *1). Only the RNA representing the *Hox*-coding DNA strand is shown (see also fig. S3A). The position of both the break point (BP2) and the 3-Mb interval is indicated. (**C**) Enlargement of the *Hoxd13* to *Hoxd8* region shown in (B) with both H3K4me3 (red) and H3K27me3 (blue) profiles in E8.5 tail buds. Elevated levels of H3K4me3 marks are scored over *Hoxd10*, *Hoxd11*, and *Hoxd12* (black arrows and arrowheads). H3K27me3 marks are reduced at and around the *Hoxd10* locus (red arrowheads) and, to a lesser extent, over *Hoxd11* and *Hoxd12* (red arrows).

the profile from *Hoxd9* to *Hoxd1* was comparable to wild type. The robust gain in H3K4me3 marks over *Hoxd12* was not scored in older wild-type tail buds (fig. S2) and did not match any transcriptional activity, neither for *Hoxd12* nor for *Hoxd11* (Fig. 3B). In this case, both *Hoxd11* and *Hoxd12* were ready to be transcribed (*28*), yet they remained silent because they were moved away from the required enhancer sequence located telomeric to the breakpoint. In contrast, increased H3K4 trimethylation on the other side of the breakpoint (Fig. 3C) matched the premature activation of *Hoxd10*.

The DNA interval decorated by H3K27me3 marks in *inv* mutants was virtually identical to wild type (Fig. 3C), indicating that an integral cluster is not necessary to define the initial extent of the repressive domain; H3K27me3 marks were positioned over posterior genes even though these genes were disconnected from the rest of the cluster, thus ruling out the existence of a spreading mechanism sensu stricto for the implementation of this repression. In addition, the overall density of these marks on both sides of the break point was considerably below the wild-type situation (Fig. 3C). In the posterior half-cluster, H3K27me3 marks were distributed almost as in wild type over *Evx2* and *Hoxd13*, whereas a decrease was scored over the *Hoxd12* to *Hoxd11* intergenic region and 3′ to *Hoxd11* (Fig. 3C). In the anterior half-cluster, a similar reduction was detected at the *Hoxd10* locus, consistent with its premature activation and, to a lesser extent, over *Hoxd9* (Fig. 3C). This weakening in H3K27me3 signal over *Hoxd10* was not observed at the wild-type locus, even in older tail buds (fig. S2). The general decrease in H3K27 trimethylation around the break point suggests that a dense coverage of the *HoxD* cluster by this histone modification requires an intact clustered configuration. Whereas isolated parts of the gene cluster can be trimethylated at H3K27 independently of one another, these various parts may cooperate and synergize to mediate a dense pattern of methylation, potentially through local cis interactions.

These results shed light on the general regulatory strategy implemented by *Hox* gene loci during the earliest steps of mouse trunk development. Unlike in *Drosophila*, mammalian *Hox* gene loci appear refractory to transcription before transcription initiates, as indicated by high levels of H3K27me3 marks covering the *HoxD* locus early on. This likely reflects the necessity to prevent the premature activation of posterior genes at a time when anterior structures are being determined, which would be deleterious to the embryo. During gastrulation, this repression is counteracted by an activity progressing from the telomeric to the centromeric extremity of the cluster, illustrated by both an elevation of H3K4me3 level and the demethylation of H3K27me3. The region of transition between these two states of chromatin corresponds to the dynamic window wherein *Hoxd* genes become transcriptionally active. Alternatively, *Hox* genes could be activated from a persisting pool of nonexpressing stem cells. In this view, the chromatin modifications observed in our samples reflect the average of successive waves of transcriptional activation rather than a dynamic process occurring in the same cells. We do not favor this possibility because such a pool of *Hox*-negative cells would constitute a large fraction of the tissue sample, yet it has never been observed in gastrulating tail buds. Also, the nucleosomes of these stem cells would lack the repressive marks over the *HoxD* cluster, unlike in ESC. Finally, *Hox* genes are activated in cells already expressing more anterior combinations thereof.

We have shown that gene clustering is not necessary for the initial definition of the H3K27me3 landscape. However, clustering is required for a full repression to be consolidated and/or maintained over the cluster, which suggests a synergistic effect due to *Hox* genes' density. Likewise, whereas an integral cluster appears dispensable for selecting the sites of H3K4 trimethylation, gene clustering helps the coordination of this general transition in chromatin status because split clusters displayed premature H3K4me3 marks on either side of the breakpoint. Although the gain of H3K4me3 and the concurrent weakening of H3K27me3 at the mutant *Hoxd10* locus coincided with its early ectopic transcription, similar imbalances at the inverted *Hoxd11* and *Hoxd12* loci did not elicit the same transcriptional response. From this, we conclude that H3K4me3 chromatin modification is necessary but not sufficient for proper *Hox* gene transcriptional control and that remote enhancer sequences must have contributed to the maintenance of clustered organization during animal evolution.

References and Notes

1. D. Duboule, P. Dollé, *EMBO J.* **8**, 1497 (1989).
2. A. Graham, N. Papalopulu, R. Krumlauf, *Cell* **57**, 367 (1989).
3. R. Krumlauf, *Cell* **78**, 191 (1994).
4. J. C. Izpisúa-Belmonte, H. Falkenstein, P. Dollé, A. Renucci, D. Duboule, *EMBO J.* **10**, 2279 (1991).
5. D. Duboule, *Development* **134**, 2549 (2007).
6. M. Kmita, D. Duboule, *Science* **301**, 331 (2003).
7. P. Dollé, J. C. Izpisúa-Belmonte, H. Falkenstein, A. Renucci, D. Duboule, *Nature* **342**, 767 (1989).
8. T. Kondo, D. Duboule, *Cell* **97**, 407 (1999).
9. S. Chambeyron, W. A. Bickmore, *Genes Dev.* **18**, 1119 (2004).
10. Y. B. Schwartz, V. Pirrotta, *Nat. Rev. Genet.* **8**, 9 (2007).
11. J. Simon, A. Chiang, W. Bender, *Development* **114**, 493 (1992).
12. M. van Lohuizen, *Cell. Mol. Life Sci.* **54**, 71 (1998).
13. R. Cao *et al.*, *Science* **298**, 1039 (2002).
14. B. Czermin *et al.*, *Cell* **111**, 185 (2002).
15. A. Kuzmichev, K. Nishioka, H. Erdjument-Bromage, P. Tempst, D. Reinberg, *Genes Dev.* **16**, 2893 (2002).
16. J. Müller *et al.*, *Cell* **111**, 197 (2002).
17. T. Kouzarides, *Cell* **128**, 693 (2007).
18. B. E. Bernstein *et al.*, *Cell* **120**, 169 (2005).
19. A. P. Bracken, N. Dietrich, D. Pasini, K. H. Hansen, K. Helin, *Genes Dev.* **20**, 1123 (2006).
20. T. I. Lee *et al.*, *Cell* **125**, 301 (2006).
21. J. L. Rinn *et al.*, *Cell* **129**, 1311 (2007).
22. J. Deschamps, J. van Nes, *Development* **132**, 2931 (2005).
23. A. P. Lee, E. G. Koh, A. Tay, S. Brenner, B. Venkatesh, *Proc. Natl. Acad. Sci. U.S.A.* **103**, 6994 (2006).
24. B. E. Bernstein *et al.*, *Cell* **125**, 315 (2006).
25. F. Spitz, C. Herkenne, M. A. Morris, D. Duboule, *Nat. Genet.* **37**, 889 (2005).
26. P. Tschopp, B. Tarchini, F. Spitz, J. Zakany, D. Duboule, *PLoS Genet.* **5**, e1000398 (2009).
27. T. Montavon, J. F. Le Garrec, M. Kerszberg, D. Duboule, *Genes Dev.* **22**, 346 (2008).
28. A. S. Chi, B. E. Bernstein, *Science* **323**, 220 (2009).

29. We thank T. Montavon, A. Puglisi, and D. Schübeler for advice; F. Chabaud for cell culture; and P. Descombes and members of the Genomics Platform for their help with tiling arrays. N.S. was supported by a European Molecular Biology Organization long-term fellowship. This work was funded by the University of Geneva, the Federal Institute of Technology in Lausanne, the Swiss National Research Fund, the National Research Center Frontiers in Genetics, and the European Union program Crescendo. Data and analysis are available for download from ArrayExpress (accession E-TABM-677).

Supporting Online Material
www.sciencemag.org/cgi/content/full/324/5932/1320/DC1
Materials and Methods
Figs. S1 to S3
References

27 January 2009; accepted 17 April 2009
10.1126/science.1171468

McsB Is a Protein Arginine Kinase That Phosphorylates and Inhibits the Heat-Shock Regulator CtsR

Jakob Fuhrmann,[1]* Andreas Schmidt,[2]* Silvia Spiess,[3] Anita Lehner,[1] Kürşad Turgay,[4] Karl Mechtler,[1,5] Emmanuelle Charpentier,[3,6] Tim Clausen[1]†

All living organisms face a variety of environmental stresses that cause the misfolding and aggregation of proteins. To eliminate damaged proteins, cells developed highly efficient stress response and protein quality control systems. We performed a biochemical and structural analysis of the bacterial CtsR/McsB stress response. The crystal structure of the CtsR repressor, in complex with DNA, pinpointed key residues important for high-affinity binding to the promoter regions of heat-shock genes. Moreover, biochemical characterization of McsB revealed that McsB specifically phosphorylates arginine residues in the DNA binding domain of CtsR, thereby impairing its function as a repressor of stress response genes. Identification of the CtsR/McsB arginine phospho-switch expands the repertoire of possible protein modifications involved in prokaryotic and eukaryotic transcriptional regulation.

One of the most intensely studied stress-response pathways is the bacterial heat-shock response. In the Gram-positive model organism *Bacillus subtilis*, the heat-shock response is mediated by a complex regulatory network (*1*, *2*) that is under control of at least four major transcriptional regulators, including the alternative sigma factor σB (*3*), the two-component response regulator CssR (*4*), and the repressors HrcA (*5*) and CtsR (*6*, *7*). The latter factor, CtsR, controls the expression of genes encoding the HSP100/Clp chaperones and the protease ClpP (*6*, *8*) that constitute the core of the bacterial protein quality control system (*9*, *10*). CtsR is encoded by the first gene of the *clpC* operon that includes *ctsR*, *mcsA*, *mcsB*, and *clpC* (*6*). The dimeric repressor consists of an N-terminal domain with a helix-turn-helix (HTH) motif and a C-terminal domain of unknown function (*11*). In *B. subtilis*, CtsR represses transcription of the *clpC* heat shock operon and the *clpE* and *clpP* genes by binding specifically to a seven-nucleotide direct repeat sequence located upstream of the transcriptional start sites (*7*). Stress-induced transcription of the *clp* genes depends on the inactivation of CtsR by McsB (*12*). McsB shows pronounced homology to phosphagen kinases (PhKs) and has been reported to exhibit tyrosine kinase activity (*12*, *13*). Under normal growth conditions, McsB is captured and inhibited by ClpC. However, when bacteria are exposed to stress situations, the ClpC chaperone preferentially interacts with misfolded proteins. It is assumed that the released McsB can now form a complex with CtsR, thereby displacing it from DNA and inducing the expression of heat-shock genes (*14*). Alternatively, the phosphorylation of CtsR by McsB may be critical for the release of the repressor from DNA (*12*). To clarify and delineate the precise function of CtsR and McsB in the bacterial stress response, we screened the respective proteins from various Gram-positive bacteria for recombinant production and succeeded in reconstituting the *Bacillus stearothermophilus* CtsR/McsB system in vitro.

To uncover how McsB modulates the repressor activity of CtsR, we performed electrophoretic mobility shift assays (EMSAs) (Fig. 1A). Addition of CtsR to the 258–base pair (bp) *clpC* promoter containing three *ctsr* half sites led to a substantial band shift caused by the formation of a $CtsR_4$/DNA complex. Addition of McsB yielded two lower migrating bands that represent $CtsR_2$/DNA and free DNA. The McsB-dependent release of CtsR was observed only in the presence of Mg/adenosine triphosphate (ATP), whereas addition of EDTA or phosphatase counteracted the effect of McsB. Because no protein-protein interaction could be detected by native gel analysis or size exclusion chromatography, we speculated that McsB and CtsR interact transiently and that phosphorylation of CtsR by McsB abolishes its binding to DNA. To test this hypothesis, CtsR was incubated with McsB in the presence of ATP, and subsequently, phosphorylated CtsR (CtsR-P) was separated from nonphosphorylated CtsR by heparin affinity chromatography (Fig. 1B). Mass spectrometry (MS) analysis of CtsR-P revealed two protein species with either one or two phosphate moieties per protomer (Fig. 1B). In contrast to unmodified CtsR, the isolated CtsR-P cannot bind to its target DNA, as deduced from isothermal titration calorimetry (ITC) and gel-shift experiments (Fig. 1, C and D). Removal of the phosphate group by alkaline phosphatase fully restored the DNA binding capability of CtsR. Thus, phosphorylation of CtsR by McsB is sufficient to inhibit the repressor function of CtsR.

To understand how phosphorylation of CtsR affects DNA binding, we determined the crystal structure of CtsR bound to a 26-bp DNA derivative of the *clpC* promoter (table S1). The $CtsR_2$/DNA structure revealed that the CtsR protomer is composed of two distinct domains: (i) an N-terminal DNA binding domain that adopts the winged HTH fold (residues 2 to 72) and (ii) a C-terminal dimerization domain (residues 79 to 153) that consists of four α helices organized in a four-helix bundle (Fig. 2A). The DNA reading heads of the major and minor groove comprise the recognition helix of the HTH motif and the extended β-hairpin wing, respectively. Key residues for recognizing and binding the *ctsr* consensus sequence are indicated in Fig. 2A and fig. S3. After obtaining a molecular model of the CtsR/DNA complex, we used MS to pinpoint individual phosphorylation sites. Our initial analyses of "in-solution" and "in-gel" digested CtsR-P were not successful; thus, we attempted to sequence mono-phosphorylated CtsR in a "top-down" MS experiment (Fig. 2B). Purified CtsR-P was directly infused into the mass spectrometer and fragmented by different techniques including electron-capture dissociation (ECD), collisionally activated dissociation (CAD), and infrared multiphoton dissociation (IRMPD). Mapping of the resulting modified protein fragments to the CtsR amino acid sequence revealed that the phosphorylation sites reside in the winged HTH domain. Furthermore, the broad distribution of modified fragments pointed to the existence of product isoforms with different phosphorylation sites. The highest probability for a phosphorylation event was observed for the region

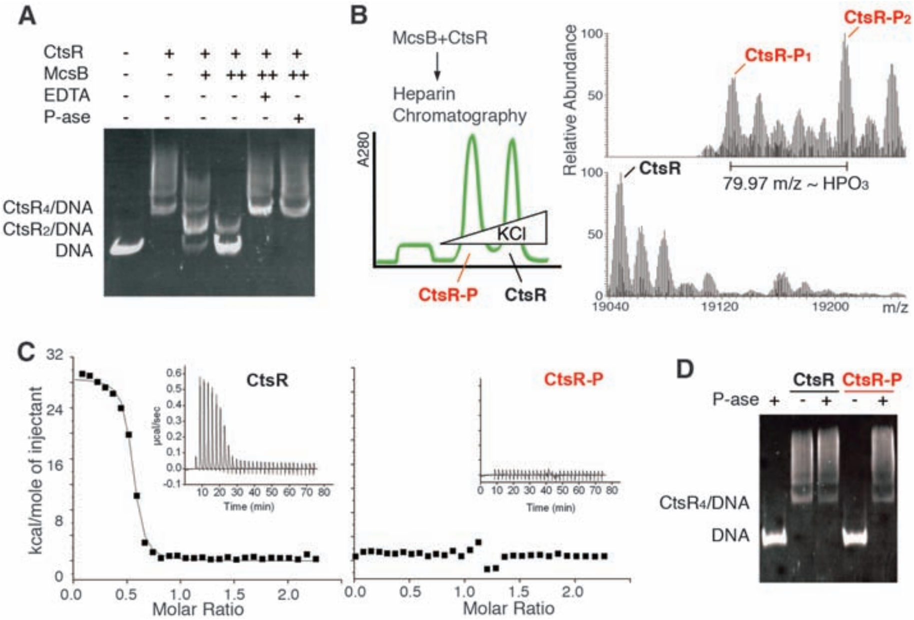

Fig. 1. Phosphorylation of CtsR impedes DNA binding. (**A**) EMSA analysis of the DNA binding capability of CtsR in the presence of McsB. CtsR was incubated with a *clpC* promoter fragment, McsB (+, 2 μM; ++, 8 μM), EDTA, and phosphatase (P-ase), as indicated. The promoter fragment, which was visualized by ethidium bromide staining of the native polyacrylamide gel, was either bound to one ($CtsR_2$/DNA) or two ($CtsR_4$/DNA) CtsR dimers. (**B**) Schematic presentation of the separation of CtsR-P from CtsR and McsB by heparin chromatography (left) and deconvoluted MS spectra of CtsR (average mass of 19047.2 daltons) and CtsR-P (19127.2 and 19207.1 daltons for mono- and di-phosphorylated isoforms, respectively) (right). (**C**) ITC analysis of $CtsR_2$/DNA complex formation. The 26-bp DNA duplex containing the *ctsr* box was injected into the sample cell containing either CtsR or CtsR-P (inset). The area under each peak was integrated and plotted against the molar ratio DNA/CtsR inside the sample cell. Thermodynamic values of CtsR/DNA complex formation are K_d = 22.2 ± 3.0 nM and n = 0.53 (reflecting the stoichiometry of bound DNA per CtsR protomer), whereas DNA binding of CtsR-P could not be detected by ITC. (**D**) EMSA analysis of the DNA binding capability of CtsR and CtsR-P, before and after phosphatase treatment.

[1]Research Institute of Molecular Pathology, Dr. Bohrgasse 7, A-1030 Vienna, Austria. [2]Christian Doppler Laboratory for Proteome Analysis, University of Vienna, Dr. Bohrgasse 3, A-1030 Vienna, Austria. [3]Max F. Perutz Laboratories, University of Vienna, Dr. Bohrgasse 9, A-1030 Vienna, Austria. [4]Institute for Biology–Microbiology, Freie Universität Berlin, Königin-Luisé-Str. 12-16, 14195 Berlin, Germany. [5]Institute for Molecular Biotechnology–IMBA, Dr. Bohrgasse 3, A-1030 Vienna, Austria. [6]The Laboratory for Molecular Infection Medicine Sweden, Umeå University, S-90187 Umeå, Sweden.

*These authors contributed equally to the work.
†To whom correspondence should be addressed. E-mail: clausen@imp.univie.ac.at

Tyr[55] to Asp[82], making up the β-hairpin wing (Fig. 2A). A lower, albeit still substantial, number of modified fragments matched the N-terminal segment from Ser[18] to Tyr[55].

To identify individual CtsR phosphorylation sites, we established a modified protocol for sample preparation and MS analysis (*15*). Most importantly, we implemented ECD and CAD fragmentation in two parallel MS/MS experiments. Only the ECD MS/MS spectrum of the phosphorylated CtsR peptide I_{57}VESKpRGGGGYIRIM$_{71}$ (*16*) allowed the unambiguous identification of Arg[62] as the site of modification (Fig. 2C). Both c- and z-fragment ion series unveiled a fragment of 236.067 daltons, reflecting the addition of a phosphate moiety (79.966 daltons) to an Arg residue (156.101 daltons). Moreover, CAD MS/MS of the I_{57}VESKpRGGGGYIRIM$_{71}$ phosphopeptide resulted in a discrete mass shift of 98 daltons, indicating the loss of phosphoric acid (fig. S1). This fragmentation behavior argues against a tyrosine kinase activity of McsB because phospho-tyrosine is stable upon CAD fragmentation (*17*). Further MS analysis led to the identification of two additional phosphorylation sites, Arg[28] and Arg[49] (fig. S2). Consistent with the results of the top-down approach, these amino acids are located within the winged HTH domain. Moreover, all Arg residues are strictly conserved in the CtsR protein family and play a crucial role in DNA binding, as predicted by our crystal structure. Arg[62] is a residue within the β wing and deeply invades the minor groove of the DNA duplex. In addition to undergoing extensive van der Waals contacts, the guanidinium group of Arg[62] forms hydrogen bonds with the DNA backbone and with one of the thymine pyrimidine carbonyls (Fig. 2A). Similarly, in the major groove of the CtsR consensus site, Arg[28] and Arg[49] bind to purine bases and coordinate the sugar-phosphate backbone, respectively (fig. S3).

To explore the functional relevance of the identified phosphosites, we conducted a mutational analysis of full-length CtsR by introducing various Arg-to-Lys mutations. Mutating the target sites in position 28, 49, and 62 (3RK) did not completely abolish, but did substantially reduce the phosphorylation of CtsR by McsB (Fig. 3A). Moreover, a mutant protein (8RK), in which the eight Arg residues located in the DNA binding region were replaced by Lys residues, was completely unsusceptible to McsB modification. Reintroduction of Arg[62] (7RK) markedly restored the phosphorylation potential. To study the direct effect of CtsR phosphorylation on DNA binding, we replaced Arg[62] by a phosphomimicking Glu residue. EMSA experiments clearly demonstrated that the Arg[62] → Glu[62] (R62E) mutant lost its capability to bind DNA (Fig. 3B), thus corroborating our finding that phosphorylation of CtsR alone is sufficient to inhibit its repressor activity. Conversely, replacing Arg[62] by Lys[62] did not alter the DNA binding ability of CtsR in band-shift assays. To test which state of CtsR is targeted by McsB, we incubated the kinase with DNA-bound and -unbound CtsR. Following the interaction with DNA over time revealed that McsB preferentially phosphorylates free CtsR, thereby preventing DNA complex formation (fig. S4). We conclude that the selective introduction of a negatively charged phosphate moiety functions as a molecular switch regulating DNA binding. Whereas the unphosphorylated CtsR binds with high affinity to its DNA consensus site and inhibits transcription of downstream genes, the McsB-phosphorylated CtsR repressor is not able to bind to DNA, thus allowing heat-shock gene expression.

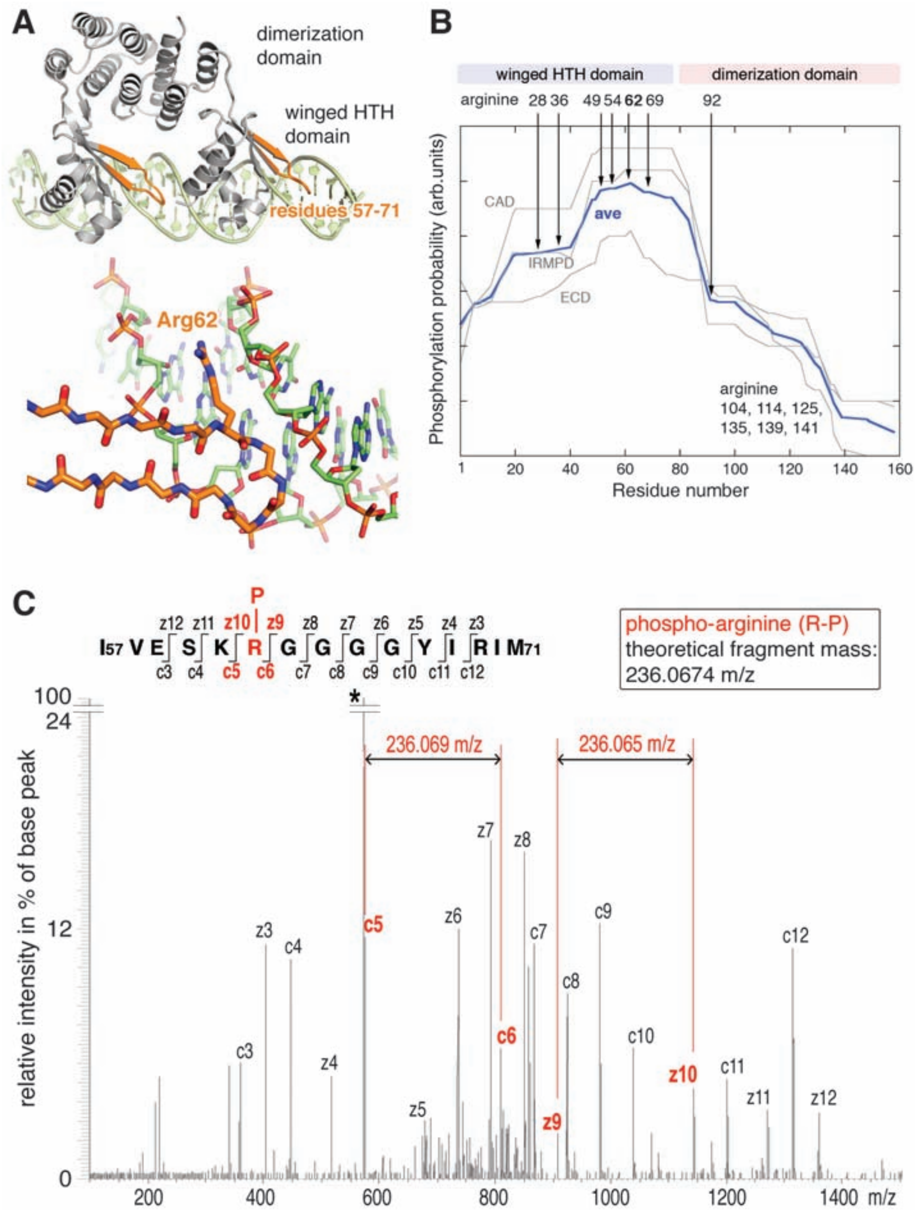

Fig. 2. Identification of arginine phosphorylation sites of CtsR. (**A**) Ribbon diagram showing the CtsR dimer (gray, with labeled domains) bound to the DNA direct repeat motif (green). The identified CtsR phosphopeptide I_{57}VESKpRGGGGYIRIM$_{71}$, which constitutes the β-hairpin of the winged HTH domain penetrating the DNA minor groove, is highlighted in orange. The lower panel illustrates the binding mode of Arg[62] (orange), the main phosphorylation site, at the floor of the DNA minor groove (green). (**B**) Phosphosite mapping with top-down MS. The mono-phosphorylated isoform of full-length CtsR was sequenced by three different fragmentation techniques. The blue line represents the average (ave) value of the three experimental setups and refers to the number of fragments additionally identified in CtsR-P, relative to unmodified CtsR. The residue with the highest phosphorylation score was Arg[62]. (**C**) ECD-MS/MS spectrum of the major phosphopeptide I_{57}VESKpRGGGGYIRIM$_{71}$ obtained after chymotryptic cleavage of phosphorylated CtsR. Individual fragments are labeled according to the c- or z-ion nomenclature. The characteristic mass difference of the phosphorylated Arg[62] is highlighted, and the threefold charged precursor ion is marked with an asterisk. m/z, mass/charge ratio.

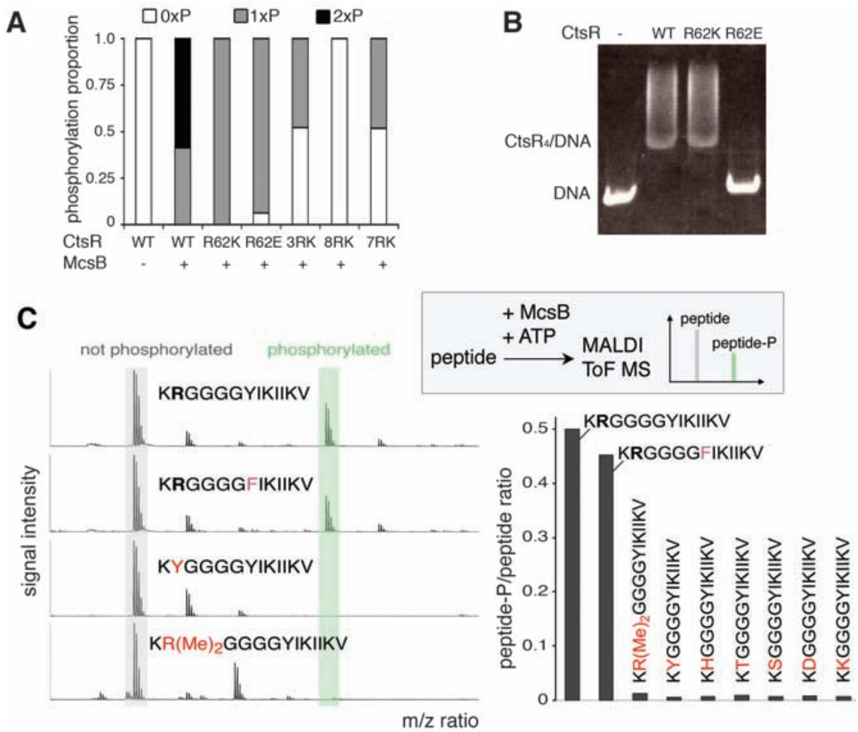

Fig. 3. Characterization of McsB-mediated arginine phosphorylation. (**A**) Phosphorylation level of CtsR Arg mutants analyzed by electrospray ionization–MS. The Arg-to-Lys mutants are 28/49/62 (3RK), 28/36/49/54/62/69/114/125 (8RK), and 28/36/49/54/69/114/125 (7RK). (**B**) DNA binding ability of different CtsR mutants in gel-shift assays. (**C**) Peptide phosphorylation assay (schematically shown in the inset). (Left) Matrix-assisted laser desorption/ionization–time-of-flight spectra of selected peptides after incubation with McsB. Non-phosphorylated and phosphorylated peptides are marked in gray and green, respectively. (Right) Effect of the exchange of Arg to other potential phospho-acceptor sites (shown in red) on the phosphorylation efficiency.

To verify our finding that McsB is a protein arginine kinase, we established an in vitro phosphorylation assay (Fig. 3C) using synthetic oligopeptides that resembled the CtsR sequence (residues 61 to 73). To avoid side effects during sample preparation that would preclude quantification of the phosphorylation reaction, we replaced one potential oxidation site (Met^{71}) and one arginine (Arg^{69}), yielding the 13-residue model substrate $K_{61}RGGGGYIKIIKV_{73}$. Systematic incorporation of potential phosphorylation sites (Tyr, Ser, Thr, His, Asp, and Lys) in position 62 revealed that only peptides with an Arg moiety are modified by McsB (Fig. 3C). Moreover, modification of the guanidinium group of Arg^{62} by asymmetric dimethylation prevented McsB-mediated modification. Additionally, we analyzed the purified phosphopeptide $K_{61}RGGGGYIKIIKV_{73}$ by ^{31}P nuclear magnetic resonance (NMR) spectroscopy (fig. S5). The chemical shift of about –2.4 parts per million (ppm) fits well to the measured NMR spectrum of free phospho-arginine (–3.0 ppm) (*18*), suggesting that the phosphate is attached via a phosphoramidate N-P linkage. Corresponding spectra of O-P linked phosphor compounds (as, for example, phospho-tyrosine, -serine, and -threonine) exhibit markedly higher chemical shifts of ~0.7 to 4.0 ppm (*18*). Thus, McsB is a protein kinase that acts exclusively on Arg residues, phosphorylating one of the amine nitrogens of the guanidinium group.

Phosphorylation of the free amino acid L-arginine by eukaryotic PhKs yields a chemically labile compound (*19*). We studied the CtsR/McsB system of a thermophilic organism living at ~55°C and thus explored the thermostability of a phosphorylated Arg residue present in a peptide context. For this purpose, we phosphorylated the $K_{61}RGGGGYIKIIKV_{73}$ peptide with McsB, incubated the purified phosphopeptide at different temperatures, and quantified the stability of the phosphorylation signal by high-performance liquid chromatography–MS analysis. The results clearly showed that peptide arginine phosphorylation is surprisingly stable up to 60°C. Dephosphorylation of the phosphopeptide occurred only at 95°C, with a half life $t_{1/2}$ of ~130 min (fig. S6). Therefore, phosphorylation of protein arginine residues should represent a relevant biological signal.

Sequence analysis indicated that the McsB protein arginine kinase exhibits no substantial homology to known Ser, Thr, Tyr, or His kinases. However, the catalytic domain of McsB is highly homologous to the catalytic domain of PhKs (*12*, *13*), which are involved in maintaining energy homeostasis but not in intermolecular signaling (*20*). Mutational analyses revealed that McsB and PhKs use a common mechanism to phosphorylate the terminal guanidinium group of substrates (fig. S7) (*14*). However, in contrast to PhKs where substrate specificity is primarily determined by the N-terminal domain, McsB harbors a distinct C-terminal domain that may redirect the substrate specificity from free Arg to protein-incorporated Arg residues.

McsB appears to be the founding member of a new class of protein kinases acting specifically on Arg residues. It should be noted that protein arginine phosphorylation has been reported previously (*21*). Remarkably, histone H3 was identified as a potential eukaryotic target (*22*), implying that Arg phosphorylation activity might be relevant for epigenetic regulation. However, these analyses failed to identify the corresponding kinase and obtained only indirect evidence for Arg modification. The thorough characterization of a protein arginine kinase presented in this work should provide the experimental tools to directly address the impact of Arg phosphorylation in prokaryotic and eukaryotic signaling pathways.

References and Notes

1. M. Hecker, W. Schumann, U. Volker, *Mol. Microbiol.* **19**, 417 (1996).
2. W. Schumann, M. Hecker, T. Msadek, in *Bacillus subtilis and Its Closest Relatives: From Genes to Cells*, A. L. Sonenshein, J. A. Hoch, R. Losick, Eds. (American Society for Microbiology Press, Washington, DC, 2002).
3. W. G. Haldenwang, R. Losick, *Nature* **282**, 256 (1979).
4. H. L. Hyyrylainen *et al.*, *Mol. Microbiol.* **41**, 1159 (2001).
5. A. Schulz, W. Schumann, *J. Bacteriol.* **178**, 1088 (1996).
6. E. Kruger, M. Hecker, *J. Bacteriol.* **180**, 6681 (1998).
7. I. Derre, G. Rapoport, T. Msadek, *Mol. Microbiol.* **31**, 117 (1999).
8. I. Derre, G. Rapoport, K. Devine, M. Rose, T. Msadek, *Mol. Microbiol.* **32**, 581 (1999).
9. S. Wickner, M. R. Maurizi, S. Gottesman, *Science* **286**, 1888 (1999).
10. R. T. Sauer *et al.*, *Cell* **119**, 9 (2004).
11. I. Derre, G. Rapoport, T. Msadek, *Mol. Microbiol.* **38**, 335 (2000).
12. E. Kruger, D. Zuhlke, E. Witt, H. Ludwig, M. Hecker, *EMBO J.* **20**, 852 (2001).
13. J. Kirstein, K. Turgay, *J. Mol. Microbiol. Biotechnol.* **9**, 182 (2005).
14. J. Kirstein, D. Zuhlke, U. Gerth, K. Turgay, M. Hecker, *EMBO J.* **24**, 3435 (2005).
15. Materials and methods are available as supporting material on *Science* Online. A detailed description of the MS approach is provided.
16. Single-letter abbreviations for the amino acid residues are as follows: A, Ala; C, Cys; D, Asp; E, Glu; F, Phe; G, Gly; H, His; I, Ile; K, Lys; L, Leu; M, Met; N, Asn; P, Pro; Q, Gln; R, Arg; S, Ser; T, Thr; V, Val; W, Trp; and Y, Tyr.
17. A. Tholey, J. Reed, W. D. Lehmann, *J. Mass Spectrom.* **34**, 117 (1999).
18. T. L. James, *CRC Crit. Rev. Biochem.* **18**, 1 (1985).
19. A. Sickmann, H. E. Meyer, *Proteomics* **1**, 200 (2001).
20. W. R. Ellington, *Annu. Rev. Physiol.* **63**, 289 (2001).
21. H. R. Matthews, *Pharmacol. Ther.* **67**, 323 (1995).
22. B. T. Wakim, G. D. Aswad, *J. Biol. Chem.* **269**, 2722 (1994).
23. We thank D. Fiegen and D. Reinert (Boehringer Ingelheim) and the staff at Swiss Light Source for assistance with collecting synchrotron data, A. Carrieri for his contribution with the kinase assays, L. Becker for the NMR analysis of phosphopeptides, T. Krojer and D. Hellerschmied for their support in the structural analysis of CtsR, and C. Stingl and M. Mazanek for assisting MS analysis. The Research Institute of Molecular Pathology is funded by

Boehringer Ingelheim. J.F., S.S., E.C., and T.C. were supported by Wiener Wissenschafts, Forschungs und Technologiefonds; A.S. by the Christian-Doppler-Society; K.T. by the Deutsche Forschungsgemeinschaft; and T.C. by the European Molecular Biology Organization Young Investigator Program. This work was further supported by the Austrian Proteomics Platform (GEN-AU). The Protein Data Bank accession number for the $CtsR_2$/DNA complex is 3H0D.

Supporting Online Material
www.sciencemag.org/cgi/content/full/324/5932/1323/DC1
Materials and Methods
Figs. S1 to S8
Table S1
References

22 December 2008; accepted 13 April 2009
10.1126/science.1170088

Rhes, a Striatal Specific Protein, Mediates Mutant-Huntingtin Cytotoxicity

Srinivasa Subramaniam, Katherine M. Sixt, Roxanne Barrow, Solomon H. Snyder*

Huntington's disease (HD) is caused by a polyglutamine repeat in the protein huntingtin (Htt) with mutant Htt (mHtt) expressed throughout the body and similarly in all brain regions. Yet, HD neuropathology is largely restricted to the corpus striatum. We report that the small guanine nucleotide–binding protein Rhes, which is localized very selectively to the striatum, binds physiologically to mHtt. Using cultured cells, we found Rhes induces sumoylation of mHtt, which leads to cytotoxicity. Thus, Rhes-mHtt interactions can account for the localized neuropathology of HD.

Huntington's disease (HD), a genetically dominant neurodegenerative disorder, reflects expansion of a polyglutamine repeat in the protein huntingtin (Htt) (*1*). Mutant Htt (mHtt) occurs uniformly throughout the brain and peripheral tissues. Yet, HD is brain-specific with profound abnormal movements related to selective, gross degeneration of the corpus striatum and lesser damage to the cerebral cortex eliciting dementia (*2*, *3*). Molecular mechanisms causing mHtt cytotoxicity are unclear. mHtt forms protein aggregates, which may be neuroprotective with soluble mHtt linked to cytotoxicity (*4*–*7*). mHtt is sumoylated, which increases the soluble form of mHtt and elicits cytotoxicity and neurotoxicity in a *Drosophila* model of HD (*8*).

Rhes (Ras homolog enriched in striatum) is a small guanine nucleotide–binding protein (G protein) very selectively localized to the striatum (*9*). To determine whether Rhes binds to Htt, we overexpressed Rhes in HEK293 cells where it bound to both wild-type (wt) Htt and mHtt (Fig. 1A) (*10*). In conditionally immortalized Htt knock-in striatal neuronal cells (*11*), which lack endogenous Rhes (fig. S1C), overexpressed Rhes bound robustly to endogenous mHtt (Fig. 1B). In HD transgenic mice (*12*), endogenous striatal mHtt coprecipitated with Rhes (Fig. 1C). In the presence of purified Rhes and Htt, Rhes bound much more to mHtt than wtHtt protein (fig. S1A). Rhes did not bind to ataxin (fig. S1B), a polyglutamine-repeat protein involved in another neurodegenerative disorder, spinocerebellar ataxia.

To ascertain whether Rhes influences mHtt cytotoxicity, we used several cell lines. In

The Solomon H. Snyder Department of Neuroscience, Johns Hopkins University School of Medicine, 725 North Wolfe Street, Baltimore, MD 21205, USA.

*To whom correspondence should be addressed. E-mail: ssnyder@jhmi.edu

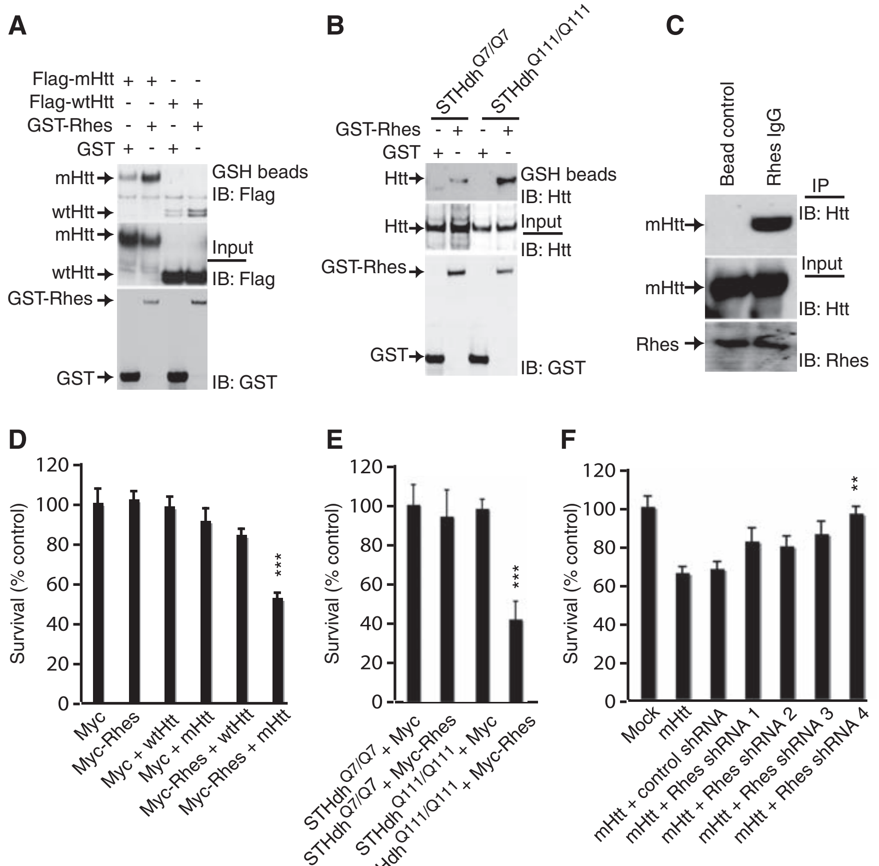

Fig. 1. Rhes binds Htt and affects cell survival. (**A**) Rhes interacts with N-terminal Htt. HEK293 cells were transfected with glutathione *S*-transferase (GST) or GST-Rhes together with Flag-tagged Htt or the N-terminal fragment containing 171 amino acids and 18 glutamines (wtHtt) or 82 glutamines (mHtt). After 48 hours, cell lysates were glutathione (GSH) precipitated and immunoblotted (IB) for Flag. (**B**) Rhes interacts with full-length Htt. Striatal cells expressing wild-type Htt (ST$Hdh^{Q7/Q7}$) or mutant Htt (ST$Hdh^{Q111/Q111}$) were transfected with GST or GST-Rhes. After 48 hours, cell lysates were GSH-precipitated and immunoblotted for Htt. Htt and GST inputs are shown. (**C**) Rhes interacts with mHtt in striatum. Striatum of transgenic mice expressing mHtt was lysed and immunoprecipitated with Rhes antibody or immunoglobulin IgG alone (bead control). Immunoprecipitates were probed with an N-terminal–specific Htt antibody (N-Htt). (**D**) Rhes reduces cell survival. HEK293 cells were transfected with Myc/Myc-Rhes and wtHtt–mHtt constructs. ***$P <$ 0.005 versus mHtt alone. (**E**) Wild-type (ST$Hdh^{Q7/Q7}$) or mutant (ST$Hdh^{Q111/Q111}$) striatal cells were transfected with Myc/Myc-Rhes. ***$P < 0.005$ versus Myc. (**F**) Depletion of Rhes prevents PC12 cell death. Control short hairpin–mediated (shRNA) or Rhes shRNA 1 to 4 were cotransfected with mHtt. Only shRNA4 was significantly cytoprotective (**$P < 0.01$ versus control shRNA). After 48 hours, cell survival was measured by MTT.

HEK293 cells, overexpression of mHtt or Rhes alone did not decrease cell survival. However, overexpression of Rhes together with mHtt reduced cell survival by 50%, whereas survival was normal in cells containing wtHtt and Rhes (Fig. 1D). We confirmed that survival of a striatal cell line with mHtt is the same as that in cells with wtHtt (*13*) (Fig. 1E). Overexpression of Rhes in mHtt knock-in striatal cells (ST*Hdh*$^{Q111/Q111}$) (*14*) reduced cell survival by 60%, whereas overexpression of Rhes in wtHtt knock-in striatal cells (ST*Hdh*$^{Q7/Q7}$) had no effect (Fig. 1E). Rhes's influences on striatal cell survival were concentration-dependent (fig. S2A). Cleaved caspase-3, an index of apoptosis, was selectively

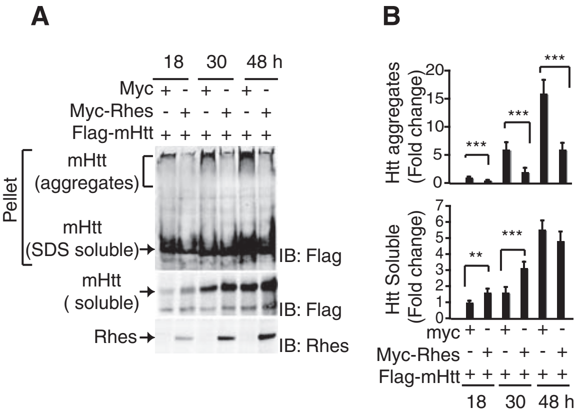

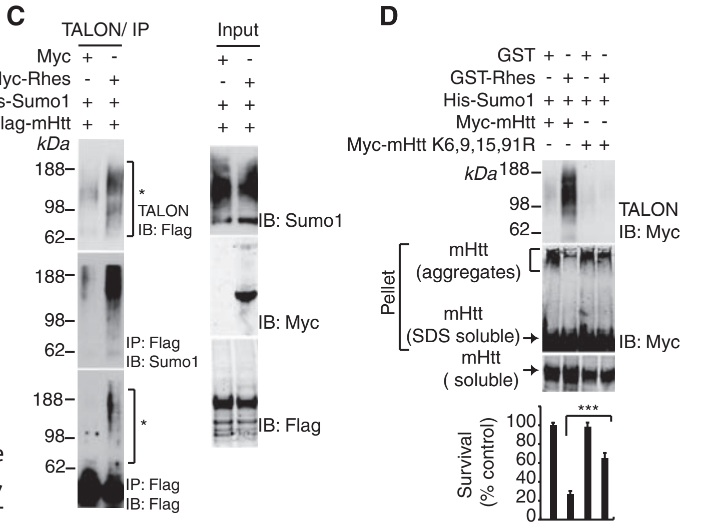

Fig. 2. Rhes inhibits mHtt aggregate formation. (**A**) HEK293 cells were transfected with Myc or Myc-Rhes and Flag-mHtt. At the indicated time points, cells were lysed, the pellet fraction (containing mHtt aggregates plus SDS-soluble mHtt), and the soluble fractions (containing only soluble Htt) were immunoblotted (IB) for Flag or Rhes. (**B**) Quantification of aggregated and soluble Htt. Fold change compared with results at 18 hours. (**C**) Rhes increases mHtt sumoylation in cells. HEK293 cells were transfected with Myc or Myc-Rhes, His-SUMO1 and Flag-mHtt. After 36 hours, cell lysates were immunoprecipitated (IP) with antibody against Flag-IgG beads and immunoblotted for Flag. SUMO-tagged proteins were enriched with TALON metal-affinity resin and immunoblotted for Flag or SUMO1. Input lysates were immunoblotted for SUMO1, Myc, or Flag. (**D**) Effect of mHtt-K6,9,15,91R mutation on sumoylation and cell survival. HEK293 cells were transfected with GST or GST-Rhes, His-SUMO1, and Myc-tagged mHtt or Myc–mHtt-K6,9,15,91R. After 48 hours, the SUMO-tagged protein was enriched with TALON metal-affinity resin and immunoblotted for Myc. The pellet fraction of the cell lysate was subjected to aggregate detection assay. Cell survival was measured by MTT.

Fig. 3. Rhes enhances sumoylation. (**A**) Rhes interacts with Ubc9. HEK293 cells were transfected with GST or GST-Rhes and Myc-Ubc9. After 48 hours, cells were lysed, precipitated with GSH beads and probed for Myc. Purified GST or GST-Rhes was incubated with purified Ubc9 and precipitated with GSH beads. The precipitates and inputs were immunoblotted for Ubc9. (**B**) Rhes sumoylates mHtt. Four μl of in vitro translated mHtt (control) and its K6,9,15,91R mutant were subjected to sumoylation [1× RB buffer, 250 ng E1, 125 ng E2, 1.5 μg SUMO1, 5 mM adenosine triphosphate (ATP), and 2 mM dithiothreitol (DTT)] in the presence of 500 ng Rhes (+) or bovine serum albumin (BSA) (–). Htt was detected by N-Htt antibody. Rhes sumoylates Htt in a time- (Rhes, 500 ng) and concentration-dependent manner. (**C** and **D**) Sumoylation of multiple substrates. Indicated substrates (500 ng) were subjected to sumoylation assay as in (B). Rhes sumoylates substrates in a (C) time- (Rhes, 200 ng) and (D) concentration-dependent manner.

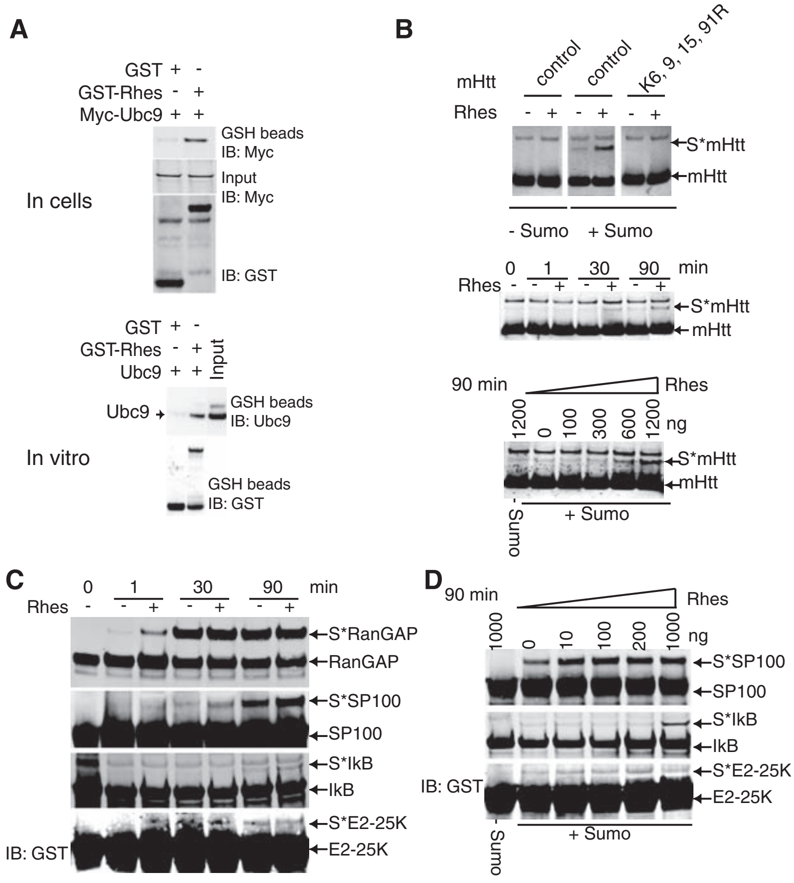

augmented in ST*Hdh*$^{Q111/Q111}$ cells overexpressing Rhes (fig. S2B). We examined the role of endogenous Rhes in cytotoxicity in PC12 cells, which contain endogenous Rhes (fig. S1C). The reduction in cell survival associated with overexpression of mHtt was reversed by depleting Rhes with RNA interference (fig. S1D and Fig. 1F).

How might Rhes facilitate mHtt neurotoxicity? When expressed in cells, mHtt, but not wtHtt, formed robust aggregates (fig. S1E). mHtt is sumoylated, that is, the small ubiquitin-like modifier (SUMO) is covalently attached to the protein, which decreases mHtt aggregation and elicits neurotoxicity (*8*). We examined the influence of Rhes on mHtt aggregation. Rhes overexpression markedly reduced aggregation and increased levels of soluble mHtt (Fig. 2, A and B). We confirmed the sumoylation of mHtt, which was markedly augmented in cells overexpressing Rhes (Fig. 2C). By contrast, Rhes failed to increase wtHtt sumoylation (fig. S3A). Because mHtt is both sumoylated and ubiquitinated at the same lysine (*8*), we examined the effect of Rhes on mHtt ubiquitination. Rhes elicited a pronounced decrease in mHtt ubiquitination (fig. S3B). To ascertain whether sumoylation at specific lysines of mHtt determines disaggregation of the protein, we evaluated mHtt with lysine-to-arginine mutations at positions 6, 9, 15, and 91 (Fig. 2D). The combined mutations abolished mHtt sumoylation, as well as disaggregation, and reversed the cytotoxicity elicited by Rhes overexpression (Fig. 2D). Sumoylation of mHtt in cells involved multiple lysines, specifically K9, K15, and K91 (fig. S4A). When Arg replaced Lys at residues 15 and 91 (K15R and K91R), these mutations of mHtt markedly diminished Rhes-elicited disaggregation of mHtt without influencing Rhes-mHtt binding (fig. S4, A and B).

We next examined the effect of SUMO1 depletion in HEK293 cells. Depletion by RNA interference of SUMO1 (fig. S5A) increased aggregation of mHtt and abolished the cytotoxicity associated with overexpression of Rhes and mHtt (fig. S5B). Conversely, overexpression of SUMO1 caused disaggregation of mHtt and increased cell death (fig. S5C). We wondered whether SUMO2/3 might sumoylate mHtt in cells lacking SUMO1 (fig. S6A). We failed to detect any sumoylation of mHtt by SUMO2 in the SUMO1-deleted cells, consistent with the observation that SUMO2/3 is exclusively nuclear, whereas mHtt exhibited a granular distribution in the cytoplasm (fig. S6B).

We explored whether Rhes directly regulates sumoylation of mHtt. Rhes bound Ubc9, the cellular E2 ligase (Fig. 3A), and enhanced sumoylation of recombinant mHtt in a time- and concentration-dependent manner (Fig. 3B). Rhes did not influence wtHtt sumoylation (fig. S7A). In these experiments in vitro, sumoylated mHtt was a single discrete band. In contrast, with intact cells, sumoylated mHtt appeared as a smear, probably because of sumoylation at multiple lysine residues and/or formation of polySUMO chains. Sumoylation was abolished in mHtt-K6,9,15,91R mutants (Fig. 3B). We explored the substrate specificity of Rhes (Fig. 3, C and D). Rhes augmented sumoylation of Ran guanosine triphosphatase (GTPase)–activating protein (RanGAP1) and SP100, but failed to elicit sumoylation of E2-25K, ubiquitin-conjugating E2 ligase (Fig. 3C). Rhes-dependent sumoylation of RanGAP1 was evident as early as 1 min (fig. S7B). Higher concentrations of Rhes were required to sumoylate inhibitor of nuclear factor κB (IκB) (Fig. 3D). Both recombinant Rhes and overexpressed Rhes in cultured cells were sumoylated (fig. S8, A and B), similar to E3 ligases (*15*, *16*).

We conducted a series of experiments to examine mechanisms whereby Rhes alters mHtt aggregation and cell death. Biological activity of small G proteins requires attachment to the cell membrane via fatty acid addition to conserved cysteines on CXXX domains (*17*). Rhes is farnesylated at cysteine 263 (*18*). Farnesylation mediates the localization of proteins to the plasma membrane, as well as to intracellular membranes (*19*). Mutation of Rhes-C263 abolished its sumoylation of mHtt, the disaggregation of mHtt, and cytotoxicity (Fig. 4A). Thus, these actions of Rhes require cysteine 263. The GTPase function of Rhes is mediated by serine 33. Rhes-S33N retained its ability to sumoylate and disaggregate mHtt and to elicit cytotoxicity and thus dissociated GTPase activity from sumoylation and/or cytotoxicity (Fig. 4, A and B). We explored the localization of the farnesylation-deficient mutant Rhes-C263S (Fig. 4C). Whereas wild-type Rhes, Ubc9, and mHtt occurred in granular structures restricted to the cytosol, Rhes-C263S was translocated to the nucleus with negligible staining in the cytoplasm. By contrast, GTPase mutant Rhes-S33N, which retains sumoylation activity,

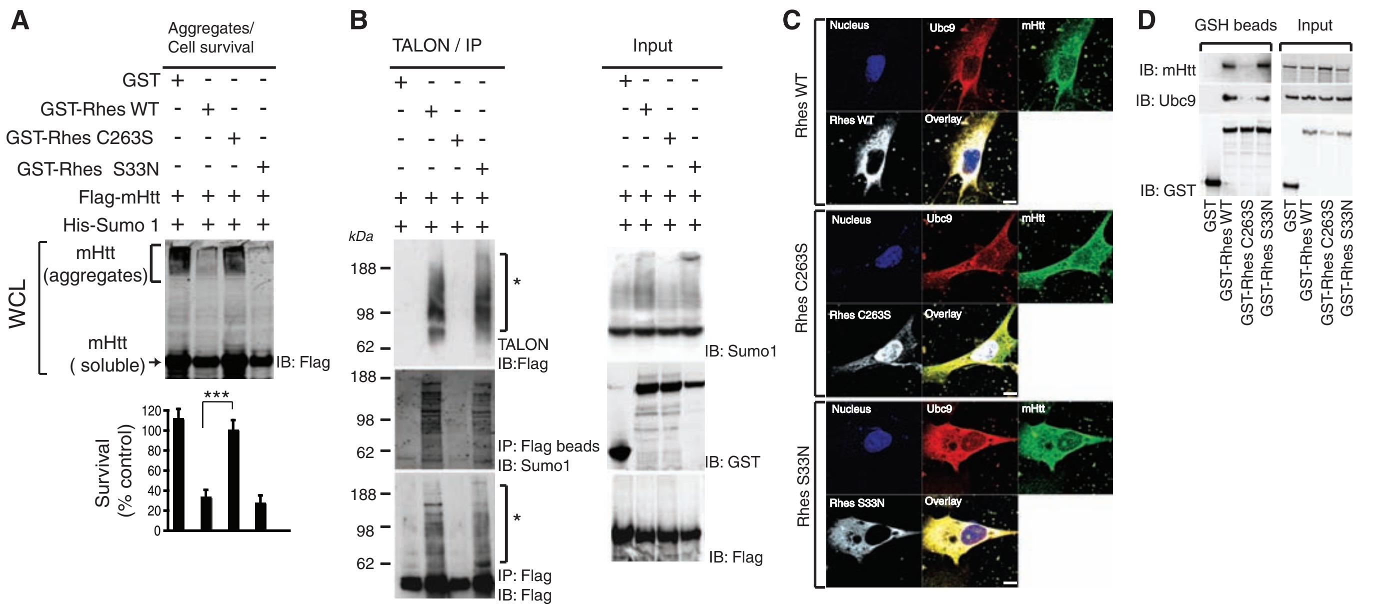

Fig. 4. Rhes function requires cysteine 263. (**A**) Disaggregation and cell death. GST or GST-tagged Rhes (WT, C263S, or S33N) were transfected along with Flag-mHtt; Htt aggregation and cell survival were assessed at 48 hours. ***$P < 0.001$ versus WT. (**B**) Sumoylation. HEK293 cells were transfected with GST, GST-tagged Rhes (WT, C263S, or S33N), His-SUMO1, and mHtt. After 36 hours, cell lysates were either immunoprecipitated (IP) with Flag-IgG beads or enriched with TALON metal-affinity resin. The precipitate and input were immunoblotted (IB) for Flag, SUMO1, or GST. (**C**) Rhes/Ubc9/mHtt colocalization. ST*Hdh*$^{Q111/Q111}$ cells were transfected with GST-Rhes WT, C263S, or S33N mutants. After 48 hours, cells were processed for nuclear staining and immunostaining with antibodies against Rhes, Ubc9, and Htt. (**D**) Rhes/Ubc9/mHtt interaction. ST*Hdh*$^{Q111/Q111}$ cells were transfected with GST or GST-Rhes with WT, S33N, or C263S. After 48 hours, cells were lysed and precipitated with GSH beads. The precipitates and inputs were probed for mHtt, Ubc9, or GST.

displayed the same intracellular localization as wild-type Rhes. Biochemical studies revealed a substantial reduction of Rhes-C263S binding to Ubc9 and mHtt (Fig. 4D). Finally, Rhes-induced mHtt sumoylation occurred both in the soluble and membrane fractions (fig. S9).

In summary, Rhes binds to mHtt and elicits its sumoylation, which is associated with mHtt disaggregation and cell death. In some animal models overexpression of full-length mHtt augments aggregates in the striatum (*20*, *21*), although, in other models, the overexpression leads to fewer or no aggregates (*22*, *23*). In human HD patients and several animal models, aggregates are not correlated with cell death (*5*, *20*, *24–26*). Sumoylated mHtt represses nuclear transcription (*8*). We observed caspase-3 activation in Rhes-mHtt cells, and mHtt is known to induce cytochrome c release (*27*).

Rhes elicits sumoylation of mHtt via a mechanism independent of its GTPase activity but which does require cysteine at CXXX domains presumably for farnesylation and membrane attachment. Sumoylation of mHtt, RanGAP1, and SP100 occurs in the absence of Rhes but is markedly augmented by Rhes. The three well-studied SUMO E3 ligases, the PIASy family, Pc2, and RanBP2, do not share obvious sequence homology with each other (*28*) or with Rhes, the only G protein with demonstrated E3 ligase activity.

Dexras1, a close homolog of Rhes, displays the highest levels in the brain, but with no marked regional differences (*29*). Dexras1 mediates linking of nitric oxide (NO) signaling by CAPON, a scaffolding protein, which links Dexras1 to neuronal NO synthase (*29*). NO serves as a guanine nucleotide–exchange factor to activate Dexras1. Dexras1 also mediates neurotoxic iron influx following glutamate–*N*-methyl-D-aspartate neurotransmission (*30*).

Our discovery that the striatal-selective protein Rhes partners with mHtt to elicit cytotoxicity can account for the striatal pathophysiology of HD. Although Rhes is uniquely enriched in the striatum, it displays detectable cerebral cortical levels with negligible values in the cerebellum (*9*, *31*). Cortical damage presumably elicits dementia; however, the cerebellum is relatively impervious to neurotoxic damage. Because HD can be diagnosed many years before the onset of symptoms, prophylactic therapy could, in principle, prevent or delay the onset of symptoms. Drugs that block the binding of Rhes and mHtt may thus have therapeutic potential.

References and Notes

1. J. F. Gusella, M. E. Macdonald, *Trends Biochem. Sci.* **31**, 533 (2006).
2. C. M. Cowan, L. A. Raymond, *Curr. Top. Dev. Biol.* **75**, 25 (2006).
3. K. A. Sieradzan, D. M. Mann, *Neuropathol. Appl. Neurobiol.* **27**, 1 (2001).
4. F. Saudou, S. Finkbeiner, D. Devys, M. E. Greenberg, *Cell* **95**, 55 (1998).
5. S. Kuemmerle *et al.*, *Ann. Neurol.* **46**, 842 (1999).
6. M. Arrasate, S. Mitra, E. S. Schweitzer, M. R. Segal, S. Finkbeiner, *Nature* **431**, 805 (2004).
7. B. Gong, M. C. Lim, J. Wanderer, A. Wyttenbach, A. J. Morton, *Brain Res. Bull.* **75**, 146 (2008).
8. J. S. Steffan *et al.*, *Science* **304**, 100 (2004).
9. J. D. Falk *et al.*, *J. Neurosci. Res.* **57**, 782 (1999).
10. Materials and methods are available as supporting material on *Science* Online.
11. F. Trettel *et al.*, *Hum. Mol. Genet.* **9**, 2799 (2000).
12. G. Schilling *et al.*, *Hum. Mol. Genet.* **8**, 397 (1999).
13. Q. Ruan, M. Lesort, M. E. MacDonald, G. V. Johnson, *Hum. Mol. Genet.* **13**, 669 (2004).
14. Single-letter abbreviations for the amino acid residues are as follows: A, Ala; C, Cys; D, Asp; E, Glu; F, Phe; G, Gly; H, His; I, Ile; K, Lys; L, Leu; M, Met; N, Asn; P, Pro; Q, Gln; R, Arg; S, Ser; T, Thr; V, Val; W, Trp; Y, Tyr; and X, any amino acid.
15. A. Pichler, A. Gast, J. S. Seeler, A. Dejean, F. Melchior, *Cell* **108**, 109 (2002).
16. M. H. Kagey, T. A. Melhuish, D. Wotton, *Cell* **113**, 127 (2003).
17. T. Magee, M. C. Seabra, *Curr. Opin. Cell Biol.* **17**, 190 (2005).
18. P. Vargiu *et al.*, *Oncogene* **23**, 559 (2004).
19. L. P. Wright, M. R. Philips, *J. Lipid Res.* **47**, 883 (2006).
20. V. C. Wheeler *et al.*, *Hum. Mol. Genet.* **9**, 503 (2000).
21. C. H. Lin *et al.*, *Hum. Mol. Genet.* **10**, 137 (2001).
22. P. H. Reddy *et al.*, *Nat. Genet.* **20**, 198 (1998).
23. M. S. Levine *et al.*, *J. Neurosci. Res.* **58**, 515 (1999).
24. J. G. Hodgson *et al.*, *Neuron* **23**, 181 (1999).
25. P. F. Shelbourne, *Hum. Mol. Genet.* **8**, 763 (1999).
26. C. A. Gutekunst, *J. Neurosci.* **19**, 2522 (1999).
27. Y. S. Choo, G. V. Johnson, M. MacDonald, P. J. Detloff, M. Lesort, *Hum. Mol. Genet.* **13**, 1407 (2004).
28. R. Geiss-Friedlander, F. Mechior, *Nat. Rev. Mol. Cell Biol.* **8**, 947 (2007).
29. M. Fang *et al.*, *Neuron* **28**, 183 (2000).
30. J. H. Cheah *et al.*, *Neuron* **51**, 431 (2006).
31. H. Usui *et al.*, *J. Neurosci.* **14**, 4915 (1994).

32. We thank I. Rao, A. Hayashi, K. Ishizuka and M. Chakraborty for technical support. We thank N. Shahani and R. Mealer for critically reading the manuscript. We thank E. Fossale and M. Macdonald for generously providing striatal cell lines. We thank M. Matunis for providing SUMO-related constructs, H. Zoghbi for ataxin constructs, S. Li and X. J.Li for purified Htt, J. Nathans for use of his cell culture facility and Alessandro Usiello for providing antibody to Rhes. Supported by USPHS grant MH18501 and Research Scientist Award DA00074 (SHS).

Supporting Online Material

www.sciencemag.org/cgi/content/full/324/5932/1327/DC1
Materials and Methods
Figs. S1 to S9
References

27 February 2009; accepted 21 April 2009
10.1126/science.1172871

Mechanoenzymatic Cleavage of the Ultralarge Vascular Protein von Willebrand Factor

Xiaohui Zhang,[1,3]* Kenneth Halvorsen,[2]* Cheng-Zhong Zhang,[1] Wesley P. Wong,[2]† Timothy A. Springer[1]†

Von Willebrand factor (VWF) is secreted as ultralarge multimers that are cleaved in the A2 domain by the metalloprotease ADAMTS13 to give smaller multimers. Cleaved VWF is activated by hydrodynamic forces found in arteriolar bleeding to promote hemostasis, whereas uncleaved VWF is activated at lower, physiologic shear stresses and causes thrombosis. Single-molecule experiments demonstrate that elongational forces in the range experienced by VWF in the vasculature unfold the A2 domain, and only the unfolded A2 domain is cleaved by ADAMTS13. In shear flow, tensile force on a VWF multimer increases with the square of multimer length and is highest at the middle, providing an efficient mechanism for homeostatic regulation of VWF size distribution by force-induced A2 unfolding and cleavage by ADAMTS13, as well as providing a counterbalance for VWF-mediated platelet aggregation.

Von Willebrand factor (VWF) is the key shear-sensing protein in hemostasis and is especially important in arterial bleeding where shear is high (*1*). VWF is biosynthesized and stored in the Weibel-Palade bodies of endothelial cells in an ultralarge form (ULVWF). The VWF 240,000 M_r monomer (Fig. 1A) is concatenated through specific disulfide bonds at both its N and C termini into multimers of up to ~50 × 10^6 M_r in ULVWF (*1*, *2*). ULVWF is secreted in response to thrombogenic stimuli. A portion of secreted ULVWF is bound locally to endothelial cells from which it is released and also through its A3 domain to collagen at sites of tissue injury. Vessel wall–bound VWF multimers, as well as multimers free in the bloodstream, are extended to a length of up to 15 μm by the hydrodynamic forces in shear flow (*2*). These forces induce a conformational change in VWF that exposes a binding site in the A1 domain for the platelet glycoprotein Ib (GPIb) molecule, which enables formation of a hemostatic platelet plug (*1*, *3*).

Within 2 hours after release from endothelium into the circulation, ULVWF is converted by ADAMTS13 to smaller multimers with a wide range of size distributions that are characteristic of the circulating pool of VWF (*4*). Because the length of VWF multimers strongly correlates with

[1]Immune Disease Institute, Harvard Medical School, Boston, MA 02115, USA. [2]Rowland Institute at Harvard, Harvard University, Cambridge, MA 02142, USA. [3]State Key Laboratory of Molecular Biology, Institute of Biochemistry and Cell Biology, Chinese Academy of Sciences, Shanghai 200031, China.

*These authors contributed equally to this work.
†To whom correspondence should be addressed. E-mail: springer@idi.harvard.edu or wong@rowland.harvard.edu

hemostatic potential, cleavage by ADAMTS13 is an important regulatory mechanism. Absence of ADAMTS13 results in increased thrombogenic potential of VWF and thrombotic thrombocytopenic purpura, a life-threatening disease caused by uncontrolled microvascular thrombosis (*5*). On the other hand, mutations in the A2 domain that presumably destabilize it cause excessive cleavage by ADAMTS13 and a shift in the size distribution to smaller VWF multimers with less hemostatic potential, resulting in the bleeding disorder known as type 2A von Willebrand disease (*3*, *6*).

VWF is cleaved by ADAMTS13 within the A2 domain at its Tyr[1605]-Met[1606] bond (*1*, *3*, *5*, *7*, *8*). Cleavage is activated by shear when A2 is present in large VWF concatamers, but not when present as the much smaller, isolated domain (*5*–*7*). Presumably, this is because the tensile forces acting on proteins in shear flow increase with protein length (*9*). Shear flow elongates VWF (*2*), and tensile force exerted on the concatamer is thought to cause conformational changes in A2 domains that enable cleavage (*3*, *5*, *8*); the scissile bond is likely buried in the native state (*10*, *11*). Therefore, partial or complete unfolding may be the mechanism for substrate activation (*6*). Here, by directly applying force with laser tweezers (*12*, *13*) to a single A2 domain, we test the hypothesis that unfolding and folding of the A2 domain may occur at forces that might be experienced by VWF in its transit through the circulation or at sites of hemostasis and thrombosis, and that force acts as a cofactor to unfold A2 for cleavage by ADAMTS13.

Single, N-glycosylated A2 domains coupled to DNA handles through N- and C-terminal Cys tags (fig. S1) were suspended between beads held in a laser trap and micropipette (Fig. 1B). A2 domains were subjected to cycles of force increase, force decrease, and clamping at a low force to enable refolding before the next cycle (Fig. 1C). A2 domain unfolding was marked by abrupt increase in length of the tether between the two beads (Fig. 1C, inset, and 1D, cycle ii). The increase in length at different forces was fitted to the wormlike chain (WLC) model (*14*) (Fig. 2A), which yielded an A2 contour length of 57 ± 5 nm and a persistence length of 1.1 ± 0.4 nm. A2 N-terminal and C-terminal residues Met[1495] and Ser[1671] are 1 nm apart in the folded state (*15*). The total length of 58 ± 5 nm divided by an extension length of 0.36 nm per residue yields unfolding of 161 ± 14 residues. This corresponds well to complete unfolding of the predicted 177-residue A2 domain.

Over a range of force loading rates, unfolding force was determined and plotted against the logarithm of the loading rate (Fig. 2B). The fit to a single-barrier kinetic model (*16*) yields an unfolding rate in the absence of force, k_u^0, of 0.0007 s^{-1} (confidence band of 0.0002 s^{-1} to 0.003 s^{-1}), and a force scale, f_β, which exponentially increases the unfolding rate $k_u = k_u^0 exp(f/f_\beta)$, of 1.1 ± 0.2 pN.

A subset of about 20% of unfolding events included a discernible pause [defined by four or more data points at a short-lived (fig. S3), partially unfolded intermediate state], which was directly observed in force-extension curves (Fig. 2C). Fit to the WLC model of the A2 extension distances (Fig. 2C, inset) shows that the intermediate state usually lies 40% of the distance between the fully folded and unfolded states.

During the pause at a clamped force between each cycle of force decrease and increase, the A2 domain had the opportunity to refold (Fig. 1C). Subsequent unfolding revealed folding during the pause (Fig. 1, C and D, cycle ii), whereas a lack of unfolding suggested an absence of refolding

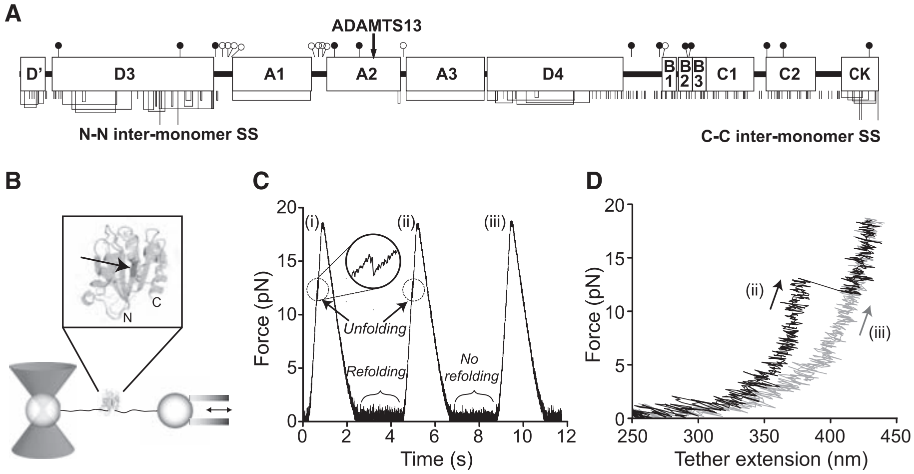

Fig. 1. A2 domain unfolding and refolding with laser tweezers. (**A**) Domain organization of VWF. Cysteines and disulfide bonds are shown beneath, and N- and O-linked sites above as filled and open lollipops, respectively. (**B**) Experimental setup. A2 domain (enlarged in inset with ADAMTS13 cleavage site indicated by an arrow) is coupled to double-stranded DNA handles, which are bound through tags at their other ends to beads held by a laser trap and a translatable (double arrow) micropipette. (**C**) Force on a molecular tether during representative cycles of force increase, decrease, and clamping at a constant low level. (**D**) Force-extension traces during force loading in cycles ii and iii from panel (C).

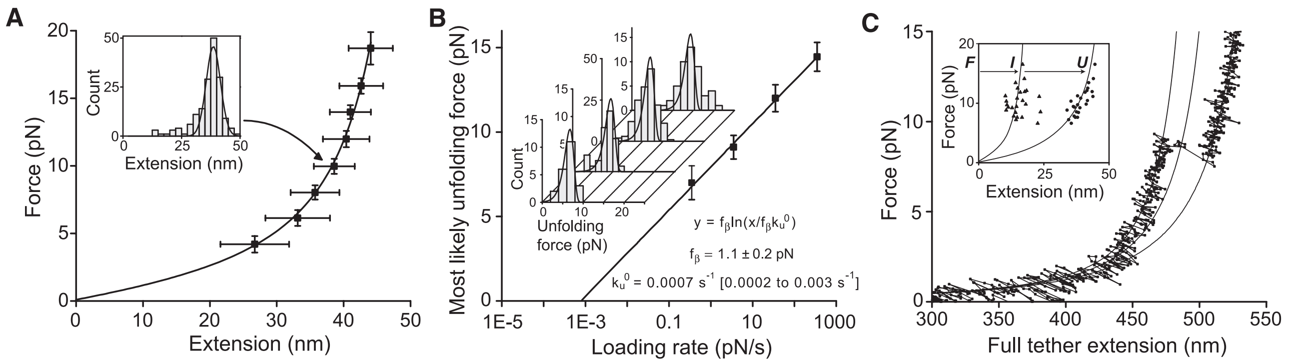

Fig. 2. Unfolding of the A2 domain. (**A**) A2 domain force-extension data with an error-weighted least squares fit to the WLC model (line) (*14*). Extension distances were sorted by unfolding force into 2-pN bins. A histogram of extensions for each bin (inset) was fitted to a Gaussian curve (inset, solid line) to find peak extension, and force was averaged for that bin. Uncertainty in extension is shown as the half width of the Gaussian fit, and uncertainty in force is shown as 1 SD. (**B**) Unfolding force as a function of loading rate. Unfolding forces were binned by loading rate and plotted as histograms (inset). The peak of each histogram was plotted against the loading rate; uncertainty in *y* is shown as half of the bin width. A linear fit to the data (line) predicts the distributions of unfolding force (inset, lines), which agree well with the histograms (inset). (**C**) Representative force-extension trace for a tether pausing at an intermediate state, with three WLC curves (solid lines) representing DNA + folded A2, DNA + partially unfolded A2, and DNA + fully unfolded A2. (Inset) Extensions of A2 to intermediate (I) and unfolded (U) lengths fit to the WLC model (lines).

(Fig. 1, C and D, cycle iii). The binary state of the domain was further confirmed with force extension curves, which have distinct branches for the unfolded and folded states (Fig. 1D). The force dependence of refolding (Fig. 3) was fitted by using maximum likelihood to an f^2 model, which takes into account the soft compliance of the unfolded state (*16*–*18*): $k_f = k_f^0 exp(-f^2/2\kappa k_B T)$ (where κ is defined as the effective compliance of the unfolded state, k_B is the Boltzmann constant, and T is the absolute temperature) (see also fig. S3). We found a refolding rate in the absence of force, $k_f^0 = 0.54 \pm 0.05$ s^{-1}, and compliance, $\kappa = 0.18 \pm 0.04$ pN/nm.

Using the folding and unfolding rates in the absence of force, we can estimate the free energy difference between the two states: $\Delta G = -k_B T \cdot \ln(k_u^0/k_f^0) = 6.6 \pm 1.5\ k_B T$ (3.9 ± 0.9 kcal/mol). This is close to the ΔG of $5.9 \pm 0.8\ k_B T$ (3.5 ± 0.5 kcal/mol) estimated from urea-induced unfolding of an *Escherichia coli* A2 fragment (*19*).

To test the hypothesis that A2 unfolding is required for cleavage by ADAMTS13, A2 was mechanically unfolded in the absence or presence of ADAMTS13 and relaxed to a clamped force of 5 pN (Fig. 4A). At this force, the lifetime of the unfolded state is >140 s, which makes refolding unlikely during the incubation with ADAMTS13. Cleavage by ADAMTS13 was detected as a drop in force on the tether to 0 pN (Fig. 4A, left). Spontaneous rupture at 5 pN, i.e., the background with no enzyme (Fig. 4A, right), was rare (Fig. 4B, inset). In experiments with a lower force ramp, unfolding sometimes did not occur, as shown by lack of the characteristic force-extension signature. No cleavage of folded A2 at 5 pN with 100 nM or 1 μM enzyme was observed.

With unfolded A2 in the presence of enzyme, the fraction of surviving tethers decreased exponentially with time, which demonstrated first-order reaction kinetics and yielded the time constant τ for cleavage at three different enzyme concentrations (Fig. 4B, inset). The observed enzymatic rate, i.e., reciprocal of τ, was fitted with the single-molecule Michaelis-Menten equation (*20*), $1/\tau = k_{cat}[\text{ADAMTS13}]/([\text{ADAMTS13}] + K_M)$ (Fig. 4B).

As the largest known soluble protein, VWF has more force exerted on it than any other free protein in the vasculature. Hydrodynamics and the overall shape and orientation of VWF multimers in flow are relevant to understanding the tensile force exerted on A2 domains within ULVWF and trimming by ADAMTS13 (*5*). In shear flow, the rate of fluid flow increases from the wall toward the center (Fig. 5, A and B). The product of shear rate and viscosity, shear stress (in units of force per area) imparts force to particles in shear flow that is related to their surface area. Compared with VWF free in flow, the hydrodynamic force at a given shear is much higher on VWF immobilized on a vessel wall or bridging two platelets free in flow and, at intermediate levels, for VWF bound to a single platelet free in flow (*9*, *21*). Because of weak attractive interactions between domains within each multimer, VWF multimers have an overall compact, yarn ball–like shape in stasis (*2*, *22*–*24*). Above a critical shear stress of 50 dyn/cm^2 (*13*), the attractive forces are overcome by hydrodynamic drag, and VWF free in flow periodically elongates and contracts (*2*, *24*) (Fig. 5C). Shear flow can be conceptualized as the superposition of rotational flow and elongational flow (Fig. 5B). The rotational flow causes particles to tumble (Fig. 5C). Tumbling is more evident for polymers such as DNA (*25*); the attractive forces between VWF monomers appear to keep it largely zipped up during tumbling, with alternating cycles of elongation and compaction that demonstrate tumbling (Fig. 5C) (*2*, *24*).

We apply concepts from the field of polymer dynamics to VWF. For an extended VWF multimer with N monomers, the tensile force on a monomer increases with distance from the nearest end of the multimer (Fig. 5D), and force at the middle of the multimer is proportional to N^2 (Fig. 5D) [see estimation of force within VWF (*13*)] (*26*). Force increases with the square of length because both multimer size and the difference in velocity between shear lamina, in which the two ends of the multimer find themselves, increase with length (*9*, *13*, *26*). This second-power dependence not only has important implications for unfolding of the A2 domain and cleavage by ADAMTS13 (Fig. 5D), but also explains the much greater potency of longer than shorter VWF multimers in shear-induced aggregation of platelets in hemostasis and thrombosis (*1*, *5*).

Could the tensile force on VWF free in the circulation reach levels in vivo sufficient to explain unfolding of the A2 domain and cleavage by ADAMTS13? The tensile force is estimated [see tumbling time scale (*13*)] to reach 10 pN in the middle of a VWF 200-monomer multimer at the maximal shear stress of 100 dyn/cm^2 (shear rate of 5000 s^{-1}) found in healthy vessels in vivo (*5*, *27*) (Fig. 5D). Using a loading rate of 25 pN/s estimated from the VWF tumbling rate in shear (*13*), the A2 domain typically unfolds at about 11 pN (peak of the unfolding force distribution) (Fig. 2B). The upper size limit of VWF in the circulation is variously estimated to correspond to a 100-monomer multimer (*1*) or a 200-monomer multimer (*2*, *13*, *22*, *23*). Thus, our single-molecule data on the A2 domain successfully predicts the observed upper size limit of VWF multimers in vivo as ~200 monomers (Fig. 5D). Caveats include uncertainty in the angle of maximally extended VWF with respect to flow direction, which could influence the magnitude of the peak force estimate by several fold [see peak force on relaxing, extending VWF (*13*)], simplifying assumptions made in the calculations, and a possible contribution of platelets to VWF trimming (*21*, *28*). The dynamics of VWF in shear flow is an important area of future investigation for understanding susceptibility to ADAMTS13, as well as activation in hemostasis.

The existence of a clear threshold for the lengths of VWF multimers has been shown in vivo; a bolus of ULVWF released from endothelium into the circulation is trimmed to the preexisting equilibrium length distribution of circulating VWF multimers within 2 hours by ADAMTS13 (*4*). Our

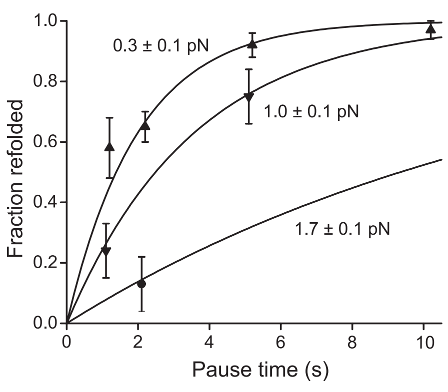

Fig. 3. A2 domain refolding kinetics. Binary refolding events were binned by clamp force and time. Standard errors (bars) were calculated as $(p \cdot (1-p)/n)^{0.5}$, where p is fraction refolded and n is number of events. Overlaid on the data are the exponential curves predicted by maximum likelihood estimation (i.e., on the data without binning) using the $\tau \approx exp(f^2)$ model.

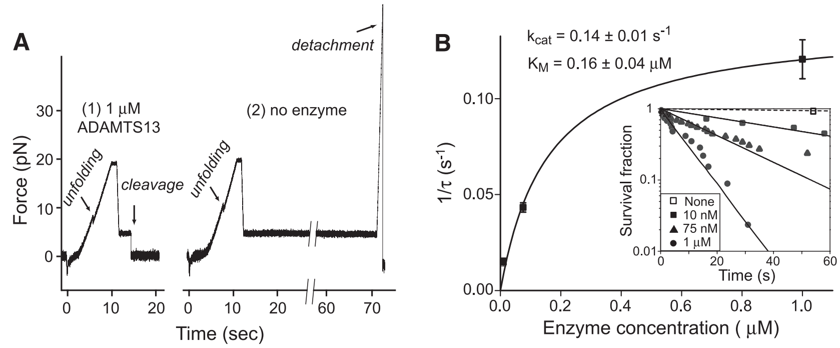

Fig. 4. Mechanoenzymatic cleavage of A2 by ADAMTS13. (**A**) Representative traces showing cleavage in the presence of enzyme (left) and no cleavage in the absence of enzyme (right). (**B**) Enzyme kinetics. The hyperbolic dependence of catalytic rate on enzyme concentration was fitted with the single-molecule Michaelis-Menten equation (*20*) (solid line). Data points and standard error were determined from single-parameter exponential fits to the survival fraction as a function of time (inset).

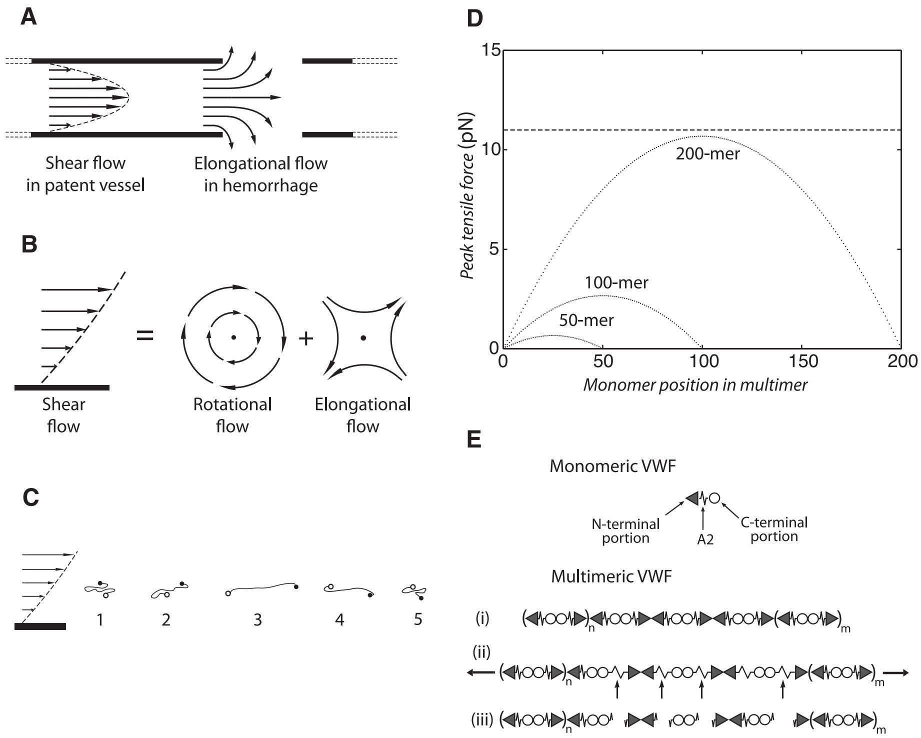

Fig. 5. Model for mechanoenzymatic cleavage of ULVWF in the circulation. (**A**) Shear flow in a vessel and elongational flow at a site of bleeding. (**B**) Shear flow may be represented as elongational flow superimposed on rotational flow [modified from (*25*)]. (**C**) Cartoon of VWF elongating, compressing, and tumbling in shear flow. (**D**) Peak force as function of monomer position in a VWF multimer chain of 200, 100, or 50 monomers at 100 dyn/cm^2. Dashed line shows the most likely unfolding force for the A2 domain at a loading rate of 25 pN/s. (**E**) Schematic of VWF, with N-terminal end as triangle, A2 as spring, and C-terminal end as circle. Elongation results in unfolding of some A2 domains, some of which are cleaved (arrows). The resulting fragments are shown.

analysis illustrates the principles that dictate the maximum length of circulating VWF multimers in vivo and suggests that the force on VWF free in the circulation is sufficient to induce unfolding of the A2 domain and cleavage by ADAMTS13.

Another concept from polymer dynamics (*25*) important for VWF is elongational flow (Fig. 5, A and B). Close to a site of hemorrhage, flow will transition from shear flow, which has both rotational and elongational components (Fig. 5A, left), to elongational flow (Fig. 5A, right). Although the actual flow pattern would be complex, the overall picture is that tumbling and alternating cycles of compression will tend to cease, and VWF will only experience elongation. Alignment of VWF with the principal direction of elongational strain could increase peak tensile force to about 10 times that experienced in shear flow [see force on VWF in elongational flow (*13*)].

We have definitively established that unfolding is required for cleavage of the A2 domain by ADAMTS13. In a portion of unfolding events, we observed an intriguing transient intermediate state. In VWF A2, the N-terminal β1 strand is central in the fold, whereas the C-terminal α6 helix is peripheral. Therefore, unfolding induced by elongational force will begin at the C terminus (*15*). Unfolding of 40% of the contour length in the intermediate state would thus correspond to the unfolding of about 70 C-terminal residues, up to and including the β4 strand, which contains the scissile Tyr^{1605}-Met^{1606} peptide bond. Studies with peptide fragments show that C-terminal, but not N-terminal, segments distal from the cleavage site are recognized by ADAMTS13 (*29*). Thus, it is possible that ADAMTS13 could recognize and cleave the intermediate unfolded state.

Our single-molecule k_{cat} for the ADAMTS13 enzyme of 0.14 s^{-1} is in the range of 0.14 to 1.3 s^{-1}, determined in bulk phase with unfolded peptide substrates corresponding to the C-terminal 70 residues of A2 (*11*, *30*). However, our K_M of 0.16 μM is lower than previous estimates of 1.7 and 1.6 μM (*11*, *30*). The lower K_M value determined here may reflect a more physiologic state of the substrate. Notably, different domains within ADAMTS13 recognize different portions of the unfolded peptide substrate that are far apart in sequence (*29*, *30*). Whereas peptide substrates have essentially random configurations, tension applied to the unfolded A2 domain partially orders it in one dimension, and this more linear configuration may improve recognition by the different domains within ADAMTS13.

VWF will only be exposed to peak shear intermittently during each tumbling cycle and only to high shear during transit through arterioles and capillaries. The lifetime of about 2 s of the unfolded state in the absence of force is longer than the time period of peak force exposure (*9*, *13*) and provides a window of opportunity for cleavage by ADAMTS13. Refolding to the correct low-energy state of the A2 domain after tension is released is another property important for function in vivo. Aberrant refolding could permit cleavage by ADAMTS13, as is observed with some A2-domain preparations from *E. coli* (*31*).

Our single-molecule enzyme assays suggest that the rate of VWF cleavage is limited by ADAMTS13 concentration in vivo, which, at 6 nM (*32*), is substantially below the K_M of 160 nM and yields a time scale for cleavage in vivo of ~200 s. Although the numbers may be altered for cleavage of unfolded A2 within intact VWF, these rough estimates are relevant to understanding events in vivo. Thus, over the short time periods of <1 s important in hemostasis, binding of VWF through the A1 domain to GPIb on platelets and through the A3 domain to collagen on the subendothelium should win out over cleavage of the A2 domain by ADAMTS13.

A further wrinkle is added by a *cis*-proline recently discovered in the A2 structure (*15*) consistent with a small number of A2 tethers that suddenly stopped refolding and, after a long delay, resumed refolding (*13*). VWF, bound to platelets at sites of hemorrhage, would be exposed to forces sufficient to accelerate cis-to-trans peptide isomerization (*33*) in unfolded A2. A *trans*-proline would be a long-lasting (100- to 1000-s) impediment to refolding that would enhance cleavage by ADAMTS13 during wound repair.

The A2 domain's unique lack of protection by disulfide bonds within VWF (Fig. 1A) and low resistance to unfolding suggest that A2 has evolved to be the shear bolt domain of VWF. A shear bolt breaks above a designed force threshold, so as to protect other parts of a machine from accidental damage. Similarly, the A2 domain unfolds when present in VWF multimers that experience high-tensile force and is cleaved by ADAMTS13, which results in down-regulation of hemostatic activity.

References and Notes

1. J. E. Sadler, *Annu. Rev. Biochem.* **67**, 395 (1998).
2. S. W. Schneider *et al.*, *Proc. Natl. Acad. Sci. U.S.A.* **104**, 7899 (2007).
3. J. E. Sadler, *Annu. Rev. Med.* **56**, 173 (2005).
4. J. Batlle *et al.*, *Blood* **70**, 173 (1987).
5. H. M. Tsai, *Semin. Thromb. Hemost.* **29**, 479 (2003).
6. H. M. Tsai, *Blood* **87**, 4235 (1996).
7. M. Furlan, R. Robles, B. Lamie, *Blood* **87**, 4223 (1996).
8. J. F. Dong *et al.*, *Blood* **100**, 4033 (2002).
9. H. Shankaran, S. Neelamegham, *Biophys. J.* **86**, 576 (2004).
10. J. J. Sutherland, L. A. O'Brien, D. Lillicrap, D. F. Weaver, *J. Mol. Model.* **10**, 259 (2004).
11. S. Zanardelli *et al.*, *J. Biol. Chem.* **281**, 1555 (2006).
12. J. R. Moffitt, Y. R. Chemla, S. B. Smith, C. Bustamante, *Annu. Rev. Biochem.* **77**, 205 (2008).
13. Materials and methods are available as supporting material on *Science* Online.
14. C. Bustamante, J. F. Marko, E. D. Siggia, S. Smith, *Science* **265**, 1599 (1994).
15. Q. Zhang, Y.-F. Zhou, C.-Z. Zhang, T. A. Springer, *Proc. Natl. Acad. Sci. U.S.A.*, 10.1073_pnas.0903679106 (2009).
16. E. Evans, K. Ritchie, *Biophys. J.* **72**, 1541 (1997).

17. P. Hanggi, P. Talkner, M. Borkovec, *Rev. Mod. Phys.* **62**, 251 (1990).
18. E. Evans, K. Halvorsen, K. Kinoshita, W. P. Wong, in *Handbook of Single-Molecule Biophysics*, P. Hinterdorfer and A. van Oijen, Eds. (Springer, New York, in press).
19. M. Auton, M. A. Cruz, J. Moake, *J. Mol. Biol.* **366**, 986 (2007).
20. S. C. Kou, B. J. Cherayil, W. Min, B. P. English, X. S. Xie, *J. Phys. Chem. B* **109**, 19068 (2005).
21. K. Shim, P. J. Anderson, E. A. Tuley, E. Wiswall, J. E. Sadler, *Blood* **111**, 651 (2008).
22. W. E. Fowler, L. J. Fretto, K. K. Hamilton, H. P. Erickson, P. A. McKee, *J. Clin. Invest.* **76**, 1491 (1985).
23. H. Slayter, J. Loscalzo, P. Bockenstedt, R. I. Handin, *J. Biol. Chem.* **260**, 8559 (1985).
24. A. Alexander-Katz, M. F. Schneider, S. W. Schneider, A. Wixforth, R. R. Netz, *Phys. Rev. Lett.* **97**, 138101 (2006).
25. D. E. Smith, H. P. Babcock, S. Chu, *Science* **283**, 1724 (1999).
26. J. A. Odell, A. Keller, *J. Chem. Phys.* **88**, 4022 (1988).
27. Z. M. Ruggeri, G. L. Mendolicchio, *Circ. Res.* **100**, 1673 (2007).
28. P. J. J. van Genderen, U. Budde, J. J. Michiels, R. van Strick, H. H. D. M. van Vliet, *Br. J. Haematol.* **93**, 962 (1996).
29. W. Gao, P. J. Anderson, J. E. Sadler, *Blood* **112**, 1713 (2008).
30. W. Gao, P. J. Anderson, E. M. Majerus, E. A. Tuley, J. E. Sadler, *Proc. Natl. Acad. Sci. U.S.A.* **103**, 19099 (2006).
31. J. L. Whitelock *et al.*, *J. Thromb. Haemost.* **2**, 485 (2004).
32. H. B. Feys *et al.*, *J. Thromb. Haemost.* **4**, 955 (2006).
33. A. Valiaev, D. W. Lim, T. G. Oas, A. Chilkoti, S. Zauscher, *J. Am. Chem. Soc.* **129**, 6491 (2007).
34. Supported by NIH HL-48675 (T.A.S.), the Rowland Junior Fellows (W.P.W.), and American Heart Association 525918T (X.Z.). The authors thank C. Bustamante, S. Marqusee, and C. Cecconi for protocols for DNA-protein coupling; J. E. Sadler, D. Schaak, J. Kim, J. Seog, C. Lu, and A. Alexander-Katz for reagents and insightful discussions; and G. Dempsey for work on the early stages of this project.

Supporting Online Material
www.sciencemag.org/cgi/content/full/324/5932/1330/DC1
Materials and Methods
SOM Text
Figs. S1 to S3
References

14 January 2009; accepted 24 April 2009
10.1126/science.1170905

Halofuginone Inhibits T_H17 Cell Differentiation by Activating the Amino Acid Starvation Response

Mark S. Sundrud,[1] Sergei B. Koralov,[1] Markus Feuerer,[2] Dinis Pedro Calado,[1] Aimee ElHed Kozhaya,[3] Ava Rhule-Smith,[4] Rachel E. Lefebvre,[1] Derya Unutmaz,[3] Ralph Mazitschek,[5,6,7] Hanspeter Waldner,[4] Malcolm Whitman,[8]* Tracy Keller,[8]* Anjana Rao[1]*

A central challenge for improving autoimmune therapy is preventing inflammatory pathology without inducing generalized immunosuppression. T helper 17 (T_H17) cells, characterized by their production of interleukin-17, have emerged as important and broad mediators of autoimmunity. Here we show that the small molecule halofuginone (HF) selectively inhibits mouse and human T_H17 differentiation by activating a cytoprotective signaling pathway, the amino acid starvation response (AAR). Inhibition of T_H17 differentiation by HF is rescued by the addition of excess amino acids and is mimicked by AAR activation after selective amino acid depletion. HF also induces the AAR in vivo and protects mice from T_H17-associated experimental autoimmune encephalomyelitis. These results indicate that the AAR pathway is a potent and selective regulator of inflammatory T cell differentiation in vivo.

Naïve $CD4^+$ T cells differentiate into diverse effector and regulatory subsets to coordinate immunity to pathogens while establishing peripheral tolerance. Besides T_H1 and T_H2 effector subsets, which produce interferon-γ (IFN-γ) and interleukin-4 (IL-4), respectively, naïve T cells can differentiate into proinflammatory T helper 17 (T_H17) cells or tissue-protective induced T regulatory (iT_{reg}) cells (*1*, *2*). T_H17 cells are key regulators of autoimmune inflammation; characteristically produce IL-17 (IL-17A), IL-17F, and IL-22; and differentiate in the presence of inflammatory cytokines, such as IL-6 or IL-21, together with transforming growth factor–β (TGF-β) (*1*, *2*).

[1]Department of Pathology, Harvard Medical School and Immune Disease Institute, Boston, MA 02115, USA. [2]Section on Immunology and Immunogenetics, Joslin Diabetes Center, Boston, MA 02215, USA. [3]Department of Microbiology and The Microbial Pathogenesis Program, New York University School of Medicine, New York, NY 10016, USA. [4]Department of Microbiology and Immunology, Pennsylvania State University College of Medicine, Hershey, PA 17033, USA. [5]Chemical Biology Program, Broad Institute, Cambridge, MA 02142, USA. [6]Department of Biological Chemistry and Molecular Pharmacology, Harvard Medical School, Boston, MA 02142, USA. [7]Chemical Biology Program, Broad Institute, Cambridge, MA 02142, USA. [8]Department of Developmental Biology, Harvard School of Dental Medicine, Boston, MA 02115, USA.

*To whom correspondence should be addressed. E-mail: whitman@hms.harvard.edu (M.W.); tkeller@hms.harvard.edu (T.K.); arao@idi.harvard.edu (A.R.)

The small molecule halofuginone (HF) is a derivative of the plant alkaloid febrifugine (*3*). HF has shown therapeutic promise in animal models of fibrotic disease and a clinical trial for scleroderma (*3*–*5*), but its mechanism of action is unclear. To investigate whether HF could modulate T cell differentiation, we stimulated murine T cells to induce T_H1, T_H2, iT_{reg}, or T_H17 differentiation and treated these cells with HF or an inactive derivative, MAZ1310 (fig. S1, A and B) (*6*). HF selectively inhibited the development of T_H17 cells with a median inhibitory concentration (IC_{50}) of 3.6 ± 0.4 nM (Fig. 1A and fig. S2A). Low concentrations of HF that impaired T_H17 differentiation did not influence T_H1, T_H2, or iT_{reg} differentiation (Fig. 1A and fig. S2A) and had no impact on T cell receptor (TCR)–induced cytokine secretion by naïve T cells (fig. S2B). HF also repressed IL-17 expression by human T cells without influencing IFN-γ production (Fig. 1B). Consistent with a previous report (*7*), 10-fold higher concentrations of HF broadly impaired lymphocyte function (Fig. 1A and fig. S2C). Inhibition of T_H17 differentiation by HF was most pronounced when added within the first 24 hours of culture (Fig. 1C), was stereospecific (fig. S2D), and was not cytotoxic below 100 nM (fig. S2E). Although HF treatment delayed S-phase entry within 24 hours of TCR activation, these T cells recovered thereafter, showing no defect in expansion kinetics between days 2 and 4 postactivation (fig. S3). Moreover, HF suppressed T_H17 differentiation, irrespective of the number of cell divisions completed (Fig. 1D), and reduced T_H17 differentiation when IFN-γ and IL-4, cytokines that inhibit T_H17 differentiation (*8*), were neutralized by antibodies (fig. S4A).

HF inhibited *Il17a* and *Il17f* mRNA production without affecting the expression of IL-2 and tumor necrosis factor, cytokines expressed by all effector T cells (fig. S4B). HF treatment did not affect the induction of RORγt and RORα, two orphan nuclear receptors induced by T_H17 polarizing cytokines that mediate lineage commitment (*9*, *10*) (fig. S4C). Ectopic expression of RORγt in T cells did not override the inhibitory effects of HF on T_H17 differentiation (fig. S4D), confirming that RORγt is not sufficient to drive the effector function of T_H17 cells (*11*).

HF did not directly inhibit signaling induced by TGF-β or IL-6, the two principal cytokines that instruct T_H17 differentiation. Although high concentrations (>50 nM) of HF were reported to impair TGF-β signaling in fibroblasts (*4*), low doses of HF that repress T_H17 differentiation inhibited neither TGF-β–induced R-Smad2 phosphorylation (fig. S5A) nor a variety of other lymphocyte responses to TGF-β (fig. S5, B to D) (*12*). In contrast, the type 1 TGF-β receptor kinase inhibitor SB-431542 (fig. S1C) abrogated all responses to TGF-β (fig. S5). Additionally, HF did not inhibit early IL-6–induced STAT3 phosphorylation (where STAT proteins are signal transducers and activators of transcription) (fig. S6), but it did reduce sustained STAT3 activation beginning 12 hours poststimulation (fig. S6), indicating that HF indirectly modulates factors that maintain STAT3 signaling. Consistent with decreased STAT3 activity (*13*), HF-treated T_H17 cells displayed a reciprocal increase in Foxp3 expression (fig. S7A). However, retroviral expression of *FOXP3* in T cells did not decrease T_H17 differentiation (fig. S7B), and HF repressed IL-17 expression in T cells lacking Foxp3 (fig. S7C). Thus, changes in Foxp3 expression are not necessary or sufficient for the effects of HF on T_H17 differentiation.

HF-treated T cells stimulated in T_H17 polarizing conditions for 3 or 6 hours showed differential expression of 81 annotated genes, the majority of which were up-regulated (Fig. 2A and table S1). Among HF-inducible transcripts, many were functionally associated with amino acid transport and biogenesis, as well as protein synthesis (table S1), a pattern characteristic of an amino acid starvation response (AAR, also called general amino acid control in yeast) (*14*). The AAR pathway is physiologically induced by unaminoacylated (i.e., uncharged) tRNAs, which accumulate during amino acid insufficiency and bind to the protein kinase GCN2 (*15*, *16*). Activated GCN2 phosphorylates and inhibits eukaryotic translation initiation factor 2A (eIF2α), leading to a transient reduction in protein synthesis, while enhancing the translation of ATF4 (fig. S8), a transcription factor that activates stress-induced gene expression (*15*–*17*). HF treatment activated ATF4 target genes (Fig. 2A; fig. S9A, red and blue dots, respectively; and table S2) (*14*, *17*), including *Asns*, *Gpt2*, and *eIF4Ebp1*, as confirmed by quantitative real-time fluorescence polymerase chain reaction(QPCR) (Fig. 2B).

HF treatment rapidly induced eIF2α phosphorylation and ATF4 expression (Fig. 2, C and D) and did so independent of stimulation and polarization conditions (fig. S9B), indicating that AAR activation by HF is not restricted to T_H17 cells. Phosphorylation of eIF2α and ATF4 expression can be initiated by multiple upstream kinases through a shared signaling cassette termed the integrated stress response (fig. S8) (*15*). GCN2 autophosphorylation was activated in response to HF treatment (Fig. 3A), indicating that HF activates the AAR pathway. Furthermore, neither HF nor depletion of cysteine and methionine (Cys/Met) activated IRE-1–dependent splicing of the transcription factor Xbp-1, a response characteristic of endoplasmic reticulum (ER) stress (*18*), in contrast to a known inducer of ER stress, tunicamycin (Fig. 3B) (*17*). Microarray analyses indicated that HF does not activate gene expression associated

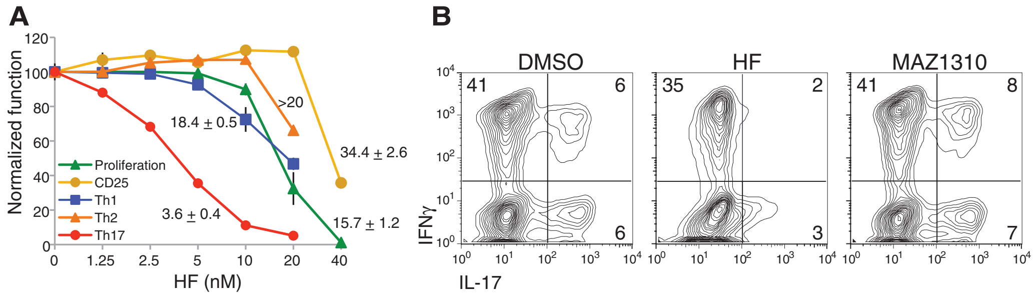

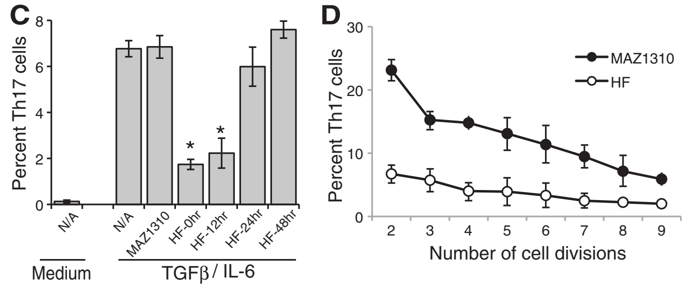

Fig. 1. Selective inhibition of T_H17 differentiation by HF. (**A**) Carboxyfluorescein diacetate succinimidyl ester (CFSE)–labeled T cells were activated in the presence of dimethyl sulfoxide (DMSO), 40 nM MAZ1310, or titrating concentrations of HF. CFSE dilution and the percentages of cells expressing CD25, IFN-γ^+ IL-4^- (T_H1 cells), IL-4^+ IFN-γ^- (T_H2 cells), or IL-17^+ IFNγ^- (T_H17 cells) cells are displayed as mean values ± SD normalized to MAZ1310-treated cells. IC_{50} values are listed next to corresponding lines ± SD. (**B**) Intracellular cytokine expression in primary human T cells treated with DMSO, HF, or MAZ1310. (**C**) Differentiating T_H17 cell cultures were incubated with HF at the indicated times after activation. Intracellular cytokine expression was determined on day four. The mean percentage of T_H17 cells is shown ± SD (error bars). *$P < 0.005$, relative to MAZ1310-treated T cells. (**D**) CFSE-labeled T cells were differentiated to T_H17 in the presence of HF or MAZ1310. After intracellular cytokine staining, CFSE peaks were gated and mean percentages of IL-17^+ T cells within each peak are displayed ± SD (error bars). All data represent at least three similar experiments.

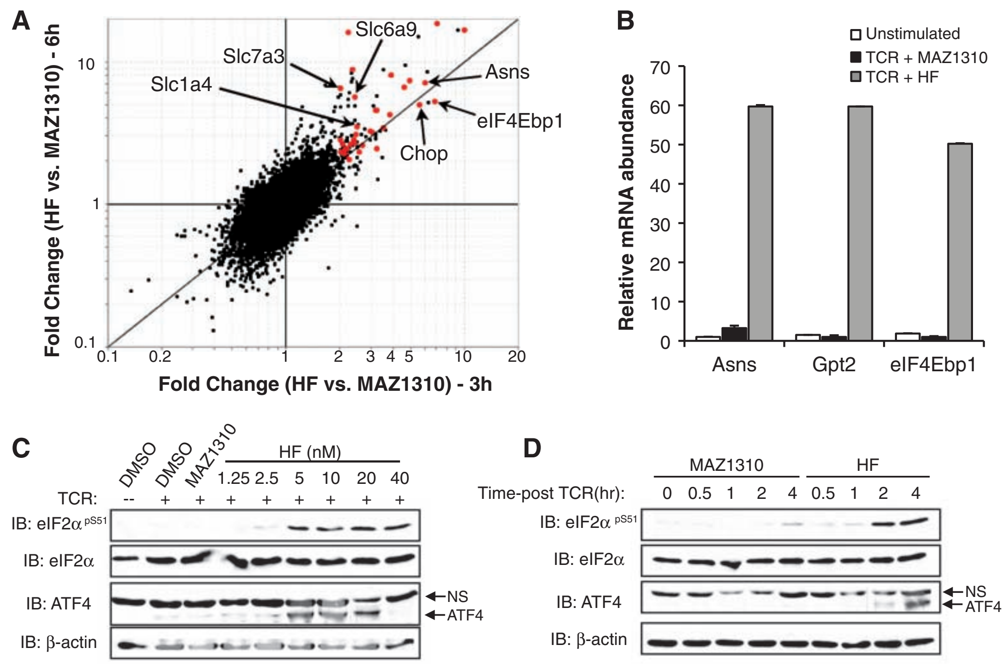

Fig. 2. HF activates the AAR pathway. (**A**) Histogram of microarray data from differentiating T_H17 cells treated with HF or MAZ1310 for 3 or 6 hours. Red dots indicate transcripts increased greater than twofold by HF-treatment at both 3 and 6 hours. Text and arrows denote several defined AAR genes (*27*). (**B**) Quantitative real-time PCR was performed on cDNA from unstimulated T cells or those activated for 4 hours in the presence of MAZ1310 or HF. *Asns*, *Gpt2*, or *eIF4Ebp1* mRNA expression was normalized to *Hprt* levels and are shown as mean values ± SD. (**C**) Unstimulated or TCR-activated T cells were treated with DMSO, 40 nM MAZ1310, or HF and were lysed for Western blotting after 4 hours. (**D**) Activated T cells were lysed at the indicated times after treatment with MAZ1310 or HF. ATF4 protein is indicated by an arrow. NS, nonspecific band. Microarray data were generated from three biological replicates. Other data represent two to three experiments.

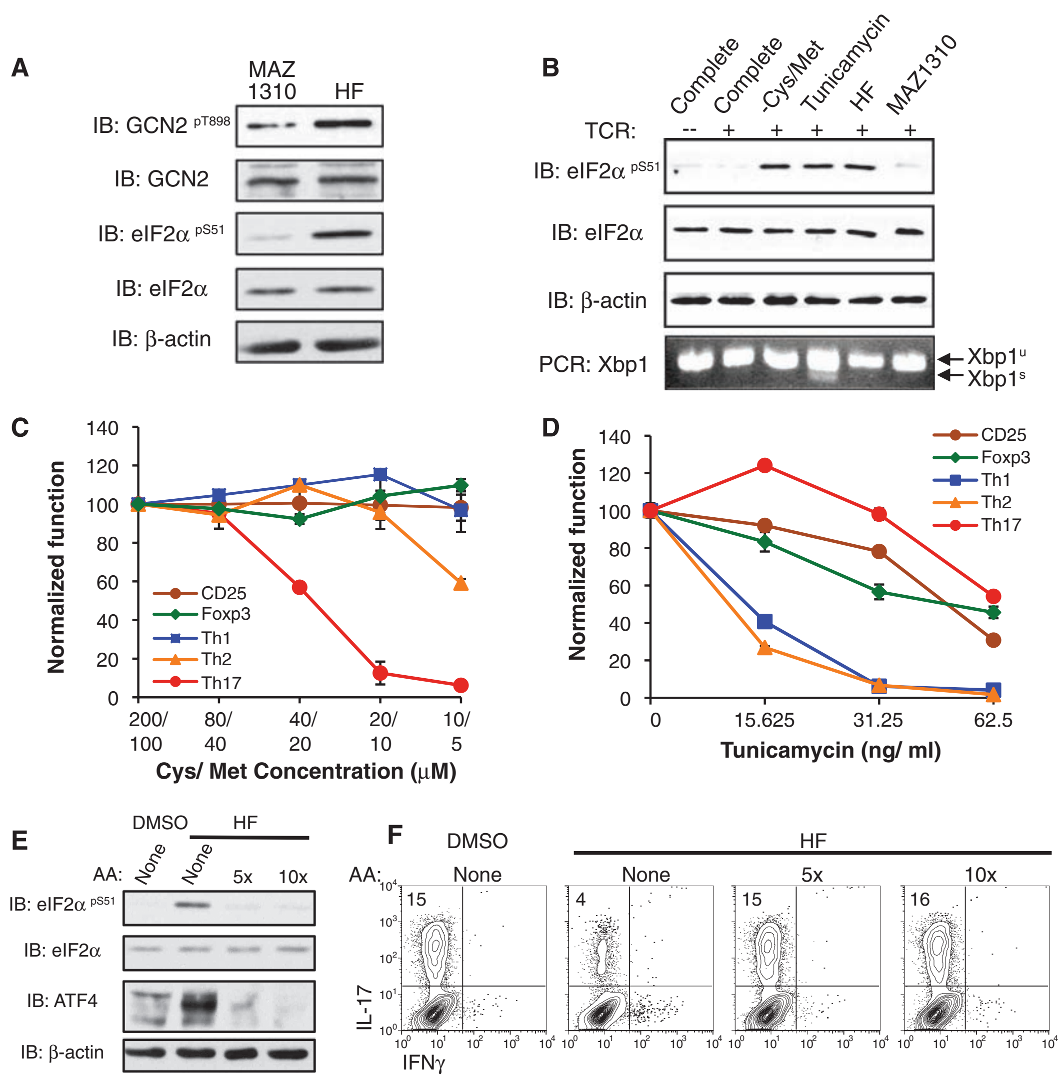

Fig. 3. Regulation of T_H17 differentiation by amino acids. (**A**) Lysates from TCR-activated T cells treated with MAZ1310 or HF for 4 hours were analyzed by Western blotting. (**B**) Unstimulated or activated T cells were cultured in complete medium, medium lacking Cys/Met (-Cys/Met), or complete medium containing tunicamycin, HF, or MAZ1310 and lysed after 4 hours for Western blot analysis. Xbp-1 splicing assay was performed on isolated cDNA (*6*). (**C**) Activated T cells were cultured without cytokines or polarized to T_H1, T_H2, iT_{reg}, or T_H17 cells. Titrating concentrations of Cys/Met are indicated. The percentages of T_H1, T_H2, and T_H17 cells, and those expressing CD25 or Foxp3, were determined as in Fig. 1A and are displayed as mean values ± SD, normalized to cells cultured in complete medium. (**D**) T cells differentiated as in (C) were treated with tunicamycin as indicated. T cell activation and differentiation was determined as in (C). (**E**) Activated T cells were treated with DMSO or HF. Some cultures were supplemented with 5× or 10× amino acids (*6*), and lysates were analyzed after 4 hours by Western blotting. (**F**) T cells activated in T_H17 polarizing conditions were treated with DMSO or HF plus amino acids, as indicated, and stained for intracellular cytokine expression. These data represent three experiments.

with ER or oxidative stress (e.g., GRP78/BiP, calreticulin) (table S1) (*18*, *19*). HF also activated the AAR in fibroblasts and epithelial cells (fig. S10) (*20*), establishing that AAR activation by HF is not limited to T cells. HF activated the AAR without concomitantly altering signaling through the nutrient sensor mTOR as determined by p70-S6K phosphorylation (fig. S11) (*21*).

We next tested whether AAR activation induced by selective amino acid deprivation (fig. S12, A and B) could mimic the effects of HF on T cell differentiation. Decreasing Cys/Met concentrations in differentiating T cell cultures impaired T_H17 cell development in a dose-dependent manner without affecting CD25 up-regulation or the differentiation of T_H1, T_H2, or iT_{reg} cells (Fig. 3C and fig. S12C). As with HF, amino acid restriction reduced T_H17 differentiation, independent of cell survival or proliferation (fig. S12D). Deprivation of leucine, or treatment with L-tryptophanol, an inhibitor of tryptophanyl-tRNA charging (fig. S12E), also diminished T_H17 differentiation, indicating that AAR activation restricts T_H17 differentiation in a manner not specific to individual amino acids. In contrast to amino acid deprivation, tunicamycin-induced ER stress suppressed the differentiation of both T_H1 and T_H2 cells at doses that did not affect T_H17 differentiation (Fig. 3D and fig. S12C). To establish whether AAR activation is required for the inhibition of T_H17 differentiation by HF, we added excess free amino acids to abrogate activation of the AAR in HF-treated cells. Under these conditions HF failed to induce eIF2α phosphorylation, up-regulate ATF4 protein expression, or prevent T_H17 differentiation (Fig. 3, E and F). Thus, activation of the AAR by HF is both necessary and sufficient for the repression of T_H17 differentiation.

Selective inhibition of T_H17 differentiation in vivo may have broad therapeutic implications. We used two distinct models of experimental autoimmune encephalomyelitis (EAE) to investigate whether systemic HF treatment could inhibit T_H17 differentiation and associated autoimmune inflammation in mice. Adjuvant-driven EAE was induced by immunizing wild-type mice with the immunodominant myelin antigen MOG33-55 emulsified in complete Freund's adjuvant (CFA) and was associated with infiltration of both T_H17- and IFN-γ–expressing T_H1 cells into central nervous system (CNS) tissue (fig. S13A). This model of EAE is sensitive to modulation of T_H17 responses (*9*, *22*, *23*). Low-dose HF treatment significantly reduced both the frequency and severity of adjuvant-driven EAE (Fig. 4A and fig. S13B). In contrast, passive EAE was initiated by transferring myelin proteolipid protein (PLP)–specific T cells into *recombination activating gene-2*$^{-/-}$ (*Rag2*$^{-/-}$) hosts (*24*), and this disease was associated with a predominant T_H1 response in the CNS (fig. S13C). HF-treated recipients developed passive EAE similar to control animals (Fig. 4B), indicating that HF specifically blunts autoimmune inflammation associated with T_H17 differentiation without inducing global immunosuppression. Both T_H1 and T_H17 cells are capable of inducing EAE upon adoptive transfer (*25*), but only adjuvant-driven, and not passive, EAE initiates a substantial T_H17 response. Thus, the protective specificity of HF in EAE is probably due to selective inhibition of T_H17, but not T_H1 differentiation.

Protection from adjuvant-driven EAE by HF was associated with fewer T_H17 cells, both in

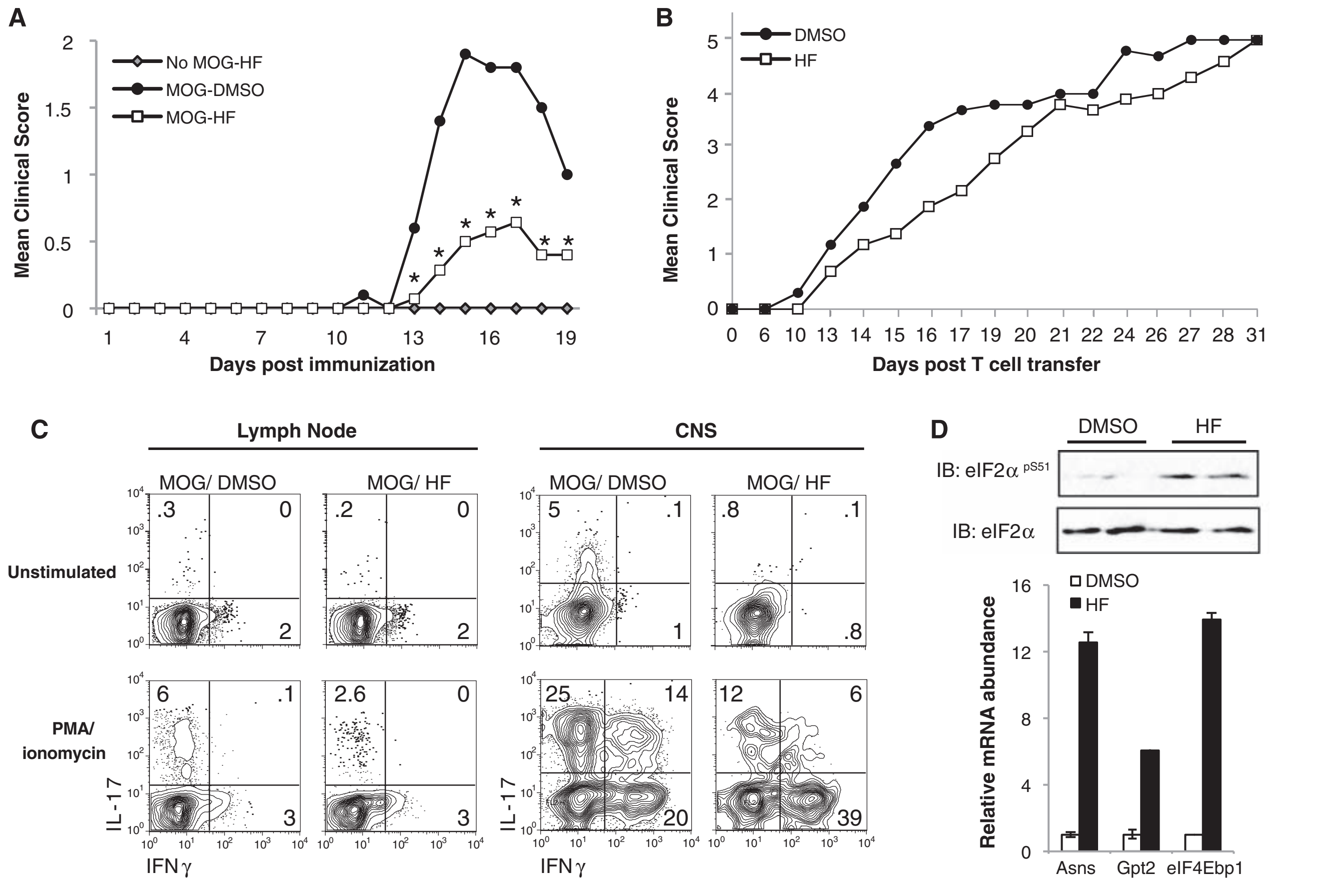

Fig. 4. HF inhibits T_H17-associated autoimmune inflammation in vivo. (**A**) Wild-type mice were immunized with phosphate-buffered saline or MOG33-55 emulsified in CFA and treated daily with DMSO or HF, and disease was monitored (*6*). (**B**) After PLP-specific T cell transfer, recipients were treated daily with DMSO or HF, and disease was monitored. Mean EAE scores are displayed. (**C**) (Left) Paraaortic lymph nodes from MOG-immunized mice treated with DMSO or HF were harvested on day 6. Mononuclear cells were cultured without (top) or with (bottom) PMA and ionomycin and stained for intracellular cytokines. (Right) Mononuclear cells isolated from CNS tissue of DMSO-treated (score = 2) or HF-treated (score = 0) mice were cultured and stained for intracellular cytokines as above. $TCR\beta^+$ $CD4^+$ cells were gated on for analyses. (**D**) (Top) Splenocyte lysates were prepared from DMSO- or HF-treated mice and analyzed by Western blotting. (Bottom) AAR-associated gene expression (*Asns*, *Gpt2*, *eIF4Ebp1*) was analyzed by QPCR on cDNA from spleens of mice treated with DMSO or HF. Transcript levels were normalized to *Hprt* and are displayed as mean expression ± SD (error bars) from triplicate samples. EAE data are cumulative from three independent experiments; other data represent two to three similar experiments.

the periphery before disease onset and the CNS during active disease (Fig. 4C). T_H17 cells initiate mononuclear cell recruitment into the CNS during adjuvant-driven EAE (*22*, *26*). HF treatment reduced T cell infiltration into the CNS (fig. S14) but did not change the proportion of T_H1 cells in the periphery or CNS (fig. S14). Moreover, splenocytes from HF-injected mice displayed increased eIF2α phosphorylation and expression of AAR-associated transcripts (Fig. 4D). Thus, HF treatment activates the AAR and selectively impairs both T_H17 differentiation and autoimmune inflammation in vivo.

In conclusion, HF selectively inhibits T_H17 differentiation and associated autoimmune inflammation via the cytoprotective AAR pathway. Endogenous amino acid restriction has been suggested to regulate inflammation (*27*). Indoleamine 2,3-dioxygenase (IDO), an IFN-γ–induced enzyme expressed by dendritic cells (DCs), metabolizes tryptophan, causes local amino acid depletion, and inhibits the proliferation of bystander T cells via the AAR (*28*). Local IDO expression also has been reported to expand, convert, and directly activate Foxp3+ T_{reg}s (*29*, *30*). Thus, AAR activation may protect against pathophysiologic inflammation by enforcing the tolerogenic effects of IDO-expressing DCs and concomitantly blunting T_H17 differentiation. Although the mechanism by which AAR activation constrains T_H17 differentiation remains unclear, these results highlight a previously unknown link between the AAR pathway and T_H17-mediated immune-pathology.

References and Notes

1. T. Korn, E. Bettelli, M. Oukka, V. K. Kuchroo, *Annu. Rev. Immunol.* **27**, 485 (2009).
2. C. Dong, *Nat. Rev. Immunol.* **8**, 337 (2008).
3. M. Pines, A. Nagler, *Gen. Pharmacol.* **30**, 445 (1998).
4. Y. Gnainsky *et al.*, *Cell Tissue Res.* **328**, 153 (2007).
5. M. Pines, D. Snyder, S. Yarkoni, A. Nagler, *Biol. Blood Marrow Transplant.* **9**, 417 (2003).
6. Materials and methods are available as supporting material on *Science* Online.
7. M. Leiba *et al.*, *J. Leukocyte Biol.* **80**, 399 (2006).
8. H. Park *et al.*, *Nat. Immunol.* **6**, 1133 (2005).
9. X. O. Yang *et al.*, *Immunity* **28**, 29 (2008).
10. I. I. Ivanov *et al.*, *Cell* **126**, 1121 (2006).
11. L. Zhou *et al.*, *Nat. Immunol.* **8**, 967 (2007).
12. M. O. Li, Y. Y. Wan, S. Sanjabi, A. K. Robertson, R. A. Flavell, *Annu. Rev. Immunol.* **24**, 99 (2006).
13. X. O. Yang *et al.*, *J. Biol. Chem.* **282**, 9358 (2007).
14. C. Deval *et al.*, *FEBS J.* **276**, 707 (2009).
15. R. C. Wek, H. Y. Jiang, T. G. Anthony, *Biochem. Soc. Trans.* **34**, 7 (2006).
16. H. P. Harding *et al.*, *Mol. Cell* **6**, 1099 (2000).
17. H. P. Harding *et al.*, *Mol. Cell* **11**, 619 (2003).
18. A. H. Lee, N. N. Iwakoshi, L. H. Glimcher, *Mol. Cell. Biol.* **23**, 7448 (2003).
19. D. Ron, P. Walter, *Nat. Rev. Mol. Cell Biol.* **8**, 519 (2007).
20. Y. Kamberov, thesis, Harvard University (2008).
21. D. C. Fingar, J. Blenis, *Oncogene* **23**, 3151 (2004).
22. S. Serada *et al.*, *Proc. Natl. Acad. Sci. U.S.A.* **105**, 9041 (2008).
23. C. L. Langrish *et al.*, *J. Exp. Med.* **201**, 233 (2005).
24. H. Waldner, M. Collins, V. K. Kuchroo, *J. Clin. Invest.* **113**, 990 (2004).
25. M. A. Kroenke, T. J. Carlson, A. V. Andjelkovic, B. M. Segal, *J. Exp. Med.* **205**, 1535 (2008).
26. A. Reboldi *et al.*, *Nat. Immunol.* **10**, 514 (2009).
27. A. L. Mellor, D. H. Munn, *Nat. Rev. Immunol.* **8**, 74 (2008).
28. D. H. Munn *et al.*, *Immunity* **22**, 633 (2005).
29. M. J. Park *et al.*, *Arthritis Res. Ther.* **10**, R11 (2008).
30. P. Puccetti, U. Grohmann, *Nat. Rev. Immunol.* **7**, 817 (2007).

31. D. Littman and A. Rudensky provided reagents for this work, and K. Otipoby prepared recombinant TAT-Cre. We thank J. Hill and K. Leatherbee for technical assistance with microarray data analysis and members of the Rao lab for critical discussion. This work was supported by grants from NIH (to A.R., D.U., and M.W.) and the Juvenile Diabetes Research Foundation (to A.R.). M.S.S. was supported by the Irvington Institute fellowship program of the Cancer Research Institute. D.P.C. was supported by a fellowship from the Portuguese Foundation for Science and Technology. S.K. was supported by an NIH training grant (T32). Further support was provided by a P01 grant to K Rajewsky. M.S.S., A.R., T.K., and M.W. have filed patent applications concerning the use of HF and its derivatives to inhibit T_H17 cell differentiation. Array data can be found at www.ncbi.nlm.nih.gov/geo/query/acc.cgi?acc=GSE15624 with the accession number of GSE15624.

Supporting Online Material
www.sciencemag.org/cgi/content/full/324/5932/1334/DC1
Materials and Methods
Figs. S1 to S14
Tables S1 and S2
References

23 February 2009; accepted 8 April 2009
10.1126/science.1172638

Endogenous Activation Patterns of Cdc42 GTPase Within *Drosophila* Embryos

Daichi Kamiyama and Akira Chiba*

Knowing when and where a given protein is activated within intact animals assists in elucidating its in vivo function. With the use of a genetically encoded A-probe (activation bioprobe), we revealed that Cdc42 guanosine triphosphatase (GTPase) remains inactive within *Drosophila* embryos during the first two-thirds of embryogenesis. Within the central nervous system where Cdc42 activity first becomes up-regulated, individual neurons display patterns restricted to specific subcellular compartments. At both organismal and cellular levels, Cdc42's endogenous activation patterns in the wild type allow predictions of where loss-of-function phenotypes will emerge in *cdc42/cdc42* mutants. Genetic tests support the importance of suppressing endogenous Cdc42 activities until needed. Thus, bioprobe-assisted analysis uncovers how ubiquitously expressed signaling proteins control cellular events through continual regulation of their activities within animals.

Proteins trigger signaling pathways upon activation (*1*). Cdc42 is a member of the monomeric Rho guanosine triphosphatase (GTPase) family expressed ubiquitously in eukaryotes (*2*). It cycles between a guanosine diphosphate (GDP)–bound inactive and GTP-bound active state. As with other family members, Cdc42 has been studied in diverse contexts such as cytoskeletal dynamics, membrane trafficking, and gene regulation (*3*–*6*) through overexpression of its wild-type, constitutively activated, and/or other mutant forms (*7*–*12*). Such approaches demonstrate profound potentials of the Rho GTPases as versatile signaling proteins. For example, Cdc42 overexpression disrupts the establishment and maintenance of polarity and mobility of various cells in early embryos. In late embryos, the complex morphology of neurons can be drastically altered after expressing mutant Cdc42 proteins. Yet, a biochemical analysis suggests that only a fraction of Rho GTPases may be activated at any given time (*13*). Advances in genetically encoded fluorescent proteins and FRET (Forster resonance energy transfer) detection allow the design of molecular bioprobes that reveal activities of specific endogenous molecules (*14*–*16*). However, this visualization approach has yet to be implemented in vivo.

To examine the activation patterns of Cdc42 within cells and tissues of intact organisms, we generated genetically encoded molecular bioprobes that can be used in *Drosophila.* We designed an A-probe (activation bioprobe) for Cdc42 by using the fact that, upon activation, Cdc42 reversibly binds to a specific peptide. In the A-probe, Cdc42 and CBD (Cdc42-binding domain) are coexpressed as a single polypeptide. An advantage of this A-probe (A-probe.1) is its FRET donor-to-acceptor ratio stays one-to-one and, thus, allows for quantification of FRET efficiency. A second design (A-probe.2) consisted of Cdc42 and CBD as separate molecules. When introduced in vivo, both A probes revealed similar FRET patterns within uniquely identified neurons (fig. S1). Use of controls defined the full range of FRET in vivo (fig. S2). Experiments shown used A-probe.1.

We expressed our Cdc42 A-probe in all cells of embryos by using a constitutive GAL4 driver (*act'-GAL4*). A-probe FRET remains rare through the first two-thirds of development (Fig. 1A and figs. S3 and S4). At hour 15:00 of embryogenesis (stage 16), the cells at the dorsal midline displayed heightened FRET. By this time, internal tissues such as the trachea and central nervous system (CNS) also exhibited similarly increased FRET. To further examine these internal tissues, we used tissue-specific GAL4 drivers (*btl'-GAL4* and *elav'-GAL4* for, respectively, trachea and CNS). In both tissues, endogenous activities of Cdc42 were suppressed until after the embryos initiated organogenesis (Fig. 1, B and C). In *Drosophila*, genetic deletion of Cdc42 results in 100% lethality. However, embryos lacking both maternal and zygotic *cdc42* gene functions still undergo normal development for much of embryogenesis. Previous work showed defects in dorsal closure, abnormal tracheal morphogenesis, and incomplete CNS maturation in *cdc42/cdc42* loss-of-function mutants (*17*, *18*). Phenotypes that manifest late during embryogenesis were puzzling because all cells maintain endogenous Cdc42 expression and, furthermore, are capable of responding to artificial activation of Cdc42 even in early stages of embryogenesis. However, a simple scenario is possible: The endogenous activation patterns of Cdc42 proteins, and not their mere presence in wild type, allow predictions of when and where loss-of-function phenotypes would emerge within *cdc42/cdc42* mutants (Fig. 1D).

Although Cdc42 proteins are ubiquitously present throughout the cytoplasm (fig. S5), their activation patterns remain uncharacterized within individual cells in vivo. The A-probe FRET patterns indicate that neurons, especially within their axons and/or dendrites in longitudinal connectives, activated Cdc42 prominently by hour 15:00 (fig. S6). Therefore, we expressed A-probe specifically in the aCC (anterior corner cell) motoneuron at different stages of its development (Fig. 2A and fig. S7). The aCC is one of the first neurons to develop complex cellular morphologies in the CNS (*19*–*21*). Within the aCC, A-probe displayed highly restricted and reproducible spatiotemporal FRET patterns (Fig. 2B and fig. S8). Before hour 13:00, FRET was rarely detected within the axon, even though it began extension 4 hours earlier. At hour 13:00, FRET became apparent within the axon, peaking at its proximal region from which dendrites were about to emerge. The local elevation of A-probe FRET continued as the neuron progressively attains dendritic complexity (fig. S9). Therefore, within an individual neuron, Cdc42's first activation coincides temporarily with the onset of dendrogenesis, and, furthermore, its activities are spatially restricted to the compartment from which dendrites emerge. Experiments with A-probe.2 produced similar results (fig. S10).

We hypothesized that removal of Cdc42 from the aCC would induce abnormal development of this neuron only when and where the protein is normally activated. To demonstrate this, we designed single-cell genetic tests that would reveal cell-autonomous functions of Cdc42 within the aCC motoneuron in the CNS, while paying attention to its normally stereotyped dendritic development (Fig. 3A and fig. S11). Despite the specific phenotype displayed by pioneer neurons (Fig. 3A and figs. S12 and S13), the CNS of mutants that lack both maternal and zygotic sup-

Department of Biology and Miami Institute of Molecular Imaging and Computation, University of Miami, Coral Gables, FL 33146, USA.

*To whom correspondence should be addressed. E-mail: akira.chiba@miami.edu

plies of *cdc42* gene (*17*) maintained an overall wild-type morphology at least up to hour 15:00 (fig. S14). There is no evidence that supports these neurons requiring Cdc42 before dendrogenesis, when the molecule would first become activated. Together, the results not only support the cell-autonomous requirement of endogenous Cdc42 during the initiation of dendrites by a model neuron but also point to spatiotemporal correlation between the activation of Cdc42 and its role within this morphologically complex cell down to the level of subcellular compartments (Fig. 3C).

To investigate the importance of controlling endogenous activity patterns of Cdc42 within a given cell, we intentionally overrode the endogenous control of Cdc42 activities in the aCC by overexpressing a constitutively activated form of Cdc42 [green fluorescent protein (GFP)::Cdc42^{V12}] (Fig. 3B). When Cdc42 was activated at high amounts and out of normal context from hour 8:00 onward, the aCC (n = 56) displayed aberrant migration of the cell body (34%), thickening of the axon (100%), and premature termination of its axonal growth cone before reaching the target muscle (77%). These abnormalities are not only qualitatively distinct from the loss-of-function phenotype but also variable from segment to segment within a given embryo and could emerge as early as hour 10:00.

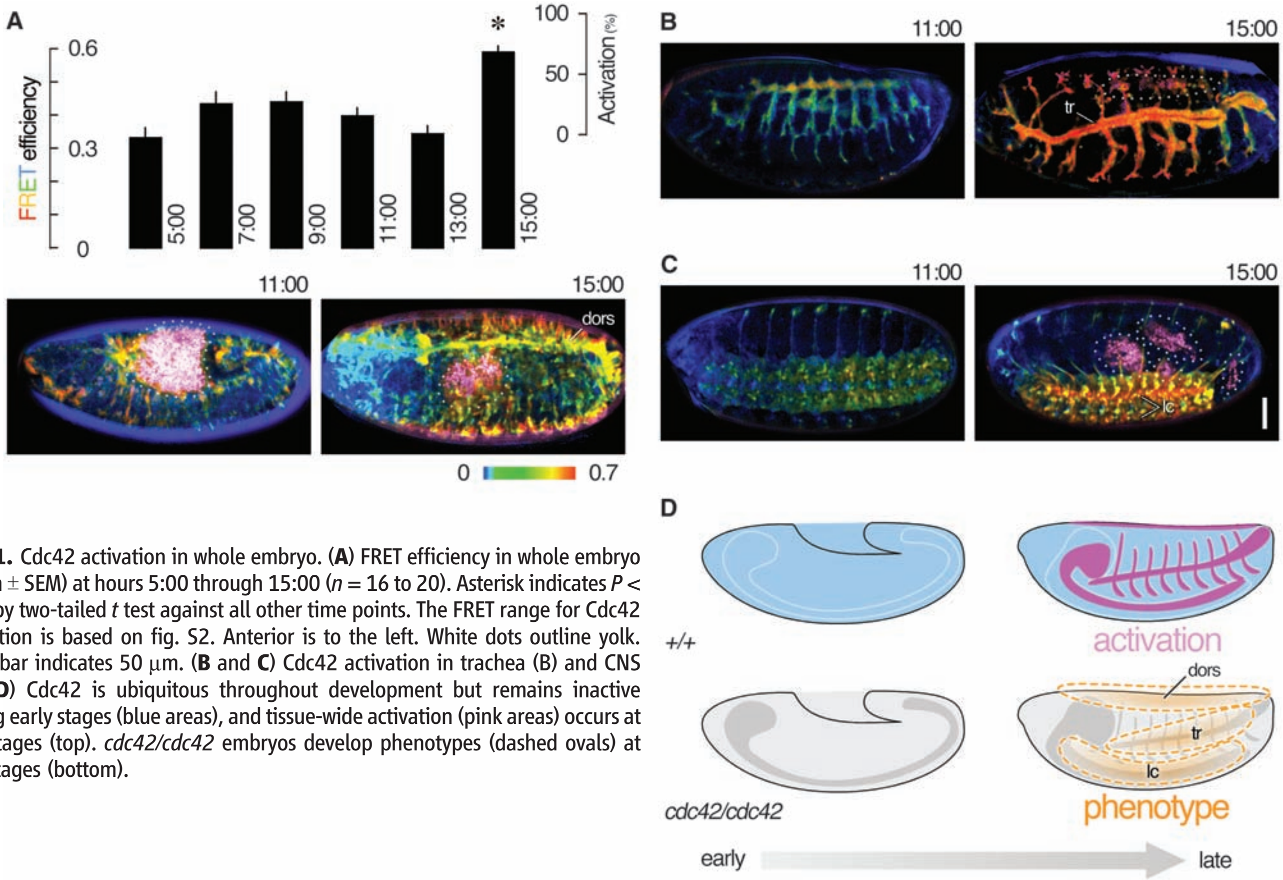

Fig. 1. Cdc42 activation in whole embryo. (**A**) FRET efficiency in whole embryo (mean ± SEM) at hours 5:00 through 15:00 (n = 16 to 20). Asterisk indicates P < 0.01 by two-tailed t test against all other time points. The FRET range for Cdc42 activation is based on fig. S2. Anterior is to the left. White dots outline yolk. Scale bar indicates 50 μm. (**B** and **C**) Cdc42 activation in trachea (B) and CNS (C). (**D**) Cdc42 is ubiquitous throughout development but remains inactive during early stages (blue areas), and tissue-wide activation (pink areas) occurs at late stages (top). *cdc42/cdc42* embryos develop phenotypes (dashed ovals) at late stages (bottom).

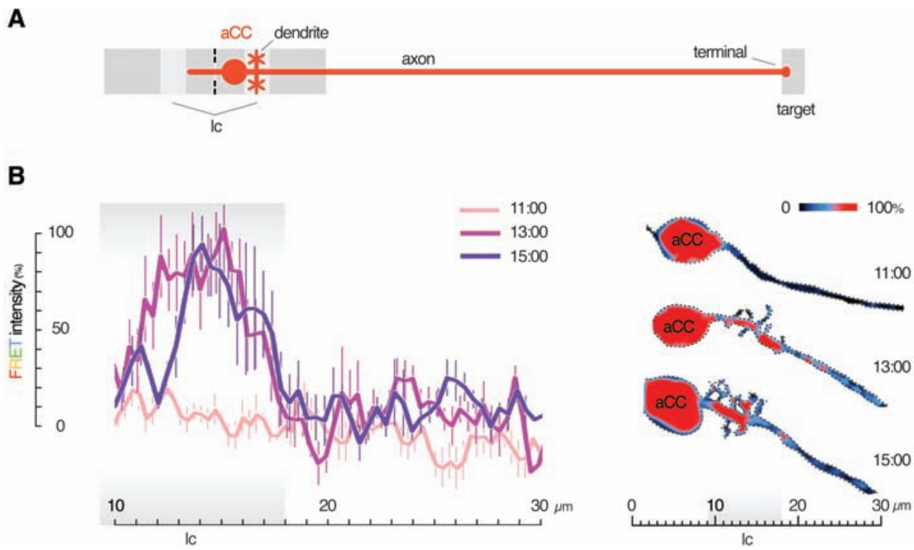

Fig. 2. Cdc42 activation in aCC motoneuron. (**A**) aCC extends its axon laterally to reach the target muscle. The dendrite develops within the longitudinal connective (lc) of the CNS. Anterior is to the top. (**B**) Relative intensity of A-probe FRET (mean ± SEM) along the proximal region of aCC axon before (11:00), during (13:00), and after (15:00) the onset of dendrogenesis (n = 6 each). The patterns at 13:00 and 15:00 differ from that at 11:00 by analysis of variance (P < 0.01). [FRET activities within cell body are mostly nuclear (fig. S1).]

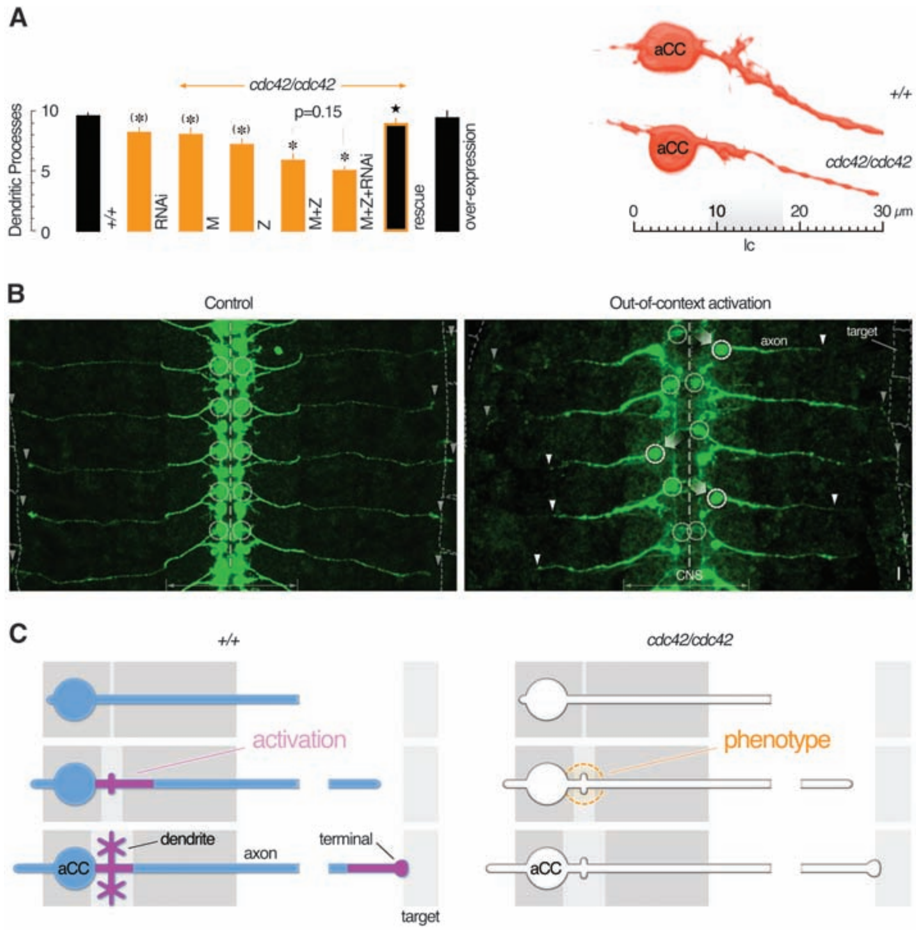

Fig. 3. Genetic tests in aCC motoneuron. (**A**) The number of dendritic processes at 15:00 in wild type (+/+, n = 21), cell-specific RNA interference (RNAi) (*eve'-GAL4/UAS-cdc42^{RNAi}*, n = 13), maternal loss of function (maternally *cdc42^4/cdc42^6*, n = 9) (*M*), zygotic loss of function (zygotically *cdc42^4/Y*, n = 13) (*Z*), maternal and zygotic loss of function (maternally *cdc42^4/cdc42^6* and zygotically *cdc42$^{4\ \mathrm{or}\ 6}$/Y*, n = 12) (*M+Z*), cell-specific RNAi plus maternal and zygotic loss of function (maternally *cdc42^4/cdc42^6* and zygotically *cdc42$^{4\ \mathrm{or}\ 6}$/Y;eve'-GAL4/UAS-cdc42^{RNAi}*, n = 14), cell-specific rescue (maternally *cdc42^4/cdc42^6* and zygotically *cdc42$^{4\ \mathrm{or}\ 6}$/Y;eve'-GAL4/UAS-cdc42*, n = 12), and cell-specific overexpression of wild-type Cdc42 (*eve'-GAL4/UAS-cdc42*, n = 15). Asterisk and parenthetical asterisk indicate, respectively, P < 0.01 and P < 0.05 against wild type, and star indicates P < 0.01 against loss-of-function mutant (*22*). (**B**) Out-of-context activation of Cdc42 in aCC (GFP in green) in the CNS (with pan-neuronal horseradish peroxidase antibody in purple) of wild-type embryos (*eve'-GAL4/eve'-GAL4;UAS-gfp::cdc42^{V12}/UAS-gfp::cdc42^{V12}*) causes changes in migration of the cell body (white circle), thickening of axons, and premature termination of axonal growth cone (arrowhead). The control expresses GFP-tagged wild-type Cdc42 (*eve'-GAL4/eve'-GAL4;UAS-gfp::cdc42/uas-gfp::cdc42*). (**C**) Cdc42 protein is present in entire cytoplasm of aCC. Its activation (pink area) occurs at the onset of dendrogenesis (left), where the phenotype (dashed circle) resulting from its genetic deletion appears (right).

They are a result of the activation of Cdc42 protein, and not its mere presence, because overexpression of wild-type Cdc42 (GFP::Cdc42) at similar amounts produces no changes in the aCC (Fig. 3B). Therefore, precise spatiotemporal control of Cdc42 activities is critical to achieve the normal development of neurons.

With use of our in vivo bioprobe imaging technology, we revealed the surprisingly restricted pattern for endogenous activities of a potent and ubiquitously expressed signaling protein both within individual cells and in whole animals. Genetic experiments further supported the causal link between the molecule's activation and its function in vivo. The bioprobe-assisted approach is indispensable in elucidating the function of molecules whose activities receive continual controls within organisms.

References and Notes

1. S. E. Egan, R. A. Weinberg, *Nature* **365**, 781 (1993).
2. S. Etienne-Manneville, A. Hall, *Nature* **420**, 629 (2002).
3. L. Luo, *Nat. Rev. Neurosci.* **1**, 173 (2000).
4. J. S. da Silva, C. G. Dotti, *Nat. Rev. Neurosci.* **3**, 694 (2002).
5. M. Fukata, M. Nakagawa, K. Kaibuchi, *Curr. Opin. Cell Biol.* **15**, 590 (2003).
6. E. E. Govek, S. E. Newey, L. Van Aelst, *Genes Dev.* **19**, 1 (2005).
7. L. Luo, Y. J. Liao, L. Y. Jan, Y. N. Jan, *Genes Dev.* **8**, 1787 (1994).
8. R. Threadgill, K. Bobb, A. Ghosh, *Neuron* **19**, 625 (1997).
9. M. L. Ruchhoeft, S. Ohnuma, L. McNeill, C. E. Holt, W. A. Harris, *J. Neurosci.* **19**, 8454 (1999).
10. Z. Li, L. Van Aelst, H. T. Cline, *Nat. Neurosci.* **3**, 217 (2000).
11. X. B. Yuan *et al.*, *Nat. Cell Biol.* **5**, 38 (2003).
12. L. Van Aelst, H. T. Cline, *Curr. Opin. Neurobiol.* **14**, 297 (2004).
13. M. A. Del Pozo *et al.*, *Nat. Cell Biol.* **4**, 232 (2002).
14. P. Nalbant, L. Hodgson, V. Kraynov, A. Toutchkine, K. M. Hahn, *Science* **305**, 1615 (2004).
15. T. Nakamura, K. Aoki, M. Matsuda, *Brain Res. Mol. Brain Res.* **139**, 277 (2005).
16. O. Pertz, L. Hodgson, R. L. Klemke, K. M. Hahn, *Nature* **440**, 1069 (2006).
17. J. L. Genova, S. Jong, J. T. Camp, R. G. Fehon, *Dev. Biol.* **221**, 181 (2000).
18. A. Lundström *et al.*, *Genes Dev.* **18**, 2161 (2004).
19. J. B. Thomas, M. J. Bastiani, M. Bate, C. S. Goodman, *Nature* **310**, 203 (1984).
20. M. Landgraf, V. Jeffrey, M. Fujioka, J. B. Jaynes, M. Bate, *PLoS Biol.* **1**, E41 (2003).
21. M. P. Furrer, S. Kim, B. Wolf, A. Chiba, *Nat. Neurosci.* **6**, 223 (2003).
22. Materials and methods are available as supporting material on *Science* Online.

23. We thank M. Hayden, K. Chittanon-Buranachai, R. Clegg, S. Rogers, S. Siechen, and I. Vasenkova for advice; S. Hsu, O. Alpcan, M. Furrer, S. Deng, and R. Kamiyama for technical assistance; Bloomington *Drosophila* Stock Center and Developmental Studies Hybridoma Bank for reagents; and E. Giniger, J. Baker, and M. Kim for comments on manuscript. Supported by grants from NIH/National Institute of Neurological Disorders and Stroke and NIH/National Institute of Mental Health (A.C.).

Supporting Online Material

www.sciencemag.org/cgi/content/full/324/5932/1338/DC1
Materials and Methods
Figs. S1 to S15
References

7 January 2009; accepted 20 April 2009
10.1126/science.1170615

New Products Focus: Imaging and Microscopy

Cell Imaging System

The IN Cell Analyzer 2000 is a flexible cell imaging system for high content analysis with high image quality, speed, and ease of use. The system can perform a wide variety of challenging experiments, from investigative microscopy through automated screening and imaging of organelles, cells, tissues, and whole organisms. New features include rapid preview scanning of a selected area of a sample at any available magnification prior to starting an acquisition run; a high-performance large-chip charge-coupled device camera combined with a widefield illumination source that is twice as bright as a conventional xenon lamp, ensuring statistically robust results in a single pass; and whole-well imaging to capture an entire well in a single image, enhancing the ability to image rare events. A wide range of objectives are available to suit a variety of sensitivity requirements.

GE Healthcare
For information +44-(0)20-7866-7862
www.gehealthcare.com/incell

CrossBeam Workstation

The Auriga CrossBeam focused ion beam/scanning electron microscope workstation features a new chamber design and unique charge compensation system for advanced analysis. The instrument's redesigned vacuum chamber includes 15 ports for different detectors. Its charge compensation system enables the local application of an inert gas flush. In this way, electrostatic charging of nonconductive samples is neutralized and detection of secondary electrons as well as backscattered electrons becomes feasible. The heart of the workstation is the field emission-scanning electron microscopy column, which enables the analysis of magnetic samples.

Carl Zeiss
For information +49-73-64-20-21-94
www.zeiss.de

Fluorescent Blot Kit

SpectraPlex provides the tools to perform quantitative, two-color fluorescent protein immunoblots. Multicolor detection makes it possible to simultaneously quantify a loading control and a protein of interest or phosphorylated isoforms of a single protein, which greatly increases the information from a single blot while saving time and reagents. The kit includes fluorescently labeled secondary antibodies as well as blocking and washing buffers optimized to provide high sensitivity; as little as 1 pg of protein can be detected. The excitation and emission spectra of the SpectraPlex secondary antibodies are compatible with common fluorescence imaging systems.

Alpha Innotech
For information 800-795-5556
www.alphainnotech.com

Scanning Probe Microscope

The Hydra is designed to open new horizons for the application of atomic force microscopy (AFM) in biology. The ground-up design of the Hydra provides no geometric or optical obstruction or interference either from above or below the scanning probe microscope system. It incorporates a tuning fork feedback mechanism to provide new sensitivities. The Hydra comes with a NanoToolKit of glass-based probes, including transparent AFM probes and nanopipette probes for conductance and structurally correlated patch-clamp applications. The instrument is suitable for all modes of optical microscopy, including standard fluorescence, confocal, total internal reflection fluorescence, fluorescence resonance energy transfer, and differential interference contrast techniques.

Nanonics Imaging
For information 800-289-7162
www.nanonics.co.il

Optical Metrology Instrument

The LEXT OLS4000 is the latest version of the LEXT confocal laser scanning microscope metrology system. It offers enhanced functionality, including near-vertical slope capabilities, large optical zoom, and a navigation overview window. Its software brings complex processes within easy reach of a broad range of users. The system has a sleek look and requires only a single control unit. It has been designed with a large and fast scanning mirror along with dual pinholes; the large mirror enables the system to provide superior optical quality, and the increased scan speed halves the time it takes to create a three-dimensional image of a sample. The 405-nm laser and dual pinholes operate simultaneously to ensure that the system provides high resolution and clarity as well as enabling steep slope detection up to 85°, so even the most complex surface topologies can be imaged and analyzed.

Olympus Europe
For information +49-40-2-37-73-5426
www.microscopy.olympus.eu

Electronically submit your new product description or product literature information! Go to **www.sciencemag.org/products/newproducts.dtl** for more information.

Newly offered instrumentation, apparatus, and laboratory materials of interest to researchers in all disciplines in academic, industrial, and governmental organizations are featured in this space. Emphasis is given to purpose, chief characteristics, and availabilty of products and materials. Endorsement by *Science* or AAAS of any products or materials mentioned is not implied. Additional information may be obtained from the manufacturer or supplier.

Release The Power of Science

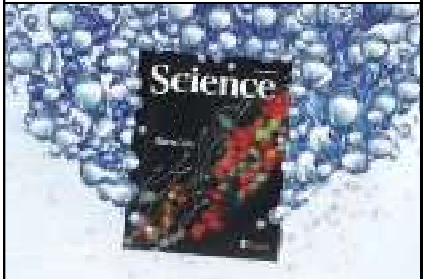

Science Careers Classified Advertising

For full advertising details, go to ScienceCareers.org and click For Advertisers, or call one of our representatives.

UNITED STATES & CANADA

E-mail: advertise@sciencecareers.org
Fax: 202-289-6742

Daryl Anderson
US Sales Manager
Phone: 202-326-6543

Joribah Able
Industry – US & Canada
Academic – Midwest/Canada
Phone: 202-326-6572

Alexis Fleming
Academic – East Coast
Phone: 202-326-6578

Nicholas Hintibidze
Academic – West and South Central
Phone: 202-326-6533

Tina Burks
Online Job Posting customer service
Phone: 202-326-6577

EUROPE & INTERNATIONAL

E-mail: ads@science-int.co.uk
Fax: +44 (0) 1223 326532

Tracy Holmes
Associate Director, *Science* Careers
Phone: +44 (0) 1223 326525

Alex Palmer
Phone: +44 (0) 1223 326527

Dan Pennington
Phone: +44 (0) 1223 326517

Susanne Kharraz Tavakol
Phone: +44 (0) 1223 326529

Lisa Patterson
Phone: +44 (0) 1223 326528

JAPAN

Mashy Yoshikawa
Phone: +81 (0) 3 3235 5961
E-mail: myoshikawa@aaas.org

To subscribe to *Science*:
In US/Canada call 202-326-6417 or 1-800-731-4939.
In the rest of the world call +44 (0) 1223 326515.

Science makes every effort to screen its ads for offensive and/or discriminatory language in accordance with US and non-US law. Since we are an international journal, you may see ads from non-US countries that request applications from specific demographic groups. Since US law does not apply to other countries we try to accommodate recruiting practices of other countries. However, we encourage our readers to alert us to any ads that they feel are discriminatory or offensive.

Science Careers
From the journal *Science* AAAS

Department of Health and Human Services
National Institutes of Health
National Institute on Aging
Intramural Research Program

Staff Scientist - Animal Program Director

The National Institute on Aging (NIA), a major research component of the National Institutes of Health (NIH) and Department of Health and Human Services (DHHS), is recruiting for a Staff Scientist-Facility Head who will serve as the Animal Program Director for the NIA Intramural Research Program (IRP). The incumbent will be responsible for an AAALAC accredited animal care and use program and for support of the animal research programs in the Institute, studying animal models of development and aging, and interventions to prevent or alleviate aging-related deficits. The supervisory and regulatory responsibilities of this position require the applicant to hold a veterinary degree (D.V.M., V.M.D., or equivalent degree) with certification or eligibility for board certification in laboratory animal medicine or veterinary pathology.

Applicants must have a proven record of management of an animal research program and demonstrated experience with the regulatory aspects of animal welfare. The expertise and experience should include, but not be limited to interaction and cooperation with scientific staff in a manner that promotes and facilitates their scientific programs. Duties will include cost-effective breeding and maintaining numerous transgenic and knockout lines (currently in excess of 600) including "difficult" lines, collaboration with scientific staff in effective production and import of new genetically manipulated lines, and, especially, in maintaining a current and accurate database on the colony status. The incumbent will take primary responsibility for the clinical aspects of the animal program and will oversee animal health surveillance and maintain both a barrier facility and a quarantine area. The incumbent will perform animal surgery and teach appropriate procedures to animal care and technical staff.

Salary is commensurate with experience and accomplishments. The salary range for Staff Scientists is $87,000 - $171,257. A full Civil Service package of benefits (including retirement, health, life and long term care insurance, Thrift Savings Plan, etc.) is available. Additional information regarding the NIA, IRP and the RRB is available at the following websites: **http://www.grc.nia.nih.gov** and **http://grc.nia.nih.gov/branches/rrb/rrb.htm** . To apply: Please send a cover letter, curriculum vitae, bibliography, statement of research interests, and three letters of recommendation to: Peggy Grothe, Intramural Program Specialist; Office of the Scientific Director; National Institute on Aging, 251 Bayview Boulevard, Suite 100-Room 04C232, Baltimore, MD 21224-6825. Position will remain open until filled; however, application reviews will begin **August 1, 2009**. Please include the following vacancy number in all correspondence: Vacancy # NIA-IRP-09-06. If additional information is needed, please call 410-558-8012 or email: **grothep@mail.nih.gov**.

DHHS and NIH are Equal Opportunity Employers

Max Planck Institute for Demographic Research

Directors: Prof. James W. Vaupel – Prof. Joshua R. Goldstein

www.demogr.mpg.de

To synthesize insights from mathematical demography and evolutionary biology, the Max Planck Institute for Demographic Research is pursuing new initiatives in the

Quantitative Analysis of Age-Specific Life-History Evolution.

The institute is looking to recruit promising scientists from diverse disciplines at the

PhD, Post-Doc, and Research Scientist levels.

The successful candidates will join a thriving Laboratory of Evolutionary Biodemography, where they will interact across disciplines with 20 other scientists, all of whom are committed to understanding how evolution can shape age-specific patterns of mortality and fertility. The research program aims to tackle this common goal by combining insights from diverse fields, including demography, life history, biology, ecology, mathematics, statistics, and actuarial science. We foster the exchange of ideas between those working both theoretically and empirically, and we aim to cultivate a range of complementary studies which use field and lab data and are based on comparative and analytical approaches. To consider a wide range of possible evolutionary outcomes, we work with a broad selection of study organisms including mammals, birds, fish, invertebrates, and plants. We will consider flexible, open appointments for strong candidates with appropriate backgrounds and relevant interests. Further information can be found at www.demogr.mpg.de.

Applications should include a CV with a statement of academic interests and relevant experience, details of all qualifications including grades, a list of any publications and the contact details of 3 referees.

Review of applications will begin on 15th June 2009. PhD positions will typically start in September or October 2009, and other positions will start as soon as possible after appointment. PhD and Postdoc appointments are made on doctoral and postdoctoral stipends respectively.

Research scientists will be employed up to salary level 15 on the basis of the German TVöD system according to the qualification of the candidate and in accordance with the rules of federal employees in Germany.

The Max Planck Society wishes to increase the share of women in areas where they are underrepresented, and strongly encourages women to apply.

The Max Planck Society is committed to employing more handicapped individuals and especially encourages them to apply.

Please send all materials (by e-mail) to Prof. James W. Vaupel, Director of the Max Planck Institute for Demographic Research, at: appl-evodemo@demogr.mpg.de.

MAX-PLANCK-GESELLSCHAFT

NATIONAL CANCER INSTITUTE

Head of Surgical Pathology And Head of Cytopathology

Position Description

The Laboratory of Pathology, Center for Cancer Research, National Cancer Institute, is seeking Heads of the General Surgical Pathology and Cytopathology Sections. These positions are among several that have become available in a restructuring of the Laboratory of Pathology. We are seeking accomplished academic diagnosticians who can take advantage of a stimulating collaborative research environment. Resources appropriate to the candidates' goals will be provided. In addition, incumbents will be responsible for leading small groups of surgical or cytopathologists, and for teaching residents and fellows.

About NCI's Center for Cancer Research

The National Cancer Institute is part of the National Institutes of Health in the Department of Health and Human Services, a fe deral government agency. The Center for Cancer Research (CCR) is the largest component of the NCI intramural biomedical research effort at NIH and a major user of the NIH Clinical Research Center, a state-of-the-art research hospital on the campus of the NIH in Bethesda, Maryland. The CCR offers tremendous depth and breadth of intellectual and technological resources, as well as opportunities for collaboration with investigators both within and outside of the NIH. The research environment is highly conducive to advancing translational research and highly collaborative, emphasizing multidisciplinary and interdisciplinary team science.

Location

The Laboratory of Pathology is located on the campus of the National Institutes of Health in Bethesda, Maryland, a suburb of Washington, D.C.

Eligibility/Salary

Applicants must have an M.D. or M.D., Ph.D. degree, be board-certified in Anatomic Pathology and be eligible to be credentialed to practice medicine at the NIH. Candidates for Head of Cytopathology should also be board-certified in Cytopathology. Successful candidates will have had both solid training and extensive experience in diagnostic pathology, a record of, and interest in, investigative pursuits as well as leadership and team-building capabilities, and a commitment to training and mentoring. Salaries are negotiable within a range and are dependent upon qualifications and experience. A full package of benefits, including health insurance, life insurance, retirement and Thrift Savings Plan, is available to all Federal employees. This position is not restricted to U.S. citizens.

Application

Interested individuals should submit a cover letter specifying which position is of interest, curriculum vitae, a career synopsis and a statement of future plans (1-2 pages) electronically to bronezm@mail.nih.gov, or by mail to the address below. Applications will begin to be considered on or around **August 1, 2009**. The positions will remain open until filled. **Dr. Mark C. Udey, Chair, Search Committee, Laboratory of Pathology, Center for Cancer Research, NIH, c/o Ms. Melissa Bronez, Executive Secretary, 9000 Rockville Pike, 31 Center Drive, Building 31, Room 31A11, MSC 2440, Bethesda, MD 20892-2440**.

NATIONAL CANCER INSTITUTE

Tenure-Track or Tenure-Eligible Molecular Pathologist

Job Description

The Laboratory of Pathology, Center for Cancer Research, National Cancer Institute, is seeking an outstanding tenure-track or tenure-eligible physician-scientist to both carry out original, innovative research and to participate in Molecular Diagnostics. This position is among several that have become available in a restructuring of the Laboratory of Pathology. The successful candidate will have a record of achievement in an area of research relevant to pathology: examples include, but are not limited to, chromosome biology and systems biology related to disease pathogenesis or diagnostics.

About NCI's Center for Cancer Research

The National Cancer Institute is part of the National Institutes of Health in the Department of Health and Human Services, a federal government agency. The Center for Cancer Research (CCR) is the largest component of the NCI intramural biomedical research effort at NIH and a major user of the NIH Clinical Research Center, a state-of-the-art research hospital on the campus of the NIH in Bethesda, Maryland. The CCR offers tremendous depth and breadth of intellectual and technological resources, as well as opportunities for collaboration with investigators both within and outside of the NIH. Investigators are supported by a wide array of research resources, including animal facilities and dedicated high-quality cores in such areas as imaging/microscopy, chemistry/purification, mass spectrometry, flow cytometry, genomics/sequencing, transgenics and knockout mice, arrays/molecular profiling, and human genetics/bioinformatics. The research environment is highly conducive to advancing translational research and highly collaborative, emphasizing multidisciplinary and interdisciplinary team science.

Location

The Laboratory of Pathology is located on the campus of the National Institutes of Health in Bethesda, Maryland, a suburb of Washington, D.C.

Eligibility/Salary

Applicants must have an M.D. or M.D., Ph.D. degree. Board certification in Anatomic Pathology, Molecular Genetic Pathology or clinical Medical Genetics is desirable but equivalent training and experience may substitute. The successful candidate will direct an independent research program supported by the NCI intramural program. Research support will be provided to develop a state-of-the-art laboratory that includes sufficient personnel, space, equipment, and a supplies budget to sustain a productive research effort. Salary is negotiable within a range and is dependent upon qualifications and experience. A full package of benefits, including health insurance, life insurance, retirement and Thrift Savings Plan, is available to Federal employees. Candidates may be eligible for the NIH Loan Repayment Program (http://www.LRP.NIH.gov). This position is not restricted to U.S. citizens.

Application

Interested individuals should submit a cover letter, curriculum vitae, brief statement of research interests and future plans (1-2 pages) electronically to bronezm@mail.nih.gov, or by mail to the address below. Applications will begin to be considered on or around **August 1, 2009**. The position will remain open until filled. **Dr. Mark C. Udey, Chair, Search Committee, Laboratory of Pathology, Center for Cancer Research, NIH, c/o Ms. Melissa Bronez, Executive Secretary, 9000 Rockville Pike, 31 Center Drive, Bldg. 31/Room 3A11, MSC 2440, Bethesda,MD. 20892-2440**.

One focus: join our shared commitment to improve the lives of cancer patients everywhere.

Millennium: The Takeda Oncology Company is developing an extensive pipeline — among the top in oncology worldwide — with more than 13 compounds in development for a broad range of solid and hematological cancers.

Postdoctoral Program – Protein Homeostasis

Millennium: The Takeda Oncology Company is renewing a Postdoctoral Fellowship Program in the rapidly advancing area of Protein Homeostasis. Following on the success of the first-in-class proteasome inhibitor, bortezomib, for the treatment of cancer, the initiation of this program presents a unique opportunity to join one of the industry's leading multidisciplinary research groups in the field.

We're looking for highly talented and motivated PhDs in the research areas of biochemistry or molecular, cellular and in vivo biology to participate in this exciting program. Research will focus on key biological questions to help define the role of Protein Homeostasis in cancer.

Fellows will integrate closely with the Discovery organization and have a real opportunity to learn the science of drug discovery. They will be encouraged to present their findings at major scientific meetings and will be expected to publish in leading peer reviewed journals. Fellows will work in state of the art facilities with access to cutting edge biology reagents and technologies.

Experience in the area of Protein Homeostasis is an advantage although candidates from other scientific backgrounds are encouraged to apply.

Please visit us at **www.millennium.com/careers** to apply to this position. Please reference req. #5968BR.

Takeda
MILLENNIUM
THE TAKEDA ONCOLOGY COMPANY

Universität Karlsruhe (TH)
Forschungsuniversität · gegründet 1825

KIT
Karlsruhe Institute of Technology

The **DFG Research Center for Functional Nanostructures (CFN)** at the Universität Karlsruhe (TH) invites applications for the position of

Leader of the Young Scientist Group „Computational Chemistry"

The Young Scientist Group will initially be funded until the 30th of June 2013.

The Young Scientist Group is intended to strengthen the CFN (www.cfn.uni-karlsruhe.de) in the field of theoretical chemistry and will be expected to participate in interdisciplinary research projects, for example in the research area **Molecular Nanostructures.** Research groups from inorganic, organic and physical/theoretical chemistry as well as from experimental and theoretical physics collaborate in this research area. Possible research topics of the Young Scientist Group are

- the interaction of molecules with nanostructured surfaces,
- surface reactions treated by density-functional theory,
- multi-scale modeling of surface processes,
- the theory of mass, charge and heat transport.

Two further researcher positions, start-up investments and consumables will be provided to the Young Scientist Group.

The applicant is expected to be an outstanding young researcher in one or more fields of theoretical chemistry related to the above research area. His/Her competence should be clear from publications in established international scientific journals, and he/she should have held a doctorate for not more than 5 years.

Universität Karlsruhe (TH) aims to increase the representation of women among the university staff and therefore explicitly encourages applications from female scientists. Universität Karlsruhe (TH) is an equal opportunity employer and will give preference to disabled candidates having the same qualifications as their competitors.

Applications including a short project outline, CV, diplomas, a list of publications and copies of the five most important publications are to be submitted not later than the **31st of August 2009** to the **Universität Karlsruhe (TH), Prof. Dr. M. Wegener, CFN coordinator, Wolfgang-Gaede-Straße 1a, 76131 Karlsruhe, Germany.**

ulm university universität uulm

The University of Ulm intends to establish a Research Group for **"Stem Cell Targeting"** within the **"Center for Biomedical Research".** We are now seeking applications from qualified individuals to head this research group:

Molecular Functions and Targeting of Stem Cells Full Professor (W3)

The successful candidate will be appointed as head of a new institute. A particular focus of the new initiative is on stem cell biology and regenerative medicine. Molecular alterations in adult stem cells contribute to regenerative dysfunction, aging, and carcinogenesis. The targeting of molecular alterations in stem cells represents an emerging focus in molecular medicine and includes genetic approaches or siRNA or compound-mediated manipulation of molecular pathways in stem cells. The new initiative will help to translate basic knowledge on stem cell biology towards targeted therapies. The appointment is tenured. The successful applicant will be appointed to a Chair at the University.

The University of Ulm has established clinical research programs in molecular medicine and stem cell aging (Max-Planck-Research Group), lympho-hematopoiesis, stem cell transplantation, characterisation of tumor stem cells, apoptosis, aging, and molecular imaging as well as programs in developmental biology (SFB 497), and tissue repair and regeneration in the pancreas (SFB 518).

Candidates should hold an MD or PhD degree in medicine, biochemistry or biology. An excellent track record, sustained external funding and a robust research program are required.

Teaching experience is advantageous. The University of Ulm runs undergraduate and graduate programs in biochemistry, biology, molecular medicine and medicine including a PhD program funded by the excellence initiative of the Federal Government.

Conditions for appointment are a completed course of studies at a university, pedagogical aptitude, doctorate and additional academic achievements (§ 47 LHG).

The University of Ulm is committed to increase the share of women in research and teaching positions and therefore explicitly encourages female candidates to apply.

Applications (including the application form, CV, a complete list of grants and publications, and a summary of current research interests and objectives) should be sent **by June 30, 2009** to: Professor Dr. G. Adler, Vice President and Head of Search Committee, University of Ulm, D-89069 Ulm, Germany. Application forms can be requested from the Vice President's Office (e-mail: almuth.stein@uniklinik-ulm.de).
Please indicate on the
envelope the index number 50.

Physically disabled applicants receive favourable consideration when equally qualified.

Zertifikat seit 2008
audit familiengerechte hochschule

Director • Laufer Center for Computational Biology and Genome Science

Stony Brook University seeks a visionary leader to direct and actively participate in the research programs of the Louis and Beatrice Laufer Center for Computational Biology and Genome Science (*www.laufercenter.stonybrook.edu*). The Center Director will have achieved national or international prominence in a field relevant to the research interests of the Laufer Center, such as systems biology, computational structural biology, and computational genomics.

The Laufer Center was designed as a focal point for research and graduate training in computational biology and genome sciences. The Center is expected to play a critical role in the recently formed Stony Brook Alliance, which involves Stony Brook University, Brookhaven National Laboratory, and Cold Spring Harbor Laboratory. Therefore, the Director must have the ability to promote and coordinate interdisciplinary research and collaborations across departments and among institutions. Resources for the Center include three endowed professorships, newly renovated space, and a substantial budget for equipment and operating funds. The Director will hold the rank of professor and report to the Provost of the University.

Required qualifications include a Ph.D. or M.D. degree and at least 10 years of research experience in a discipline relevant to the goals of the Laufer Center. He or she will have successfully obtained research funding from major granting institutions and research foundations and will have compiled an outstanding record of professional achievement. Candidates must possess excellent leadership and management skills and have the decision-making and collaborative skills required to establish and lead a world-class interdisciplinary research center. Experience will include the ability to stimulate innovation and to effectively collaborate with faculty and staff to ensure the emergence of a vibrant and productive Center.

Qualified applicants should submit a comprehensive curriculum vitae that includes their educational background, academic/visiting appointments held, honors and awards received, external research funding, list of publications, invited/keynote presentations, work with learned societies, service on editorial boards, conferences organized, and memberships in professional organizations. Applications will be accepted until the position is filled.

To apply submit to: Chair, Search Committee
Laufer Center Director, Basic Science Tower
T-8, Room, 160, Stony Brook University, SUNY
Stony Brook, NY 11794-8651; or fax (631) 444-7641

Equal Opportunity/Affirmative Action Employer. Women, people of color, individuals with disabilities, and veterans are encouraged to apply.

STONY BROOK

DTRA

Defense Threat Reduction Agency

The Defense Threat Reduction Agency (DTRA) makes the world safer by reducing the threat posed by weapons of mass destruction. In the 21st century few tasks are as challenging or demanding. We are looking to employ a skilled technical manager and leader with the vision to help keep America safe from weapons of mass destruction.

We are actively recruiting for the position of Chief, Physical Science and Technology Division, Chemical and Biological Technologies Directorate (located at Ft. Belvoir, VA). Highly qualified candidates will have excellent collaborative leadership skills, in-depth technical knowledge, and the demonstrated capability to plan, coordinate, integrate and execute a science and technology program that provides timely and effective physical countermeasures against Chemical, Biological, and Radiological threats and direct Division technical staff.

US CITIZENSHIP IS REQUIRED.

Applications will be accepted **June 1, 2009 thru June 19, 2009** at **www.usajobs.gov** (Click on Agency Search, then select Defense Threat Reduction Agency) or Resumes may be submitted thru **June 19, 2009** directly to: **Human Capital Office, Attn: Mr. Howard Staik, 8725 John J. Kingman Road, Ft. Belvoir, VA 22060-6201**.

UNC
ESHELMAN SCHOOL OF PHARMACY

Assistant/Associate Professor in Nanomedicine

The Center for Nanotechnology in Drug Delivery announces the appointment in the Division of Molecular Pharmaceutics in the UNC Eshelman School of Pharmacy in Partnership with the Lineberger Comprehensive Cancer Center at the University of North Carolina at Chapel Hill.

Candidates possessing a Ph.D. degree in an engineering discipline, pharmaceutical sciences, chemistry or related discipline with expertise in nanomedicine, nanotechnology and cancer drug delivery are invited to apply for this 12-month tenure-track position. The ideal candidate will have already established a highly competitive independent research program, or possess the clear potential to do so with a primary focus in targeted nanoparticle-based therapeutics and/or molecular and nanotechnology-based imaging and diagnostic probes. The candidate must have an interest in translating novel technologies into clinical investigation, and have the ability to collaborate with other basic and clinical researchers.

The deadline for applications is **August 1, 2009**. Applications should be in PDF format including the following four items: (1) a cover letter, (2) CV, (3) detailed statement of research program and interests, and (4) the names and contact information of four references. Interested applicants should apply directly to the search committee chair: **Michael Jay, Ph.D.** at **mjay@unc.edu**. *Women and minority groups are encouraged to apply.*

Baylor College *of* Medicine

Baylor College of Medicine is recruiting McNair Scholars.

The best minds in medicine seek emerging leaders in:

Breast Cancer Research
Dan L. Duncan Cancer Center of Baylor College of Medicine

Type 1 Diabetes Research
Division of Diabetes, Endocrinology and Metabolism

Neuroscience Research
Departments of Neuroscience and Neurology

Pancreatic Cancer Research
Dan L. Duncan Cancer Center of Baylor College of Medicine

Through a $100 million gift from the Robert and Janice McNair Foundation, Baylor College of Medicine in Houston is recruiting up-and-coming researchers and physician scientists to serve as McNair Scholars. These new faculty members will join the best minds in medicine in a uniquely collaborative work environment as we transform the future of healthcare through groundbreaking basic or translational research and the delivery of personalized medicine. A very generous recruiting package will be offered to these new faculty members.

Are you a McNair Scholar candidate?

- A promising investigator with an exciting research program and high impact publications in your field
- A junior faculty or senior postdoctoral fellow
- Extraordinary potential for significantly advancing human health and novel treatments for human disease through highly innovative, cutting-edge research
- Committed to collaboration and willing to share discoveries for the benefit of the larger medical community

Baylor College of Medicine is an Equal Opportunity/Affirmative Action/Equal Access Employer.

For more information and to learn how to apply, visit www.bcm.edu/mcnair or call 713.798.9134.

BCM
Baylor College *of* Medicine

McNAIR SCHOLAR

AARHUS UNIVERSITY

Three Professor/Group Leader Positions at NeuroCampus Aarhus, Denmark

NeuroCampus Aarhus (NCA) is a crosscutting research cluster within neuroscience and cognition at Aarhus University (AU). NeuroCampus is a focus area of AU and receives strong support from the Lundbeck Foundation, the Danish National Research Foundation, Aarhus University Hospital, the Danish Ministry of Science, Technology and Innovation, and numerous industrial partners.

NCA comprises basic sciences ranging from neurogenetics, molecular and cellular neurobiology to clinical neuroscience, rehabilitation research and cognitive neuroscience. NeuroCampus Aarhus research has strong translational traditions and is partly embedded in Aarhus University Hospital. It has strong international collaborations and a strong infrastructure with cutting edge neuroimaging research facilities, bio-imaging equipment, biomedical engineering and animal models.

NeuroCampus Aarhus wishes to strengthen basic research within neurotransmission and neuropharmacology, plasticity, degeneration and regeneration as well as ischemia, extending our emphasis on understanding the molecular and cellular biology of neurological and psychiatric diseases.

We are offering several professor/group leader positions in specific research fields:

- Professor/Group Leader, *in vivo* molecular imaging
- Tenured Professor/Group Leader, Positron Emission Tomography Neuroimaging
- Tenured Professor/Group Leader, Neurobiology

Read full job description at **www.neurocampus.au.dk**

Application containing full CV, publication list and a brief statement of research plans should be submitted **by noon, July 15th 2009** to **Aarhus University, Faculty of Health Sciences, Vennelyst Boulevard 9, DK-8000 Aarhus C, Denmark, marked '2009-NeuroCampus'**.

Select candidates will be invited to interview in **October 2009**.

Head of Division (Neurophysiology)

MRC | National Institute for Medical Research

Situated in Mill Hill, North West London, NIMR is the largest MRC institute, supporting some 70 research groups and 500 bench scientists. The Institute provides excellent training for researchers in a multi-disciplinary environment and is equipped with state of the art facilities. **http://www.nimr.mrc.ac.uk/employment/**

The NIMR intends to appoint an outstanding neuroscientist to head the division of Neurophysiology. This is one of the leadership posts at NIMR, and the successful candidate will have made major contributions to research in one or more fields involving in vivo or in vitro analysis of single cells and circuits, synaptic transmission and plasticity, or any area of systems neuroscience.

The candidate should have a successful record of team leadership, and an enthusiasm for promoting and developing neuroscience in a multi-disciplinary environment. The candidate will benefit from the Institute's open culture of collaboration across all disciplines, relevant strengths in developmental neuroscience and molecular genetics, world class animal facilities, and excellent core infrastructure and services.

Informal enquiries to **Professor Iain Robinson** by e-mail **irobins@nimr.mrc.ac.uk** or call **0208 816 2049**.

Salary range is from £55,550 per annum + £1,469 per annum (London Allowance). MRC final salary Pension Scheme is also available.

Applications, along with a full CV and covering letter, should be made online at **http://jobs.mrc.ac.uk**. If you do not have internet access or you experience technical difficulties please call **01793 301157** quoting reference **NIMR09/239**.

The closing date is **2 July 2009**.

Final appointments will be subject to a pre employment screening.

The MRC is an Equal Opportunities Employer.

SYMPOSIUMS

DEPARTMENT OF THE NAVY
ONR
Science & Technology

PROGRAM OFFICER, WARFIGHTER & APPLICATIONS RESEARCH
(Biologist, Pharmacologist, Physiologist)

The Office of Naval Research is seeking a qualified individual to manage sponsored basic/applied research, and advanced technology development programs and projects in the broad areas of physiology, pharmacology, and psychology. The sponsored efforts are conducted principally at U.S. universities and industry or Federal laboratories. This is a Federal Civil Service position at the GS-14/15 level ($102,721 - $153,200) depending on individual qualifications.

The position requires knowledge and experience in the fundamental theories, concepts, and current-state-of-the art research and/or technology development in the broad areas of physiology, pharmacology, and psychology, including but not limited to, hemostasis, transfusion safety, resuscitations, critical care, traumatic brain injury, post traumatic stress disorder, wound repair, regenerative medicine, pain management.

For information on qualifications and how to apply, see the job announcement at our website http://www.onr.navy.mil/hr. Applications must be submitted by the date noted in the job announcement. For technical information contact CDR Elizabeth Montcalm-Smith at elizabeth.montcalms@navy.mil.

U.S. CITIZENSHIP REQUIRED   AN EQUAL OPPORTUNITY EMPLOYER

POSITIONS OPEN

INFECTIOUS DISEASE FACULTY POSITION

The Virginia-Maryland Regional College of Veterinary Medicine at the University of Maryland in College Park, Maryland, invites applications from qualified individuals for a tenured/tenure-track faculty position in infectious diseases. The appointment will be at the **ASSISTANT, ASSOCIATE or FULL PROFESSOR** level, depending upon the qualifications of the successful candidate. A D.V.M.-Ph.D. or Ph.D. degree with relevant postdoctoral training in an area of Department research focus is required for this position. Salary will be commensurate with rank and experience.

Current focus is on host-pathogen interaction with emphases on virology, immunology, bacterial pathogenesis, zoonotic diseases, and public health. Preference will be given to candidates with demonstrated abilities in attracting extramural funding, a strong publication record, and experience in graduate education. The position comprises 80 percent research and 20 percent teaching responsibilities. The research portion focuses on basic and/or applied aspects of infectious disease/host-pathogen interaction with pathogens important for human and animal health, zoonosis, and/or public health. Active participation in the University's graduate program is required. The successful candidate will be expected to develop, maintain, and conduct a productive, extramurally funded research program that will strengthen the current research goals of the College. Excellent opportunities exist for collaborations with federal agencies (USDA, FDA, NIH) and other University departments. The Department has excellent in-house shared facilities that include advanced ultraviolet-visible laser confocal and electron microscopy, DNA sequencing, fluorescent-activated cell sorting analyzer with sorting capabilities, and laboratories/animal rooms to work with BSL-2 and select BSL-3 agents.

Please submit electronically a letter of interest, curriculum vitae, statement of career goals, and contact information of three professional references to **e-mail: aferrero@umd.edu.** Please indicate in the Subject header "application for faculty position" to the attention of **Dr. Daniel R. Perez, Search Committee Chair, VA-MD Regional College of Veterinary Medicine, University of Maryland, 8075 Greenmead Drive, College Park, MD 20742-3711. Telephone: 301-314-7345; fax: 301-314-6855.** Applications will be accepted until June 30, 2009, or until a successful candidate is identified. The position is available immediately.

The University of Maryland is an Affirmative Action/Equal Opportunity Employer. Women and minorities are encouraged to apply.

POSTDOCTORAL AND STAFF POSITIONS

available in **Professor Jingdong Tian**'s synthetic biology and genomics laboratory at Duke University to develop technologies for high-throughput gene and genome synthesis and protein, genome engineering.

(1) Postdoctoral Fellow in protein design, engineering, and evolution: Experimental candidates should have extensive experience in molecular biology, protein biochemistry, enzymology, directed evolution, protein structure determination and simulation. Computational candidates should have good programming skills, solid mathematics and algorithms background, and working experience in protein design. The project will involve the upkeep of existing code and development of algorithmic procedure to aid in the redesign of proteins which bind and process nucleic acids.

(2) Postdoctoral Fellow in microfabrication, microfluidics, and instrumentation: The candidate should have extensive hands-on experience in microfabrication and microfluidic techniques. Expertise in inkjet technology, electronics, robotics, or polymer and surface chemistry is desirable. The project will involve development of integrated microfluidic platforms for high-throughput gene synthesis and genomics.

(3) Laboratory Technician/Manager: Requires B.S./M.S. degree and extensive work experience in molecular cell biology and biochemistry. The candidate should be able to stay for at least two to three years and will be responsible for routine nucleic acids, protein, cell culture work, and laboratory management.

Candidates should send curriculum vitae, statement of research interests, and names of two references to: **Professor Jingdong Tian at e-mail: jtian@duke.edu.**

POSITIONS OPEN

SIBCB

CAS-NN GREAT WALL PROFESSORSHIP IN PROTEIN SCIENCE

Institute of Biochemistry and Cell Biology, Shanghai Institutes for Biological Sciences, Chinese Academy of Sciences

中国科学院上海生命科学研究院
生物化学与细胞生物学研究所

Institute of Biochemistry and Cell Biology (IBCB), Shanghai Institutes for Biological Sciences (SIBS), Chinese Academy of Sciences (CAS) (**website: http://www.sibcb.ac.cn**) is seeking applicants for a CAS-Novo Nordisk (NN) Great Wall Professorship position in protein science with research focus on the structural and functional studies of key protein regulators that are involved in epigenetics in diabetes. Applicants should have a Ph.D. or an equivalent degree, postdoctoral experience, demonstrated excellence in research, and potential of developing independent, outstanding research work. The successful candidate will be expected to develop vigorous, extramurally funded research programs and to contribute to graduate and postdoctoral training programs. The Professorship recipient will be provided with excellent laboratory space, substantial startup fund, competitive salary, housing subsidy, and fringe benefit package. In addition, the recipient will have extra support from the CAS-NN Research Foundation to improve employment conditions, such as supplementary salary and benefits to the recipient and his/her family.

Applicants should send curriculum vitae with a complete list of publications, a concise summary of past research accomplishments and future research plans, and three letters of references to: **Dr. Jianping Ding, Faculty Search Committee, IBCB, SIBS, CAS, 320 Yue-Yang Road, Shanghai 200031, China.** Or electronically to **e-mail: jpding@sibs.ac.cn; telephone: 086-21-54921619; fax: 086-21-54921610.** Applications will be accepted until position is filled. Interviews may be conducted at any time upon arrangement.

IBCB is an Equal Opportunity Employer.

CAREER OPPORTUNITY

Doctor of Optometry (O.D.) degree in 27 months for Ph.D.s in science and M.D.s. Excellent career opportunities for O.D./Ph.D.s and O.D./M.D.s in research, education, industry, and clinical practice. This unique program starts in March 2009, and features small classes and 12 months devoted to clinical care.

Contact the **Admissions Office, telephone: 800-824-5526** at the **New England College of Optometry, 424 Beacon Street, Boston, MA 02115.** Additional information at **website: http://www.neco.edu, e-mail: admissions@neco.edu.**

The Olympic Analytical Laboratory in the Department of Pathology and Laboratory Medicine at UCLA has a **POSTDOCTORAL POSITION** available to develop hormone isolation and detection techniques to identify the use of doping agents by athletes. A Ph.D. in chemistry, biochemistry, toxicology, or molecular biology is required. Knowledge of and experience with hormones and protein analysis using techniques such as SDS-PAGE, Western blots, isoelectric focusing, GC/MS, and/or LC/MS/MS are highly desirable. Send curriculum vitae and contact information for three references to **e-mail: abutch@mednet.ucla.edu.** *The David Geffen School of Medicine at UCLA is an Equal Opportunity Employer.*

POSTDOCTORAL POSITIONS

Two Postdoctoral positions available to study differentiation mechanisms of the eye and brain using molecular and genetic approaches. Candidates with experience in molecular biology and a Ph.D. degree are encouraged to send their curriculum vitae, statement of research interests, and the names of three references to: **Dr. Renping Zhou, Laboratory for Cancer Research, School of Pharmacy, Rutgers University, 164 Frelinghuysen Road, Piscataway, NJ 08854. E-mail: bachorik@rci.rutgers.edu.**

POSITIONS OPEN

UTD

SENIOR RESEARCH SCIENTIST

The University of Texas at Dallas
Sickle Cell Disease Research Center

Requires a Ph.D. in molecular biology or a closely related field and three years of postdoctoral training or research-based experience in molecular biology techniques including reporter systems, chromatin immunoprecipitation, gene expression profiling by microarray analysis, stem cell tissue culture techniques, cloning, and basic protein analysis. This position will require comprehensive reports for grant application, scientific publications, and graduate student supervision. Applications from U.S. citizens or permanent residents preferred.

Review of applicants begins June 1, 2009, and continues until filled.

Submit curriculum vitae to: **Betty S. Pace, M.D., at e-mail: bpace@utdallas.edu.**

POSTDOCTORAL FELLOWSHIPS AND JUNIOR FACULTY POSITIONS

in Diabetes and Beta Cell Biology
University of Pittsburgh
Division of Endocrinology and Metabolism

Pancreatic beta cell–diabetes group seeks Postdoctoral Fellows and Junior Faculty, M.D. or Ph.D., with excellence in cell biological techniques (including co-immunoprecipitation, immunohistochemistry, confocal imaging, intracellular trafficking) and molecular techniques (including adenoviral and retroviral gene delivery). Send resume to: **Andrew Stewart, M.D., Chief, Endocrinology, University of Pittsburgh School of Medicine, U.S.A., via e-mail: mkc20@pitt.edu.**

The University of Pittsburgh is an Affirmative Action, Equal Opportunity Employer.

MARKETPLACE